

Title: Solution Based Synthesis of Perovskite-Type Oxide Films
and Powders

Author: James M. McHale
Los Alamos National Laboratory
Nuclear Materials Technology Division
NMT-6, Mail Stop E510
Los Alamos, NM 87545

505 667 3763



LOS ALAMOS NATIONAL LABORATORY

DISTRIBUTION OF THIS DOCUMENT IS UNLIMITED

DISCLAIMER

Portions of this document may be illegible in electronic image products. Images are produced from the best available original document.

DISCLAIMER


This report was prepared as an account of work sponsored by an agency of the United States Government. Neither the United States Government nor any agency thereof, nor any of their employees, makes any warranty, express or implied, or assumes any legal liability or responsibility for the accuracy, completeness, or usefulness of any information, apparatus, product, or process disclosed, or represents that its use would not infringe privately owned rights. Reference herein to any specific commercial product, process, or service by trade name, trademark, manufacturer, or otherwise does not necessarily constitute or imply its endorsement, recommendation, or favoring by the United States Government or any agency thereof. The views and opinions of authors expressed herein do not necessarily state or reflect those of the United States Government or any agency thereof.

SOLUTION BASED PREPARATION
OF PEROVSKITE-TYPE OXIDE
FILMS AND POWDERS

A Dissertation
Submitted to
the Temple University Graduate Board

in Partial Fulfillment of
the Requirements for the Degree
DOCTOR OF PHILOSOPHY

by
James M. McHale Jr.
January, 1995


DISTRIBUTION OF THIS DOCUMENT IS UNLIMITED

MASTER

SOLUTION BASED PREPARATION OF PEROVSKITE-TYPE
OXIDE FILMS AND POWDERS

James M. McHale Jr.

Doctor of Philosophy

Temple University

January, 1995

Major Advisor: Dr. Robert E. Salomon

ABSTRACT OF DISSERTATION

Conventional solid state reactions are diffusion limited processes that require high temperatures and long reaction times to reach completion. In this work, several solution based methods were utilized to circumvent this diffusion limited reaction and achieve product formation at lower temperatures. The solution methods studied all have the common goal of trapping the homogeneity inherent in a solution and transferring this homogeneity to the solid state, thereby creating a solid atomic mixture of reactants. These atomic mixtures can yield solid state products through "diffusionless" mechanisms. The effectiveness of atomic mixtures in solid state synthesis was tested on three classes of materials, varying in complexity. A procedure was invented for obtaining the highly water soluble salt, titanyl nitrate, $\text{TiO}(\text{NO}_3)_2$, in crystalline form, which allowed the production

of titanate materials by freeze drying. The freeze drying procedures yielded phase pure, nanocrystalline BaTiO_3 and the complete SYNROC-B phase assemblage after ten minute heat treatments at 600°C and 1100°C , respectively. Two novel methods were developed for the solution based synthesis of $\text{Ba}_2\text{YCu}_3\text{O}_{7-x}$ and $\text{Bi}_2\text{Sr}_2\text{Ca}_2\text{Cu}_3\text{O}_{10}$. Thin and thick films of $\text{Ba}_2\text{YCu}_3\text{O}_{7-x}$ and $\text{Bi}_2\text{Sr}_2\text{Ca}_2\text{Cu}_3\text{O}_{10}$ were synthesized by an atmospheric pressure, chemical vapor deposition technique. Liquid ammonia solutions of metal nitrates were atomized with a stream of N_2O and ignited with a hydrogen/oxygen torch. The resulting flame was used to coat a substrate with superconducting material. Bulk powders of $\text{Ba}_2\text{YCu}_3\text{O}_{7-x}$ and $\text{Bi}_2\text{Sr}_2\text{Ca}_2\text{Cu}_3\text{O}_{10}$ were synthesized through a novel acetate glass method. The materials prepared were characterized by XRD, TEM, SEM, TGA, DTA, magnetic susceptibility and electrical resistivity measurements.

ACKNOWLEDGMENTS

Although this dissertation is attributed to a single author, the work reported here would not have been completed without the help of several individuals, to whom I am deeply indebted. Of these individuals, I would like to first acknowledge my advisor, Professor Robert E. Salomon, for four years of constant instruction, guidance, and encouragement. He has devoted countless hours to my education. I thank him sincerely for his dedication and friendship, and hope to honor his name in the future.

I am also greatly indebted to Dr. Nicholas V. Coppa of Los Alamos National Laboratory. Although he did not know me personally or professionally, Dr. Coppa hired me as a Graduate Research Assistant at Los Alamos on the recommendation of Dr. Salomon. I have benefited greatly from the opportunity to work with him. I believe him to be one of the most energetic and creative individuals that I have had the privilege to know.

In my early years as a graduate student, I learned a great deal about research and chemistry from Dr. Richard W. Schaeffer of Franklin and Marshall College (who, at the time was a fellow graduate student in Dr. Salomon's group). Rick was always willing to explain a concept or contribute to scientific discussions. In addition, the research reported in Chapter 7 of this work would not have been possible had Dr. Schaeffer not introduced the author to use of liquid ammonia as a solvent in the preparation of cuprate superconductors. I wholeheartedly thank him.

Professor George H. Myer has played an integral role in my education and research. I have greatly benefited from his instruction, discussions, and expertise in powder x-ray diffraction. I am also indebted to Dr. Myer for his allowing me ample time for analysis on his x-ray diffractometer, and for serving on my graduate committee.

I would also like to express my gratitude to Professor Mortimer M. Labes for his assistance in the final preparation of this manuscript and for serving on my graduate committee. In addition, I thank Professor Labes for the use of his electrical resistivity measuring equipment, which was a vital part of this research.

Professor Donald D. Titus is to be recognized for his discussions and input in several areas of this research, and for serving on my graduate committee. I have had the opportunity to attend several of his courses and have learned a great deal about chemistry, and teaching chemistry from Professor Titus.

Several individuals have contributed valuable pieces of data to compliment this research, and I am indebted to them for their services. From Los Alamos National Laboratory, the author acknowledges P. C. McIntyre and K. E Sickafus for their TEM analysis and interpretation and E. L. Brosha for his TGA studies. From Temple University, the author acknowledges the assistance of A. Kebede, and the outstanding group of graduate students with whom I have had the privilege to work; R. W. Schaeffer, J. Macho, A. Thomas, B. Ahn, H. Y. Chen, M. Seyedahmadian, Z. Zou, E. Manas, and D. Wolko.

The author acknowledges the support of the U. S. Department of Energy through the Graduate Research Assistant program at Los Alamos National Laboratory.

I would like to wholeheartedly thank my parents, James and Joan McHale, for a lifetime of love and support. This work would have surely not been completed without their help and motivation.

Finally, I thank my best friend and fiancée, Maureen Donaher, for her love, support, patience, understanding, and encouragement, throughout the past four years.

TABLE OF CONTENTS

ABSTRACT.....	iii
ACKNOWLEDGMENTS.....	v
LIST OF FIGURES.....	xiv
LIST OF TABLES.....	xxii

PART I INTRODUCTION AND BACKGROUND

CHAPTER	Page
1. SOLID STATE REACTIONS.....	2
1.1 The Diffusion Limited Solid State Reaction.....	2
1.2 The Diffusionless (Atomically Mixed) Solid State Reaction	7
1.3 Notes and References.....	14
2. SOLID STATE MATERIALS.....	16
2.1 The Perovskite Structure.....	17
2.2 Properties and Applications of Simple Perovskite Materials.....	19
2.2.1 Barium Titanate.....	20
2.2.2 SYNROC.....	24
2.3 High Temperature Superconducting Cuprates.....	26
2.3.1 Ba ₂ YCu ₃ O ₇ and Related Cuprates.....	27

TABLE OF CONTENTS (cont.)

2.3.2 The Bismuth Cuprates.....	30
2.4 Applications of High Temperature Superconductors.....	32
2.5 Notes and References.....	34
3. SYNTHESIS OF BULK POWDERS AND SUPPORTED FILMS OF PEROVSKITE MATERIALS	38
3.1 Synthesis of Perovskite Materials in Bulk Form.....	38
3.1.1 Conventional Ceramic Processing.....	38
3.1.2 Solution Methods.....	40
3.1.2.1 Solute Removal Techniques.....	41
3.1.2.2 Solvent Removal Techniques.....	45
3.2 Synthesis of Perovskite Materials as Supported Films.....	49
3.2.1 Preparation of Thin Films.....	51
3.2.1.1 Ion Beam Sputtering.....	51
3.2.1.2 Molecular Beam Epitaxy.....	52
3.2.1.3 Laser Ablation.....	52
3.2.1.4 Coevaporation.....	53
3.2.1.5 Metalorganic Chemical Vapor Deposition.....	54
3.2.2 Preparation of Thick Films.....	55
3.2.2.1 Screen Printing.....	55
3.2.2.1 Spray Pyrolysis.....	55
3.3 Notes and References.....	57

TABLE OF CONTENTS (cont.)

PART II EXPERIMENTAL METHODS AND RESULTS

CHAPTER	Page
4. CHARACTERIZATION OF SOLID STATE MATERIALS.....	65
4.1 Characterization of Chemical Properties.....	65
4.1.1 Thermogravimetric Analysis.....	66
4.1.2 Gross Gravimetric Analysis.....	67
4.1.3 Differential Thermal Analysis.....	67
4.2 Characterization of Structural and Morphological Properties.....	68
4.2.1 Powder x-ray Diffraction.....	68
4.2.2 Scanning Electron Microscopy.....	70
4.2.3 High Resolution Transmission Electron Microscopy.....	72
4.3 Characterization of Physical Properties.....	73
4.3.1 Electrical Measurements.....	73
4.3.2 Magnetic Measurements.....	74
4.4 Notes and References.....	77
5. PREPARATION OF NANOCRYSTALLINE BARIUM TITANATE VIA THERMAL DECOMPOSITION OF FREEZE DRIED NITRATE PRECURSORS	78
5.1 Preparation of Titanyl Nitrate.....	79
5.1.1 Hydrous Titania.....	80
5.1.2 Titanyl Nitrate.....	82

TABLE OF CONTENTS (cont.)

5.1.3 Experimental Procedure.....	83
5.1.4 Results.....	84
5.2 Preparation of BaTiO ₃ from Freeze Dried Nitrate Solutions.....	88
5.2.1 Solution Preparation.....	88
5.2.2 Freezing the Solution.....	89
5.2.3 Sublimation.....	90
5.2.4 Thermal Processing.....	92
5.2.5 Results and Discussion.....	94
5.2.6 Conclusions.....	108
5.3 Notes and References.....	110
6. EVOLUTION OF THE SYNROC-B PHASE ASSEMBLAGE FROM FREEZE DRIED NITRATE PRECURSORS.....	112
6.1 Preparation of SYNROC-B from Freeze Dried Nitrates.....	113
6.1.1 Experimental Procedure.....	113
6.1.2 Results and Discussion.....	114
6.2 Preparation of SYNROC-B Constituent Phases.....	121
6.2.1 Experimental Procedure.....	121
6.2.2 Results and Discussion.....	122
6.2.2.1 Hollandite.....	122
6.2.2.2 Zirconolite.....	124
6.2.2.3 Perovskite.....	125

TABLE OF CONTENTS (cont.)

6.3 Conclusion.....	126
6.4 Notes and References.....	128
7. PREPARATION OF OXIDE FILMS FROM COMBUSTION OF NON-AQUEOUS SOLUTIONS.....	129
7.1 General Considerations.....	132
7.1.1 Solvent.....	132
7.1.2 Reagents.....	132
7.1.3 Pilot Flame and Propellant Gas.....	134
7.1.4 Substrate.....	135
7.1.5 Substrate Preparation.....	135
7.2 Preliminary Studies With Organic Solvents.....	136
7.2.1 Experimental Procedure.....	136
7.2.2 Results and Discussion.....	139
7.3 Preparation of Thick Films of $Ba_2YCu_3O_{7-x}$ From Combustion of Liquid Ammonia Solutions.....	145
7.3.1 Experimental Procedure.....	146
7.3.2 Results and Discussion	150
7.4 Preparation of Thin Films of From Combustion of Liquid Ammonia Solutions.....	159
7.4.1 Experimental Procedure.....	161
7.4.2 Results and Discussion	163

TABLE OF CONTENTS (cont.)

7.5 Conclusions.....	166
7.6 Notes and References.....	169
8. SYNTHESIS OF BULK HIGH T _c SUPERCONDUCTORS FROM ACETATE GLASS PRECURSORS.....	171
8.1 Experimental Procedure.....	172
8.1.1 Reagents.....	172
8.1.2 Sample Preparation.....	173
8.1.3 Mechanistic Studies.....	174
8.2 Characterization of Final Products.....	176
8.2.1 Ba ₂ (RE)Cu ₃ O _{7-x}	176
8.2.2 (Bi,Pb) ₂ Sr ₂ Ca ₂ Cu ₃ O ₁₀	178
8.3 Results of Mechanistic Studies.....	180
8.4 Discussion and Conclusions.....	185
8.4.1 The Ba-RE-Cu-O Acetate System.....	185
8.4.2 The (Bi,Pb)-Sr-Ca-Cu-O Acetate System.....	188
8.5 Notes and References.....	190
9. SUMMARY AND CONCLUSIONS.....	192
COMPREHENSIVE BIBLIOGRAPHY.....	198

LIST OF FIGURES

<u>Figure</u>	<u>Page</u>
Figure 1.1. A schematic depicting product formation at the contact points of reactant grains. The rate of the solid state reaction is slowed as the reactants are forced to diffuse through an ever increasing, inert layer of product for subsequent product formation. The double headed arrows represent the length of the diffusion paths.	3
Figure 1.2. A plot of the extent of the reaction, α , versus time for the reaction $\text{MgO} + \text{Al}_2\text{O}_3 \rightarrow \text{MgAl}_2\text{O}_4$ at 1300°C . The solid boxes represent the reaction between $\sim 1\ \mu\text{m}$ particles and the empty boxes represent the reaction between $\sim 50\ \mu\text{m}$ particles. The data is from reference 15.....	8
Figure 2.1. The ideal perovskite structure consisting of a cube with a B atom at the center, A atoms at the corners and O atoms on the center of each face.	18
Figure 2.2. A pseudo-phase diagram of the structural changes of BaTiO_3 with respect to temperature and particle size. Crystallites below $10\ \text{nm}$ in diameter are cubic due to surface effects. The curvature of the tetragonal to cubic transition line is arbitrary. The structure of the surface layer of BaTiO_3 at low temperatures is undetermined.	21
Figure 2.3 A schematic of the variance in the relative permittivity of BaTiO_3 with increasing temperature. The Curie temperature, T_C , occurs at $\sim 120^\circ\text{C}$	23
Figure 2.4. The crystal structure of $\text{Ba}_2\text{YCu}_3\text{O}_7$ showing one half of the unit cell. The buckled Cu-O planes labeled B carry the supercurrents.	29
Figure 4.1. A schematic of the basic components of a transmission electron microscope (from reference 5).	73

LIST OF FIGURES (cont.)

<u>Figure</u>	<u>Page</u>
Figure 4.2. A schematic of the experimental setup used for measuring the Meissner force exerted between a permanent magnet and a superconducting pellet with varying temperature. The labeled parts correspond to; a) permanent magnet, b) Styrofoam support, c) superconducting sample, d) silicon diode temperature sensor, e) liquid nitrogen, f) Lakeshore Cryogenics temperature controller, and g) desk top computer.	76
Figure 5.1. A TGA plot for titanyl nitrate.	87
Figure 5.2. A schematic depicting the experimental setup for rapid freezing of solutions. The labeled parts correspond to; a) stainless steel support holding inner Pyrex tube, b) mechanical stirrer, c) ultrasonic spray nozzle, d) solution inlet, e) liquid nitrogen inlet, f) cross section of Dewar flask, and g) stainless steel fine mesh screen.	90
Figure 5.3. A schematic diagram of the apparatus used for freeze drying the solutions. It is the difference in the temperature dependent vapor pressure of water at -70°C (condenser temperature) and -30°C (sample temperature) that drives the mass transport.	91
Figure 5.4. A schematic diagram of the furnace setup for thermally processing the freeze dried precursor. The labeled parts correspond to; a) gas outlet, b) needle valve, c) pressure gauge, d) stainless steel rod, e) Ultratorr seal welded to KF flange, f) Pt or Au boat, g) furnace heating element, h) Pt radiation shield, i) quartz tube, j) gas inlet, and k) furnace temperature control thermocouple.	93
Figure 5.5. The x-ray diffraction pattern for the freeze dried barium and titanyl nitrate precursor. Data was collected with the sample sealed behind Kapton tape. The scattering due to blank Kapton tape is provided for comparison (upper pattern). Barium nitrate peaks are evident in the precursor.	94
Figure 5.6. A TGA curve for the barium and titanyl nitrate precursor.	95
Figure 5.7. The XRD pattern of a BaTiO_3 sample calcined for 10 min at 600°C in an atmosphere of pure O_2 . No impurity phases (Ba_2TiO_4 , TiO_2 , BaCO_3 , etc.) were detected.	96

LIST OF FIGURES (cont.)

<u>Figure</u>	<u>Page</u>
Figure 5.8. The XRD pattern of a mechanical mixture of Ba(NO ₃) ₂ and TiO(NO ₃) ₂ , calcined for 10 min at 600° C in an atmosphere of pure O ₂ , and the atomic mixture calcined under identical conditions.	99
Figure 5.9. A bright field TEM image of a BaTiO ₃ sample heated at 600° C for 10 min in O ₂ . Photograph courtesy of K. E. Sickafus, Los Alamos National Laboratory.	101
Figure 5.10. A bright field TEM image of a BaTiO ₃ sample heated at 600° C for 1 h in O ₂ . Photograph courtesy of K. E. Sickafus, Los Alamos National Laboratory.	102
Figure 5.11. A bright field transmission electron micrograph of a larger area of the BaTiO ₃ sample heated for 10min at 600° C showing the bimodal distribution of particle sizes. Photograph courtesy of K. E. Sickafus, Los Alamos National Laboratory.	103
Figure 5.12. A plot of the inverse of the full width at half maximum (1/F _{WHM}) of the powder x-ray diffraction data for the 110 peak of BaTiO ₃ versus annealing time at 600° C (solid squares), 800° C (empty squares), and 1000° C (empty circles). An increase in the value of 1/F _{WHM} is consistent with an increase in the average particle size of the sample.	106
Figure 5.13. X-ray diffraction patterns for a BaTiO ₃ samples calcined at 1000° C for (from bottom) 10 min, 30 min, 60 min and 120 min. The splitting indicative of tetragonal BaTiO ₃ can be seen in the peak(s) at ~45° 2θ.	107
Figure 6.1. The XRD patterns of the SYNROC-B nitrate precursor behind a layer of Kapton tape and the XRD pattern of blank Kapton tape.	115
Figure 6.2. A TGA of the SYNROC-B nitrate precursor.	116
Figure 6.3. The XRD pattern of SYNROC-B prepared from freeze dried nitrates after calcination at 1100° C for 10 min and the standard JCPDS files for perovskite, hollandite and zirconolite. Peaks marked P correspond to perovskite, H correspond to hollandite and Z correspond to zirconolite.	117

LIST OF FIGURES (cont.)

<u>Figure</u>	<u>Page</u>
<p>Figure 6.4. X-ray diffraction patterns for the SYNROC-B precursor heated for ten minutes at 1100° C (lower pattern) and 20h at 1100° C (upper pattern). The two patterns are virtually identical, indicating that the thermodynamically stable mixture of phases forms extremely rapidly upon calcination of the freeze dried nitrates.</p>	118
<p>Figure 6.5. Evolution of the SYNROC-B phases, perovskite, hollandite and zirconolite, from the amorphous mixture of nitrates after calcination for 10min at temperatures ranging from 600° C to 1100° C. The material is amorphous to XRD until 800°C, where peaks corresponding to the fluorite-type CaZrTi₂O₇ (labeled F) appear. Peaks labeled P correspond to perovskite, Z to zirconolite and H to hollandite.</p>	119
<p>Figure 6.6. X-ray diffraction patterns for SYNROC-B samples heated at 1000° C for (from bottom) 10 min, 30 min, 1h, 2h, and 15h. Peaks labeled P correspond to perovskite, Z correspond to zirconolite, F correspond to fluorite type CaZrTi₂O₇, and H correspond to hollandite peaks.</p>	120
<p>Figure 6.7. The XRD pattern of the hollandite phase obtained from calcination of atomically mixed nitrates for 10min at 1100° C and the JCPDS standard files for the two proposed hollandite phases. The d-spacing data collected in this work are slightly larger than those of both hollandite phases in the JCPDS files.</p>	123
<p>Figure 6.8. X-ray diffraction pattern of the freeze dried, calcium and titanyl nitrate precursor calcined for 10min at (from bottom) 500°C, 600°C, 800°C, and 1000°C. Peaks labeled P correspond to perovskite, C correspond to CaO (lime), and T correspond to TiO₂ (rutile).</p>	125
<p>Figure 7.1 A schematic top view of the FSS experimental setup. The tip of the spray gun was fixed at 19 cm from the steel plate. The spray nozzle was motor driven across a region 10 cm in length. The labeled parts correspond a) steel plate, b) substrate, c) Teflon guides, d) natural gas burner (or H₂/O₂ torch), e) 7 or 1 r.p.m. motor, f) carrier gas inlet, and g) solution inlet.</p>	138

LIST OF FIGURES (cont.)

<u>Figure</u>	<u>Page</u>
<p>Figure 7.2. An XRD pattern for an ethanol FSS film after thermal processing at 940 C for 24h. The film shows some alignment of the c-axis with the polycrystalline MgO substrate. Peaks labeled A correspond to $Ba_2YCu_3O_{7-x}$, B to BaY_2CuO_5, and C to substrate (MgO) peaks.</p>	140
<p>Figure 7.3. The resistivity versus temperature plot for a $Ba_2YCu_3O_{7-x}$ film prepared via ethanol FSS.</p>	141
<p>Figure 7.4. An XRD pattern of a film with nominal composition, $Ag_{0.5}Ba_2YCu_3O_{7-x}$, prepared via ethylene glycol FSS. The peaks labeled A correspond to $Ba_2YCu_3O_{7-x}$, B to metallic silver, and C to BaY_2CuO_5.</p>	142
<p>Figure 7.5. The resistivity versus temperature plot for a film of nominal composition $Ag_{0.5}Ba_2YCu_3O_{7-x}$, prepared via ethylene glycol FSS.</p>	143
<p>Figure 7.6. The XRD pattern for a film of nominal composition $Bi_{1.7}Pb_{0.3}Sr_2Ca_2Cu_3O_{10}$, prepared via ethanol FSS. Peaks labeled A correspond to MgO (substrate). Peaks labeled X correspond to an unidentified phase.</p>	144
<p>Figure 7.7. The resistivity versus temperature plot for a film of nominal composition $Bi_{1.7}Pb_{0.3}Sr_2Ca_2Cu_3O_{10}$, prepared via ethanol FSS.</p>	145
<p>Figure 7.8. A schematic of the experimental setup for ammonia solution FSS. The labeled parts correspond to (a) spray nozzle, (b) hydrogen oxygen torch (pilot flame), (c) liquid ammonia solution reservoir, (d) $N_{2(g)}$ and $NH_{3(g)}$ outlet to oil bubbler, and (e) rotameters. The distance from the spray nozzle to the substrate (not pictured) was constant throughout the experiments at 19 cm.</p>	148
<p>Figure 7.9. An XRD pattern of an ammonia FSS, $Ba_2YCu_3O_{7-x}$ thick film before thermal processing. Significant amounts of $Ba_2YCu_3O_{7-x}$ are present in the pre-annealed sample. The stick pattern of $Ba_2YCu_3O_{7-x}$ is superimposed on the pattern (JCPDS 38-1433). Peaks labeled Y correspond to Y_2O_3, C to CuO, and B to $BaCO_3$.</p>	151

LIST OF FIGURES (cont)

<u>Figure</u>	<u>Page</u>
<p>Figure 7.10. An XRD pattern for a thermally processed ammonia FSS $Ba_2YCu_3O_{7-x}$ film deposited from a 0.048M solution. The pattern is typical of the ammonia FSS films. All major peaks can be attributed to $Ba_2YCu_3O_{7-x}$, except the peaks at $\sim 43^\circ 2\theta$ and $\sim 62.5^\circ 2\theta$, which are due to reflections from the substrate, MgO.</p>	153
<p>Figure 7.11. Resistivity versus temperature plots for four thermally processed films prepared via ammonia FSS.</p>	154
<p>Figure 7.12. A scanning electron micrograph of a $Ba_2YCu_3O_{7-x}$ film prepared via FSS of a 0.05 M ammonia solution. The random orientation of grains and poor grain contact, indicative of a spray deposition, is evident. Each bar=$10\mu m$.</p>	156
<p>Figure 7.13. Scanning electron micrographs of ammonia FSS films from varying solution concentration. (A) 0.016M as-sprayed film, (B) 0.016M film heated 2h at $940^\circ C$, (C) 0.008M as-sprayed film, and (D) 0.008M film heated 2h at $940^\circ C$.</p>	157
<p>Figure 7.13. (cont) Scanning electron micrographs of (E) 0.0033M as-sprayed film, and (F) 0.0033M film heated 2h at $940^\circ C$.</p>	158
<p>Figure 7.14. A schematic of a single droplet of a liquid ammonia solution during the FSS process. If deposition occurs when some of the ammonia is still in the liquid phase, the method is spray pyrolysis. If deposition occurs when the ammonia has essentially all evaporated, then the concentration of the solution will determine the size of the particles deposited. The optimal situation for the production of a thin epitaxial film is deposition of extremely small particles, approaching a gas phase deposition.</p>	160
<p>Figure 7.15 The XRD patterns of a thin film of $Ba_2YCu_3O_{7-x}$ as-prepared via ammonia FSS (lower pattern) and the same film, annealed for 30 min under flowing Ar at $900 C$ (upper pattern). The 031 peak of $Ba_2YCu_3O_{7-x}$, which has the highest relative intensity in randomly oriented samples of $Ba_2YCu_3O_{7-x}$ can be seen in the lower pattern at $\sim 32.8^\circ 2\theta$. The (hkl) values of the intense reflections in the upper pattern are given.</p>	164

LIST OF FIGURES (cont.)

<u>Figure</u>	<u>Page</u>
Figure 7.16. The resistance versus temperature plot for an ammonia FSS thin film. The sample does not reach zero resistance above 15K.	165
Figure 7.17. Scanning electron micrographs of (A) an as-prepared ammonia FSS thin film, and (B) the same film at higher magnification.	166
Figure 8.1 The XRD patterns for (from bottom) $Ba_2YCu_3O_{7-x}$, $Ba_2LaCu_3O_{7-x}$, $Ba_2NdCu_3O_{7-x}$, $Ba_2GdCu_3O_{7-x}$, and $Ba_2EuCu_3O_{7-x}$	177
Figure 8.2. The resistance vs. temperature plot for a $Ba_2YCu_3O_{7-x}$ sample, prepared via the acetate method.	177
Figure 8.3. A scanning electron micrograph of an $Ba_2YCu_3O_{7-x}$ sample prepared via the acetate method.	178
Figure 8.4. The XRD pattern of a $(Bi,Pb)_2Sr_2Ca_2Cu_3O_{10}$ sample prepared via the acetate method. The JCPDS standard file for $Bi_2Sr_2Ca_2Cu_3O_{10}$ is superimposed.	179
Figure 8.5. A plot of Meissner force versus temperature for a $(Bi,Pb)_2Sr_2Ca_2Cu_3O_{10}$ sample prepared via the acetate method.	179
Figure 8.6. The x-ray diffraction pattern of the acetic acid mixed precursor (upper pattern) and mechanically mixed acetates (lower pattern). The large broad diffraction from 3° to $30^\circ 2\theta$ is due to the Kapton tape in which the samples were enclosed.	181
Figure 8.7. The x-ray diffraction patterns of an acetic acid mixed sample (upper pattern) and a solid state mixture of the acetates, subjected to the same thermal treatment (2h at $900^\circ C$). Peaks labeled A correspond to $BaCO_3$, B correspond to CuO , C correspond to BaY_2CuO_5 , and D correspond to $Ba_2YCu_3O_{7-x}$	182
Figure 8.8. The XRD patterns of $Ba_2YCu_3O_{7-x}$ acetate method samples heated from 300° to $800^\circ C$. The precursor is completely amorphous except for metallic copper at $300^\circ C$. Peaks marked X correspond to an unidentified phase. The stick patterns superimposed are; $300^\circ Cu$ (metal), $400^\circ Cu_2O$, $500^\circ CuO$, $600^\circ BaCO_3$, $700^\circ Y_2O_3$, and $800^\circ Ba_2YCu_3O_7$	183

LIST OF FIGURES (cont.)

<u>Figure</u>	<u>Page</u>
Figure 8.9 X-ray diffraction patterns of (from bottom) the dried precursor of yttrium acetate boiled in acetic acid, barium acetate boiled in acetic acid and a 1:1 mixture (per mole) of yttrium acetate and barium acetate boiled in acetic acid. The two salts are necessary for the amorphous pattern.	184

LIST OF TABLES

<u>Table</u>	<u>Page</u>
Table 2.1. Some simple perovskite type oxides and their applications in electronics. Adapted from reference 14.	20
Table 2.2. The weight percentages of the metal oxides that make up SYNROC-B. Adapted from reference 20.	25
Table 2.3 The current families of high temperature superconductors. From reference 27.	27
Table 2.4 Devices which can be fabricated from high temperature superconductors, the applications of these devices and the phenomena associated with superconductivity that makes the application possible Adapted from references	33
Table 5.1 Variation in the gross gravimetrically determined formula weight for $\text{TiO}(\text{NO}_3)_2$ over the course of 20 days. The compound appears to be stable at room temperature. An error occurred during the first determination of day 7 and the data was discarded.	86
Table 5.2. A comparison of the collected powder x-ray diffraction data for a sample of BaTiO_3 from freeze dried nitrates calcined for 10 min at 1000°C with a standard diffraction file for tetragonal BaTiO_3 . Peaks designated by the Sintag computer program with relative intensities equal to 1 were discarded from the data.	98
Table 7.1 Anion of reagents, pilot flame, and carrier gas used for the three solvent systems.	135
Table 7.2. Flow rates used in the preparation of thick films of $\text{Ba}_2\text{YCu}_3\text{O}_{7-x}$ via ammonia FSS.	152
Table 7.3. Flow rates used in the preparation of thin films of $\text{Ba}_2\text{YCu}_3\text{O}_{7-x}$ via ammonia FSS.	162
Table 8.1 Nominal composition of metal acetates and solvent in several precursors and the resulting x-ray diffraction.	183

PART I

INTRODUCTION AND BACKGROUND

CHAPTER 1

SOLID STATE REACTIONS

In this dissertation, solution based synthetic methods and the concept of atomic level mixing will be introduced as a potential solution to the common problems associated with solid state reactions. As background for the experimental discussion to come, the first chapter of this work will discuss the kinetics of the diffusion limited solid state reaction and how atomic level mixing can be used to eliminate this diffusion limited mechanism. Later chapters in the first part of this dissertation will discuss the structure, properties, applications, and common methods of synthesis of the materials that were studied in this work. Part II of this dissertation will concern the experimental details and results of the utilization of solution based synthesis and atomic mixtures in overcoming the problems discussed in this chapter. To better understand the chemistry of atomic mixtures and evaluate their applicability and utility in solid state reactions, this work focuses on several multi-cation oxide phases. The phases synthesized range from a simple, two cation perovskite oxide, to three and four cation high temperature superconducting cuprates, up to a five cation oxide, multi-phase mineral assemblage.

1.1 The Diffusion Limited Solid State Reaction

Under subsolidus conditions, the rate determining step of a reaction between two phases, one labeled A, the other B, to form the binary phase AB, can be either a chemical

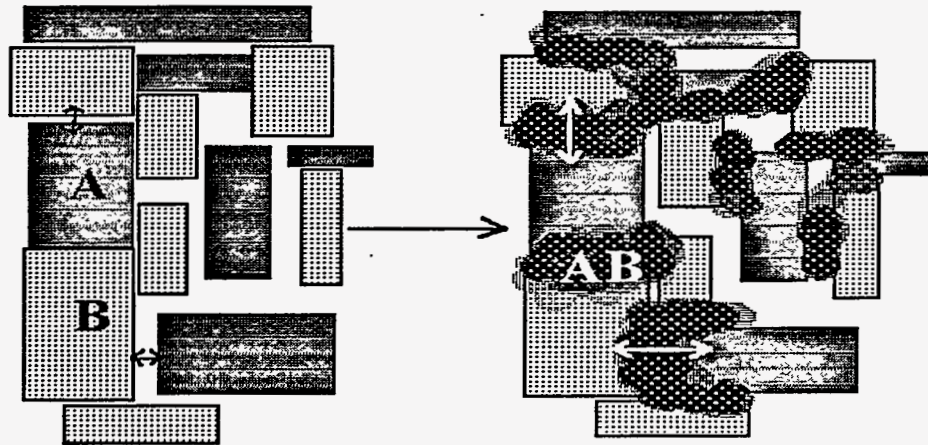


Figure 1.1. A schematic depicting product formation at the contact points of reactant grains. The rate of the solid state reaction is slowed as the reactants are forced to diffuse through an ever increasing, inert layer of product for subsequent product formation. The double headed arrows represent the length of the diffusion paths.

reaction or diffusion.^{1,2} A chemical reaction could be the rate limiting step if several energetically unfavorable bond redistributions must occur for the reactants to form products. In ionic phases (or predominantly ionic phases), bond redistribution is rarely a problem and the second factor, diffusion, becomes the rate limiting step. This diffusion limited mechanism, for a reaction of the type $A + B \rightarrow AB$, has been described by Wagner.³ The mechanism assumes that the reaction takes place entirely in the solid state. Therefore, the only mode of transport for A to come into physical contact with B (a necessary condition for the reaction to occur) is ionic diffusion. If the temperature is high enough to allow a reasonably fast rate of ionic diffusion, and the product, AB, is thermodynamically more stable than the reactants, A and B, the reaction will proceed swiftly. However, the rate of the reaction will drop off as product forms. This can be

understood by considering Figure 1.1. When the individual grains of pure A and pure B become covered with a layer of product, AB, the distance that ions must diffuse to form product is increased. Consequently, the rate of the reaction slows as the reaction proceeds. If it is further assumed that the reactant particles are spherical, the kinetics of the diffusion can be characterized by the three dimensional rate equation;

$$[1-(1-\alpha)^{1/3}]^2 = kt/r_A^2 \quad \text{eq. 1.1}$$

where α is the extent of the reaction (the volume fraction of the product), k is the rate constant ($k \propto e^{-1/T}$, where T is temperature), t is the time, and r_A is the radius of the particles.⁴ This equation, which is usually referred to as the Jander equation,⁵ predicts initial rapid product formation and gradual slowing of the rate as the barrier layer of inert product increases in thickness. This description of a solid state reaction, however, is still grossly over-simplified.⁶ Some of the problems with the mechanism are; (1) perfect parabolic growth is only expected for a one dimensional system, (2) the assumption that B completely envelops A will be only true if the particle size of B is much smaller than that of A, and (3), there is no term accounting for possible differences in molar volumes of A and B.⁶ These discrepancies were considered by R. E. Carter^{7,8} who derived the rate equation;

$$[1+(z-1)\alpha]^{2/3} + (z-1)(1-\alpha)^{2/3} = z + 2(1-z) kt/r_A^2, \quad \text{eq. 1.2}$$

where z is the volume of product formed from a unit volume of reactant A. This rate equation agrees very well with the experimental determination of the reaction rate for a fine powder mixture of ZnO and Al₂O₃ reacting to form ZnAl₂O₄.⁹ Modifications of the Jander equation have also been made in which lattice imperfections are taken into account.¹⁰

Since the only method of transport in the solid state reaction considered here is ionic diffusion, it is necessary that high temperatures are used in the reaction to facilitate this diffusion. It is also beneficial to have the reactants well mixed. A small particle size is desired as the square of the radius of the reactant particles is inversely proportional to the rate of the reaction (see eq. 1.2). A third aspect which can effect the rate of a solid state reaction is the amount of contact between reactant grains. To maximize these factors, conventional ceramic processing entails high temperature calcination of compacted, mechanically mixed, fine powders.

The conventional procedures for solid state reactions, briefly described above, are the source of many synthetic problems. As has already been pointed out, a solid state reaction can take long periods of time to go to completion. Another problem which can be difficult to avoid using conventional ceramic processing is contamination. Contamination can be a significant problem if electronic materials (superconductors, dielectric etc.) which have properties particularly sensitive to impurities are being prepared.^{11,12} The three basic steps in conventional ceramic processing (grinding, pressing, and heating) are all potential sources of contamination. Grinding can lead to contamination of the reactant material with the grinding medium. This problem can be minimized by the use of a relatively hard

grinding medium such as agate or alumina. The pressing of reactants into pellets can lead to contamination from the die (usually hardened steel) as well as materials which were previously pressed in the die and were imbedded in scratches. The high temperature anneal can lead to contamination from the reaction container (boat or crucible) and loss of stoichiometry through evaporation or sublimation of one or more reactant.

There are some materials which can not be synthesized by conventional ceramic processing due to the high temperature reaction conditions needed to facilitate ionic diffusion. Using high temperatures can become problematic if the material being synthesized decomposes at such temperatures. The cuprate superconductor, $\text{Ba}_2\text{YCu}_4\text{O}_8$, can not be synthesized in phase pure form by conventional ceramic processing (due to high temperature instability of the phase with respect to $\text{Ba}_2\text{YCu}_3\text{O}_{7-x}$ and CuO) but can be synthesized by a low temperature, diffusionless route.¹³ The tetragonal phase of SrCuO_2 (which is the simplest example of an infinite layer cuprate superconductor) is also inaccessible by conventional ceramic processing (due to the high temperature stability of orthorhombic SrCuO_2), but can be synthesized by a novel, low temperature technique.¹⁴ In addition, many materials which can be synthesized through conventional ceramic processing do not melt homogeneously, but decompose into two or more liquid or solid phases above a certain *peritectic* melting temperature. If a material undergoes incongruent melting, as some of the materials synthesized in this work do (e.g., $\text{Ba}_2\text{YCu}_3\text{O}_{7-x}$), an upper limit is effectively placed on the processing temperature, and consequently, the rate of the reaction. Since the high temperatures used in conventional ceramic processing are a direct result of the need for ionic diffusion, these

problems can all be avoided if product formation occurs through a low temperature, *diffusionless* mechanism.

1.2 The Diffusionless (Atomically Mixed) Solid State Reaction

In a powder mixture of reactants, as particles get smaller the degree of mixing between the reactants increases (the contact area between reactant grains increases). Enhancement of solid state reaction rates with decreasing particle size of the reactants has been experimentally demonstrated. Beretka and Brown¹⁵ studied the reaction between Al_2O_3 and MgO to yield MgAl_2O_4 and measured the extent of the reaction, α , versus time for several different particle size mixtures. The result is a fine example of how the rate of a solid state reaction is highly dependent upon the degree of mixing (see Figure 1.2). A plot of α versus reaction time showed that when $\sim 1\mu\text{m}$ reactant particles were annealed at 1300°C , the reaction neared completion after about 70 hours. Whereas when $\sim 50\mu\text{m}$ reactant particles were used, the reaction was less than 50% complete after the same time period at temperature.

In a conventional, mechanical mixture of two solid reactants, such as Al_2O_3 and MgO , individual phases are not mixed on an atomic scale. Even with crystallite sizes on the order of $\sim 1\mu\text{m}$, diffusion path lengths require the migration of reactants over many (~ 1000) unit cells for complete reaction to occur. Consequently, the reaction of $1\mu\text{m}$ particles studied by Beretka and Brown took over 70h to reach completion (at 1300°C). If reactants could be homogeneously mixed on the atomic scale, and individual crystallites were on the order of 1 to 10 nm, the need for long range diffusion would be eliminated,

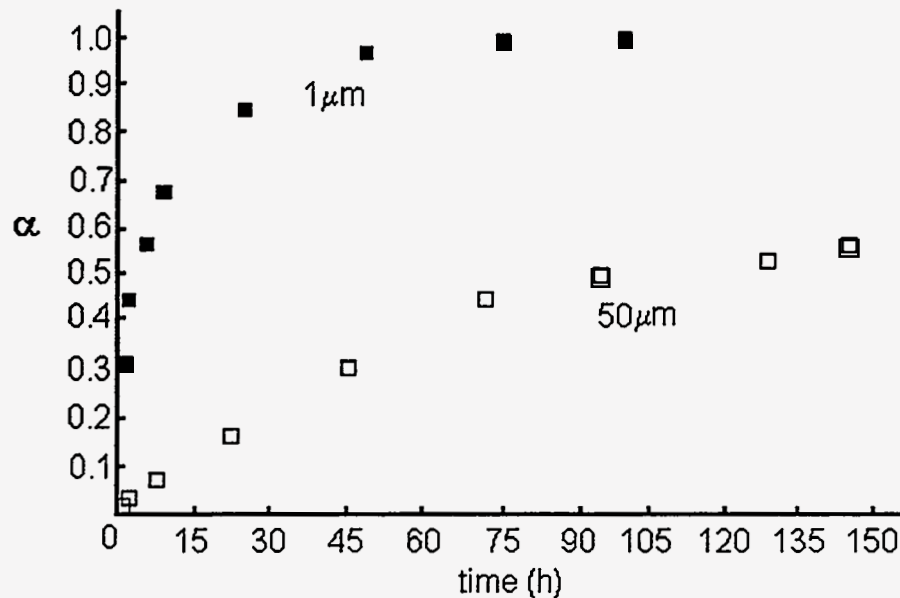


Figure 1.2. A plot of the extent of the reaction, α , versus time for the reaction $\text{MgO} + \text{Al}_2\text{O}_3 \rightarrow \text{MgAl}_2\text{O}_4$ at 1300°C . The solid boxes represent the reaction between $\sim 1\ \mu\text{m}$ particles and the empty boxes represent the reaction between $\sim 50\ \mu\text{m}$ particles. The data are from reference 15.

and the rate of the reaction would be greatly influenced. This was experimentally demonstrated by Schnettler, Monforte, and Rhodes, who developed a freeze drying procedure for the preparation of MgAl_2O_4 . An aqueous solution of magnesium and aluminum sulfates was rapidly frozen, trapping the Mg^{2+} and Al^{3+} ions the random configuration inherent in the solution state. Sublimation of the solvent left behind an intimate mixture of the two metal sulfates which yielded phase pure MgAl_2O_4 after only a one hour heat treatment at 870°C .¹⁶ When a mechanical mixture of $1\ \mu\text{m}$ MgO and Al_2O_3 particles was calcined for 1h at 1100°C (lowest temperature investigated), Beretka and

Brown found that only 3.1% (volume fraction) had reacted to form MgAl_2O_4 . The freeze drying procedure resulted in over a thirty-fold increase in the rate of product formation at a much lower temperature, which implies that the level of mixing (radius of reactant particles) achieved through freeze drying is far greater than that of $1\ \mu\text{m}$ particles.

Consider again the rate equation for a solid state reaction between spherical particles (for clarity, see equation 1.1). When the radius of the reactant particles approaches zero, the rate of the reaction, $d\alpha/dt$, approaches infinity, and this rate law breaks down. This suggests that the kinetics of solid state reactions between phases which are mixed on the atomic scale requires a more accurate model, based on a diffusionless mechanism. Such reactions are dominated by thermodynamics and nucleation, rather than kinetics (diffusion), and resemble a phase transformation more than a reaction.

The level of reactant mixing achievable through freeze drying was explored in the early 1970's by A. C. C. Tseung.¹⁷ Tseung studied the uniformity of mixing achievable through freeze drying by measuring the electrical conductivity of cadmium doped silver chloride. The conductivity of silver chloride is highly dependent upon the uniformity of cadmium doping. Tseung found that the electrical conductivity of silver chloride was over an order of magnitude greater when the cadmium ions were doped by freeze drying (of silver and cadmium chloride solutions) than when they were doped by mechanical mixing. He later demonstrated a similar effect on the electrical conductivity of lithium doped nickel sulfate prepared by freeze drying.¹⁸ Tseung attributed the increase in conductivity to an *atomic mixing* of ions achieved through the freeze drying process. In this work, the term *atomic mixture* will be used to describe precursors to solid state materials that contain

reactants which are mixed on a level greater than that of a mechanical mixture. The term is not meant to imply that a perfectly random mixture of ions exists on the atomic level, but to distinguish the precursors from conventional mixtures of reactants. It is likely that the precursors are not truly atomically mixed, and that, at minimum, they consist of clusters of several hundred atoms. However, these precursors behave, when calcined, as if they were atomically mixed. That is, product formation occurs too rapidly for diffusion to be considered as a limiting step.

In this work, the major piece of evidence which will be used to support the formation of an atomically mixed precursor is an amorphous x-ray diffraction pattern. To observe a loss of diffracted intensity due to a small particle size powder, crystallites must be <50nm in diameter.¹⁹ This implies that what is referred to here as an atomic mixture is, in reality, a mixture of reactants which are (at least) on the order of tens of nanometers in diameter. Based on the results (rate of product formation) of this work and the work of others,^{13,20,21} this degree of mixing seems to be sufficient to effectively eliminate the diffusion limited solid state reaction mechanism.

Additional consequences arise from the use of extremely small particles as starting materials in a solid state reaction due to the greater surface to volume ratio of the reactants. This larger ratio should result in the release of excess surface energy during the course of the reaction. Furthermore, it has been shown by thermogravimetric analysis, that smaller reactant particles, due to the inherent better mixing, decompose at lower temperatures than the same reactants of larger particle size.²² This implies that the lowest possible reaction temperatures could be used if reactants were truly atomically mixed.

There has been little work to date on the kinetics of atomically mixed solid state reactions. The use of freeze drying (see section 3.1.2.2 for a discussion of freeze drying) has been studied as a means of producing metastable atomic mixtures of nitrate salts for the preparation of high temperature superconductors.^{13, 23, 24} The kinetics of formation of $(\text{Bi, Pb})_2\text{Sr}_2\text{Ca}_2\text{Cu}_3\text{O}_{10}$ from thermal processing of freeze dried nitrate salts has been studied.²⁵ The extent of product formation, α , from an atomic mixture as a function of annealing time was obtained by both powder x-ray diffraction and magnetic susceptibility measurements. To elucidate the kinetic pathway of the reaction, the curve obtained by a plot of α , the extent of the reaction, versus time, was compared to similar curves for various reaction mechanisms. The phase development of $(\text{Bi, Pb})_2\text{Sr}_2\text{Ca}_2\text{Cu}_3\text{O}_{10}$ at 865°C (3°C below the determined melting point) was found to follow a Hulbert and Klawitter²⁶ nucleation and growth mechanism (HKN&G) with a very good correlation. The empirical HKN&G rate law is;

$$\ln(1-\alpha) = -(kt)^m, \quad \text{eq. 1.3}$$

where k is the rate constant, and m is a parameter that takes into account the number and geometry of the nuclei. The goal of this research was to utilize atomically mixed precursors in the preparation of solid state phases, thereby circumventing the diffusion limited reaction and allowing product formation through other mechanisms (i.e. nucleation and growth). In addition to improved reaction conditions due to shortened diffusion paths, the synthetic methods explored provided a control of particle morphology.

Uniform, sub-micron (or nanocrystalline) particles could be produced that should display favorable sintering characteristics. The end result of this work was the production of very high quality samples of technologically important materials, and a better understanding of the solid state reactions of atomically mixed precursors.

The techniques used in this work to achieve atomic mixing all originate with solutions containing the desired metal ions. The perfect mixing of ions, inherent in the solution, is then trapped and transferred into the solid state by a number of different methods. Usually this “trapping” and “transferring” occurs in a single step, such as rapid evaporation of the solvent, or rapid precipitation of the solute. In the first synthetic part of this dissertation (Chapters 5 and 6), an established solution method of atomic mixing, freeze drying, is used in the preparation of BaTiO_3 and the multi-phase system, SYNROC-B. In freeze drying, the trapping and transferring steps are separated. Aqueous solutions are rapidly frozen, trapping the ions in a random state, after which the water is removed by sublimation (transferring) leaving behind an atomically mixed powder. In later chapters, two novel methods of atomic level mixing which have been developed are presented. The first of these novel methods entails the combustion of a flammable solution for the production of metal oxide films (Chapter 7). The combustion of the solvent acts as a means of rapid solvent removal which prevents phase separation and extensive crystallization in the deposited film. The second novel method entails the use of glacial acetic acid solutions of metal acetates which, rather than crystallizing, form a glassy precursor upon solvent removal (Chapter 8). Although seemingly very different

techniques, they all the common objective of achieving a greater degree of mixing of reactants in the solid state, and thereby enable product formation through a diffusionless mechanism.

1.3 Notes and References

- ¹ N. B. Hannay, *Solid State Chemistry*, Prentice-Hall Inc., Englewood Cliffs, NJ, 1967.
- ² A. R. West, *Solid State Chemistry*, Wiley, New York, 1989.
- ³ C. Wagner, *Z. Anorg. Allg. Chem.* **236**, 320 (1938).
- ⁴ W. E. Brown, D. Dollimore, and A. K. Galwey, *Comprehensive Chemical Kinetics*,
Volume 22, Reactions in the Solid State, Edited by C. H. Bamford and C. H. F.
Tipper, Elsevier Scientific (New York, 1980).
- ⁵ W. Jander, *Z. Anorg. Chem.* **163**, 1 (1927).
- ⁶ H. Schmalzred, *Monographs in Modern Chemistry 12, Solid State Reactions*, Edited By
Hans F. Ebel, Verlag Chemie (Deerfield Beach, FL, 1981).
- ⁷ R. E. Carter, *J. Chem. Phys.* **34**, 2010 (1961).
- ⁸ R. E. Carter, *J. Chem. Phys.* **35**, 1137 (1961).
- ⁹ C. A. Duckwitz, and H. Schamlzried, *Z. Phys. Chem. NF* **76**, 173 (1971).
- ¹⁰ S. F. Hulbert, *J. Br. Ceram. Soc.* **6**, 11 (1969).
- ¹¹ P. P. Phule, and S. H. Risbud, *J. Mater. Sci.* **25**, 1169 (1990).
- ¹² P. Dumas and J. A. T. Taylor, *J. Am. Ceram. Soc.* **74**, 2663 (1991).
- ¹³ E. Brosha, E. Sanchez, P. K. Davies, N. V. Coppa, A. Thomas, and R. E. Salomon,
Physica C **184**, 353 (1991).
- ¹⁴ C. Nui and C. M. Lieber, *J. Am. Chem. Soc.* **114**, 3570 (1992).
- ¹⁵ J. Beretka and T. Brown, *J. Am. Ceram. Soc.* **66**, 383 (1983).
- ¹⁶ F. J. Schnettler, F. R. Monforte, and W. W. Rhodes, *Sci. Ceram.* **4**, 79 (1968).

- ¹⁷ A. C. C. Tseung and H. L. Bevan, *J. Mater. Sci.* **5**, 604 (1970).
- ¹⁸ J. Kelly, D. B. Hibbert, and A. C. C. Tseung, *J. Mater. Sci.* **13**, 1053 (1978).
- ¹⁹ See reference 2, page 173.
- ²⁰ N. V. Coppa, Doctoral Dissertation, Temple University (Philadelphia PA, 1990).
- ²¹ R. W. Schaeffer, Doctoral Dissertation, Temple University (Philadelphia PA, 1992).
- ²² G. S. Grader, P. K. Gallagher, and D. A. Flemming, *Chem. Mater.* **1**, 665 (1989).
- ²³ N. V. Coppa, G. H. Myer, R. E. Salomon, A. Bura, J. W. O'Reilly, J. E. Crow, and P. K. Davies, *J. Mater. Res.* **7**, 2017 (1992).
- ²⁴ N. V. Coppa, A. Bura, J. W. Schwegler, R. E. Salomon, G. H. Myer, and J. E. Crow, *Mat. Res. Soc. Proc.* Vol. **180**, 935 (1990).
- ²⁵ N. V. Coppa, W. L. Hults, J. L. Smith, and J. Brynestad, *J. Mater Res.* **9**, 2510 (1994).
- ²⁶ S. F. Hulbert and J. J. Klawitter, *J. Am. Ceram. Soc.* **50**, 484 (1967).

CHAPTER 2

SOLID STATE MATERIALS

In this chapter, the structure, properties and applications of perovskite-type oxides, the main structural family of the phases synthesized in this work, will be reviewed. The first topic to be covered will be the structure and applications of simple perovskite-type oxides such as BaTiO_3 . This will be followed by an introduction to SYNROC-B, a possible material for immobilization of radioactive waste. Finally, a discussion of the structure and applications of high temperature superconductors, which have a stacked perovskite structure (tetragonal or orthorhombic perovskites) will be provided. These systems were chosen to probe the effectiveness of atomic mixing on three related (all can be said to consist of *perovskite-type* phases with the exception of the zirconolite and hollandite-type phases in SYNROC-B) but very different systems. Barium titanate is a simple, but technologically important, ternary oxide. The benefits of atomic mixing of reactants should be clearly evident in this system. The high temperature superconductors are technologically important as well, but are quaternary and pentenary oxides. In such systems, many intermediate phases are possible en route to product formation. In addition to the benefits observed in the BaTiO_3 system, atomic mixing may allow product formation through intermediates not observed in a reaction of a conventional mixture. The SYNROC-B system is different from the previous two in that the end goal is not single phase material, but a mixture of three phases, perovskite (CaTiO_3), a barium aluminum

titanate with a hollandite-type¹ structure ($\text{BaAl}_2\text{Ti}_5\text{O}_{14}$), and zirconolite ($\text{CaZrTi}_2\text{O}_7$). In this system, the benefits of atomic mixing, apart from the initial high reactivity of such mixtures, may be slightly obscured. A completely homogeneous starting material is being used for the production of an inhomogeneous (on the atomic scale) product. For example, the originally, completely dispersed aluminum ions must all migrate, or nucleate, by diffusion, to form hollandite crystallites. The following discussion of the structure and applications of the materials studied in this work will be on a cursory level for economy of space. The interested reader is directed to references 2 and 3 for a more detailed discussion of simple perovskite type oxides (i.e. BaTiO_3), references 4, 5, and 6 for a more thorough discussion of the structure, properties and applications of high temperature superconductors, and reference 7 for a more complete discussion on SYNROC.

2.1 The Perovskite Structure

Perovskite oxide materials are represented by the general formula ABO_3 . The ideal perovskite structure is cubic and falls into the space group $Pm\bar{3}m$ (see Figure 2.1). The structure consists of a cube with one B atom in the center, $\frac{1}{8}$ A atoms at each of the eight corners and $\frac{1}{2}$ O atoms at the center of the six faces. The structure was named after the natural mineral perovskite, CaTiO_3 , the first material found to exhibit the structure.^{8,9} Although the "ideal" perovskite structure is cubic, its namesake, CaTiO_3 , is actually orthorhombic.¹⁰ Single crystals of CaTiO_3 exhibit strong optical double reflection; evidence for the less than cubic symmetry of the structure. Relatively few of the known materials which have the perovskite structure are cubic (SrTiO_3 is truly cubic at room

temperature).¹¹ More often, the materials have slightly less than cubic symmetry. In BaTiO_3 , the ratio of the c axis of the unit cell to the a axis is 1.0134 at room temperature. In true cubic lattices (by definition) this ratio, c/a , must be equal to one.¹²

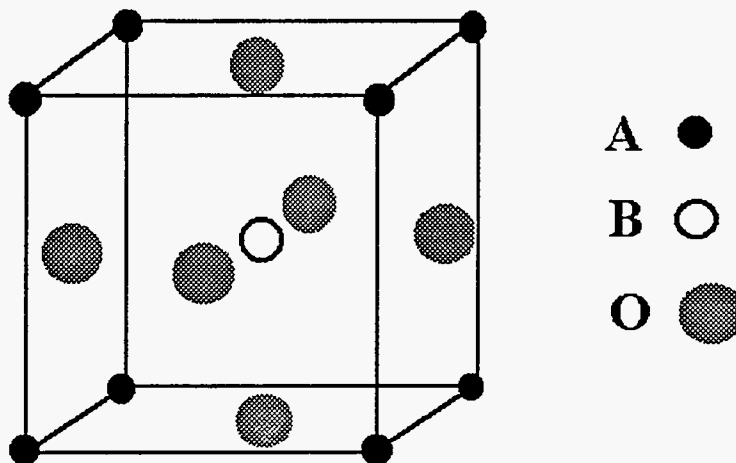


Figure 2.1. The ideal perovskite structure consisting of a cube with a B atom at the center, A atoms at the corners and O atoms on the center of each face.

The perovskite structure is exhibited by many crystal phases (e.g., SrTiO_3 , BaTiO_3 , BaPuO_3 , LaAlO_3 , BaLiF_3 , RbCaF_3 , etc.). The structure can be formed for A and B atoms of varying charge where the total positive charge is balanced by the charge of the anions (e.g. $\text{A}^{+1}\text{B}^{+5}\text{O}_3$, $\text{A}^{+2}\text{B}^{+4}\text{O}_3$, $\text{A}^{+3}\text{B}^{+3}\text{O}_3$, or $\text{A}^{+1}\text{B}^{+2}\text{F}_3$, $\text{A}^{+2}\text{B}^{+1}\text{F}_3$ etc.). A distorted version of the structure can be formed for materials in which the total positive charge is balanced through anion deficiencies. The high temperature superconducting cuprates are prime

examples of oxygen deficient perovskites. There are also numerous complex perovskites where varying levels of differently charged cations occupy the B site (e.g., $A^{+2}(B^{3+}_{0.67}B^{6+}_{0.33})O_3$).

There is a tolerance factor, τ , based on the ionic radii of A and B that must be met for a material to assume the perovskite structure. If the value of τ obtained by the equation;

$$R_A + R_B = 1.414\tau (R_B + R_O) \quad \text{eq. 2.1}$$

is between 0.80 and 0.90, the material assumes the ideal cubic perovskite structure.¹³ If the value of τ falls slightly outside of this range (0.75 to 1.00), a distorted perovskite is formed.

There are some materials that have perovskite-like structures which consist of stacked units of the basic CaTiO_3 structure. These materials are usually referred to as tetragonal perovskites (e.g., $\text{Bi}_2\text{Sr}_2\text{CaCu}_2\text{O}_8$) or orthorhombic perovskites (e.g., $\text{YBa}_2\text{Cu}_3\text{O}_7$). The structure of these materials will be discussed below in the section on high temperature superconductors.

2.2 Properties and Applications of Simple Perovskite Materials

Many perovskite-type oxides have applications in electronics. Some of these are listed in Table 2.1. The synthesis of barium titanate, BaTiO_3 , was a particular focus of this

work. Consequently, only this phase and its application as a dielectric material will be discussed here in relative detail.

Table 2.1. Some simple perovskite type oxides and their applications in electronics. Adapted from reference 14 .

Application	Perovskite phase
Multilayer capacitor	BaTiO ₃
Piezoelectric transducer	Pb(Zr,Ti)O ₃
Thermistor	doped BaTiO ₃
Second harmonic generator	KNbO ₃
Electrooptical modulator	(Pb, La) (Zr,Ti)O ₃
Switch	LiNbO ₃
Dielectric resonator	BaZrO ₃
Thick film resistor	BaRuO ₃
Electrostrictive actuator	Pb(Mg, Nb)O ₃
Superconductor	Ba(Pb, Bi)O ₃
Magnetic bubble memory	GdFeO ₃
Laser host	YAlO ₃
Ferromagnet	(Ca, La)MnO ₃
Refractory electrode	LaCoO ₃

2.2.1 Barium Titanate

There are seven stable ternary phases formed in the Ba-Ti-O system. These are Ba₂TiO₄, BaTi₂O₅, Ba₆Ti₁₇O₄₀, Ba₄Ti₁₃O₃₀, BaTi₄O₉, Ba₂Ti₉O₂₀ and BaTiO₃.^{15,16} Of these phases, the BaTiO₃ composition is most widely used as a dielectric and reports of its preparation, properties, phase diagrams, and applications are abundant in the scientific

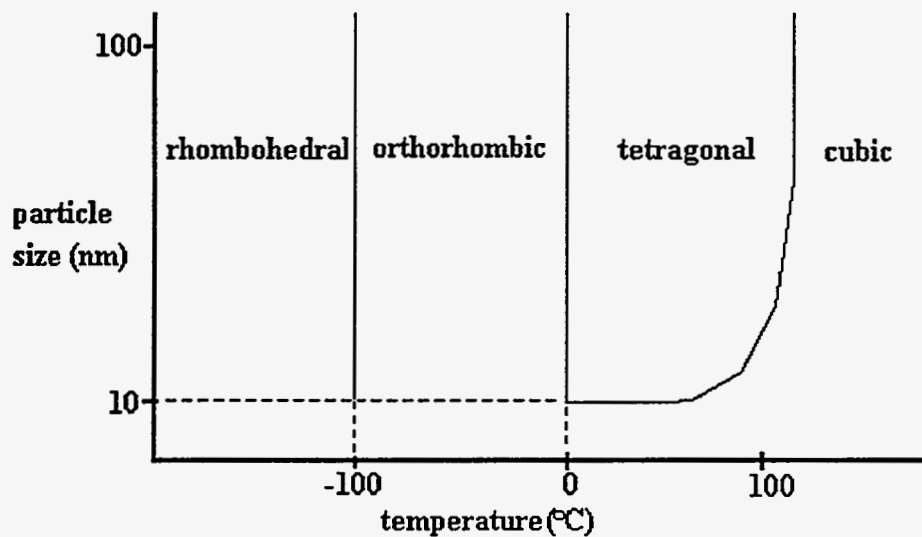


Figure 2.2. A pseudo-phase diagram of the structural changes of BaTiO_3 with respect to temperature and particle size. Crystallites below 10 nm in diameter are cubic due to surface effects. The curvature of the tetragonal to cubic transition line is arbitrary. The structure of the surface layer of BaTiO_3 at low temperatures is undetermined.

literature. At room temperature, BaTiO_3 has a tetragonal unit cell with cell dimensions $a=3.989\text{\AA}$ and $c=4.029\text{\AA}$.¹¹ Below 0°C , BaTiO_3 has an orthorhombic structure and below -100°C the material is rhombohedral.¹⁷ The surface layer of barium titanate has a cubic structure at room temperature. The thickness of this layer at room temperature has been measured at $\sim 5\text{nm}$.¹⁸ Consequently very small crystallites of BaTiO_3 display predominantly cubic diffraction patterns due to the large surface to volume ratio in the particles. Crystallites with a diameter of less than ten nanometers can be assumed to be entirely cubic (if the cubic surface layer is 5 nm thick). A pseudo-phase diagram of the structure of BaTiO_3 with respect to temperature and particle size is pictured in Figure 2.2.

The applications of BaTiO_3 in electronics arise from its dielectric and ferroelectric properties. Barium titanate is widely used as a dielectric material due to its high relative

permittivity. The relative permittivity (a dimensionless quantity) is the ratio of the capacitance of a parallel plate capacitor when the space between the plates is filled with the dielectric material and when the space is a vacuum. For most ionic crystals, the relative permittivity, ϵ' , ranges from 5 to 10. For BaTiO_3 , ϵ' ranges from 10^3 to 10^4 ,¹⁹ due to the phenomenon of ferroelectricity. This unusually high permittivity allows for more powerful insulators and capacitors to be made with BaTiO_3 . When a sample of BaTiO_3 is placed in an electric field, a polarization occurs in the material which increases with increasing voltage. However, the process is not completely reversible. When the voltage is reduced, a partial electrical polarization in the material remains resulting in a hysteresis loop in a plot of P , the polarization, versus V , the applied voltage. This ferroelectric effect is a direct result of the perovskite structure of BaTiO_3 . The large difference in size of the O^{2-} and Ti^{4+} ions allows for significant displacements ($\sim 0.1 \text{ \AA}$) of the smaller Ti^{4+} ion to occur, resulting in the formation of dipoles. Since BaTiO_3 is tetragonal ($c/a=1.010$) at room temperature, these dipoles are not symmetrically oriented and a net dipole moment can arise. Applying a voltage serves to orient these dipoles into domains that align with the applied field. However, an increase in temperature results in a decrease in the ratio of the length of the c axis to the a axis of the BaTiO_3 unit cell. It converts to a cubic structure ($c = a$) at the Curie temperature, which, for BaTiO_3 , is $\sim 120^\circ \text{ C}$.¹¹ At the Curie temperature, T_C , thermal vibrations are sufficient to break down the domain of aligned dipoles and the material becomes a normal dielectric. This conversion from tetragonal to cubic is accompanied by a sharp increase in permittivity with its peak at the Curie temperature (see Figure 2.3). This effect results in extremely high dielectric constants

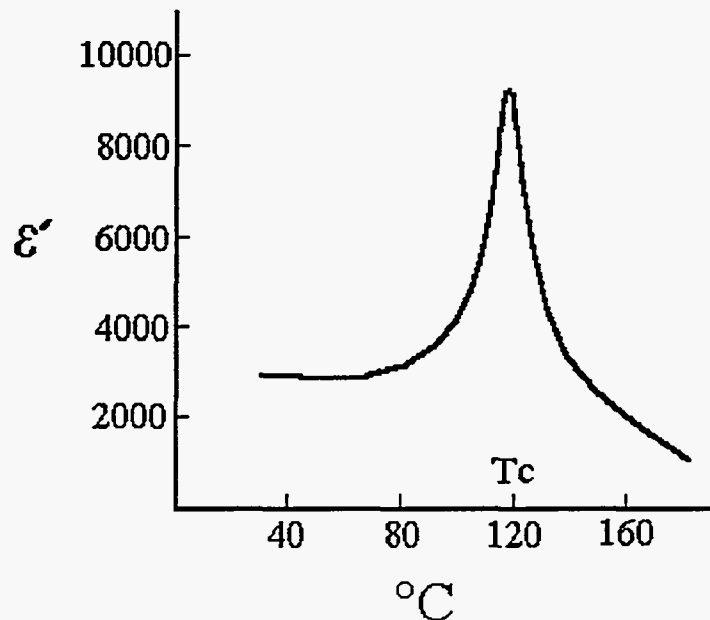


Figure 2.3 A schematic of the variance in the relative permittivity of BaTiO₃ with increasing temperature. The Curie temperature, T_C, occurs at ~120° C.

(relative permittivity) at T_C, making ferroelectrics widely used as capacitors. The high permittivity of ferroelectrics allows the production of capacitors that have >1000 times the capacitance (for a given thickness) that they would otherwise have if a normal dielectric material was used. Obtaining small and uniform particle size dielectric material is extremely important in the production of thin film capacitors by screen printing (see section 3.2.2.1 for a discussion of screen printing).

2.2.2 SYNROC

SYNROC (an abbreviation for synthetic rock) is a titanate or alumino-silicate ceramic, developed by A. E. Ringwood,^{7,20} that is being considered as a possible crystalline material for immobilization of high level nuclear waste (HLNW). It was first proposed by L. P. Hatch,²¹ in 1953, that immobilization (as solid solution) of nuclear waste in stable phases will help prevent leaching of the radioactive components into ground water when the waste is buried in deep geological formations.

There are several different versions of SYNROC. SYNROC-A is a titanate and alumino-silicate mixture consisting of a hollandite-type barium aluminum titanate ($\text{BaAl}_2\text{Ti}_5\text{O}_{14}$), perovskite (CaTiO_3), zirconolite ($\text{CaZrTi}_2\text{O}_7$), barium-feldspar ($\text{BaAl}_2\text{Si}_2\text{O}_8$), kalsite (KAlSiO_4), and leucite (KAlSi_2O_6), that can incorporate (as solid solution) up to 10 wt% HLNW. SYNROC-B, which was synthesized in this work, is a titanate based ceramic, consisting of the above hollandite-type barium aluminum titanate, zirconolite, and perovskite, that can incorporate up to 10 wt% HLNW. The weight percentages of the metal oxides in SYNROC-B are outlined in Table 2.2. A SYNROC-C (the C is said to stand for Commercial) and a SYNROC-D (D for defense waste) phase assemblies have also been developed.

An alternative to immobilization of HNLW in crystalline phases is immobilization in borosilicate glass. However, the crystalline nature of SYNROC makes it inherently more stable than a glass, which is a metastable state. It has been shown that under conditions simulating burial in deep geological formations (i.e. high pressures and temperatures, exposure to water at high pressures and temperatures, possibly supercritical

water), borosilicate glasses completely devitrify; potentially allowing complete leaching of HLNW into groundwater.^{20, 22, 23, 24} SYNROC, under the identical conditions, emerges virtually unscathed. This is an extremely important factor considering the length of time ($>10^6$ yr)²⁰ that will be needed for radioactive decay to reach safe levels.

Table 2.2. The weight percentages of the metal oxides that make up SYNROC-B. Adapted from reference 20.

Metal Oxide	Weight %
TiO ₂	57
ZrO ₂	11
Al ₂ O ₃	10
CaO	13
BaO	9

The obstacle preventing utilization of SYNROC as a HLNW immobilization medium is the preparation conditions proposed by Ringwood.²⁵ These involve hot pressing (5 to 10 x 10⁷ Pa and 1200° C) of SYNROC constituents, mechanically mixed with 10% HLNW. These harsh conditions are incompatible with the radiological glovebox environment in which nuclear waste is normally handled.²⁶ The low pressure preparation (atmospheric pressure) of SYNROC-B reported in Chapter 7 of this work may make application of the material more feasible.

2.3 High Temperature Superconducting Cuprates

Superconductivity is a state of matter that is marked by the sudden onset (at some critical temperature, T_c , dependent on the material) of two phenomena, zero resistivity and perfect diamagnetism. In addition to an increase in temperature, superconductivity can be destroyed by exceeding a critical current density, J_c , or exceeding a critical magnetic field, H_c . The critical current density is an important factor in determining the feasibility of superconducting materials for applications, especially in the high temperature superconducting cuprates. In this work, T_c will denote the critical temperature at which a superconducting transition occurs, whereas T_C (a larger c) will denote the Curie temperature. A discussion of the various theories, or a detailed, phenomenological review of the characteristics of superconducting materials will not be given in this section, as there are numerous sources of this information in the chemical and physical literature.²⁷ A review of the structure and properties of the high transition temperature superconductors prepared in this work will be given. To date, there are nine general families of cuprate superconductors.²⁸ These families appear in Table 2.3. This discussion will concern only the $Ba_2YCu_3O_7$ cuprates and bismuth cuprates, which were studied in this work. Several intensive reviews on the structure of high temperature superconductors have been published and the interested reader is directed to references 29, 30, and 31 for a more complete discussion.

Table 2.3 The current families of high temperature superconductors. From reference 28.

Family of superconductor	Example	T_c (K)
La ₂ CuO ₄ related cuprates	La _{1.6} Sr _{0.4} CaCu ₂ O ₆	~60
Ba ₂ YCu ₃ O ₇ and related cuprates	Ba ₂ YCu ₃ O _{7-x}	92
Bismuth cuprates	Bi ₂ Sr ₂ Ca ₂ Cu ₃ O ₁₀	110
Thallium cuprates	Tl ₂ Ba ₂ Ca ₂ Cu ₃ O ₁₀	128
Lead cuprates	(Pb _{0.5} Sr _{0.5})Sr ₂ (Y _{0.5} Ca _{0.5})Cu ₂ O _x	100
Electron-doped cuprates	Nd _{2-x} Ce _x CuO _{4-y}	30
Infinite layer cuprates	Ca _{1-x} Sr _x CuCuO ₂	110
Mercury cuprates	HgBa ₂ Ca ₂ Cu ₃ O _x	133

2.3.1 Ba₂YCu₃O₇ and Related Cuprates

This group of cuprates, which contains the first material discovered with a superconducting transition temperature above the boiling point of liquid nitrogen, Ba₂YCu₃O₇ ($T_c = 92\text{K}$),³² was a major focus of the synthetic work in this thesis. The Ba₂YCu₃O₇ phase has a variable oxygen content which O₆ to O₇. Consequently, samples with experimentally undetermined oxygen contents will be (and often have been in the literature) referred to as Ba₂YCu₃O_{7-x}. The phase is superconducting and orthorhombic for oxygen content greater than Ba₂YCu₃O_{6.5}. The T_c does rise, however, reaching a maximum value, 92 K, as the value of x in the formula Ba₂YCu₃O_{7-x}, approaches zero.

The orthorhombic, fully oxygenated, superconducting form of the phase has lattice parameters of $a=3.8856(3)\text{\AA}$, $b=11.6804(7)\text{\AA}$, and $c=3.8185(4)\text{\AA}$.³³ The unit cell structure is pictured in Figure 2.4. Assuming that all barium ions are in the 2+ state, all yttrium ions are in the 3+ state, and all copper ions are in the 2+ state, the material is fully oxygenated with a nominal composition of $\text{Ba}_2\text{YCu}_3\text{O}_{6.5}$. However, a greater oxygen content is needed for the material to display superconductivity. Since the oxygen content can change, the varying charge (accepting that the oxygen charge stays a constant 2-) is accounted for by the copper ions which can be 1+, 2+ or 3+. When the material is further oxidized to $\text{Ba}_2\text{YCu}_3\text{O}_7$, the average copper oxidation state is $\text{Cu}^{2.33+}$. The $\text{Ba}_2\text{YCu}_3\text{O}_7$ phase crystallizes as an oxygen deficient perovskite. The oxygen deficiencies create two nonequivalent copper-oxygen planes labeled A and B in Figure 2.4. The buckled $\text{Cu}(\text{O})_2$ planes labeled B are believed to carry the supercurrents through the material. Hence, the material is highly anisotropic with respect to its current carrying ability (supercurrents preferentially flow in a-c plane). For this reason, epitaxial films (with the b-axis perpendicular to the substrate) or highly oriented composites are necessary to increase the current carrying ability. Several methods, such as melt texturing,³⁴ have been developed to enhance the alignment of the a-c planes in bulk $\text{YBa}_2\text{Cu}_3\text{O}_7$.

A closely related phase in the system is $\text{Ba}_2\text{YCu}_4\text{O}_8$. The phase was noticed as an impurity in the Ba-Y-Cu-O system and first synthesized in relatively pure form by Karpinski et al.³⁵ with the use of high oxygen pressures. The transition temperature of this phase is 82 K but it has the distinct advantage over its higher T_c counterpart of having a stable oxygen content. Doping the material with calcium (about 10 mol%) to give

$Ba_2Y_{1-x}Ca_xCu_4O_8$ is reported to raise the T_c to near 90 K.³⁶ The structure of the material is very similar to $Ba_2YCu_3O_{7-x}$, with the additional copper and oxygen ions forming Cu-O chains adjacent to the copper oxide chains of $Ba_2YCu_3O_{7-x}$ but displaced in the unit cell by $1/2 a$.

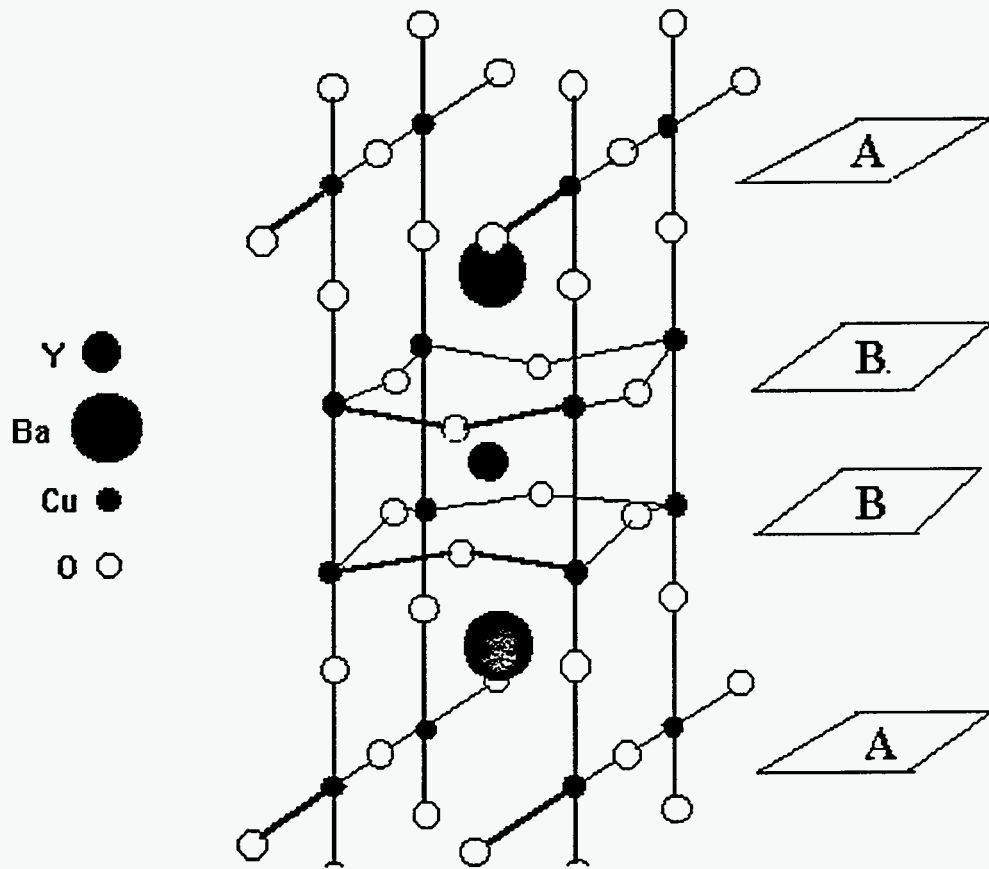


Figure 2.4. The crystal structure of $Ba_2YCu_3O_7$ showing one half of the unit cell. The buckled Cu-O planes labeled B carry the supercurrents.

A third superconducting phase in the Ba-Y-Cu-O system is, $\text{Ba}_4\text{Y}_2\text{Cu}_7\text{O}_{15}$. This phase, first synthesized in pure form by Bordet et al.,³⁷ has a T_c of 90 K. As with $\text{Ba}_2\text{YCu}_4\text{O}_8$, doping with Ca has a beneficial effect on the T_c . A substitution of 5 mol% Ca for Y raises the T_c of the phase to 94 K.

The Ba-Y-Cu-O family is more accurately described as the Ba-RE-Cu-O family (where RE stands for a rare earth element) since all of the rare earths, with the exception of cerium, praseodymium, and terbium, will substitute for yttrium in the $\text{Ba}_2\text{YCu}_3\text{O}_7$ phase with little or no change in structural or superconducting properties. Phases of composition $\text{Ba}_2\text{RECu}_4\text{O}_8$ and $\text{Ba}_4\text{RE}_2\text{Cu}_7\text{O}_{15}$ also exist, but studies on such materials are relatively few.^{38,39}

2.3.2 The Bismuth Cuprates

Discovered by Maeda et al.,⁴⁰ this family of cuprates consists of phases having the general formula; $\text{Bi}_2\text{Sr}_2\text{Ca}_x\text{Cu}_{1+x}\text{O}_{7+x}$. This formula results in $\text{Bi}_2\text{Sr}_2\text{CuO}_7$ for $x=0$, $\text{Bi}_2\text{Sr}_2\text{CaCu}_2\text{O}_8$ for $x=1$, and $\text{Bi}_2\text{Sr}_2\text{Ca}_2\text{Cu}_3\text{O}_{10}$ for $x=3$. The critical temperatures for these phases are 40 K, 82 K and 110 K respectively.²⁸ The bismuth cuprates appear to be more promising for bulk applications (silver clad wires etc.,) due the tendency for the material to form large, aligned platelets upon recrystallization. The unit cells of the bismuth based compounds are stacked perovskites, or pseudo-tetragonal perovskites. A goal of this work was the synthesis of the $\text{Bi}_2\text{Sr}_2\text{Ca}_2\text{Cu}_3\text{O}_{10}$ phase of the bismuth system in bulk powder and thick film form, consequently, the discussion of structure will center on this composition.

The $\text{Bi}_2\text{Sr}_2\text{Ca}_2\text{Cu}_3\text{O}_{10}$ phase crystallizes as a tetragonal stacked perovskite with lattice parameters of $a=5.40 \text{ \AA}$, $b=37.18 \text{ \AA}$, and $c=5.41 \text{ \AA}$. The material is structurally complicated due to ordered dislocations and vacancies which extend over several unit cells giving rise to a type of superstructure.⁴¹ The phase, like $\text{Ba}_2\text{YCu}_3\text{O}_{7-x}$, is anisotropic in its current carrying ability. The supercurrents flow preferentially in the a-c plane of Cu-O chains. The $\text{Bi}_2\text{Sr}_2\text{Ca}_2\text{Cu}_3\text{O}_{10}$ phase is one of the most difficult of the high temperature superconductors to synthesize in phase pure form.⁴² It is also a technologically important phase since its T_c of 110K is higher than space temperatures suggesting applications in space requiring only passive cooling. It is also safer to work with than its slightly higher T_c counterparts ($\text{Tl}_2\text{Ba}_2\text{Ca}_2\text{Cu}_3\text{O}_{10}$ and $\text{HgBa}_2\text{Ca}_2\text{Cu}_3\text{O}_{10}$), due to the relatively low volatilities of the metals involved (the addition of Pb does present a health concern, though not as severe as Tl and Hg). The material is almost always contaminated, mainly with lower T_c bismuth phases (e.g., $\text{Bi}_2\text{Sr}_2\text{CaCu}_2\text{O}_8$). Many reports of "phase pure" $\text{Bi}_2\text{Sr}_2\text{Ca}_2\text{Cu}_3\text{O}_{10}$ state the necessity of extended annealing times (over ten days).⁴³ It has been shown that partial substitution of lead for bismuth stabilizes the $\text{Bi}_2\text{Sr}_2\text{Ca}_2\text{Cu}_3\text{O}_{10}$ phase with respect to the lower T_c phases. The usual lead doped composition is $\text{Bi}_{1.7}\text{Pb}_{0.3}\text{Sr}_2\text{Ca}_2\text{Cu}_3\text{O}_{10}$. Some research groups have reported the synthesis of high phase purity $\text{Bi}_{1.7}\text{Pb}_{0.3}\text{Sr}_2\text{Ca}_2\text{Cu}_3\text{O}_{10}$ through off stoichiometric starting compositions⁴⁴ (due to volatility of Pb, Cu, Ca, and Bi and extended firing times necessary for phase purity) such as $\text{Bi}_{2.5}\text{Pb}_{0.5}\text{Sr}_{2.0}\text{Ca}_{3.0}\text{Cu}_{3.5}\text{O}_{10}$.

2.4 Applications of High Temperature Superconductors

Due to the difficulty in obtaining bulk samples that are capable of carrying substantial currents in the superconducting state (the result of weak links created by poor grain alignment and the anisotropic current carrying ability of the materials), it is generally accepted that the first commercial applications of high temperature superconductors will utilize the materials in the form of thin films. Thin films of high temperature superconductors have several potentially important industrial applications. Some of these applications are outlined in Table 2.4. Most applications utilize a series of tunneling effects predicted by Josephson in 1962, which are collectively known as the *Josephson effects*.⁵ An important application for thin films is in the fabrication of superconducting quantum interference devices (SQUIDs). SQUIDs are essentially a loop containing two Josephson junctions connected in parallel, biased with a constant current. Such an arrangement enables the detection of extremely small changes in the magnetic field within the loop via the production of an output voltage in response to a small input magnetic flux.⁴

Table 2.4. Devices which can be fabricated from high temperature superconductors, the applications of these devices and the phenomena associated with superconductivity that makes the application possible. Adapted from references 45 and 46 .

Phenomenon	Devices	Applications
Zero resistivity, high critical current density	Micro-strip lines, patterned layer structures, wires, cables, tapes	Passive microwave devices,* Interconnects in microelectronics,* Electrical energy transport
High critical current density and critical magnetic field	Magnetic coils	Medicine (NMR topography) Electrical power industry (energy storage, generators) Transport (levitating trains) Plasma confinement.
Meissner effect	Magnetic shields	Medicine (shielding for NMR experiments) High energy physics (shielding)
	Magnetic bearings	Low friction bearings
Josephson tunneling	SQUIDs	Detection of extremely small magnetic fields, magnetic susceptibility measurements, voltage measurements* Medicine (magnetic encephalography)*
	Josephson devices	Computers (faster circuits)* Microwave detectors*
Sharp resistive transition	Bolometer	Plasma and space physics (detection of far-infrared radiation)*

*This application requires epitaxial thin films.

2.5 Notes and References

- ¹ This phase is referred to as "hollandite-type" because it crystallizes with a structure similar to that of the natural mineral hollandite, $\text{BaMn}_8\text{O}_{16}$.
- ² L. G. Tejuca and J. L. G. Fierro, Editors, *Properties and Applications of Perovskite Type Oxides*, Marcel Dekker Inc. (New York, 1993).
- ³ F. S. Galasso, *Perovskites and High Tc Superconductors*, Gordon and Breach (New York, 1990).
- ⁴ S. T. Ruggiero and D. A. Rudman, *Superconducting Devices*, Academic Press Inc. (Boston, MA, 1990).
- ⁵ M. Cryot and D. Pavuna, *Introduction to Superconductivity and High Temperature Superconductivity*, World Scientific (Singapore, 1992).
- ⁶ B. Raveau, C. Michel, M. Hervieu, and D. Groult, *Crystal Chemistry of High Tc-Superconducting Oxides*, Springer-Verlag (New York, 1991).
- ⁷ A. E. Ringwood, *Safe Disposal of High Level Nuclear Reactor Wastes: A New Strategy*, Australian National University Press (Norwalk, CT, 1978).
- ⁸ H. F. Kay and P. C. Bailey, *Acta. Cryst.* **10**, 219 (1957).
- ⁹ T. Barth, *Norsk. Geol. Tidsk.* **8**, 201 (1925).
- ¹⁰ H. D. Megaw, *Proc. Phys. Soc.* **58**, 326 (1946).
- ¹¹ R. S. Roth, *J. Research NBS* **58**, RP 2736 (1957).
- ¹² I. Naray-Szabo, *Inorganic Crystal Chemistry*, Akademiai Kiado (Budapest, 1969).
- ¹³ V. M. Goldschmidt, *Geochemische Verteilungsgesetze der Elemente. VII, VIII*, Skrift. Norske Vidensk Akad. I. Mat. nat. Kl. Oslo, Nos. 2 and 8.

- ¹⁴ J. Twu and P. K. Gallagher, in *Properties and Applications of Perovskite Type Oxides*, Edited by L. G. Tejuca and J. L. G. Fierro, Marcel Decker Inc. (New York, 1993).
- ¹⁵ D. E. Rase and R. Roy, *J. Am. Ceram. Soc.* **38**, 102 (1955).
- ¹⁶ T. Negas, R. S. Roth, H. S. Parker, and D. Minor, *J. Solid State Chem.* **9**, 297 (1974).
- ¹⁷ See reference 3, page 6.
- ¹⁸ T. Takeuchi, K. Ado, T. Asai, H. Kageyama, Y. Saito, C. Masquelier, and O. Nakamura, *J. Am. Ceram. Soc.* **77**, 1665 (1994).
- ¹⁹ H. C. Graham, N. M. Tallin, and K. S. Mazdizyasni, *J. Am. Ceram. Soc.* **54**, 548 (1971).
- ²⁰ A. E. Ringwood, S. E. Kesson, N. G. Ware, W. Hibberson, and A. Major, *Nature* **278**, 219 (1979).
- ²¹ L. P. Hatch, *Am. Sci.* **41**, 410 (1952).
- ²² L. Werme, I. K. Bjorner, G. Bart, H. U. Zwicky, B. Grambow, W. Lutze, R. C. Ewing, and C. Magrabi, *J. Mater. Res.* **5**, 1130 (1990).
- ²³ G. J. McCarthy, *Nucl. Technol.* **32**, 92 (1977).
- ²⁴ R. Roy, *J. Am. Ceram. Soc.* **60**, 350 (1977).
- ²⁵ T. Ringwood, *Amer. Sci.* **70**, 201 (1982).
- ²⁶ N. V. Coppa, Personal Communication (Los Alamos, NM, 1994).
- ²⁷ For example, see reference 5.
- ²⁸ C. N. R. Rao, R. Nagarajan, and R. Vijayaraghavan, *Supercond. Sci. Technol.* **6**, 1 (1993).

- ²⁹ C. P. Poole, T. Datta, and H. A. Farrah, *Copper Oxide Superconductors*, John Wiley and Sons, New York, 1988.
- ³⁰ V. Z. Kreslin and S. A. Wolf, *Fundamentals of Superconductivity*, Plenum Press (New York, 1989).
- ³¹ R. J. Cava, *Scientific American*, August, **42** (1990).
- ³² C. W. Chu, P. H. Hor, R. L. Meng, L. Gao, and Z. H. Huang, *Science* **235**, 567 (1987).
- ³³ F. Beech, S. Miraglia, A. Santoro, and R. S. Roth, *Phys. Rev. B* **35**, 8778 (1987).
- ³⁴ K. Salama and D. F. Lee, *Supercond. Sci. Technol.* **7**, 177 (1994).
- ³⁵ J. Karpinski, E. Kaldis, E. Jilek, S. Rusiecki, and B. Bucher, *Nature* **338**, 328 (1989).
- ³⁶ T. Miyatake, S. Gotoh, N. Koshizuka, and S. Tanaka, *Nature* **341**, 41 (1989).
- ³⁷ P. Bordet, C. Chailout, J. Chevanas, J. L. Hoveau, M. Marezio, J. Karpinski, and E. Kaldis, *Nature* **334**, 596 (1988).
- ³⁸ D. M. Pooke, R. G. Buckley, M. R. Pressland, and J. L. Tallon, *Phys. Rev. B* **41**, 6616 (1990).
- ³⁹ S. Adachi, H. Adachi, K. Stesune, and K. Wasa, *Physica C* **175**, 523 (1991).
- ⁴⁰ H. Maeda, Y. Tanaka, M. Fukutomi, and T. Asano, *Jpn. J. Appl. Phys.* **27**, L209 (1988).
- ⁴¹ See for example, Z. Zhang and C. M. Lieber, *J. Phys. Chem.* **96**, 2030 (1992).
- ⁴² M. T. Ruiz, G. F. de la Fuente, A. Badia, J. Blasco, M. Castro, A. Sotelo, A. Larrea, F. Lera, C. Rillo, and R. Navarro, *J. Mater. Res.* **8**, 1668 (1993).
- ⁴³ A. Briggs, B. A. Bellamy, I. E. Denton, and J. M. Perks, *J. Less-Common Metals* **164 & 165**, 559 (1990).

- ⁴⁴ N. Balchev, D. Kovacheva, V. Lovchinov, K. Konstantinov, and K. Petrov, J. Supercon. **6**, 49 (1993).
- ⁴⁵ H. J. Scheel, M. Berkowski, and B. Chabot, J. Crystal Growth **115**, 19 (1991).
- ⁴⁶ M. Leskela, H. Molsa, and L. Niinisto, Suprecon. Sci. Technol **6**, 627 (1993).

CHAPTER 3

SYNTHESIS OF BULK POWDERS AND SUPPORTED FILMS OF PEROVSKITE MATERIALS

In this chapter, commonly used synthetic procedures for the preparation of perovskite-type oxides will be outlined. This material is provided for comparison of the synthetic methods developed or utilized in this work with the present technology. The chapter will cover the preparation of bulk powders as well as thin and thick films. The preparation of high temperature superconductors will be used as an example of most synthetic techniques due to the relative abundance of these examples in the scientific literature and relevance to the present work. The techniques discussed are applicable for synthesis other oxide phases except where precluded by chemical properties of the constituent elements (aqueous solubility, melting point, etc.,).

3.1 Synthesis of Perovskite Materials in Bulk Form

3.1.1 Conventional Ceramic Processing

The simplest method for the preparation of perovskite-type oxides is *conventional ceramic processing*. Sometimes referred to as the grind and calcine method, conventional ceramic processing entails the mixing of several starting reagents and subjecting the mixture to high temperatures to facilitate diffusion and reaction in the solid state. The

most common method of synthesis of barium titanate is the grind and calcine method.^{1,2,3,4} The preparation of this material will be reviewed as an example.

The starting reagents, TiO_2 and BaCO_3 , are weighed out in stoichiometric quantities. The two powders are mechanically mixed by ball milling or manual grinding with a mortar and pestle. A hard grinding medium (agate, Al_2O_3 , etc.) is preferred to lessen the chance of contamination during mixing. After grinding and mixing, sieving of powders may be incorporated to achieve a relatively uniform particle size distribution. The mixed powder may then be pressed into compacts to increase the grain contact between reactants. The mixture is then calcined at high temperatures (1200° to 1400° C) for long periods of time ($>24\text{h}$). The compact is then pulverized and mechanically mixed again to expose unreacted grains. This material is then compacted and calcined, repeating the cycle, until the desired phase purity is obtained.

It can be seen from the above procedure that conventional ceramic processing, although simple in theory and practice (and consequently so widely used), has the disadvantages of being slow, labor intensive, and is often impractical for commercial preparation of large amounts of high purity materials. The high temperatures needed to facilitate diffusion result in additional problems. As discussed in Chapter 1, some materials are not stable (with respect to other, undesired phases) at high temperatures. These materials are often inaccessible by conventional ceramic processing. Other materials do not melt congruently, but decompose into two or more solid or liquid phases above a certain *peritectic* melting temperature. In such systems, an upper limit is placed on the processing temperature. This lower temperature slows the rate of diffusion, and

consequently, necessitates longer reaction times (or more intermittent grindings). Finally, the high temperatures and long reaction times, common in conventional ceramic processing, result in excessive and uncontrollable grain growth. Often, material of small and uniform particle size is desired for forming sintered compacts or thick films. Powders with small (submicrometer) and uniform particle size achieve higher *green body densities* upon pressing. The green body density is the density of a powder compact before the sintering step. The final density of the ceramic is highly dependent upon this green body density. The production of a homogenous, sub-micron particle size material is not possible through the grind and calcine method.

3.1.2 Solution Methods

The drawbacks of conventional ceramic processing result from the diffusion limited reaction pathway they follow (see Chapter 1). Several synthetic methods have been developed in attempts to minimize (or eliminate) these drawbacks by achieving a greater degree of mixing of reactants and thereby shorten diffusion paths. These methods are solution methods. Solutions are homogeneous. For example, a solution of Ba^{2+} and Cu^{2+} contains a random, completely homogenous mixture of the two cations. Simply evaporating the solvent will result in a loss of homogeneity as the solute salts crystallize and separate due to differences in solubility. Solution methods try to “trap” this homogeneity and “transfer” it into the solid state.

There are several different ways to trap the homogeneity of a solution and transfer it into the solid state (some more effective than others). These methods fall into two

distinct categories; *solute removal techniques* and *solvent removal techniques*. Solute removal techniques, which include coprecipitation and the sol gel methods, rely on rapid precipitation or gelation of the solute, to both trap the solution homogeneity and transfer it (after filtering or drying) into the solid state. The solvent removal techniques, spray drying and freeze drying, have different trapping and transferring processes. In spray drying, extremely rapid evaporation of the solvent serves as both trapping (solvent removal occurs too fast for extensive crystallization) and transferring mechanisms. In freeze drying, the solution is rapidly frozen, which serves to trap the homogeneity. Sublimation of the solvent then preserves this homogeneity, and transfers it to the solid state.

The choice of the solution anion in a solvent removal technique is an important decision. After a solvent removal process, the resulting precursor (and product) depends directly on the anion of the solution. Therefore, anions which produce salts with low melting points, high decomposition temperatures, or high volatility are to be avoided. In the solute removal techniques, the salts in the original solution undergo some chemical change and the choice of this anion is not as important. A discussion of the four commonly used solution techniques follows.

3.1.2.1 Solute Removal Techniques

3.1.2.1.1 Coprecipitation

The simplest in theory of the solution methods, coprecipitation, is based on a precipitation reaction. A solution of the desired metal salts is added to a second solution containing a large excess of a precipitating agent, optimally resulting in uniform,

simultaneous precipitation of the desired metals as insoluble salts. For preparation of $\text{Ba}_2\text{YCu}_3\text{O}_{7-x}$, a common procedure involves the addition a solution containing stoichiometric quantities of yttrium, barium, and copper nitrates to a nearly concentrated solution of oxalic acid. The result is the precipitation of the metals as insoluble oxalates.^{5,6,7} The oxalates are then filtered, washed, and calcined at $\sim 900^\circ\text{C}$ to yield $\text{Ba}_2\text{YCu}_3\text{O}_{7-x}$. The oxalate coprecipitation method was used by Bednorz and Muller in the preparation of the first high temperature superconductors.⁸ Alternatively, the nitrate solution can be added to a concentrated solution of Na_2CO_3 or K_2CO_3 , which causes precipitation of the transition metals as the insoluble carbonates; $\text{Y}_2(\text{CO}_3)_3$, BaCO_3 , and $\text{Cu}_2(\text{CO}_3)(\text{OH})_2$.⁹ Sodium hyponitrite, NaN_2O_2 , has also been used as a coprecipitating agent for the low temperature synthesis of $\text{Ba}_2\text{YCu}_3\text{O}_{7-x}$. The tetragonal phase of $\text{Ba}_2\text{YCu}_3\text{O}_{7-x}$ was obtained from the hyponitrite precursor after calcination in argon at 700°C . The lower reaction temperature was attributed to intimate mixing and the noncarbonaceous nature of the precursor. The absence of carbon allows lower reaction temperatures by avoiding the formation of the relatively stable intermediate, BaCO_3 .¹⁰

Coprecipitation can also be carried out in non-aqueous solvents. Glacial acetic acid has been explored as a solvent for coprecipitation of oxalates as a precursor to $(\text{Bi,Pb})_2\text{Sr}_2\text{Ca}_2\text{Cu}_3\text{O}_{10}$ and $\text{Bi}_2\text{Sr}_2\text{CaCu}_2\text{O}_8$.¹¹ Liquid ammonia has been utilized as the solvent for coprecipitation of yttrium, barium, and copper carbamates as precursors to $\text{Ba}_2\text{YCu}_3\text{O}_{7-x}$ and $\text{Bi}_2\text{Sr}_2\text{CaCu}_2\text{O}_8$. An interesting difference between this liquid ammonia coprecipitation method and aqueous coprecipitation methods is that in the former, the solvent, in addition to the solute, reacts with the coprecipitating agent (gaseous CO_2)

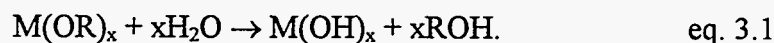
forming insoluble ammonium carbamate. This is believed to make for a more intimate mixture since nucleation of the precipitating metal salts is hampered by the coprecipitating ammonium carbamate.^{12,13}

Oxalate coprecipitation is also widely used for the preparation of BaTiO_3 .^{14,15,16,17} The coprecipitation (after addition of a barium and titanyl chloride solution to an oxalic acid solution) yields a single phase double oxalate salt, barium titanyl oxalate, $\text{BaTiO}(\text{C}_2\text{O}_2)_2 \cdot 4\text{H}_2\text{O}$. Since a double salt is formed, the mixing of barium and titanium cations is perfectly homogeneous. However, phase separation occurs during thermal decomposition of this salt and BaTiO_3 forms through a reaction of BaCO_3 and TiO_2 . Due to the greater degree of mixing of BaCO_3 and TiO_2 achieved through $\text{BaTiO}(\text{C}_2\text{O}_2)_2 \cdot 4\text{H}_2\text{O}$ decomposition, calcination conditions for BaTiO_3 synthesis can be as mild as 700°C for 1h for oxalate coprecipitation precursors.¹⁸

Although relatively simple in practice and theory, coprecipitation is not an effective method of achieving atomic level mixing and frequently results in mixing on the same order as mechanical grinding. An additional problem with the method is loss of stoichiometry through finite solubilities of the precipitated salts. This factor can be somewhat minimized by lowering these finite solubilities by judicious selection and control of reaction $p\text{H}$, carrying out the coprecipitation reaction at $\sim 0^\circ\text{C}$, and adding a miscible organic solvent (ethanol, methanol, etc.).

3.1.2.1.2 Sol Gel Methods

Sol gel methods have been widely used in preparative solid state chemistry. There are many variations which all have the common goal of producing a colloidal suspension or sol gel from a solution of desired reagents. A widely used sol gel method of $\text{Ba}_2\text{YCu}_3\text{O}_{7-x}$ preparation is often referred to as the alkoxide method.¹⁹ Yttrium isopropoxide, $\text{Y}(\text{OC}_3\text{H}_7)_3$, copper methoxide, $\text{Cu}(\text{OCH}_3)_2$, and barium metal (which reacts with the solvent to form barium ethoxide, $\text{Ba}(\text{OC}_2\text{H}_5)_2$) are dissolved in ethanol. To increase the solubility of the alkoxides, 2-methylaminoethanol is added and the solution is refluxed for 3h. Other additives, such as β -diketones,²⁰ have also served this purpose. The solution is then hydrolyzed to form the sol gel by addition of a controlled amount of H_2O according to the general reaction;



The solvent can then be removed under reduced pressure to yield a colloidal precursor.

Calcination of the precursor at 850°C for 3h in O_2 yields single phase $\text{Ba}_2\text{YCu}_3\text{O}_{7-x}$.¹⁹

A similar alkoxide based procedure has been used for the preparation of CaTiO_3 ,²¹

BaTiO_3 ,^{22,23,24} and SrTiO_3 .²⁵

Another sol gel method for $\text{Ba}_2\text{YCu}_3\text{O}_{7-x}$ preparation involves the addition of a chelating agent, citric acid, to an aqueous solution of $\text{Y}(\text{NO}_3)_3 \cdot x\text{H}_2\text{O}$, $\text{Ba}(\text{NO}_3)_2$ and $\text{Cu}(\text{NO}_3)_2 \cdot x\text{H}_2\text{O}$.²⁶ Ethylene glycol is then added and the mixture is heated to 120°C until most of the original water has evaporated. At this time, a colloidal precipitate forms in the

ethylene glycol solution. This gel is heated at 200° to 300° C for organic decomposition. The resulting powder is fired at 940°C for 2 h to achieve the high temperature superconductor.

The sol gel methods are effective methods of achieving atomic level mixing of reactants. A drawback of some sol gel methods is the need for costly organometallic reagents. Several of the sol-gel methods require a careful control of pH to prevent phase separation during gel formation. Many of the sol-gel methods form carbonaceous precursors. The presence of carbon may lead to the formation of carbonates as intermediate products. Some alkaline earth carbonates are relatively stable and require temperatures in excess of 800° C for complete decomposition. The presence of BaCO₃ has been shown to necessitate longer reaction times in the synthesis of Ba₂YCuO_{7-x}.²⁷ Even after decomposition of carbonates, a precursor with a high carbon to metal ratio may result in the buildup of amorphous carbon at grain boundaries. This buildup has been shown to be detrimental to the superconducting properties of Ba₂YCu₃O_{7-x}.²⁸

3.1.2.2 Solvent Removal Techniques

3.1.2.2.1 Spray Drying

Spray drying, or spray pyrolysis²⁹ (also sometimes referred to as aerosol decomposition) consists of spraying a solution (usually an aqueous solution) of salts containing the desired metals through a heated reaction zone, wherein the solvent is vaporized and complete or partial decomposition of the constituent salts occurs. The starting reagents are usually nitrates^{30,31,32} or acetates³³ due to their favorable solubility,

low decomposition temperature, and non-volatility with most metals. Although acetates are commonly used, spray drying aqueous solutions of organic acid salts can result in the build up of amorphous carbon at grain boundaries of the final product. Free carbon has been detected in samples of MgO prepared by spray pyrolysis of aqueous $\text{Mg}(\text{O}_2\text{CCH}_3)_2$ solutions after extensive firing at 1000°C .³⁴ Other anions, such as metal chlorides, have been used in a spray pyrolysis preparation of MgO and some ferrites.³⁵

A novel method utilizing anionic oxidation-reduction has been developed for a spray pyrolysis preparation of $\text{Ba}_2\text{YCu}_3\text{O}_{7-x}$ ³⁶ and $\text{Ba}_2\text{YCu}_4\text{O}_8$.³⁷ Briefly, the method consists of spray drying an aqueous solution containing oxidizing salts (nitrates) and reducing salts (acetates). An exothermic redox reaction occurs which converts the acetate/nitrate precursors to an intimate mixture of oxides below 300°C . This mixture is then fired at high temperatures to obtain the desired phase.

If the solvent is removed rapidly, spray drying is a very effective method of atomic mixing. The main problems associated with spray drying are engineering in nature. The system must be designed so that the water vapor created upon the rapid evaporation of the solution is quickly removed. A high percentage of water vapor in the system will cause agglomeration of spray dried particles and possible phase separation if a water soluble species exists in the dried powder. It is possible that some salts with high decomposition temperatures (e.g. $\text{Ba}(\text{NO}_3)_2$ decomposes at $>600^\circ\text{C}$)³⁸ could remain after the drying process and dissolve in condensed water resulting in phase separation.

3.1.2.2.2 Freeze Drying

Freeze drying, (sometimes referred to as the cryochemical technique) which is the least commonly used of the four solution methods discussed here, is perhaps the most effective method for producing solid atomic mixtures. The technique was used in this work for the preparation of BaTiO₃ and SYNROC-B. It is similar in concept to spray drying; removal of the solvent without allowing for extensive crystallization. In freeze drying, however, the solvent removal step and salt decomposition step are separated. An aqueous solution is sprayed into stirred liquid nitrogen (or another cryogen) where it is rapidly frozen. The rapid freezing traps the ions in the random state they were in when in solution. In order for the random mixture of cations to be trapped in the freezing process, the speed at which the ice front moves through the droplet of solution must be greater than the rate at which the solute can diffuse to form precipitates.

After the solution is rapidly frozen, the snow-like substance is placed in a commercial freeze drying apparatus. The pressure in the sample chamber is lowered to a few millitorr, and the temperature is kept below the eutectic point of the solution to facilitate sublimation and prevent melting, respectively. Heat for sublimation is supplied to the frozen solution by radiation, or by conduction through frozen solution. The heat supplied is precisely controlled to keep the temperature of the "snow" below the eutectic point of the solution. The sublimed water is collected on a condenser that is cooled to about -70° C. Although a vacuum pump is included in most freeze drying systems, it serves only to remove the noncondensable gases and thereby increase the mean free path of the H₂O molecules. The main driving force in the sublimation is the difference in the

temperature dependent vapor pressure of water at the sample temperature (-5° to -40° C) and the condenser temperature (-70° to -100° C). When the water has completely sublimed, a very fine powder (particle size depends on concentration of the starting solution and droplet size of the spray) remains which is subject to the appropriate thermal treatment.

Ceramic synthesis through freeze drying was first explored in the late 1960's by Schnettler, Monforte, and Rhodes,³⁹ who used sulfate salts for the preparation of alumina (Al_2O_3) and spinel (MgAl_2O_4). More recently, the technique has been used in the synthesis of cuprate superconductors. A four fold increase in the rate of formation of the $(\text{Bi}, \text{Pb})_2\text{Sr}_2\text{Ca}_2\text{Cu}_3\text{O}_{10-x}$ phase has been reported with the calcination of freeze dried nitrate powders over the grind and calcine method.^{40,41,42} Freeze drying of nitrate solutions has also been shown to allow the formation of $\text{Ba}_2\text{YCu}_4\text{O}_8$ at atmospheric pressure.⁴³ Complete formation of the $\text{Ba}_2\text{YCu}_4\text{O}_8$ phase requires high O_2 pressures,^{44,45} or the use of an alkali metal catalyst⁴⁶ when a mechanical mixture is heat treated. Very high quality $\text{Ba}_2\text{YCu}_3\text{O}_{7-x}$ powders⁴⁷ and the perovskite $\text{La}_{1-x}\text{Sr}_x\text{CoO}_3$ ⁴⁸ have also been synthesized via freeze drying of nitrate solutions.

Freeze drying was used in this work (Chapters 5 and 6) due to its unrivaled effectiveness in producing solid atomic mixtures. The technique has the advantage over spray drying that every step of the process can be controlled and adjusted to prevent phase separation. The critical step in the process is the freezing of the solution. If the freezing is rapid enough, the atomic mixture is created in this step. Subsequent steps

(sublimation and thermal processing) need only preserve this atomic mixture. A more detailed discussion of the freeze drying procedure will be presented in Chapter 5.

3.2 Synthesis of Perovskite Materials as Supported Films

Thin and thick films of perovskite materials, and in particular, high T_c superconductors have important practical applications in areas such as electronics and magnetic shielding (see section 2.4 for a more complete discussion of the applications of high T_c films). Consequently, a great amount of research has looked into better ways of producing high T_c films. A few general comments are in order before beginning a discussion on the preparation of high T_c films.

A film with a thickness of $>1\mu\text{m}$ is generally referred to as a thick film. Thin films ($\leq 1\mu\text{m}$ thick), have a tendency to grow epitaxially on the substrate.⁴⁹ That is, the film will grow as a single crystal-like sheet on top of the single crystal substrate. For good epitaxial growth to occur, the lattice spacing of the substrate should be close to that of the material being deposited. This epitaxial growth is extremely important for the preparation of high temperature superconductors. The anisotropic current carrying nature of the materials, which limits the current carrying ability in bulk samples, is not a problem if the film can be grown so that the current carrying a-c plane is grown parallel to the substrate (b-axis perpendicular to the substrate). Critical current densities in thin epitaxial films have been reported as high as $5 \times 10^6 \text{ A/cm}^2$ (at 77K).⁵⁰ It has been shown, however, that when a thickness of a few hundred nanometers is exceeded in $\text{Ba}_2\text{YCu}_3\text{O}_{7-x}$ films, the orientation switches from b-axis perpendicular to the substrate to a-axis perpendicular to the

substrate.⁵¹ The critical current density perpendicular to the a-c plane of $\text{Ba}_2\text{YCu}_3\text{O}_{7-x}$ is only 2-3% of the J_c in the a-c plane.⁵² This causes the critical current density for thick films to be considerably lower (good samples produced by screen printing can have $J_c \sim 3 \times 10^3 \text{ A/cm}^2$ for a 30-40 μm thick film).⁵³

The choice of material for substrate is governed by four general considerations.

(1) The substrate material must not melt or undergo any other phase transformation between the preparation temperature and the temperature of operation. (2) The substrate material should have a crystal plane with lattice parameter close to the lattice parameter of the material of interest, i.e. $\sim 3.8 \text{ \AA}$ for $\text{Ba}_2\text{YCu}_3\text{O}_{7-x}$ (this property is especially important if epitaxial growth is desired). (3) The substrate material should have thermal expansion coefficients close to that of the compound of interest, and (4), the substrate material should be (or allow the growth of a buffer layer that is) chemically inert to reaction with the coating. These four considerations lead to the two most common choices of substrates for $\text{Ba}_2\text{YCu}_3\text{O}_{7-x}$ film growth; MgO and LaAlO_3 . Single crystal, 100 oriented wafers of LaAlO_3 are considered the optimum substrate for thin film growth of $\text{Ba}_2\text{YCu}_3\text{O}_{7-x}$ due to the close lattice match between the phases. Single crystal, 100 oriented MgO is also widely used for thin films but suffers from a slightly less perfect lattice match. For thick films, the most important property of a substrate is inactivity to chemical reaction with the coating. Consequently, polycrystalline MgO is widely used. MgO has been shown to be extremely inert to reaction with the Ba-Y-Cu-O system at temperatures below 1000° C .⁵⁴ Other materials, such as yttria-stabilized zirconia (YSZ), SrTiO_3 , NdGaO_3 , Ag, and Al_2O_3 (sapphire), have also been used for both thin and thick films.

A distinction has developed between two general types of film production, *in-situ* and *ex-situ*. In-situ refers to techniques that result in production of superconducting phases without a post-anneal. Ex-situ techniques prepare a non-superconducting film which requires a high temperature anneal to obtain the superconducting phase. It is generally accepted that in-situ techniques are desirable since the complication of a post-deposition heat treatment is unnecessary. In-situ techniques are usually implemented for thin film production, whereas ex-situ techniques dominate thick film production. Most in-situ techniques require high vacuum conditions. The most widely used techniques⁵⁵ for the synthesis of thin films of high temperature superconductors are ion beam sputtering, molecular beam epitaxy, laser ablation, coevaporation, and chemical vapor deposition (CVD). The literature on thick film production is dominated by screen printing, and spray pyrolysis. A brief discussion of the various techniques developed for the production of films of high T_c superconductors follows. For simplicity and consistency, all techniques discussed will be explained in terms of the $Ba_2YCu_3O_{7-x}$ system. In most cases, changing starting materials to produce a different film composition will have little effect on the general procedure.

3.2.1 Preparation of Thin Films

3.2.1.1 Ion Beam Sputtering

Ion beam sputtering (IBS)^{56,57} is a high vacuum technique, wherein an energized, ionic beam of a high mass gas (Ar) impinges upon a target consisting of the desired film constituents. Particles are sputtered from the target and nucleate on a nearby substrate.

The substrates are radiatively heated to the required temperature for nucleation, diffusion, and growth, which varies from system to system. The particle beam is generated by a direct current arc (DCS), or a radio frequency plasma. There are several problems with both sputtering techniques. Due to a phenomenon of backsputtering (from film to target), the stoichiometry of the target does not have a direct correlation to the stoichiometry of the resultant film.⁵⁸ Consequently, target stoichiometry has to be varied to obtain the optimum film composition.

3.2.1.2 Molecular Beam Epitaxy

In molecular beam epitaxy,^{59,60} the individual components (usually metallic) which will combine to form the desired film are evaporated from separate sources in a background pressure of $<1 \times 10^{-4}$ torr. Atomic particles then nucleate and grow into a thin film on a radiatively heated substrate. For preparation of $\text{Ba}_2\text{YCu}_3\text{O}_{7-x}$ films, an activated oxygen source is added near the substrate to yield a sufficiently oxygenated film.⁶¹ Since each elemental component can be heated separately, the method is widely used for the preparation of layered superconducting devices of only a few nanometers in thickness.⁶² The technique, although able to produce exceptionally high quality films ($J_c > 4.5 \times 10^6 \text{ A/cm}^2$)⁵⁹ has a very low deposition rate.⁵⁵

3.2.1.3 Laser Ablation

Laser ablation, or pulsed laser deposition,^{63,64,65} is in principle, very much like the sputtering techniques. A target composed of the desired starting material, $\text{Ba}_2\text{YCu}_3\text{O}_{7-x}$, is

placed in a vacuum chamber which is then evacuated to below 1×10^{-3} torr. A high powder Nd: YAG, CO₂, or excimer laser is directed through a window of the vacuum chamber and onto the target. The laser ablates atomic size fragments away from the target which travel in a plume, toward a thermally controlled substrate. Laser ablation does not suffer from deviations in stoichiometry and, with precise control of substrate temperature, can be implemented to produce very high quality thin films of Ba₂YCu₃O_{7-x} with $J_c > 5 \times 10^6 \text{ A/cm}^2$.⁵⁰ Laser ablation, although generally used for the production of thin films, has also been used for the synthesis of thick films ($> 6 \mu\text{m}$ thick) with $J_c > 1 \times 10^6 \text{ A/cm}^2$.⁶⁶ The technique has an acceptably high deposition rate but has the disadvantage of being costly due to the need for a high power laser and suitable vacuum chamber.

3.2.1.4 Coevaporation

Coevaporation^{67,68,69} is related to molecular beam epitaxy except that in coevaporation, the deposition of the film constituents is carried out simultaneously and at a much higher deposition rate. For Ba₂YCu₃O_{7-x} films, three sources are individually heated. The sources contain samples of metallic yttrium, metallic copper, and barium fluoride (BaF₂). They are resistively heated to over the boiling points of the materials in a low pressure (1×10^{-3} torr) oxygen containing chamber. The materials evaporate and condense on the substrates. BaF₂ is preferentially used over barium metal due to the high reactivity of the latter with water vapor, oxygen, and CO₂. Such reactions produce very high boiling point compounds (e.g. BaCO₃ b.p. $> 1740^\circ \text{C}$, BaO b.p. $\sim 2000^\circ \text{C}$)³⁸ and will result in a barium deficiency in the finished film. The use of BaF₂, however, necessitates a

post anneal to remove fluorine from the film. Fluorine has been shown to adversely affect the superconducting properties of films produced by coevaporation.⁷⁰ The post anneal is usually performed in wet oxygen (O₂ gas bubbled through water to saturate it with water vapor), which more effectively removes the absorbed fluorine.⁷⁰ This need for a post anneal keeps coevaporation from being a true in-situ technique.

3.2.1.5 Metalorganic Chemical Vapor Deposition

Chemical vapor deposition (CVD)^{71,72,73} is fast becoming an important synthetic technique in many areas of materials chemistry. It is used for the preparation of diamond films⁷⁴ and is extremely important in the semiconductor industry. The production of high T_c films through CVD is mainly a subdivision known as metalorganic chemical vapor deposition (MOCVD). Large, chelating, anions are used to "hide" the metals, making compounds that are relatively volatile. A typical anion used in the Ba-Y-Cu-O system is the dipivalomethanate (dpm). The volatile metalorganic compounds, Y(dpm)₃, Ba(dpm)₂, and Cu(dpm)₂ are mixed with oxygen (carrier gas) and metered into the reaction chamber. The chamber, which may be partially evacuated, contains radiatively heated substrates (600° to 900° C). The gaseous metalorganics decompose on the hot substrate to the much higher boiling point oxides (or possibly carbonates) resulting in an oxide film. The technique is adaptable to large area deposition (the previously discussed sputtering techniques are not adaptable to large area deposition due to geometrical restraints), but often produces films which need a post anneal to achieve full oxidation. Some researchers

have explored the use of more oxidizing carrier gases such as ozone⁷⁵ and nitrous oxide⁷⁶ in attempts to avoid the post anneal.

3.2.2 Preparation of Thick Films

3.2.2.1 Screen Printing

Screen printing^{77,78,79,80} is a commonly used technique for the preparation of thick films of high temperature superconductors. The method starts with preparing (or obtaining) high quality, bulk superconducting material of small and uniform particle size ($<1\mu\text{m}$). The powder is sifted through a fine mesh screen and mixed with an organic solvent/vehicle into a type of paste. This paste is then screen printed using a rolling device onto the substrate of choice. The films are dried and then sintered to improve the grain contact. Screen printing generally produces films with poor superconducting transport properties, usually due to a total lack of orientation. Some success in grain alignment has been achieved by using special post annealing procedures. Melt texturing and other grain aligning techniques have resulted in screen printed thick films of $\text{Ba}_2\text{YCu}_3\text{O}_{7-x}$ with $J_c > 3 \times 10^3 \text{ A/cm}^2$ at 77K.⁵³

3.2.2.2 Spray Pyrolysis

Spray pyrolysis^{81,82,83} is a technique for thick or thin film production, related to the spray drying method of powder production. A solution (usually aqueous), containing the desired metals, is sprayed onto a heated (200° to 1000° C) substrate. The solvent is quickly vaporized at the surface of the substrate leaving the metal salts (or their

decomposition products) at the substrate surface. If the surface temperature is sufficiently high, the superconducting phase can result after the initial decomposition of the salts.

Most spray pyrolysis techniques produce films which require a post anneal. The size of the droplets and flow rate of the spray are extremely important parameters to be controlled.

Ultrasonic spray nozzles are frequently used.^{84,85} Large droplets form large particulates on the surface of the film and result in a very inhomogeneous, rough coating. The aerosol flow has to be kept at a level that is fast enough for good nucleation and the thermal power at the substrate must be sufficient to maintain the desired temperature. The technique, in addition to its simplicity, has the advantage of being able to coat large areas with superconducting material, a desired feature for magnetic shielding applications.

However, film quality (J_c , T_c etc.) is usually far below that of vacuum produced thin films.⁸⁶

3.3 Notes and References

- ¹ T. Kubo and K. Shinriki, *J. Chem. Soc. Jpn., Ind. Chem. Sect.* **55**, 49 (1952).
- ² L. K. Templeton and J. A. Pask, *J. Am. Ceram. Soc.* **42**, 212 (1959).
- ³ A. Beauger, J. C. Multin, and J. C. Neipce, *J. Mater. Sci.* **18**, 3041, (1983).
- ⁴ A. Beauger, J. C. Multin, and J. C. Neipce, *J. Mater. Sci.* **18**, 3543, (1983).
- ⁵ A. Manthiram and J. B. Goodenough, *Nature* **329**, 701 (1987).
- ⁶ X. Z. Wang, M. Henry, J. Livage, and I. Rosenman, *Solid St. Commun.* **64**, 881 (1987).
- ⁷ A. Das Sharma, R. N. Basu, and H. S. Maiti, *J. Mater. Sci.* **11**, 122 (1992).
- ⁸ J. G. Bednorz and K. A. Muller, *Z. Phys. B* **64**, 189 (1986).
- ⁹ A. M. Kini, U. Geiser, H-C. I. Kao, K. D. Carlson, H. H. Wang, M. R. Monaghan, J. M. Williams, *Inorg. Chem.* **26**, 1836 (1987).
- ¹⁰ H. S. Horowitz, S. J. McLain, A. W. Sleight, J. D. Druliner, P. L. Gai, M. J. Van Kavelaar, J. L. Wagner, B. D. Biggs, and S. J. Poon, *Science* **243**, 66 (1989).
- ¹¹ D. I. Dos Santos, U. Balacandran, R. A. Guttschow, and R. B. Poeppel, *J. Non-Cryst. Sol.* **121**, 448 (1990).
- ¹² R. W. Schaeffer, J. Macho, R. E. Salomon, G. H. Myer, J. E. Crow, and P. Wise, *J. Supercon.* **4**, 5 (1991).
- ¹³ R. W. Schaeffer, *Doctoral Dissertation*, Temple University, Philadelphia, PA, 1992.
- ¹⁴ W. S. Clabaugh, E. M. Swiggard, and R. Gilchrist, *J. Res. Natl. Bur. Stand.* **56**, 289 (1956).
- ¹⁵ P. K. Gallagher, F. Schrey, and F. V. DiMarcello, *J. Am. Ceram. Soc.* **46**, 359 (1963).

- ¹⁶ K. Kiss, J. Madger, M. S. Vukasovich, and R. J. Lockhart, *J. Am. Ceram. Soc.* **49**, 291 (1966).
- ¹⁷ T. Tunkasiri and G. Rujjanagul, *J. Mater. Sci. Lett.* **13**, 165 (1994).
- ¹⁸ M. Stockenhuber, H. Mayer, and J. A. Lercher, *J. Am. Ceram. Soc.* **76**, 1185 (1993).
- ¹⁹ S. Katayama and M. Sekine, *J. Mater. Res.* **5**, 683 (1990).
- ²⁰ C. Sanchez, J. Livage, M. Henry, and F. Babonneau, *J. Non-Cryst. Solids* **100**, 65 (1988).
- ²¹ G. Pfaff, *Chem. Mater.* **6**, 58 (1994).
- ²² G. Pfaff, *J. Mater. Chem.* **2**, 591 (1992).
- ²³ S. Barboux-Doeuff and C. Sanchez, *Mater. Res. Bull.* **29**, 1 (1994).
- ²⁴ P. P. Phule and S. H. Risbud, *J. Mater. Sci.* **25**, 1169 (1990).
- ²⁵ K. R. Thampi, M. Subba Rao, W. Schwartz, M. Gratzel, and J. Kiwi, *J. Chem. Soc. Faraday Trans.* **84**, 1703 (1988).
- ²⁶ M. Kakihana, L. Borjesson, S. Eriksson, and P. Svendlindh, *J. Appl. Phys.* **69**, 867 (1991).
- ²⁷ E. Ruckenstein, S. Narain, and N. L. Wu, *J. Mater. Res.* **4**, 267 (1989).
- ²⁸ T. M. Shaw, D. Dinos, P. E. Batson, A. G. Schrott, D. R. Clarke, and P. R. Duncombe, *J. Mater. Res.* **5**, 1176 (1990).
- ²⁹ G. L. Messing, S. C. Zhang, and G. V. Jayanthi, *J. Am. Ceram. Soc.* **76**, 2707 (1993).
- ³⁰ G. Gyurov, I. Kristova, P. Peshev, and M. V. Abrashev, *Mat. Res. Bull.* **28**, 1067 (1993).

- ³¹ T. L. Ward, T. T. Kodas, A. H. Carim, D. M. Kroeger, and H. Hsu, *J. Mater. Res.* **7**, 827 (1992).
- ³² M. Awando, K. Kani, Y. Takao, and H. Tagaki, *Jpn. J. Appl. Phys.* **30**, L806 (1991).
- ³³ T. G. Carreno, A. Misfud, C. J. Cerna, and J. M. Palacios, *Mater. Chem. Phys.* **27**, 287 (1991).
- ³⁴ T. J. Gardner and G. L. Messing, *Am. Ceram. Soc. Bull.* **64**, 1498 (1984).
- ³⁵ M. J. Ruthner, *Sci. Sintering* **6**, 81 (1974).
- ³⁶ K. Kourtakis, M. Robbins and P. K. Gallagher, *J. Solid St. Chem.* **82**, 290 (1989).
- ³⁷ K. Kourtakis, M. Robbins and P. K. Gallagher, and T. Teifel, *J. Mater. Res.* **4**, 1289 (1989).
- ³⁸ T. M. Orza, J. C. Jha, and E. I. Ezekiel, *J. Indian Chem. Soc.* **45**, 420 (1968).
- ³⁹ F. J. Schnettler, F. R. Monforte, and W. W. Rhodes, *Sci. Ceram.* **4**, 79 (1968).
- ⁴⁰ K. H. Song, H. K. Liu, S. X. Dou, and C. Sorrel, *J. Amer. Ceram. Soc.* **73**, 1771 (1990).
- ⁴¹ P. Krishnaraj, M. Lelovic, N. G. Eror, and U. Balachandran, *Physica C* **215**, 305 (1993).
- ⁴² N. V. Coppa, W. L. Hults, J. L. Smith, and J. Brynestad, *J. Mater. Res.* **10**, 2510 (1994).
- ⁴³ E. L. Brosha, E. Sanchez, P. K. Davies, N. V. Coppa, A. Thomas, and R. E. Salomon, *Physica C* **184**, 353 (1991).
- ⁴⁴ J. Karpinski, E. Kaldis, E. Jilek, S. Rusiecki, and B. Bucher, *Nature* **336**, 660 (1988).

- ⁴⁵ D. E. Morris, J. H. Nickel, J. Y. T. Wei, N. G. Asmer, J. S. Scott, U. M. Scheven, C. T. Hultgren, A. G. Markelz, J. E. Post, P. J. Heaney, D. R. Velben, and R. M. Halzen, *Phys. Rev. B* **37**, 9353 (1989).
- ⁴⁶ R. J. Cava, J. J. Krajewski, W. F. Peck Jr., B. Batlogg, L. W. Rupp Jr., R. M. Flemming, W. P. James, and P. Marsh, *Nature* **338**, 328 (1989).
- ⁴⁷ N. V. Coppa, G. H. Myer, R. E. Salomon, A. Bura, J. W. O'Reilley, J. E. Crow, and P. K. Davies, *J. Mater. Res.* **7**, 2017 (1992).
- ⁴⁸ J. Kirchnerova and B. D. Hibbert, *Mat. Res. Bull.* **25**, 585 (1990).
- ⁴⁹ H. G. Schneider and V. Ruth, Editors, *Advances in Epitaxy and Endotaxy*, VEB Deutscher Verlag für Grundstoffindustrie (Leipzig, 1971).
- ⁵⁰ L. Luo, X. D. Wu, R. C. Dye, R. E. Muenchausen, S. R. Foltyn, Y. Coulter, and C. J. Marriore, *Appl. Phys. Lett.* **59**, 2043 (1991).
- ⁵¹ A. Mogro-Campero, L. G. Turner, E. L. Hall, M. F. Garbauskus, and N. Lewis, *Appl. Phys. Lett.* **54**, 2719 (1989).
- ⁵² A. Mogro-Campero, L. G. Turner, and E. L. Hall, *J. Appl. Phys.* **65**, 4951 (1989).
- ⁵³ J. Tabuchi and K. Utsumi, *Appl. Phys. Lett.* **53**, 606 (1988).
- ⁵⁴ C. T. Cheung and E. Ruckenstein, *J. Mater. Res.* **4**, 1 (1989).
- ⁵⁵ C. H. Stroessel, R. F. Bunshah, S. Prakash, and H. R. Fetterman, *J. Supercon.* **6**, 1 (1993).
- ⁵⁶ J. Gao, Y. Z. Zhang, B. R. Zhao, P. Out, C. W. Yuan, and L. Li, *Appl. Phys. Lett.* **53**, 2675 (1988).

- ⁵⁷ K. Setsune, T. Kamada, H. Adachi, and K. Wasa, *J. Appl. Phys.* **65**, 1318 (1988).
- ⁵⁸ T. I. Selinder, G. Larsson, U. Helmersson, and S. Rudner, *Supercond. Sci. Technol.* **4**, 379 (1991).
- ⁵⁹ J. Kwo, *J. Crystal Growth* **111**, 965 (1991).
- ⁶⁰ H. S. Wang, D. Eissler, W. Dietsche, A. Fischer, and K. Ploog, *J. Crystal Growth* **127**, 655 (1993).
- ⁶¹ B. R. Johnson, K. M. Beauchamp, T. Wang, J. X. Lui, K. A. McGreer, J. C. Wan, M. Tuominen, Y. J. Zhang, M. L. Mecartney, and A. M. Goldman, *Appl. Phys. Lett.* **56**, 1911 (1990).
- ⁶² R. H. Ono, *MRS Bull.* **8**, 34 (1992).
- ⁶³ D. Dijkamp, T. Venkatesan, X. D. Wu, S. A. Shaheen, N. Jisrawi, Y. H. Min-Lee, W. L. McLean, and M. Croft, *Appl. Phys. Lett.* **51**, 619 (1987).
- ⁶⁴ T. Venkatesan, E. W. Chase, X. D. Wu, A. Inam, C. C. Cheng, and F. K. Skokoohi, *Appl. Phys. Lett.* **53**, 243 (1988).
- ⁶⁵ X. X. Xi, T. Venkatesan, X. D. Wu, A. Inam, C. C. Chang, R. Ramesh, D. M. Hwang, T. S. Ravi, A. Findikoglu, D. Hemmick, S. Etemad, J. A. Martinez, and B. Wilkens, *IEEE Trans. Magnet.* **27**, 928 (1991).
- ⁶⁶ S. R. Foltyn, P. Tiwari, R. C. Dye, M. Q. Le, and X. D. Wu, *Appl. Phys. Lett.* **63**, 1848 (1993).
- ⁶⁷ H. J. Chang, Y. Doshida, Y. Watanabe, K. Shimizu,, Y. Okamoto, R. Akihama, and J. T. Song, *Cryogenics* **32**, 279 (1992).

- ⁶⁸ T. Terashima, K. Ijima, K. Yamamoto, Y. Bando, and H. Mazaki, *Jpn. J. Appl. Phys.* **55**, 504 (1989).
- ⁶⁹ S. Prakash, D. M. Umarjee, H. J. Doerr, C. V. Deshpandey, and R. F. Brunshah, *Appl. Phys. Lett.* **55**, 504 (1989).
- ⁷⁰ Q. Li, O. Meyer, X. X. Xi, J. Geerk, and G. Linker, *Appl. Phys. Lett.* **55**, 1560 (1989).
- ⁷¹ M. Leskela, H. Mosla, and L. Niinisto, *Supercond. Sci. Technol.* **6**, 627 (1993).
- ⁷² O. Thomas, E. Mossang, J. Fick, F. Weiss, R. Madar, J. P. Senateur, S. K. Agarwal, C. Schlenker, M. Ingold, P. Germi, and M. Pernet, *Physica C* **185-189**, 2113 (1991).
- ⁷³ H. G. Lee, S. D. Park, S. W. Yang, H. S. Shin, and D. Y. Won, *Jpn. J. Appl. Phys.* **31**, L157 (1992).
- ⁷⁴ See for example, J. C. Angus and C. C. Hayman, *Science* **241**, 913 (1988).
- ⁷⁵ H. Onishi, H. Harima, Y. Kusakabe, M. Kobayashi, S. Hoshinouchi, and K. Tachibana, *Jpn. J. Appl. Phys.* **29**, L2041(1990).
- ⁷⁶ T. Tsuruoka, R. Kawasaki, and H. Abe, *Jpn. J. Appl. Phys.* **28**, L1800 (1989).
- ⁷⁷ P. Stastny, R. Kuzel, and V. Skacel, *J. Less. Comm. Metals* **164 & 165**, 464 (1989).
- ⁷⁸ J. M. Aponte and M Octavio, *J. Appl. Phys.* **66**, 1480 (1990).
- ⁷⁹ J. Tabuchi and K. Utsumi, *Appl. Phys. Lett.* **53**, 606 (1989).
- ⁸⁰ L. Zeng, Z. Zijiang, L. Zhang, H. Chen, Z. Quain, and D Wu, *Appl. Phys. Lett.* **56**, 1573 (1990).
- ⁸¹ S. J. Golden, H. Isotalo, M. Lanham, J. Mayer, F. F. Lange, and M. Ruhle, *J. Mater. Res.* **5**, 1605 (1990).

- ⁸² A. A. Hussain and M. Sayer, *J. Supercon.* **4**, 385 (1991).
- ⁸³ M. Jergel, S. Chromik, V. Strbik, V. Smatko, F. Hanic, G. Plesch, S. Buchta, and S. Valtynoiva, *Supercond. Sci. Technol.* **5**, 225 (1992).
- ⁸⁴ M. Langlet, E. Senet, J. L. Deschanvres, G. Delabouglise, F. Weiss, and J. C. Jourbert, *J. Less Comm. Metals* **151**, 399 (1989).
- ⁸⁵ S. P. S. Arya, and H. E. Hintermann, *Thin Solid Films* **193-194**, 841 (1990).
- ⁸⁶ For example, see reference 81.

PART II

EXPERIMENTAL METHODS AND RESULTS

CHAPTER 4

CHARACTERIZATION OF SOLID STATE MATERIALS

In this chapter, the first of the experimental part of this dissertation, the analytical techniques that were used to characterize the perovskite oxide films and powders synthesized in this work will be reviewed and the general experimental procedures will be given. The techniques will be divided into three general areas; characterization of chemical properties, characterization of structural and morphological properties, and characterization of physical properties. The characterization of chemical properties included thermogravimetric analysis (TGA), and differential thermal analysis (DTA). These methods were used to characterize precursor samples. TGA was used as the basis for the protocol of thermal treatments to which precursor powders were subjected. DTA was used to screen for melting of precursor powders during thermal processing, a possible source of phase separation and loss of atomic level mixing. This information was important in helping to determine the thermal processing protocols for freeze dried powders. The structural and morphological properties of final products and precursors were studied by powder x-ray diffraction (XRD), transmission electron microscopy (TEM), and scanning electron microscopy (SEM). XRD was used to determine the phase composition and purity of the powder and film samples produced in this work. In the production of ceramic phases (films or powders), the particle size and morphology is of great importance. Small uniform particles improve the sintering characteristics of ceramic

compacts by allowing for higher green body densities. The morphology of the powders and films prepared in the work was studied with TEM and SEM. Finally, the high temperature superconductors prepared in this work have interesting physical properties that are as indicative of sample quality as the structural and morphological properties mentioned above. When cooled to below the superconducting transition temperature, samples should exhibit zero resistance to electric current and perfect diamagnetism (below the critical magnetic field). The temperature of this superconducting transition can be measured by the onset of either of these two phenomena and the result correlated to the quality of the sample.

4.1 Characterization of Chemical Properties

4.1.1 Thermogravimetric Analysis

Thermogravimetric analysis (TGA) was performed on freeze dried precursors and acetate glass precursors with a Perkin Elmer TGS-2 thermogravimetric analyzer. Precursors were placed in gold or platinum sample pans, ramped to $\sim 1000^{\circ}\text{C}$ at a rate of $10^{\circ}\text{C}/\text{min}$, and the mass was recorded with increasing temperature. A plot of these data versus sample mass indicated the decomposition temperature of the precursor. This technique also made evident any evaporative loss of reactants. The complete decomposition of the salts was indicated by the lowest temperature where no mass change occurred with increasing temperature ($dm/dT=0$).

4.1.2 Gross Gravimetric Analysis

Gross gravimetric analysis was performed to determine the formula weight of certain unknown compounds, or samples with varying water content. Samples were decomposed to their oxides by heating them to temperatures well beyond the decomposition temperatures of the compounds. The percent of mass lost was used to calculate the formula weight of the starting compound. The procedure consisted of heating clean, platinum crucibles (with lids) to 900° C in a box furnace until a constant mass was achieved upon weighing. Quantitative analytical techniques were used throughout this procedure. A known amount of the sample to be analyzed was added to the crucibles and they were calcined in a box furnace at 900° C for 2 to 6h. After this time period the samples were cooled while in the furnace to ~100° C, and then cooled to room temperature in a dessicator. They were then weighed again to determine the mass of oxide recovered. The formula weight of the oxide was used to determine the formula weight of the unknown sample. Samples were analyzed in triplicate.

4.1.3 Differential Thermal Analysis

Differential thermal analysis (DTA) was performed on freeze dried SYNROC precursors in a TA Instruments 2100 Simultaneous TGA-DTA. Samples were run at 20° C/min in flowing O₂ (120 mL/min) while simultaneously recording the sample mass, the sample temperature and the temperature of a reference material (α -Al₂O₃). Phase changes in the sample are evident when a discontinuity occurs between the sample temperature and the reference temperature.

4.2 Characterization of Structural and Morphological Properties

4.2.1 Powder x-ray Diffraction

For both films and powders, the method used for phase characterization was powder x-ray diffraction (XRD). In this procedure, a powder or series of small crystallites is placed in the path of a monochromatic beam of x-rays. The x-rays are diffracted by the individual planes of the crystallites when the Bragg equation;

$$n\lambda=2d\sin\Theta, \quad \text{eq. 3.1}$$

where n is an integer representing the order of a particular reflection, d is the spacing between reflecting planes, and Θ is the angle between the incident x-ray beam and plane of the sample, is satisfied. The instrument rotates the sample surface while scanning the detector through a designated range of degrees of 2Θ at a predetermined rate. Reflected x-ray intensity measurements are made at close intervals (usually every $0.02^\circ 2\Theta$) and are plotted against 2Θ to give the XRD pattern. It is accepted that only the three most intense peaks of a phase need be detected for qualitative identification of that phase in a sample.¹ However, in this work all diffraction lines and their intensities were considered in analysis of collected data.

The XRD measurements made for this work were taken at two different locations, and the experimental procedures for each location differ due to instrumental specifications. The XRD patterns of the high temperature superconductor samples (Chapters 7 and 8) were performed at Temple University with a Rigaku D/max-B x-ray diffractometer using

Cu $K\alpha_1$ radiation ($\lambda=1.54060\text{\AA}$), which was filtered from a Cu x-ray tube by the use of a graphite monochromator. The patterns were typically taken from 3° to $90^\circ 2\Theta$ for the Bi-Sr-Ca-Cu-O system but were generally only taken from 20° to $70^\circ 2\Theta$ for the Ba-Y-Cu-O system since no peaks of interest for $\text{Ba}_2\text{YCu}_3\text{O}_{7-x}$ or any common impurities of the system lie in these upper or lower regions of 2Θ . The scan rate was set at $3^\circ 2\Theta/\text{min}$ for preliminary scans and lowered to $1^\circ 2\Theta/\text{min}$ if a more precise pattern was desired. Samples were automatically rotated to minimize preferred orientation effects. The Rigaku D/max-B was fitted with an automatic sample changer capable of holding and changing up to forty samples at a time.

The samples for powder XRD analysis were prepared by grinding the powder in an agate mortar and pestle until no inhomogeneities were visually apparent. This powder was then placed into circular glass slides with a circular, ground glass depression on one side. The powder was gently set into the depression by sliding a glass slide across the surface. This procedure also served to sufficiently smooth out the surface of the powder. A rough surface destroys the planar geometry necessary for proper determination of the angles of reflection. However, sliding the glass across the surface of the sample may serve to orient several reflections with the plane of the slide.² The powder was then held in place by adding a few drops of a solution of Duco cement in acetone (~ 3 wt% Duco cement). The non-reactivity of this Duco cement solution to both the Ba-Y-Cu-O and Bi-Sr-Ca-Cu-O systems has been previously established.³

Thin and thick films were studied in XRD by mounting the films directly into circular aluminum discs in which a square $1\frac{1}{4}$ in. x $1\frac{1}{4}$ in. depression was cut. The films

were held in place by the positioning of an Apiezon clay between the back of the film and the aluminum disc. This clay also served to allow the film to be optically flattened with respect to the aluminum disc by placing the film under a plate of glass and applying manual pressure.

The XRD data were analyzed using Rigaku software and standard XRD card files on cd-ROM from the Joint Committee on Powder Diffraction Standards (JCPDS). The Rigaku software contained several programs of which the most commonly used were for peak finding, search matching against JCPDS standard files, and a charting program for producing hard copies of the patterns. The software was also capable of calculating unit cell dimensions for a given, single phase pattern.

The XRD patterns of SYNROC-B and BaTiO₃ samples (Chapters 5 and 6) were taken at Los Alamos National Laboratory using a Sintag 5000 x-ray diffractometer. Data was collected using CuK_{α1} radiation ($\lambda=1.54060 \text{ \AA}$) while rotating the sample and continuously scanning 2Θ at $1^\circ/\text{min}$ from $3^\circ 2\Theta$ to $90^\circ 2\Theta$. Samples were ground to fine powders and horizontally mounted on quartz zero-background plates. A thin layer of randomly textured Dow Corning high vacuum grease was used to hold the powder samples in place. Standard diffraction file analysis was performed using Sintag software and JCPDS files, or by comparing d-spacings to those found in the literature.

4.2.2 Scanning Electron Microscopy

Determining the extent of phase purity is not the only important analysis for complete judgment of the quality of a particular sample of a ceramic material. The particle

size, shape, and uniformity (morphology) are also of great importance for industrial application as all of these factors have an effect on the overall sintering characteristics of the materials. In this work, the morphology of bulk powders and thin film superconductors was studied using scanning electron microscopy.

Scanning electron microscopy (SEM) allows resolution at higher magnification than optical microscopy due to the shorter wavelength (with respect to visible light) of the electrons used. The method suffers from the drawback that the samples studied must be relatively good electrical conductors to prevent charge buildup. Non-conducting samples can be studied by sputtering the samples with a thin layer of gold to allow surface conduction and charge dissipation. Using this technique, the morphology of sub-micrometer particles could be observed, compared, and measured.

A Phillips, 501-SEM was used throughout the scanning electron microscopy studies.⁴ Powder samples of $\text{Ba}_2\text{YCu}_3\text{O}_{7-x}$ and $\text{Bi}_2\text{Sr}_2\text{Ca}_2\text{Cu}_3\text{O}_{10}$ final products, as well as other electrically conductive samples, were prepared for SEM analysis by gently dusting the powder onto 3M copper conductive tape which was then attached to an aluminum sample mount. Alternatively, the sample could be dusted onto a aluminum sample holder onto which a thin layer of silver paint has been applied. Mounting the sample on copper tape has several advantages over the silver paint method. (1) A smoother background is evident in the finished micrograph. (2) The aluminum sample mounts are more easily reused, and (3), the solvent of the silver paint wets the grains of the sample, possibly causing agglomeration through surface tension. Samples which were not sufficiently

conducting (usually precursor samples) were sputtered with a thin layer of gold to allow charge dissipation.

Film samples were prepared for SEM analysis by attaching the film to an aluminum sample holder with conductive, double sided graphite tape. The tape was allowed to slightly overlap to the coated side of the substrate to allow electric conduction around the highly resistive substrate. A measurement of the thickness of the film could be obtained by mounting the film perpendicular to the aluminum sample holder.

4.2.3 High Resolution Transmission Electron Microscopy

In transmission electron microscopy (TEM), a focused beam of electrons passes through a sample, a series of magnetic lenses, and eventually to a fluorescent screen, where an image of the sample forms. The basic components of a transmission electron microscope are given schematically in Figure 4.1. Samples for TEM must be very thin (~200nm) because the electron beam must pass through the sample. TEM can also be utilized to gather structural information about small regions of a sample (<1 μ m in diameter) by obtaining an electron diffraction pattern. The results can be used in combination with x-ray diffraction for a more complete structural determination of a sample.⁵ The fine powder BaTiO₃ samples were prepared for TEM analysis by dispersing the powder in an ultrasonic acetone bath and allowing the particles to fall into a holey carbon grid.⁶

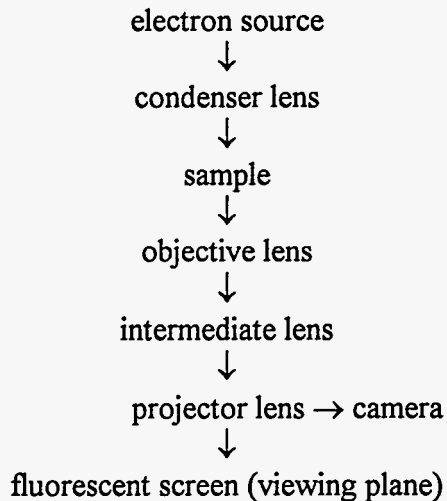


Figure 4.1. A schematic of the basic components of a transmission electron microscope (from reference 5).

4.3 Characterization of Physical Properties

4.3.1 Electrical Measurements

The resistivity versus temperature of high temperature superconducting samples was measured via the standard four point probe method. Bulk samples were pressed (1 kbar) into bars of 3mm x 3mm x 20mm and sintered under varying conditions, depending on composition. Four thin copper wire (Belden #36) leads were attached to the bars with silver conducting paint. The samples were mounted on a cold stage which was subsequently sealed, evacuated and cooled to 15 K via a closed cycle refrigerator. The sample temperature was monitored by a silicon diode temperature sensor and controlled by a Lakeshore Cryogenics (model # DRC 91C) temperature controller. The sample temperature was raised to room temperature while a direct current (0.1 to 10 mA) was sent through the outer leads of the sample. The voltage between the inner two leads was

read with a Keithley Model 181 Nanovoltmeter. A computer program was written in BASIC to take readings of the voltage at 1 K intervals and store the data in a desk top computer. The resistivity versus temperature measurements on thick and thin film samples were also made with this instrument. The copper wire leads were wrapped around the film several times and attached to the superconducting surface with silver conducting paint.

The same instrument was used for determination of critical current densities (J_c). For J_c measurements, the temperature of the sample was maintained at a constant value (below the superconducting transition temperature) and the current was gradually raised while voltage measurements between the two inner sample contacts were made. When the sample is superconducting, there was no voltage measured between the inner leads of the sample. When the critical current was exceeded, a voltage was measured which increased linearly with increasing current, in accordance with Ohm's Law. The onset current of Ohmic behavior was defined as the critical current for the sample. The critical current density, J_c , was determined by dividing this value by the cross sectional area of the sample.

4.3.2 Magnetic Measurements

A simple device for measuring the magnetic properties of the high temperature superconductors prepared in this work was developed.⁷ The device consisted of an enclosed analytical balance (Fisher A-200DS) with a permanent magnet supported in a position close to the upper glass door of the balance. The magnetic field at the surface of the permanent magnet was 150 gauss. The base of the support rested on the pan of the

balance and the mass of it and the permanent magnet was negated by taring the balance. A styrofoam cup containing a high temperature superconducting sample was then placed directly above the magnet on the glass door. Liquid nitrogen was added to the cup to cool the sample. If the superconducting transition temperature of the material was above 77 K, the balance responded to the force exerted between the sample and the magnet.

Multiplying the balance response in kilograms by the acceleration of gravity ($\sim 9.8\text{m/s}^2$) resulted in a determination of the Meissner force in Newtons. Using this technique, a quick and nondestructive judgment of sample quality was attained. Comparative studies could be performed if pellets of equal mass and dimensions were used. This device was later expanded upon⁸ to give a magnetic determination of the superconducting transition temperature in high temperature superconducting samples (see Figure 4.2). Positioning of a silicon diode temperature sensor in thermal contact with the superconducting sample allowed simultaneous monitoring of the sample temperature and Meissner force. Balance response and temperature data were recorded by a desk top computer, allowing a plot of magnetic response versus temperature to be produced. The superconducting transition temperature of the sample was defined as the onset temperature of diamagnetic response.

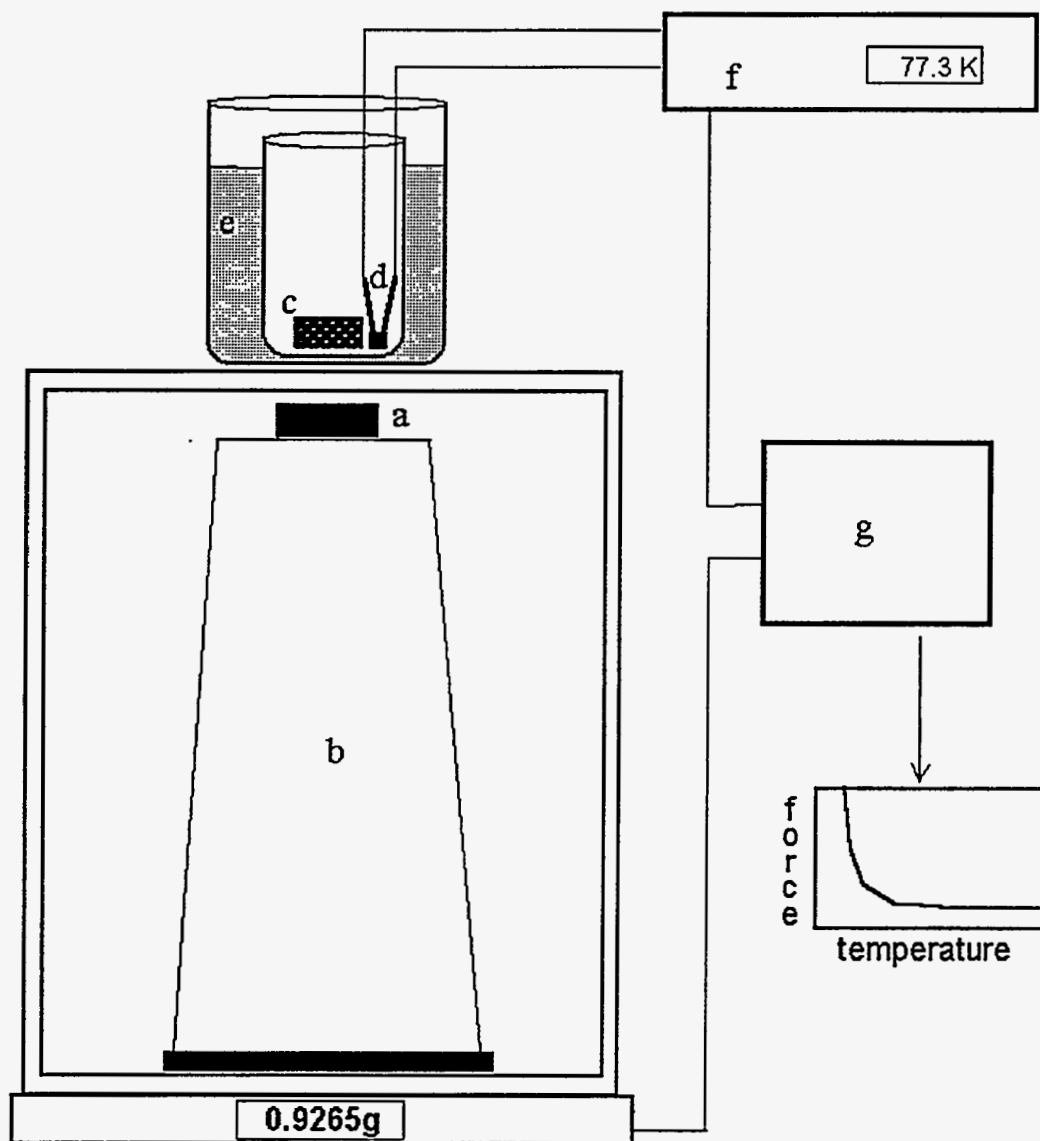


Figure 4.2. A schematic of the experimental setup used for measuring the Meissner force exerted between a permanent magnet and a superconducting pellet with varying temperature. The labeled parts correspond to; a) permanent magnet, b) low mass styrofoam support, c) superconducting sample, d) silicon diode temperature sensor, e) liquid nitrogen, f) Lakeshore Cryogenics temperature controller, and g) desk top computer.

4.4 Notes and References

- ¹ B. D. Cullitty, *Elements of X-ray Diffraction*, Addison-Wesley Publishing Co (Reading, MA, 1978).
- ² See reference 1, page 295.
- ³ R. W. Schaeffer, Doctoral Dissertation, Temple University, Philadelphia, PA 19122, (1992).
- ⁴ The author acknowledges Professor Robert Hilfer of the Temple University biology department for the use of the SEM.
- ⁵ A. R. West, *Solid State Chemistry And Its Applications*, John Wiley and Sons (New York, 1984).
- ⁶ The author acknowledges P. C. McIntyre and K. E. Sickafus of Los Alamos National Laboratory for their assistance and TEM work on the nanocrystalline BaTiO₃ powders.
- ⁷ J. McHale, R. W. Schaeffer, and R. E. Salomon, *J. Chem. Ed.* **69**, 1031 (1992).
- ⁸ E. Manas, unpublished research, Temple University, Philadelphia, Pa 19122 (1993).

CHAPTER 5
PREPARATION OF NANOCRYSTALLINE BARIUM TITANATE
VIA THERMAL DECOMPOSITION OF FREEZE DRIED
NITRATE PRECURSORS

The conventional preparation of the technologically important dielectric material, BaTiO₃, was described in section 3.1.1. To briefly summarize this procedure, BaCO₃ and TiO₂ powders are mechanically mixed in a mortar and pestle (or mechanically ball milled), compacted, and calcined at temperatures ranging from 1200° C to 1400° C for up to 48 h. To achieve a reasonable degree of phase purity, and optimum electrical properties, several intermittent grindings and re-pressings are necessary during the thermal treatment. This regimen of repeated high temperature annealing leads to large and non-uniform particle morphology, as sintering occurs between adjacent grains. In this work, an atomically mixed titanium and barium precursor, prepared by freeze drying of nitrate solutions, was used for the preparation of BaTiO₃, and resulted in a drastic reduction in reaction times and temperatures. A degree of control of particle morphology was also possible with the use of freeze dried nitrate precursors and nanocrystalline material was produced.

The success of the freeze dry preparation of BaTiO₃ reported here depended upon the development of a routine for obtaining stable, well characterized (with respect to metal concentration) titanium solutions. A procedure was developed for obtaining the highly water soluble Ti⁴⁺ salt, titanyl nitrate, in powder form. This compound was subsequently

used in the preparation of barium and titanyl nitrate solutions for freeze drying. In this chapter, difficulties in preparing aqueous Ti^{4+} solutions, and the preparation of titanyl nitrate in solution and powder form will be discussed. This will be followed by the experimental details, results, and a discussion of the advantages of the freeze drying route to $BaTiO_3$.¹

5.1 Preparation of Titanyl Nitrate

The successful implementation of the freeze drying route to $BaTiO_3$ rested upon the development of a procedure for obtaining nitrate solutions of titanium. A brief review of the possible choices of anion in the aqueous Ba-Ti system will underscore this necessity. The use of halides is prevented by the volatility and high decomposition temperature of BaF_2 , $BaCl_2$, etc. Thermal processing of a freeze dried mixture of Ba and Ti chlorides would result in a loss of stoichiometry as barium chloride vaporizes. The use of sulfates is prevented by the extreme insolubility of barium sulfate in water. The use of carboxylic acid salts (formates, acetates, etc.,) would result in the formation of barium carbonate upon decomposition of the organic anion. Barium carbonate is a relatively stable phase which requires temperatures in excess of $900^\circ C$ for complete decomposition and has been responsible for lower reaction rates in some systems.² The use of carbonaceous precursors may also result in the buildup of amorphous carbon at grain boundaries in the final ceramic. Amorphous carbon has been shown to be detrimental to the electrical properties of some ceramics.³ Nitrates were the anion of choice for several reasons.

Among these reasons were; (1) they generally have a low decomposition temperature, (2) they are relatively non-volatile, and (3) they have a high aqueous solubility.

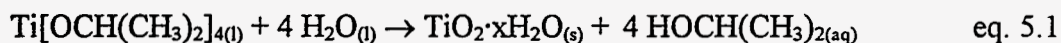
The choice of anion was further complicated by the limited number of commercially available titanium salts and the insolubility of Ti, TiO, Ti₂O₃ and TiO₂. Commercially available⁴ titanium (IV) compounds include TiF₄, TiCl₄, TiBr₄, TiI₄, TiO₂, Ti(OCH₂CH₃)₄ and Ti[OCH(CH₃)₂]₄. Of these compounds, the halides are volatile liquids (TiCl₄) or solids (TiF₄, TiBr₄, TiI₄) which are hydrolyzed by even slightly moist air, and can not be accurately weighed without the use of a dry box. The reaction is vigorous in the case of the volatile liquid TiCl₄. Titanium dioxide, whether in its rutile or anatase structure, is an extremely resistant material to attack by mineral acids. The material is practically insoluble in hot sulfuric, nitric, and hydrochloric acids and only slightly attacked by hydrofluoric acid. The lower oxides of titanium, Ti₂O₃ and TiO, are also scarcely soluble in concentrated mineral acids. The metal itself is attacked by concentrated sulfuric and hydrochloric acids but nitric acid has no effect.⁵ Although nitrates were the anion of choice, a titanium nitrate was not commercially available, and could not be directly prepared (e.g., by dissolving titanium oxide or metallic titanium in nitric acid) from a commercially available compound.

5.1.1 Hydrrous Titania

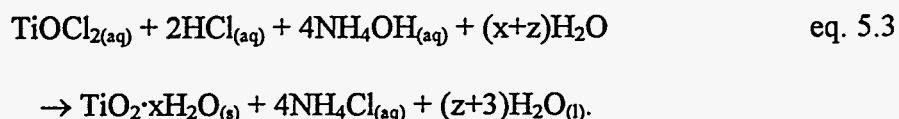
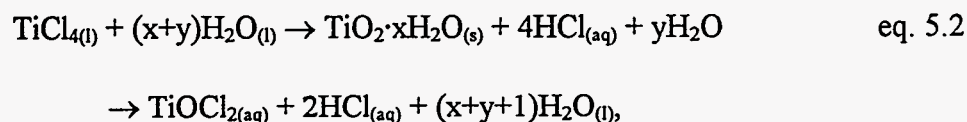
The solubility of TiO₂ in mineral acids strongly depends upon the thermal history of the sample. Strongly roasted samples of TiO₂ (such as those commercially available) are chemically inert. However, freshly prepared TiO₂ can be brought into acidic solution. The

gelatinous precipitate obtained upon the hydrolysis of Ti^{4+} salts ($TiCl_4$, $Ti[OCH(CH_3)_2]_4$, etc.), hydrous titanium dioxide, also called hydrous titania,^{6,7} was used in this work as the source of titanium for the preparation of titanyl nitrate solutions. Hydrous titania exists in two forms, which are designated alpha and beta. The beta form of hydrous titania, $\beta-TiO_2 \cdot xH_2O$, is obtained from hydrolysis of Ti^{4+} solutions on heating to near boiling. The beta form of hydrous titania is only slightly soluble in mineral acids. The alpha form, $\alpha-TiO_2 \cdot xH_2O$, which is readily soluble in acid, results from hydrolysis of cold Ti^{4+} solutions. Aging of the alpha form at room temperature results in a slow conversion to the beta form. An increase in temperature will speed this conversion.⁵ Little is known about the structure of these hydrous oxides.

In this work, there were two independent procedures used for the preparation of hydrous titania. In the first of these, titanium tetra-isopropoxide (TiOPR) was hydrolyzed with excess deionized water (d. H_2O). About 15 g of water was used to hydrolyze each gram of TiOPR by the reaction;



Alternatively, titanium chloride was hydrolyzed by the addition of d. H_2O to produce hydrous titania which subsequently dissolved in the reaction by-product, $HCl_{(aq)}$, to give an aqueous solution of titanyl chloride, $TiOCl_2$. Hydrous titania was then precipitated from this solution by the addition of ammonium hydroxide. The complete reaction sequence is;



The hydrous titania, regardless of the method of preparation, was filtered and washed five times with cold (<10° C) d. H₂O to remove either the ammonium chloride or isopropanol.

5.1.2 Titanyl Nitrate

Dissolving hydrous titania in aqueous nitric acid results in the formation of titanyl nitrate solutions.⁸ These solutions are unstable and concentrated solutions (>1.0 M) and mildly acidic solutions (pH>1.5) will precipitate an amorphous form of titania after a few days (probably β-TiO₂·xH₂O). Dilute solutions (~0.1M) with a pH less than 1.0 have remained stable for a matter of months (longest time period investigated). The instability of these titanyl nitrate solutions prevents the use of “stock solutions” as a quantitative Ti source. In order to guarantee an accurate Ti concentration, each solution need be prepared and subsequently analyzed immediately before it is used. Attempts at crystallizing titanyl nitrate from these solutions were unsuccessful. Evaporation of the water at room temperature results in decomposition of TiO(NO₃)₂ into HNO₃ and an amorphous form of TiO₂ (probably β-TiO₂·xH₂O). The evaporation process was also

hampered by the inability of these solutions to withstand extended heating without precipitation of β - $\text{TiO}_2 \cdot x\text{H}_2\text{O}$.

The preceding problems were overcome with the use of freeze drying technology. A solution of $\text{TiO}(\text{NO}_3)_2$ was frozen by atomization into stirred liquid nitrogen. The water was then removed from the frozen solution by sublimation in a commercial freeze drying apparatus. This yielded a stable, powder form of $\text{TiO}(\text{NO}_3)_2$, which was readily soluble in water, could be accurately analyzed for Ti content and used for the preparation of stoichiometric Ti solutions. The experimental details of the preparation of $\text{TiO}(\text{NO}_3)_2$ in powder form and determined properties of the solid follow.

5.1.3 Experimental Procedure

The reagents used in the preparation of $\text{TiO}(\text{NO}_3)_2$ solutions were titanium tetraisopropoxide, $\text{Ti}[\text{OCH}(\text{CH}_3)_2]_4$, (ultrapure, min 99.999%, obtained from Johnson Matthey) and nitric acid (Baker Ultrex II, Ultrapure Reagent, 70%). To prepare 1.0 mol of $\text{TiO}(\text{NO}_3)_2$, 1.0 mol of TiOPR was hydrolyzed with 2000 mL of d. H_2O and the resulting $\text{TiO}_2 \cdot x\text{H}_2\text{O}$ was filtered and washed five times with 750 mL portions of d. H_2O . The $\text{TiO}_2 \cdot x\text{H}_2\text{O}$ was then dissolved in a mixture of 500 mL HNO_3 and 1500 mL d. H_2O . The mixture was slowly heated and maintained between 60° and 70° C until the solution had completely cleared. The resulting $\text{TiO}(\text{NO}_3)_2$ solution was filtered to remove any suspended particles and dissolved gases and subsequently frozen by atomization into stirred liquid nitrogen. The frozen solution was then placed in a commercial freeze dryer (Vertis XL500) and the water was removed by sublimation at reduced temperature

(-35° C) and pressure (~10 $\mu\text{m Hg}$) over the course of several days. The complete procedure for freeze drying will be covered later in this chapter. After the completion of sublimation and the slow ramping of the sample temperature from -35° C to room temperature (2° C/ h), a solid form of $\text{TiO}(\text{NO}_3)_2$ resulted. The chamber of the freeze drying apparatus was back filled with dry helium and the powder was removed from the sample trays and stored in air tight glass jars. The powder was characterized by powder x-ray diffraction, electron spin resonance, gross gravimetric analysis, thermogravimetric analysis and aqueous solubility experiments.

The freeze drying process used in the preparation of solid $\text{TiO}(\text{NO}_3)_2$ served a different purpose than the freeze drying procedures that follow (for preparation of BaTiO_3 , etc.). In this experiment, freeze drying served to extract a solid product from an unstable solution which would decompose if simply evaporated. In subsequent freeze drying experiments the technique is used as a means of achieving atomic level mixing. For this reason, little attention was paid to the freezing step (atomization into liquid nitrogen) in the preparation of powdered $\text{TiO}(\text{NO}_3)_2$. This step, however, becomes extremely important if atomic mixing is the desired outcome of freeze drying.

5.1.4 Results

The powder had a purple tint when first taken from the freeze dryer but quickly took on a uniform light yellow appearance. The purple tint may be indicative of some Ti^{3+} in the sample which was quickly oxidized to Ti^{4+} by contact with air. The powdered $\text{TiO}(\text{NO}_3)_2$ proved extremely soluble in H_2O . The aqueous solubility was measured at over

200g $\text{TiO}(\text{NO}_3)_2$ per 100 g H_2O . The resulting yellow solution was extremely viscous and decomposed into white TiO_2 and clear HNO_3 after about 48 h. The powder was also found to be hygroscopic. Samples left exposed to air picked up enough atmospheric moisture to become solution. These concentrated solutions precipitated TiO_2 after a short time. This precipitate was dried at room temperature and analyzed by powder x-ray diffraction (XRD). The diffraction pattern of this material consisted of mainly amorphous scattering but displayed some very broad peaks which were centered around the d-spacings of rutile and anatase reported in the JCPDS data files.

The powdered titanyl nitrate was studied using XRD. Samples were sealed under Kapton tape to protect the powder from adsorption of water. The powder, however, proved to be amorphous to XRD, and no structural information could be gathered. At the time of this writing, experiments are underway wherein the $\text{TiO}(\text{NO}_3)_2$ solutions have been frozen very slowly, to possibly obtain a more crystalline material for structural analysis after freeze drying.

Gross gravimetric analysis was performed on the powder to obtain a formula weight for the compound. Three Pt crucibles with lids were cleaned and heated to 900°C until all three displayed a constant mass when weighed. An accurately weighed mass (between 0.2 and 0.5 g) of $\text{TiO}(\text{NO}_3)_2$ was placed in each crucible and calcined at 800°C for 2 h. The crucibles were then cooled to room temperature in a dessicator and weighed. The mass of the resulting powder was calculated and assumed to be TiO_2 . Dividing this mass by the formula weight of TiO_2 (79.9g/ mol) results in the number of moles of Ti present in the sample of $\text{TiO}(\text{NO}_3)_2$. The determined formula weight for the compound

was 179.12g/mol. This number is slightly lower than the theoretical formula weight for anhydrous $\text{TiO}(\text{NO}_3)_2$ of 187.9 g/mol. This low formula weight may be due to some contamination with TiO_2 (e.g., 93% $\text{TiO}(\text{NO}_3)_2$, 7% TiO_2). Table 5.1 shows that this formula weight remained quite consistent with time, suggesting that the compound is relatively stable at room temperature.

Table 5.1 Variation in the gross gravimetrically determined formula weight* for $\text{TiO}(\text{NO}_3)_2$ over the course of 20 days. The compound appears to be stable at room temperature. An error occurred during the first determination of day 7 and the data was discarded.

Days out of freeze dryer	1st determination	2nd determination	3rd determination	average
1	178.49	179.15	178.54	178.73
7	-----	178.60	179.64	179.12
13	178.75	179.58	179.42	179.25
20	179.37	178.91	179.08	179.12

* All values are in g/mol.

Thermogravimetric analysis (TGA) was used to verify this formula weight and determine the temperature of decomposition for the powdered $\text{TiO}(\text{NO}_3)_2$. The TGA plot can be seen in Figure 5.1. The compound begins to lose weight rapidly at about 100° C. The formula weight for the compound that results from the percent weight loss of this TGA is 177.48 g/ mol. This number is in reasonable agreement with the gross gravimetrically determined value.

Gross gravimetric analysis of a more recently prepared batch of $\text{TiO}(\text{NO}_3)_2$ yielded a formula weight of 187.87g/mol, a value very close to the theoretical value.⁹ This latter

sample of $\text{TiO}(\text{NO}_3)_2$ was held in the vacuum chamber of the freeze dryer at a temperature of 25°C and a pressure of $\sim 10\mu\text{m Hg}$ for one week after the low temperature drying step. It is possible that the first batch was not completely dry, and the residual water promoted decomposition of some $\text{TiO}(\text{NO}_3)_2$ into TiO_2 and HNO_3 . This would account for the low formula weight of the first sample.

Although the crystal structure of $\text{TiO}(\text{NO}_3)_2$ could not be determined due to the amorphous nature of the powder, electron spin resonance (ESR) studies have indicated that there are two distinct nitrate groups in the material.¹⁰ One of the nitrate ions had ESR active nitrogen and the other was ESR inactive, indicating that the former was closer to the Ti^{4+} ion. No nitrogen to nitrogen coupling was observed. These observations can be explained using the structural formula $[\text{TiO}(\text{NO}_3)]^+(\text{NO}_3)^-$ instead of $\text{TiO}(\text{NO}_3)_2$.¹¹

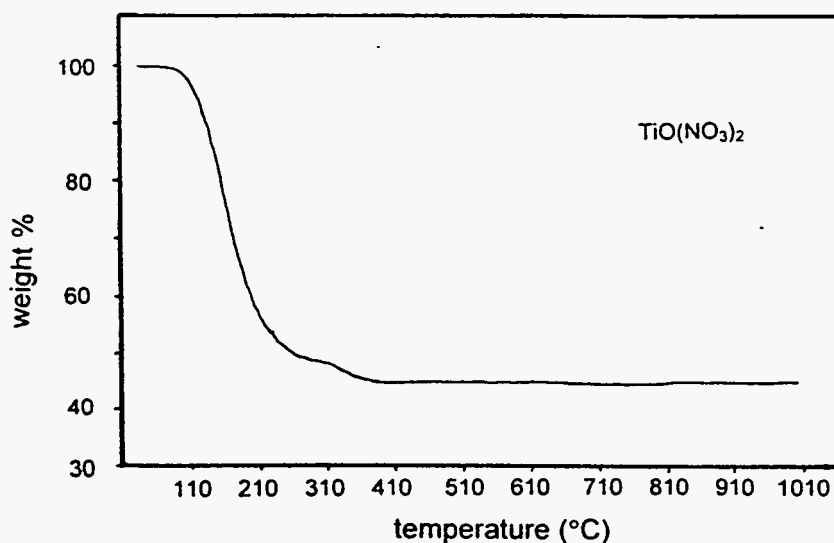


Figure 5.1. A TGA plot for titanyl nitrate.¹²

5.2 Preparation of BaTiO₃ from Freeze Dried Nitrate Solutions

With a ready supply of a water soluble titanium salt, titanyl nitrate solutions were prepared and used for the synthesis of titanate materials by freeze drying. Barium titanate, BaTiO₃, was chosen as the prototype system. Preparation of ceramic materials by freeze drying consists of four general steps; (1) preparation of the solution, (2) rapidly freezing the solution, (3) sublimation of the solvent, and (4) thermal processing of the freeze dried salts. These steps, as they apply to the synthesis of BaTiO₃, are outlined below; followed by the results and a discussion of the preparation of BaTiO₃ from freeze dried nitrate solutions.

5.2.1 Solution Preparation

The typical batch size for preparation of BaTiO₃ was 3 L and contained 0.1500 mol Ti. The concentration of the solutions was kept below 0.06 M in Ba to prevent Ba(NO₃)₂ precipitation in the aerosol before freezing. This limiting value for Ba(NO₃)₂ concentration has been previously established.¹³ The solution was prepared by adding 0.1500 mol powdered TiO(NO₃)₂ and 0.1500 mol crystalline Ba(NO₃)₂ in 1:1 Ti to Ba stoichiometry to 3000 mL of d. H₂O. The purity of the water used is an important factor since any impurities will be concentrated in the solid product. The barium and titanyl nitrate solution was then vacuum filtered through a medium pore size glass fritted filter (Pyrex) to remove dissolved gases and stored in Teflon bottles until ready for the freezing step.

5.2.2 Freezing the Solution

The rate of the freezing of the solution was a critical factor in the preparation of an atomic mixture by freeze drying. The rate must be as high as possible to prevent precipitation and nucleation of the solute and assure that the random dispersion of cations that exists in the solution state is transferred into the solid state. The solutions were rapidly frozen by atomization into stirred liquid nitrogen. To assure a quick rate of freezing the solution was atomized with an ultrasonic spray nozzle capable of producing droplet sizes on the order of $10\mu\text{m}$. An aerosol droplet of pure water with a $10\mu\text{m}$ diameter will freeze in 10^{-5} sec or less when suddenly introduced to temperatures around 77 K .¹⁴ This corresponds to freezing rates of $>10^6\text{ K sec}^{-1}$.

The experimental setup for the rapid freezing of solutions has been described elsewhere in great detail.^{13,15} Briefly, an ultrasonic spray nozzle (Sonotek, 8700-120MS/PS-8S) was used to atomize the solution (see Figure 5.2). The spray nozzle was wrapped with a band heater, maintained at about 65°C , to guarantee that the liquid exiting the nozzle was $\geq 25^\circ\text{C}$. The resulting fine mist fell by gravity into a large Dewar flask of stirred liquid nitrogen. The liquid nitrogen level was automatically controlled at 2.0 to 2.5 cm below the tip of the spray nozzle by the use of a level control. This distance, 2.0 to 2.5 cm, was chosen so that the droplets of solution would enter an area where the temperature was close to 77K almost instantly after leaving the spray nozzle. A distance less than 2 cm from the surface of the liquid nitrogen to the spray nozzle would result in freezing of the solution in the tip of the spray nozzle. A larger distance ($>2.5\text{ cm}$) would introduce the

droplets into an area where the temperature was significantly greater than 77 K, which would result in slower freezing rates and possible phase separation.

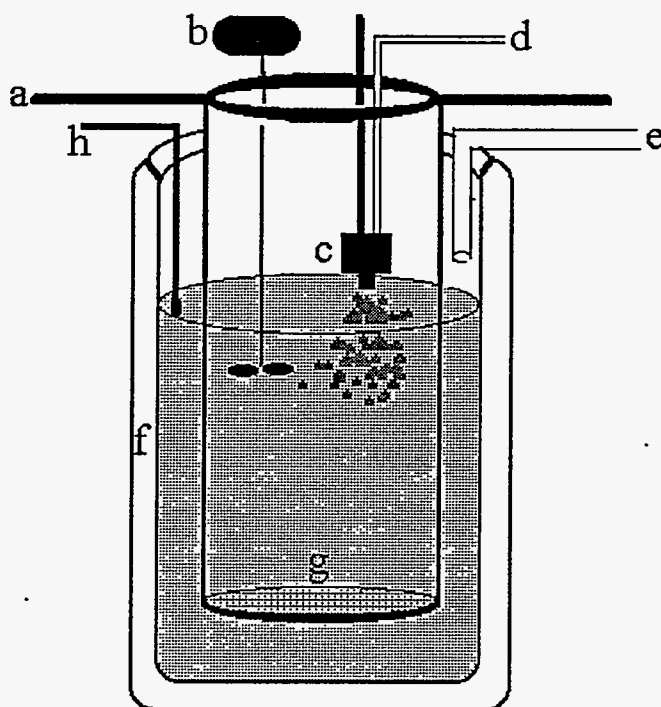


Figure 5.2. A schematic depicting the experimental setup for rapid freezing of solutions. The labeled parts correspond to; a) stainless steel support holding inner Pyrex tube, b) mechanical stirrer, c) ultrasonic spray nozzle, d) solution inlet, e) liquid nitrogen inlet, f) cross section of Dewar flask, and g) stainless steel fine mesh screen.

5.2.3 Sublimation

Once the solute was trapped in a random, atomically mixed state by rapid freezing of the solution, the water was removed via sublimation using a commercial freeze dryer (Vertis XL500). The unit consisted of three shelves in a vacuum chamber on which the

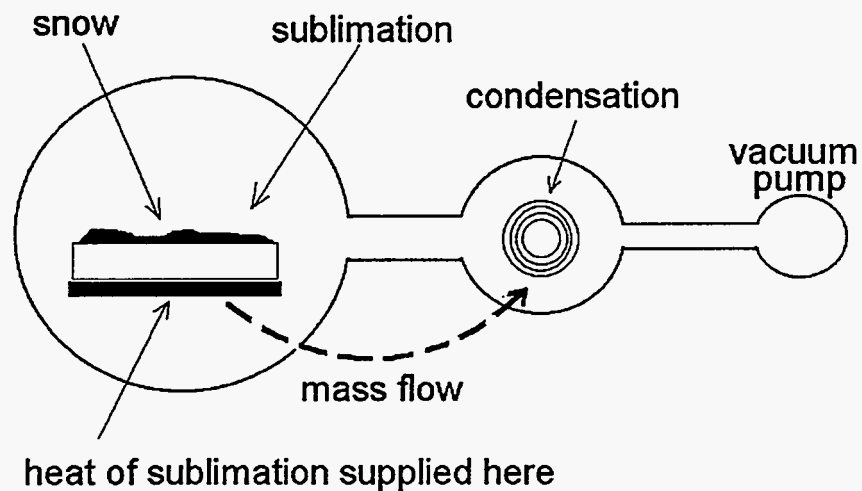


Figure 5.3. A schematic diagram of the apparatus used for freeze drying the solutions. It is the difference in the temperature dependent vapor pressure of water at -70°C (condenser temperature) and -30°C (sample temperature) that drives the mass transport.

frozen sample was uniformly divided in Teflon coated trays. This sample chamber was connected to a condenser that was maintained at -70°C . To speed sublimation, non-condensable gases were removed by a rotary vacuum pump and the pressure in the vacuum chamber was held at $\sim 10\ \mu\text{m Hg}$ at the condenser. The temperature of the shelves was controlled at -30°C by the circulation of a chilled silicon oil. The difference in the temperature dependent vapor pressure of water at -30° and -70°C drives the mass transport. A schematic diagram of the freeze dryer can be seen in Figure 5.3. Although the drying of the $\text{BaTiO}(\text{NO}_3)_x$ sample was carried out at a shelf temperature of -30°C , the temperature of the snow was usually 5 to 10°C lower than the shelf temperature due to the loss of the heat of sublimation. Under these conditions, the sublimation of three liters

of solvent was completed in about five days. The rate of sublimation is primarily limited by the power of the condenser. The end of sublimation is indicated by the equilibration of the shelf temperature and tray temperature (no heat loss in the trays due to the heat of sublimation). When sublimation had ceased, the temperature was raised to 25° C at a rate of 1° C/h to slowly remove any chemically bound water, the concentration of which is temperature dependent. The freeze dried powder, referred to as the *precursor*, was stored in clean glass jars until the thermal processing step.

5.2.4 Thermal Processing

The precursor powder was subjected to various thermal treatments using a Lindberg Model #55035, horizontal tube furnace equipped with a 1 inch inner diameter quartz tube (Figure 5.4). The center of the length of the quartz tube was wrapped in a 5 inch x 4 inch section of platinum foil to provide a more uniform temperature profile. The tube was sealed at both ends with Ultratorr connectors, fitted with o-ring seals, connected to KF flanges. Samples were placed in platinum or gold boats and into the quartz tube at the outer, relatively cool section. The system was then closed and flushed with pure oxygen for 10 min. An oxygen atmosphere was used to prevent the possible formation of BaCO₃ via reaction with atmospheric CO₂. The pressure in the tube was controlled via the use of needle valves at the oxygen inlet and outlet. The pressure was measured with the use of a MKS Baritron 1000 torr pressure gauge, which was placed before the oxygen outlet. With this arrangement, the pressure in the quartz tube could be varied and maintained between 590 torr (atmospheric pressure at Los Alamos, NM) and 1000 torr.

The sample was then plunged into the center of the furnace, without opening the system, by sliding a $\frac{1}{8}$ inch diameter stainless steel rod of proper length through an o-ring seal at the gas outlet side of the tube. The temperature of the furnace was measured and accurately controlled by a chromel-alumel thermocouple which was positioned inside the quartz tube at the center of the heat zone. The platinum or gold boats rested directly on top of this thermocouple during heat treatments. Samples were annealed for ten minutes at 100°C intervals from 300°C , to 1000°C . Based on these preliminary studies, longer anneals at selected temperatures were also performed.

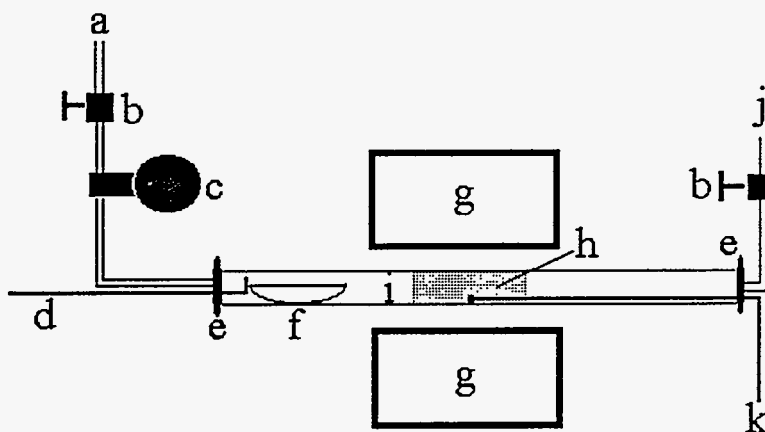


Figure 5.4. A schematic diagram of the furnace setup for thermally processing the freeze dried precursor. The labeled parts correspond to; a) gas outlet, b) needle valve, c) pressure gauge, d) stainless steel rod, e) Ultratorr seal welded to KF flange, f) Pt or Au boat, g) furnace heating element, h) Pt radiation shield, i) quartz tube, j) gas inlet, and k) furnace temperature control thermocouple.

Throughout this work, freeze dried nitrate precursors are referred to as mixed metal nitrates. For example, the freeze dried barium and titanyl nitrate precursor will be

referred to as $\text{BaTiO}(\text{NO}_3)_x$. This is not meant to imply that a double salt has been synthesized, but simply that the mixing of Ba^{2+} , TiO^{2+} , and NO_3^- ions is on the molecular length scale.

5.2.5 Results and Discussion

The freeze dried barium and titanyl nitrate precursor was a very fine, free flowing, light yellow powder. The precursor was studied via XRD to probe for long range order in the sample. The XRD of the precursor (Figure 5.5) showed peaks corresponding to

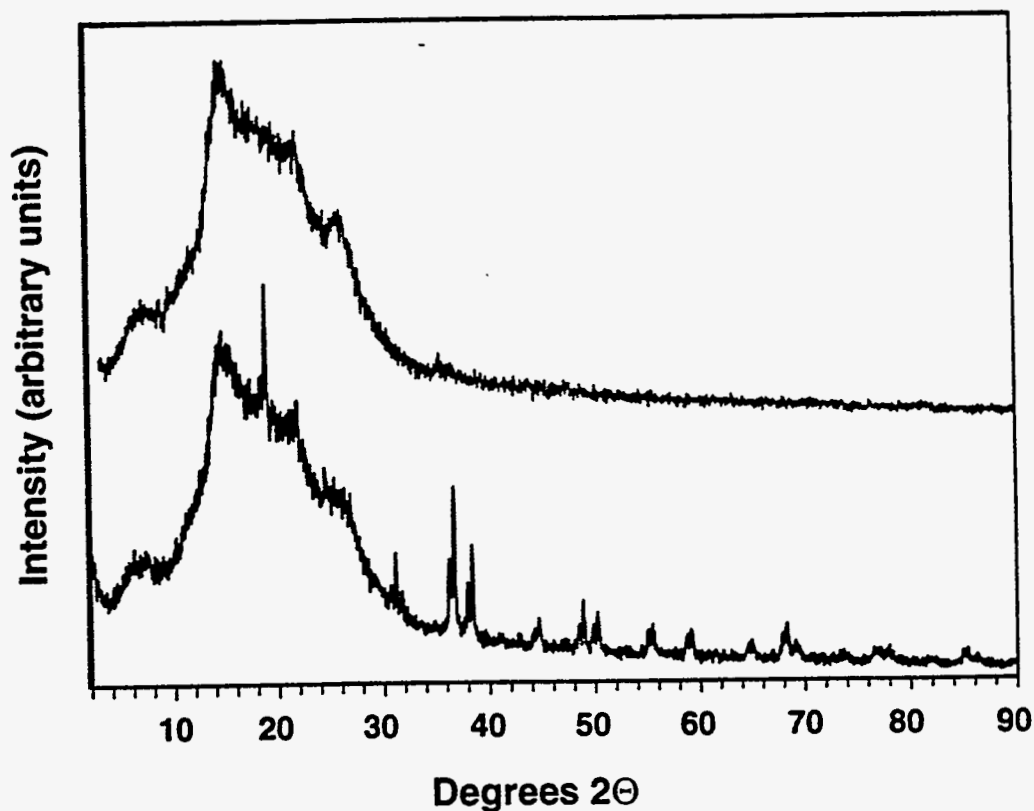


Figure 5.5. The x-ray diffraction pattern for the freeze dried barium and titanyl nitrate precursor. Data was collected with the sample sealed behind Kapton tape. The scattering due to blank Kapton tape is provided for comparison (upper pattern). Barium nitrate peaks are evident in the precursor.

$\text{Ba}(\text{NO}_3)_2$. However, the pattern still displayed a large degree of amorphous scattering. Barium nitrate peaks have been previously seen in the freeze dried precursor powders of yttrium, barium, and copper nitrates.¹⁵ No titanium containing phases could be identified in the precursor. This fact was not surprising, however, since the XRD of pure, freeze dried titanyl nitrate displayed only amorphous scattering.

The precursor powder was subjected to thermogravimetric analysis (TGA) to determine the minimum processing temperature. The TGA was run at a rate of $20^\circ \text{C}/\text{min}$ from room temperature to 1000°C and can be seen in Figure 5.6. The inflection point of the final decomposition occurs at about 620°C . Decomposition is complete at 650°C . The complete decomposition of pure $\text{Ba}(\text{NO}_3)_2$ usually occurs between 600° and 750°C .

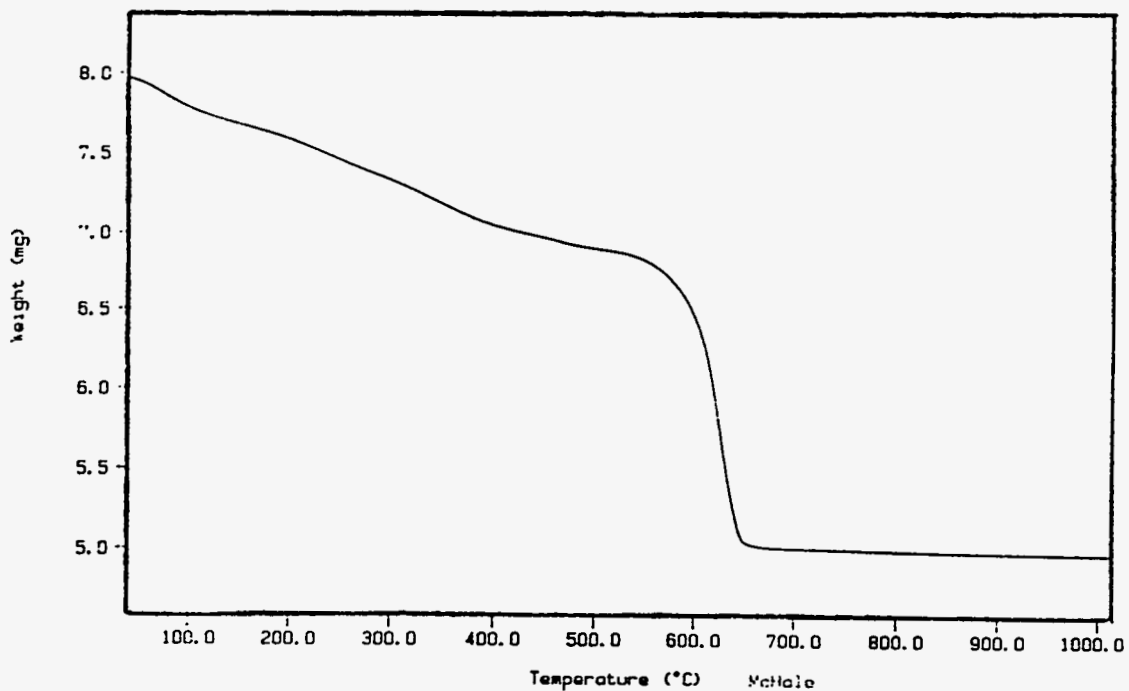


Figure 5.6. A TGA curve for the barium and titanyl nitrate precursor.

This lowering of the decomposition temperature of $\text{Ba}(\text{NO}_3)_2$ is typical of atomic mixtures.¹⁵ Also noteworthy at this time is the lack of melting of $\text{Ba}(\text{NO}_3)_2$ in the freeze dried precursor. The accepted melting point for $\text{Ba}(\text{NO}_3)_2$ is 592°C .¹⁶ Yet there is no visual or microscopic evidence of melting in the precursor after thermal processing at temperatures between 300° and 1000°C .

The XRD pattern of the freeze dried barium and titanium nitrate precursor heated to 1000°C in an O_2 atmosphere at 600 torr (slightly above atmospheric pressure at Los Alamos, NM) for 10 min is that of phase pure BaTiO_3 . Table 5.2 compares the collected

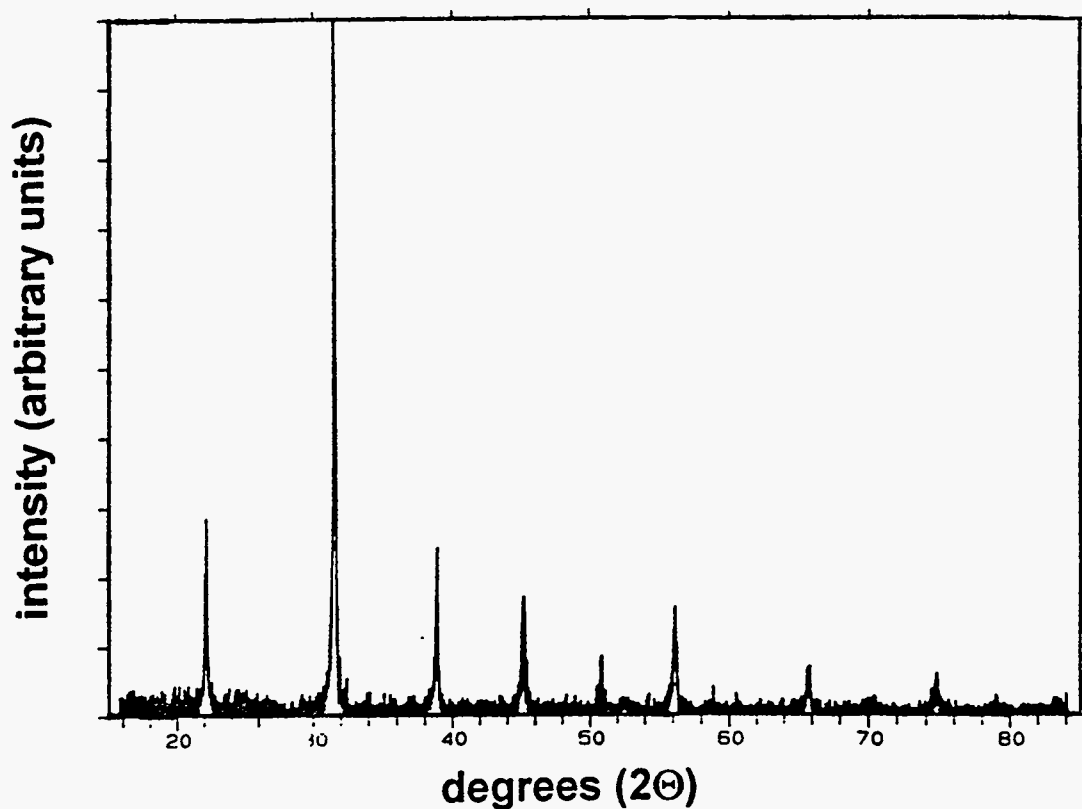


Figure 5.7. The XRD pattern of a BaTiO_3 sample calcined for 10 min at 600°C in an atmosphere of pure O_2 . No impurity phases (Ba_2TiO_4 , TiO_2 , BaCO_3 , etc.,) were detected.

XRD data for the BaTiO₃ sample calcined for 10 min at 1000° C with a standard JCPDS pattern for tetragonal BaTiO₃. According to a study by Templeton and Pask,¹⁷ a mechanical mixture of BaCO₃ and TiO₂ reacted at 1050° C for 15 min showed only 12 mol% BaTiO₃. Clearly the freeze dried nitrates were far more reactive than a mechanical mixture. In fact, furnace temperatures of 1000° C were more than sufficient. Thermal processing of the precursor in an oxygen atmosphere at 600° C for 10 min also resulted in phase pure BaTiO₃ (Figure 5.7). These conditions were extremely mild as compared to the conditions used in the conventional ceramic preparation of the material. Phase pure BaTiO₃ was also obtained after a 10 min calcination in air. No BaCO₃ was detected by XRD. However, for reproducibility, subsequent experiments were all carried out in an O₂ atmosphere. BaTiO₃ was also produced by calcination of the precursor for 10 min at 500° C. However, some Ba(NO₃)₂ peaks were evident in the XRD pattern. Increasing the calcination time at 500° C to 20 h resulted in phase pure BaTiO₃.

To determine if the mixing of reactants achieved through freeze drying was indeed responsible for the enhanced reactivity of the precursor, or if the phenomenon was due to the use of nitrates, a mechanical mixture of TiO(NO₃)₂ and Ba(NO₃)₂ was prepared and calcined. The mechanical mixture was calcined for 10 min at 600° C in an O₂ atmosphere. Figure 5.8 shows the XRD pattern of the mechanical mixture along with that of the freeze dried nitrates subjected to the same thermal treatment. The XRD pattern of the mechanical mixture consisted of mainly Ba(NO₃)₂ peaks, although some BaTiO₃ was present. Under the same calcination conditions, as has already been noted, the freeze dried precursor formed phase pure BaTiO₃.

Table 5.2. A comparison of the collected powder x-ray diffraction data for a sample of BaTiO₃ from freeze dried nitrates calcined for 10 min at 1000° C with a standard diffraction file for tetragonal BaTiO₃. Peaks designated by the Sintag computer program with relative intensities equal to 1 were discarded from the data.

JCPDS (5-626)			freeze dried nitrates		
BaTiO ₃	relative	h k l	1000° C, 10 min	relative	
d-spacing (Å)	intensity		d-spacing (Å)	intensity	
---	---	---	5.222	2	
---	---	---	4.248	2	
4.03	12	0 0 1	---	---	
3.99	25	1 0 0	4.002	22	
2.838	100	1 0 1	2.834	100	
2.825	100	1 1 0	---	---	
2.314	46	1 1 1	2.313	29	
2.019	12	0 0 2	---	---	
1.997	37	2 0 0	2.000	14	
1.802	6	1 0 2	1.792	3	
1.790	8	2 0 1	1.789	3	
1.786	7	2 1 0	---	---	
1.642	15	1 1 2	---	---	
1.634	35	2 1 1	1.635	16	
1.419	12	2 0 2	1.418	7	
1.412	10	2 2 0	---	---	
1.337	5	2 1 2	1.336	2	
1.332	2	3 0 0	---	---	
1.275	5	1 0 3	1.273	2	
---	---	---	1.271	2	
1.264	7	3 0 1	1.266	4	
1.263	9	3 1 0	---	---	
1.214	3	1 1 3	---	---	
1.205	5	3 1 1	1.207	2	
1.1569	7	2 2 2	1.157	3	
1.1194	1	2 0 3	---	---	
1.1161	1	[3 0 2]	---	---	

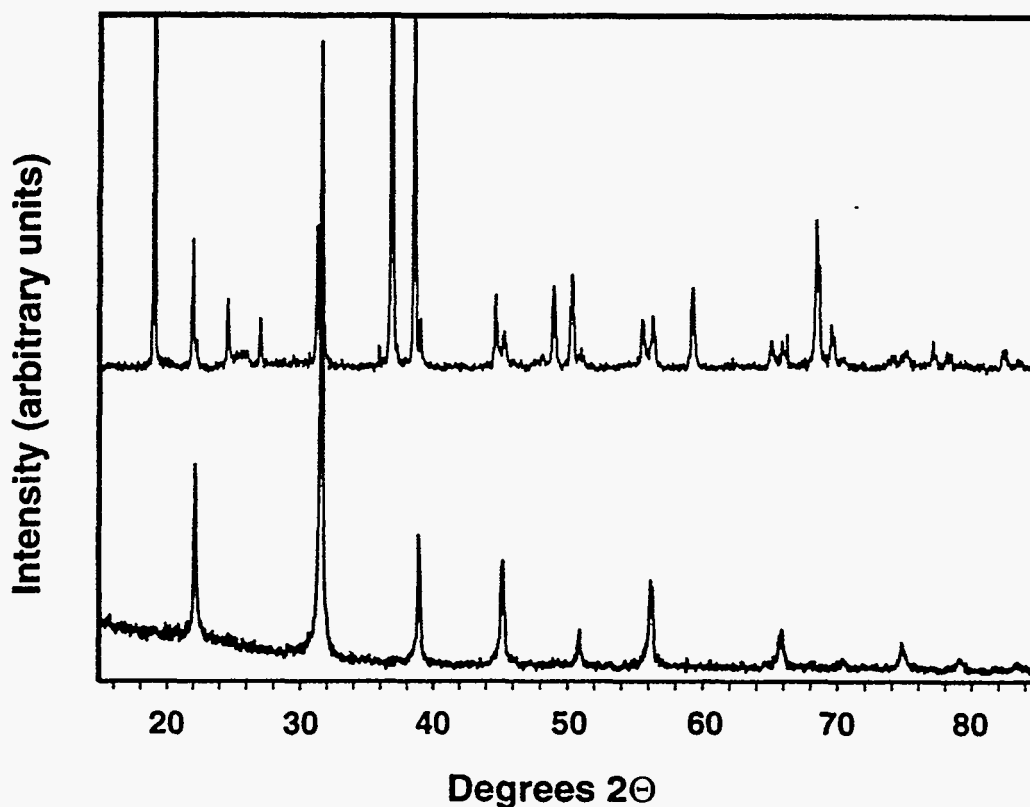


Figure 5.8. The XRD pattern of a mechanical mixture of $\text{Ba}(\text{NO}_3)_2$ and $\text{TiO}(\text{NO}_3)_2$, calcined for 10 min at 600°C in an atmosphere of pure O_2 , and the atomic mixture calcined under identical conditions.

The XRD of the freeze dried precursor calcined for 10 min to 20h (longest and shortest time periods investigated, respectively) at 600° in O_2 displayed a cubic phase of BaTiO_3 . Although BaTiO_3 is tetragonal below the Curie temperature (110°C), the surface layer of BaTiO_3 crystallites is cubic. The thickness of this cubic surface layer was estimated by Takemuchi et al.¹⁸ to be about 5 nm. It can be seen that very small particles would have a high surface to volume ratio and produce a predominantly cubic diffraction pattern. Particles which are $\leq 10\text{nm}$ should consist of entirely cubic material. A bright field

transmission electron micrograph (TEM) of the BaTiO₃ sample calcined for 10 min at 600° C in O₂ can be seen in Figure 5.9. The material was nanocrystalline with particles in the range of 8 to 12 nm. These very small particles account for the appearance of a cubic XRD pattern. Each crystallite was essentially *all* surface. Figure 5.10 shows a bright field TEM image of a BaTiO₃ sample heated at 600° C for 1 h in O₂. Some grain growth was evident but the material was still nanocrystalline, with crystallites in the range of 10 to 15nm.

Although the material is largely nanocrystalline, it appears that there is a bimodal distribution of particle size in the BaTiO₃ samples. Figure 5.11 shows a bright field image of a larger area of the sample calcined for 10 min at 600°C. In addition to nanocrystalline material previously discussed, there are several larger, single crystallites with linear dimensions on the order of 100nm. However, no intermediate particle size material can be seen.. The larger grains can also be seen in micrographs of samples calcined at higher temperatures. The appearance of these larger grains and bimodal distribution may be due to one of two possible situations. (1) They may have been the result of enhanced nucleation around impurities. (2) It is possible that the excess surface energy inherent in the nanocrystalline BaTiO₃ was being released in a catastrophic fashion, resulting in sudden grain growth.

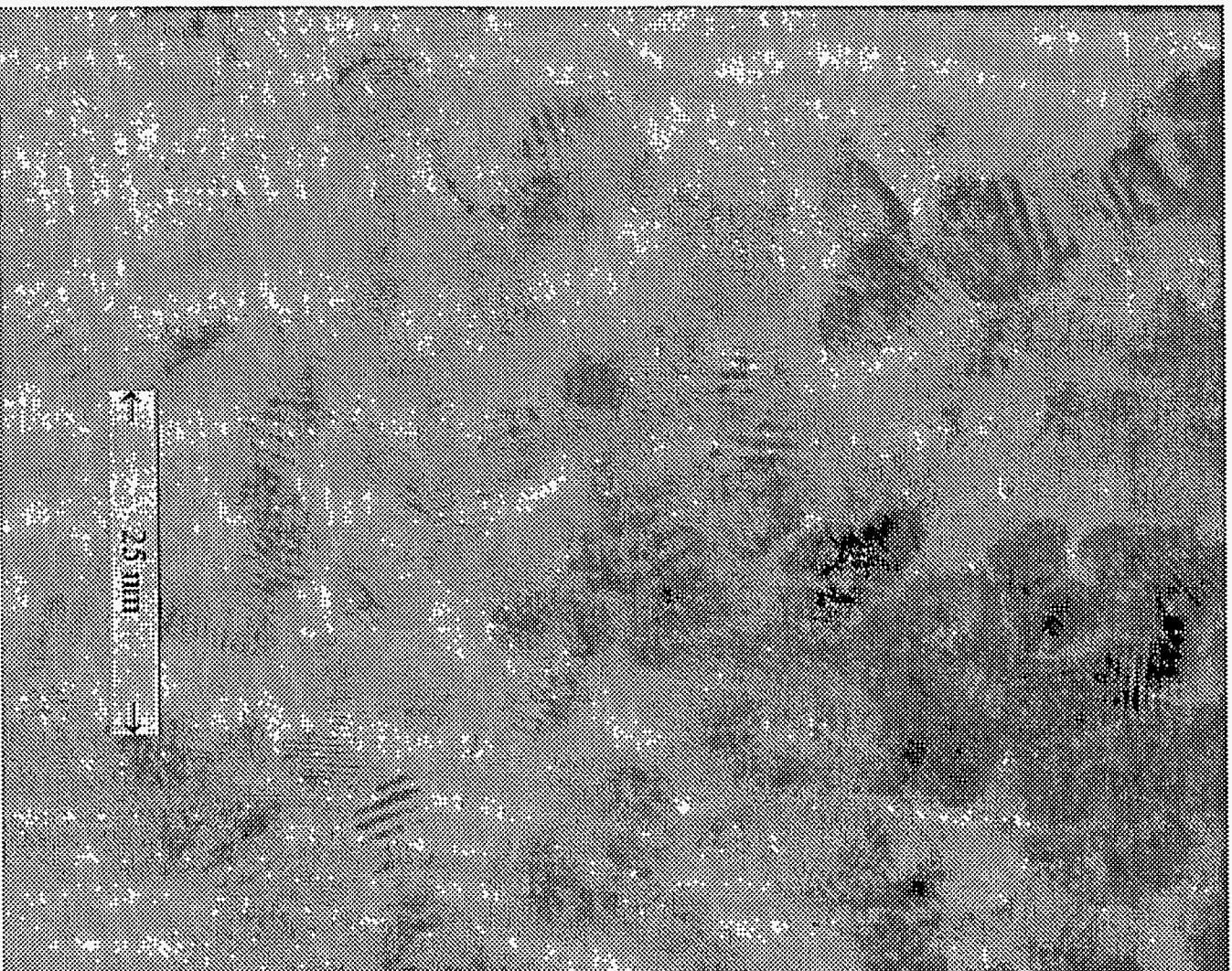


Figure 5.9. A bright field TEM image of a BaTiO₃ sample heated at 600° C for 10 min in O₂. Photograph courtesy of K. E. Sickafus, Los Alamos National Laboratory.

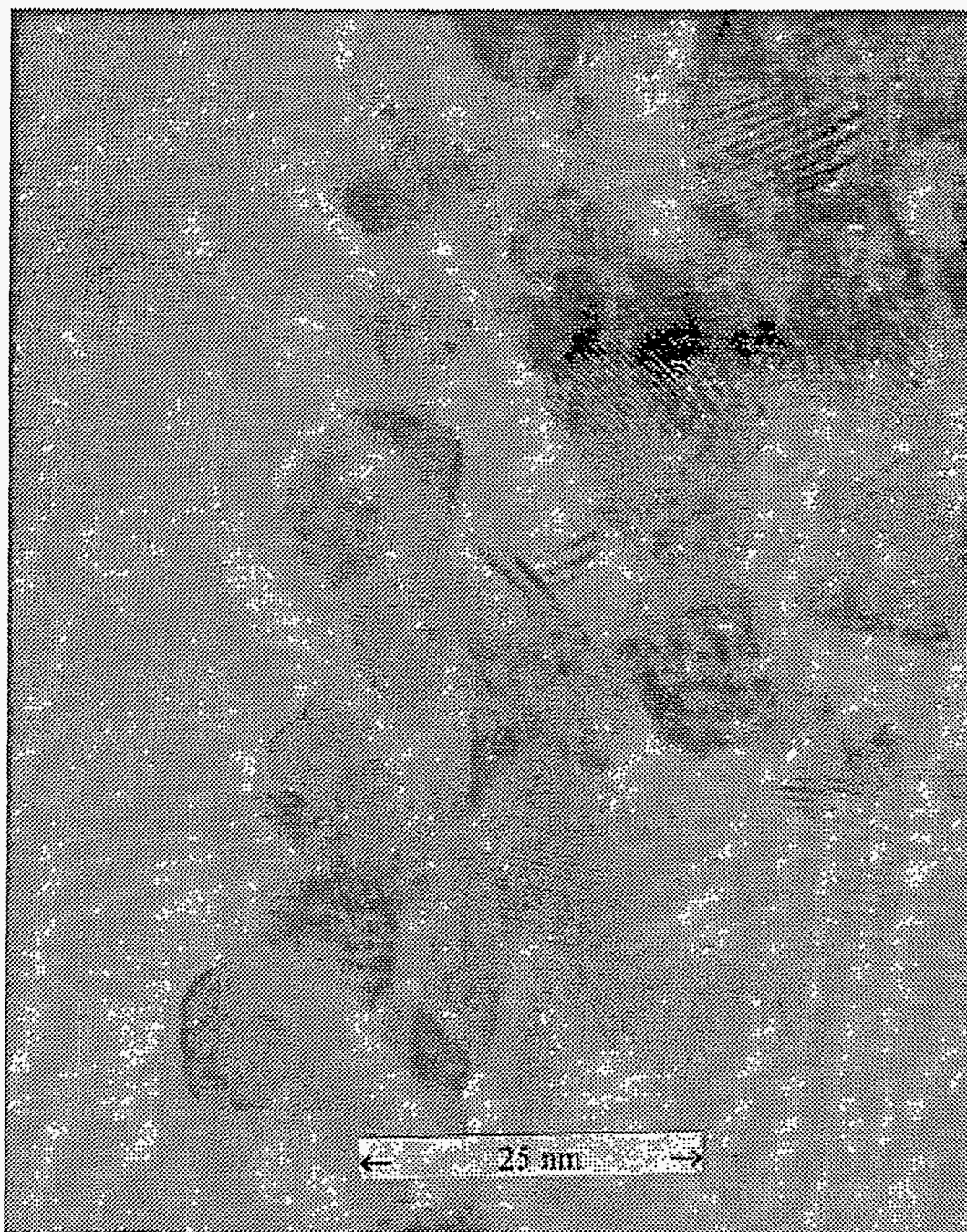


Figure 5.10. A bright field TEM image of a BaTiO₃ sample heated at 600° C for 1 h in O₂. Photograph courtesy of K. E. Sickafus, Los Alamos National Laboratory.

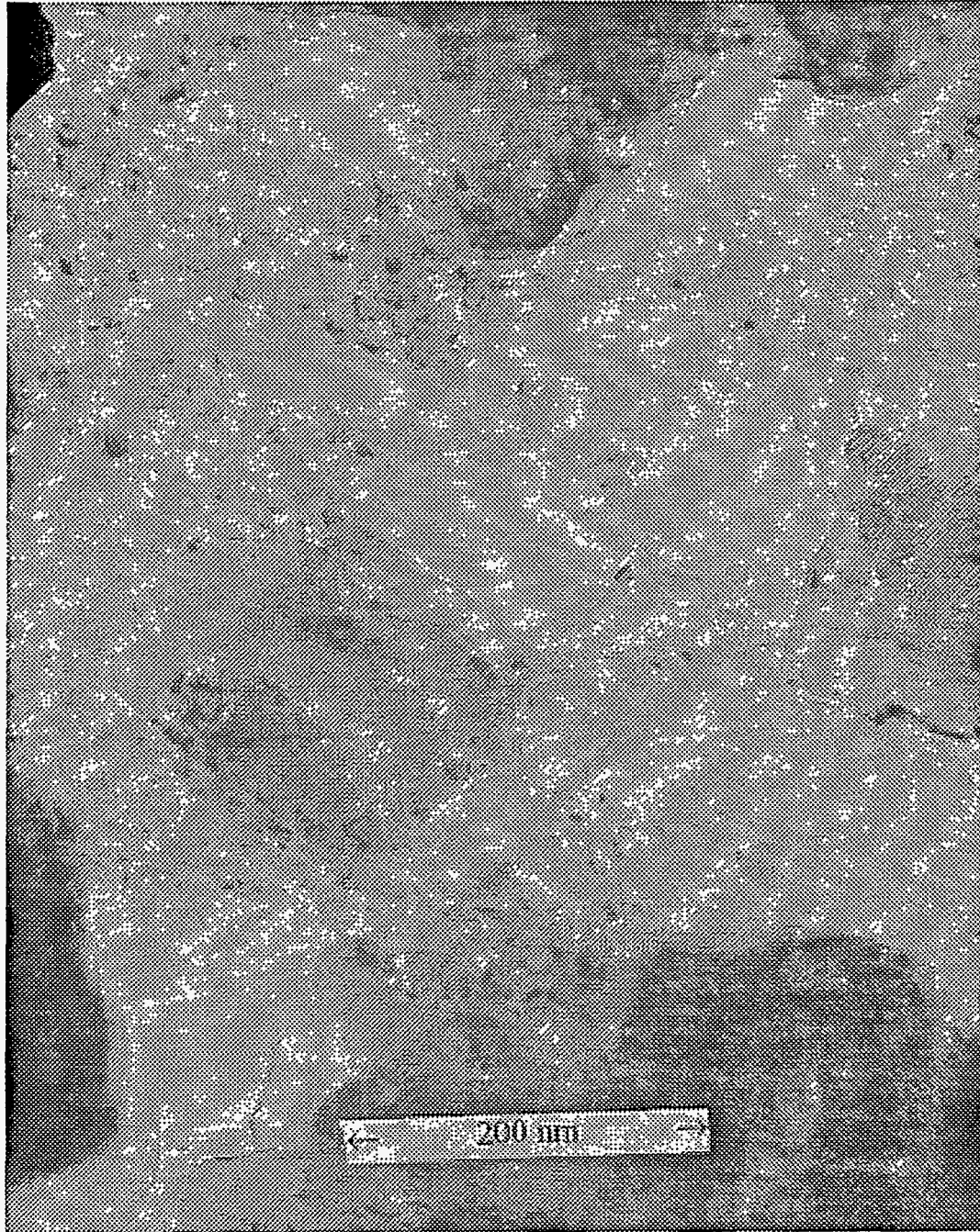


Figure 5.11. A bright field transmission electron micrograph of a larger area of the BaTiO₃ sample heated for 10min at 600° C showing the bimodal distribution of particle sizes. Photograph courtesy of K. E. Sickafus, Los Alamos National Laboratory.

Additional TEM data,¹⁹ which will be more fully discussed in a forthcoming publication,²⁰ reveal that the grain growth with time at temperatures between 600° C and 1000° C is very slow. Although some agglomeration of grains occurred, the material was still largely nanocrystalline (10 to 18 nm crystallites) after 20h at 600° C. There appeared to be no increase in the number of large (~100nm) crystallites present with increased annealing time at 600° C. Electron diffraction patterns obtained from the samples of BaTiO₃ showed no splitting of the diffraction rings, indicating that the material had a cubic structure. These data are consistent with the observations from powder x-ray diffraction. The particle distribution in samples which were calcined at 1000° C for 10 min appeared to be trimodal. The material consisted of small, 20 to 30nm crystallites, intermediate sized crystallites on the order of 100 to 150 nm, and some large crystallites, with linear dimensions of ~500nm. Electron diffraction patterns indicated that the material calcined for 10 min at 1000° C has a tetragonal structure (also consistent with XRD). Increasing the calcination time at 1000° C to 20h, did not result in significant grain growth.²¹

Additional information on grain growth in the BaTiO₃ samples was obtained from powder x-ray diffraction data. A Sintag program was used to calculate the full width at half maximum (FWHM) for the 110 peak of BaTiO₃ samples annealed for different time periods. The FWHM of a diffraction peak is related to the size of the particles by the Scherrer formula;

$$B = \frac{0.9 \lambda}{t \cos \Theta} \quad \text{eq. 5.1}$$

where B is the broadening of the diffraction line, λ is the wavelength of the radiation, Θ is the angle of the reflection, and t is the particle size. The broadening, however, refers only to "extra broadening" (over instrumental broadening) and the formula cannot be used to directly calculate particle size, without the use of an internal standard of known particle size.²² However, the FWHM is inversely proportional to the particle size, so a change in FWHM can be related to a change in the average particle size of the material. In Figure 5.12, the inverse of the full width at half maximum ($1/F_{\text{WHM}}$) of the 110 peak of BaTiO_3 (d-spacing = 2.850\AA) is plotted versus annealing time at 600°C , 800°C , and 1000°C . At 600°C , the FWHM of the 110 peak of BaTiO_3 decreased through 60 minutes of annealing and then saturated. It appears that some grain growth occurred quickly in the initial stages of annealing (calcination) at 600°C , but extended annealing at 600°C had little effect on the particle size. These data were supported by the TEM observations (Figures 5.9 and 5.10). At 800°C , the FWHM decreased ($1/F_{\text{WHM}}$ increased) through 2h of annealing and then saturated. However, all of the FWHM for the samples annealed at 800°C were smaller than those of the 600°C samples, indicating a larger average particle size in the 800°C samples. In samples calcined and annealed at 1000°C , there was no observed decrease in FWHM with time at temperature, indicating minimal grain growth with extended annealing. This observation is also consistent with the TEM studies. Conversely, at 1000°C , there is a slight increase in FWHM with annealing time. This effect probably was due to an increase in the tetragonality of the 1000°C samples with extended annealing times. When BaTiO_3 transforms from cubic to tetragonal, the 110 peak splits into the 110 and 101 peaks (with d-spacings of 2.825\AA and 2.838\AA , respectively). This

splitting, if not completely resolved, would appear to be an increase in the FWHM of the 110 peak. The Sintag computer program calculated the FWHM data based on the assumption that the peak was a single reflection. Consequently, any splitting was included into the value of the FWHM.

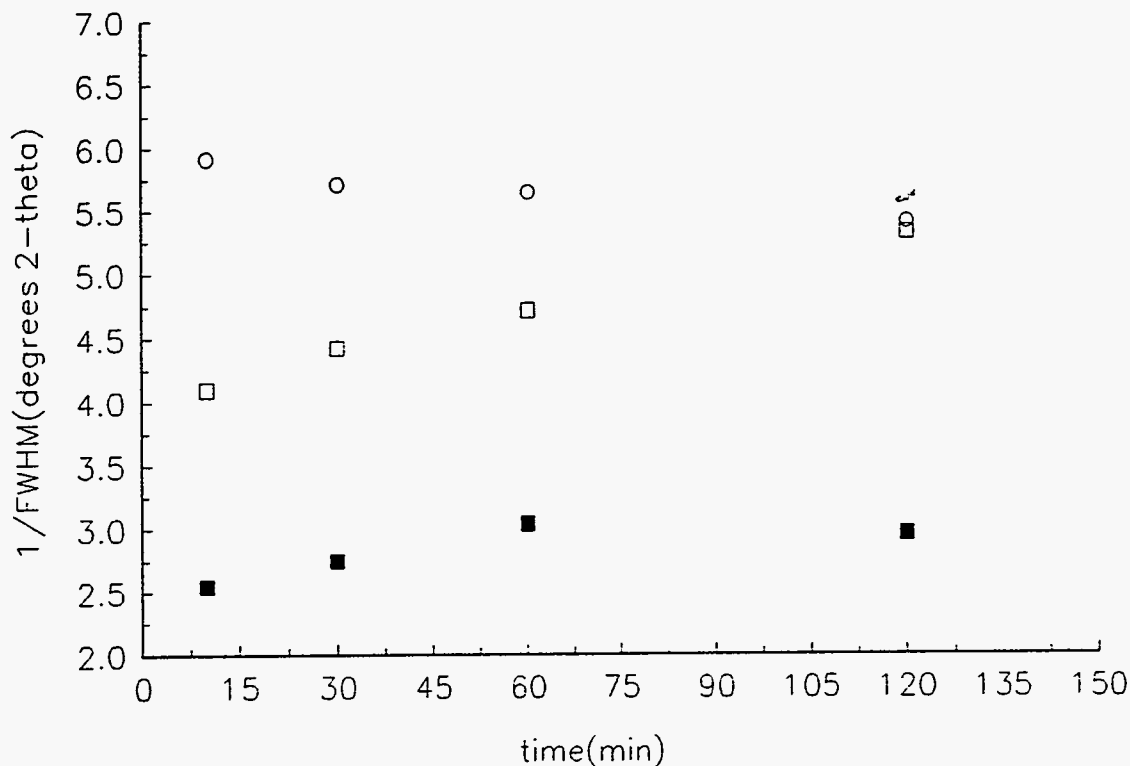


Figure 5.12. A plot of the inverse of the full width at half maximum ($1/F_{WHM}$) of the powder x-ray diffraction data for the 110 peak of $BaTiO_3$ versus annealing time at 600° C (solid squares), 800° C (empty squares), and 1000° C (empty circles). An increase in the value of $1/F_{WHM}$ is consistent with an increase in the average particle size of the sample.

The grain growth in the $BaTiO_3$ samples with prolonged annealing was also studied through XRD by observing the increase in the resolution of the splitting of the 002 and 200 peaks (d-spacings of 2.019Å and 1.997Å, respectively) at $\sim 45^\circ 2\Theta$.²³ As the average particle size of the powder became larger, the surface (cubic) to volume

(tetragonal) ratio became smaller. The XRD pattern of the powder took on the characteristics of the bulk and became tetragonal, as was evidenced by the splitting of the peak at $\sim 45^\circ 2\theta$. After calcination times of 20 h at 600°C , the material still gave a predominantly cubic pattern. As would be expected, grain growth was very slow at this low temperature. The precursor was also subjected to heat treatments at higher temperatures. At 800°C , the cubic diffraction pattern gradually developed into the expected tetragonal pattern with extended firing times. However, the splitting was not clearly present until 20 h at 800° . When the calcination temperature was raised to 1000°C , the tetragonality of the pattern was evident after only 30 min (Figure 5.12).

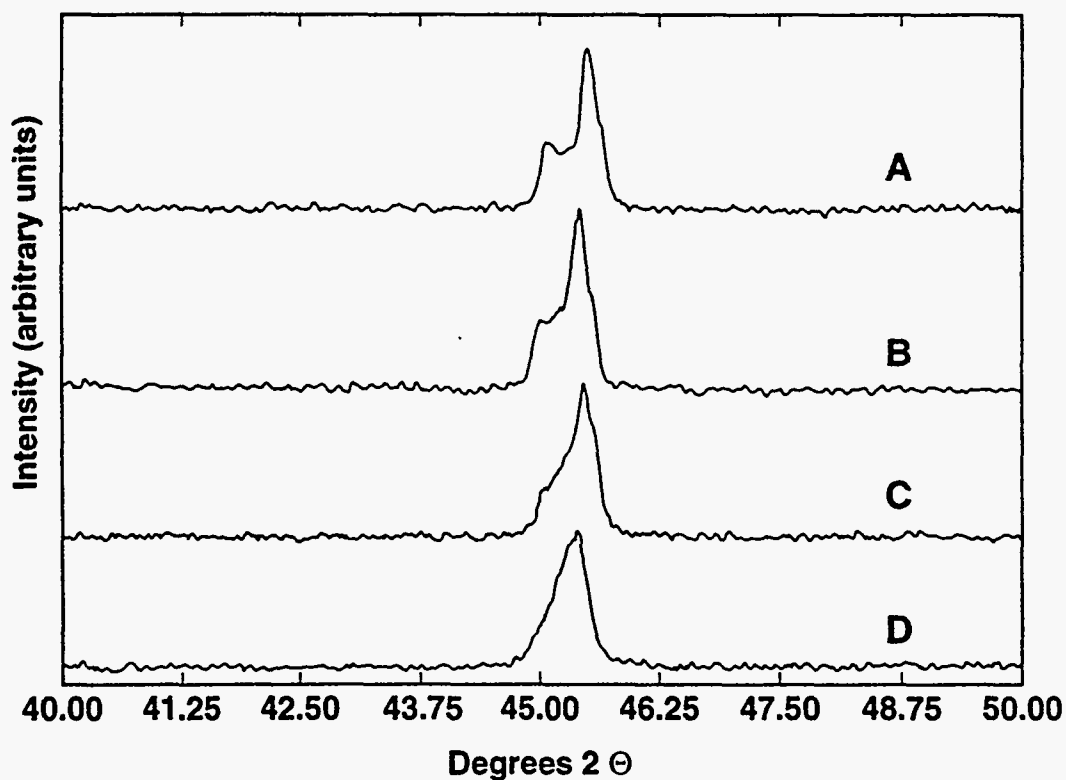


Figure 5.12. X-ray diffraction patterns for BaTiO_3 samples calcined at 1000°C for A, 120 min; B, 60 min; C, 30 min; and D, 10 min. The splitting indicative of tetragonal BaTiO_3 can be seen in the peak(s) at $\sim 45^\circ 2\theta$.

5.2.6 Conclusions

A procedure for the preparation of stable, powdered titanyl nitrate was developed. This compound was subsequently used in the preparation of accurately stoichiometric barium and titanyl nitrate aqueous solutions. Rapid freezing, followed by freeze drying of these barium and titanyl nitrate solutions yielded fine, free flowing, highly reactive precursor powders. A heat treatment of this precursor at 600° C for 10 min (shortest time period investigated) in pure O₂ (or air) was sufficient for complete formation of BaTiO₃. The synthesis of BaTiO₃ via conventional ceramic processing requires temperatures in excess of 1000°C and calcination times of greater than 24h. The high reactivity of the precursor has been shown to be a result of the atomic level mixing achieved through the freeze drying process by comparison with the reactivity of mechanical mixtures of barium and titanyl nitrates. The rapid freezing of the barium and titanyl nitrate solution trapped the homogeneity and mixing of cations inherent in the solution. Removal of the water by sublimation preserved this homogeneity during transfer to the solid state.

Bright field TEM micrographs revealed that the material produced at 600° C is nanocrystalline with an average grain size of about 10 nm. The resulting XRD pattern from the 10 nm crystallites was dominated by intensities originating from the cubic surface layer of BaTiO₃. Longer annealing times resulted in a modest growth of grain size. Conversion to the expected tetragonal form of BaTiO₃ occurred at higher temperatures. The observations from TEM micrographs agreed with the growth of particle size observed through a decrease in the full width at half maximum of powder x-ray diffraction data. In addition to the advantages of milder calcination conditions, nanocrystalline powders

should achieve higher green body densities and display improved sintering characteristics over conventionally prepared samples of BaTiO_3 . Furthermore, it has been demonstrated that the annealing temperature played a much larger role in determining the final grain size of the material than the annealing time. This implies that the particle size of BaTiO_3 powders produced from freeze dried nitrates can be controlled via judicious selection of the calcination and annealing temperature. This factor could lead to application of these materials in nanocrystalline compacts.

5.3 Notes and References

- ¹ J. M. McHale and N. V. Coppa, *Titanate Materials from Freeze Dried Nitrate Solutions*, Patent applied for: DOE Application # S-80, 469 (1994).
- ² E. Ruckenstein, S. Narain, and N. L. Wu, *J. Mater. Res.* **4**, 267 (1989).
- ³ T. M. Shaw, D. Dinos, P. E. Batson, A. G. Schrott, D. R. Clarke, and P. R. Duncombe, *J. Mater. Res.* **5**, 1176 (1990).
- ⁴ Johnson Matthey, 1994 AESAR catalogue.
- ⁵ J. Barksdale, *Titanium Its Occurrence, Chemistry, and Technology, Second Edition*, The Ronald Press Co., New York, 1966.
- ⁶ H. B. Weiser, *Inorganic Colloid Chemistry, Volume II The Hydrous Oxides and Hydroxides*, John Wiley and Sons, Inc. (London, 1935).
- ⁷ A. W. Hixson and W. W. Plechner, *Ind. Eng. Chem.* **25**, 262 (1933).
- ⁸ H. Yamamura, A. Watanabe, S. Shirasaki, Y. Moriyoshi, and M. Tanada, *Ceram. Int.* **11**, 17 (1985).
- ⁹ N. V. Coppa, Personal Communication (Los Alamos, NM, 1994).
- ¹⁰ The author acknowledges Nancy Buecheler (Temple University, Department of Chemistry) for her assistance with the ESR experiments.
- ¹¹ S. Jansen-Varnum, Personal Communication (Philadelphia, PA, 1994).
- ¹² The author acknowledges E. L. Brosha of Los Alamos National Laboratory for his TGA work with the titanate powders.
- ¹³ N. V. Coppa, Doctoral Dissertation, Temple University, Philadelphia, PA 19122 (1990).
- ¹⁴ A. V. Luikov, *Analytical Heat Diffusion Theory*, Academic Press, p. 452 (1968).

- ¹⁵ N. V. Coppa, G. H. Myer, R.E. Salomon, A. Bura, J. W. O'Reilly, J. E. Crow, and P. K. Davies, *J. Mater. Res.* **7**, 2017 (1992).
- ¹⁶ R. C. Weast, Editor, *CRC Handbook of Physics and Chemistry, 56th Edition*, CRC Press, Cleveland, Ohio, (1976)
- ¹⁷ L. K. Templeton and J. A. Pask, *J. Am. Ceram. Soc.* **42**, 212 (1959).
- ¹⁸ T. Takemuchi, K. Ado, T. Asai, H. Kageyama, Y. Saito, C. Masqueleir, and O. Nakamura, *J. Am. Ceram. Soc.* **77**, 1665 (1994).
- ¹⁹ The author acknowledges P. C. McIntyre of Los Alamos National Laboratory for his TEM analysis and interpretation.
- ²⁰ J. M. McHale, P. C. McIntyre, K. E. Sickafus, and N. V. Coppa, To be submitted to the *Journal of Materials Research*, November, 1994.
- ²¹ P. C. McIntyre, Personal Communication (Los Alamos, NM, 1994).
- ²² B. D. Cullity, *Elements of X-Ray Diffraction*, Addison-Wesley Publishing Co. (Reading, MA, 1978).
- ²³ S. Naka, F. Nakakita, Y. Suwa, and M. Inagaki, *Bull. Chem. Soc. Jpn.* **47**, 1168 (1974).

CHAPTER 6

EVOLUTION OF THE SYNROC-B PHASE ASSEMBLAGE FROM FREEZE DRIED NITRATE SOLUTIONS

It has already been shown that atomic level mixing via freeze drying can lead to extremely rapid product formation in a simple, binary system such as BaTiO_3 . The research reported in this chapter utilized freeze drying of nitrate solutions for the synthesis of the complex titanate phase assemblage, SYNROC-B (see section 2.2.2 for a discussion of the composition and application of SYNROC-B). First proposed as a high level nuclear waste immobilization medium by A. E. Ringwood in 1978, SYNROC-B, a mixture of a hollandite-type barium aluminum titanate, $\text{BaAl}_2\text{Ti}_5\text{O}_{14}$ (which will be referred to in this work as hollandite), zirconolite, $\text{CaZrTi}_2\text{O}_7$, and perovskite, CaTiO_3 , served as a complex, yet well studied phase assemblage, to probe the benefits of atomic mixing on a multi-phase system. With five different metals (which do not form a single oxide phase) in the "mix," there is a great number of possible intermediates and products. Under hot pressing conditions, hollandite, zirconolite and perovskite are the thermodynamically stable phases in the SYNROC-B system. Hot pressing, however, the method Ringwood proposed^{1,2} for synthesis of SYNROC, is incompatible with the radiological glove box environment and prevents the practical application of SYNROC-B. True atomic mixtures should react by a diffusionless mechanism to yield the most thermodynamically stable products in very short time periods. Presented in this chapter is the application of atomically mixed precursors in

an ambient pressure synthesis of SYNROC-B. In addition, the three individual phases were synthesized from atomic mixtures to better understand the phase development in the assemblage.

6.1 Preparation of SYNROC-B from Freeze Dried Nitrates

6.1.1 Experimental Procedure

Based on Ringwood's reported metal oxide weight percentages for SYNROC-B (see Table 2.3), an imaginary phase of nominal composition; $\text{TiZr}_{0.125} \text{Al}_{0.275} \text{Ca}_{0.350} \text{Ba}_{0.082} \text{O}_{3.1}$ was formulated. Three liters of a metal nitrate solution with the preceding stoichiometry was prepared by dissolving powdered $\text{TiO}(\text{NO}_3)_2$, $\text{Ca}(\text{NO}_3)_2 \cdot 4\text{H}_2\text{O}$, $\text{ZrO}(\text{NO}_3)_2 \cdot x\text{H}_2\text{O}$, $\text{Ba}(\text{NO}_3)_2$, and $\text{Al}(\text{NO}_3)_3 \cdot 9\text{H}_2\text{O}$ in d. H_2O . The solution was diluted to a Ti concentration of 0.25M, filtered to degas, and stored in Teflon bottles. The solution was rapidly frozen under the identical conditions used for barium and titanyl nitrate solutions (see section 5.2.2). The frozen solution, or snow, was then placed in the freeze drying unit and dried at a pressure of $\sim 10\mu\text{m Hg}$ and a shelf temperature of -40°C . After seven to eight days at -40°C , the powder was sufficiently dry (as evidenced by the meeting of the shelf and tray temperatures) and the shelf temperature was raised to 20°C at a rate of 2°C/h . The resulting freeze dried precursor was stored in clean glass jars until ready for thermal processing.

Precursor powders were studied by TGA and XRD to determine decomposition temperature and probe for long range order, respectively. Thermal processing of the precursor was carried out at 600 torr (slightly above 590 torr, atmospheric pressure at Los

Alamos, altitude = 2200m) in the tube furnace described in section 5.2.4, which appears schematically in Figure 5.4. A reducing atmosphere of 6% H_2 in Ar was used throughout the experiments. It had been previously established that a reducing atmosphere was necessary for the production of the hollandite phase.³ Calcination conditions ranged from 700° to 1100° C for time periods of 10 min to 15 h. The development and crystallization of the SYNROC-B phases was studied by XRD. Samples were plunged into a preheated furnace under flowing H_2 /Ar for ten minutes each at 100° C intervals from 500° C to 1100° C. After the ten minute time period the samples were pulled out of the hot zone of the furnace and allowed to cool to room temperature under 6% H_2 in Ar. The high thermal conductivity of the platinum boats allowed cooling rates to be high enough so that the samples would not glow red hot for more than a few seconds after removal from the hot zone of the furnace. These samples were then studied by XRD to determine phase composition.

6.1.2 Results and Discussion

The freeze dried SYNROC-B precursor was a free flowing, light yellow powder. The powder filled nearly the same volume as the frozen solution (snow). The XRD pattern of the SYNROC-B freeze dried precursor was indistinguishable from that of blank Kapton tape (see Figure 6.1). This was evidence for a lack of long range order in the precursor, a phenomenon consistent with atomic mixing. A TGA trace of the precursor powder can be seen in Figure 6.2. Decomposition of the nitrates was essentially complete by 600° C. Over 70% of the mass loss occurs before 200° C. This low temperature decomposition

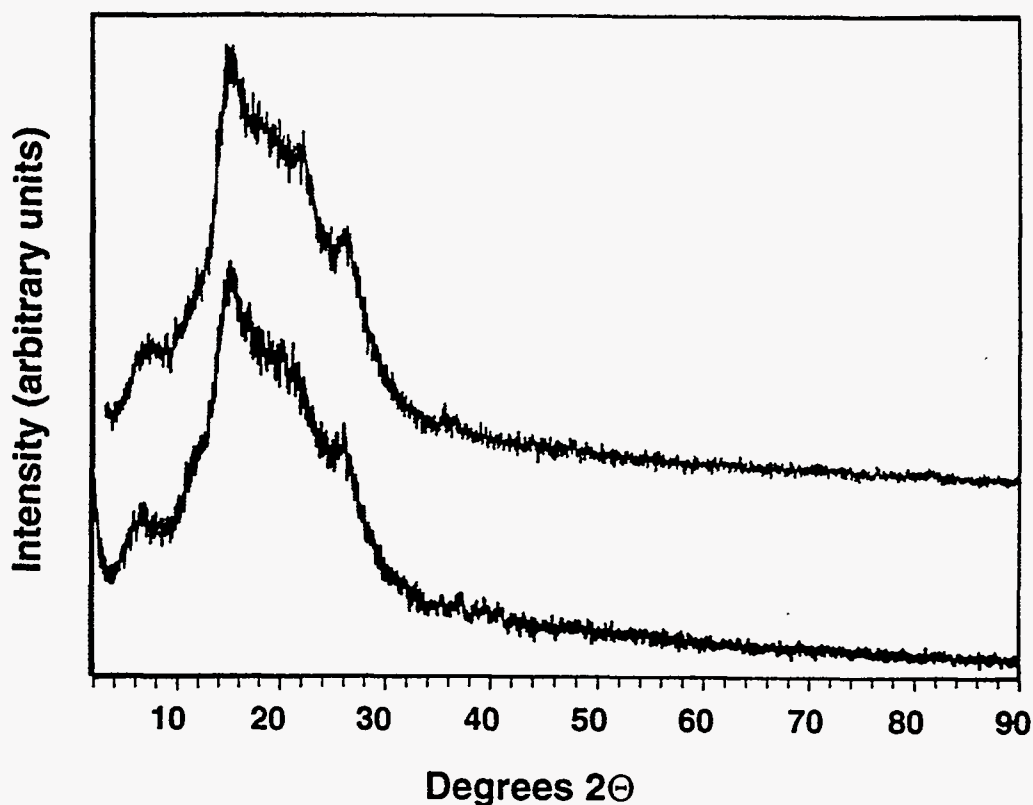


Figure 6.1. The XRD patterns of the SYNROC-B nitrate precursor behind a layer of Kapton tape (lower pattern) and the XRD pattern of blank Kapton tape.

was consistent with the TGA curve for $\text{TiO}(\text{NO}_3)_2$ (Figure 5.1). The XRD pattern of the SYNROC-B precursor calcined for 10 min at 600°C , however, was amorphous.

Calcination of the freeze dried nitrate precursor for ten minutes at 1100°C in an atmosphere of $6\%\text{H}_2$ in Ar resulted in the complete formation of the SYNROC-B phase assemblage. Figure 6.3 shows the XRD pattern SYNROC-B, prepared from thermal processing (10 min at 1100°C) of freeze dried nitrates. All major peaks in the pattern

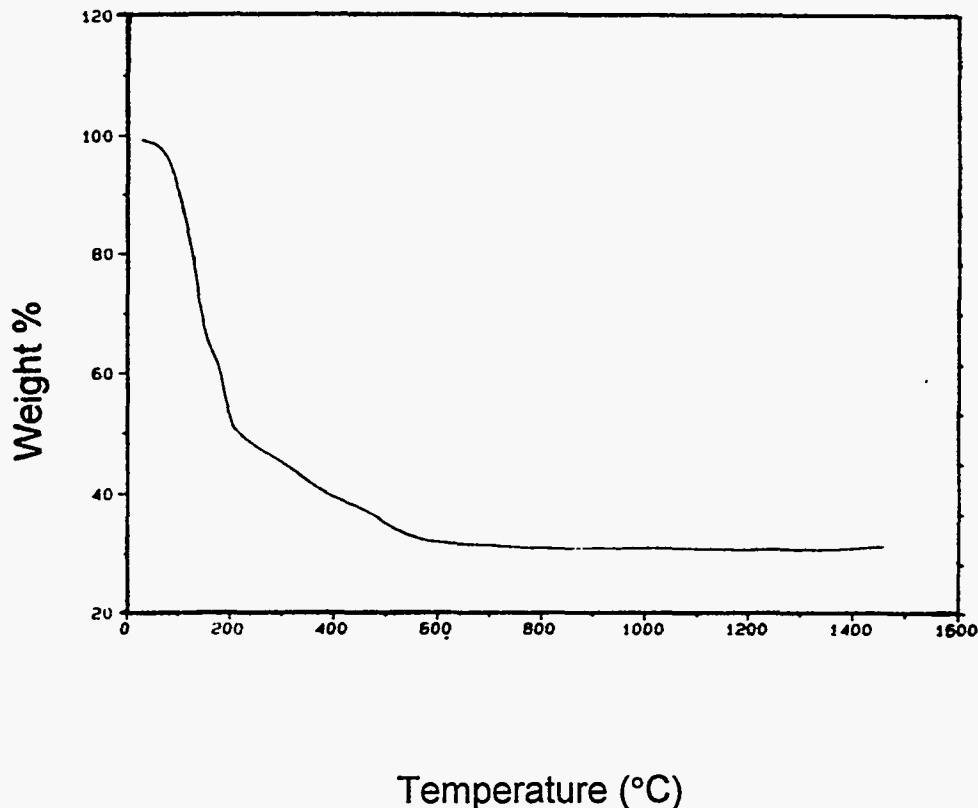


Figure 6.2. A TGA of the SYNROC-B nitrate precursor

were attributed to the three phases which comprise SYNROC-B, hollandite, zirconolite and perovskite. However, there was a slight shifting of the hollandite peaks to a larger d-spacing (lower 2θ). The XRD pattern of this sample was nearly identical to a sample calcined for 15 h at 1100° C (see Figure 6.4), neglecting narrowing of peaks due to improved crystallinity in the 15 h sample. This showed that the thermodynamically stable products were formed after very short processing times, as would be expected for a solid state reaction of an atomic mixture.

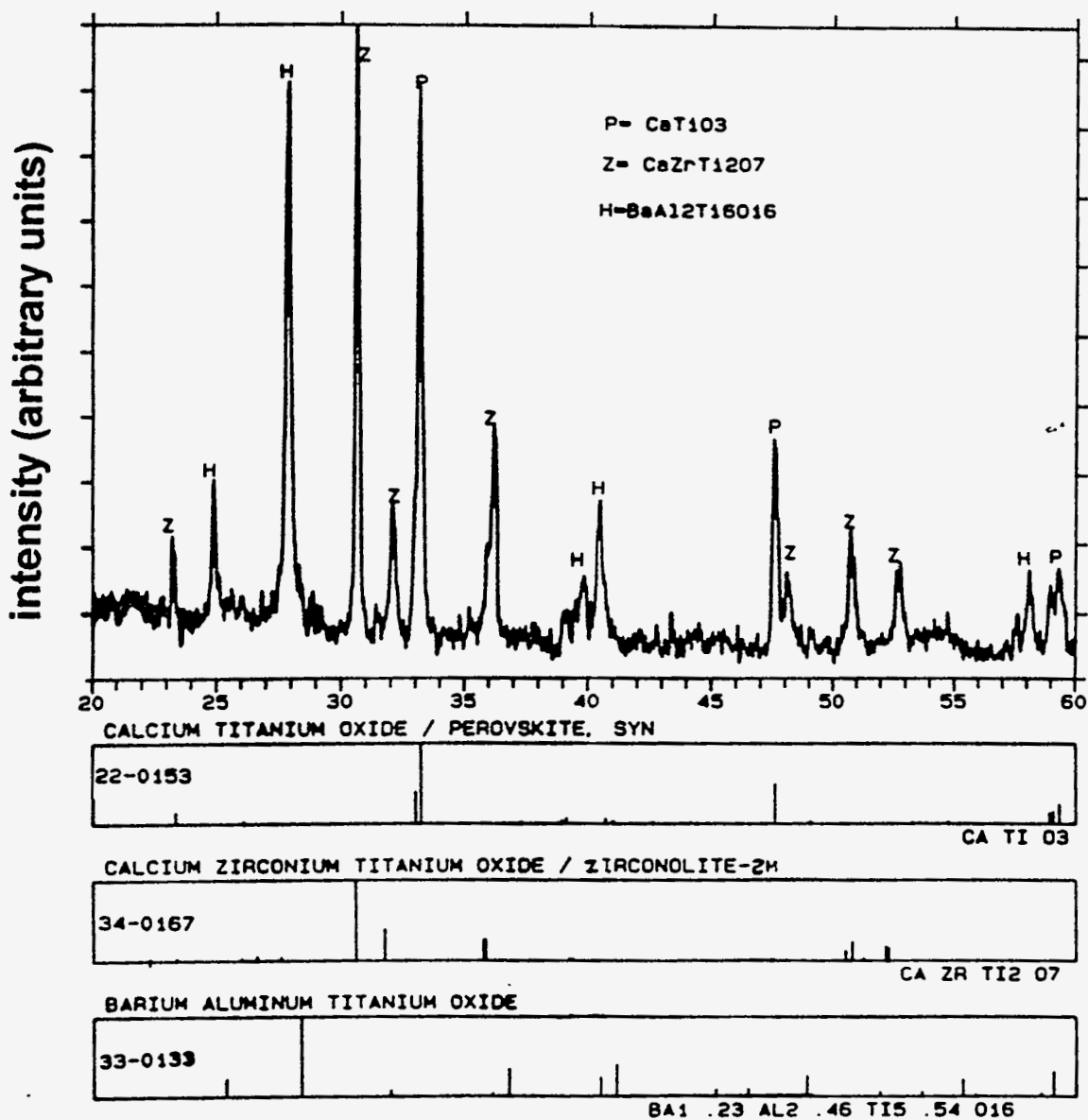


Figure 6.3. The XRD pattern of SYNROC-B prepared from freeze dried nitrates after calcination at 1100° C for 10 min and the standard JCPDS files for perovskite, hollandite and zirconolite. Peaks marked P correspond to perovskite, H correspond to hollandite and Z correspond to zirconolite.

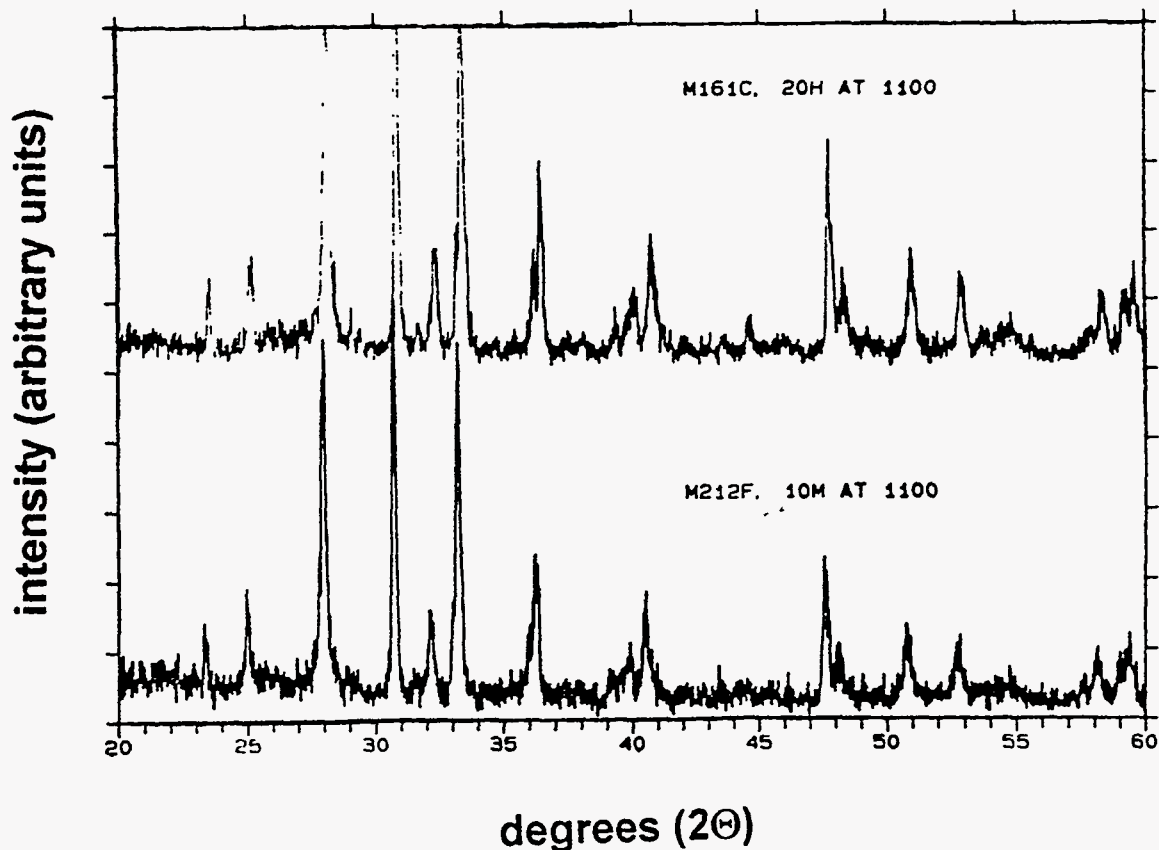


Figure 6.4. X-ray diffraction patterns for the SYNROC-B precursor heated for ten minutes at 1100° C (lower pattern) and 20h at 1100° C (upper pattern). The two patterns are virtually identical, indicating that the thermodynamically stable mixture of phases forms extremely rapidly upon calcination of the freeze dried nitrates.

To determine the lowest possible processing temperature for SYNROC-B preparation from freeze dried nitrates, samples were plunged into the furnace for ten minute intervals at temperatures ranging from 700° C to 1100° C. The XRD pattern of a SYNROC-B sample heated at 700° C for 10 min was completely amorphous. After 10 min at 800° C, a $\text{CaZrTi}_2\text{O}_7$ phase with a fluorite type structure crystallized (see Figure 6.5). This fluorite type phase has been observed upon calcination of zirconolite precursors prepared by hydrolysis of metal alkoxides.⁴ At 900° C, peaks which corresponded to the

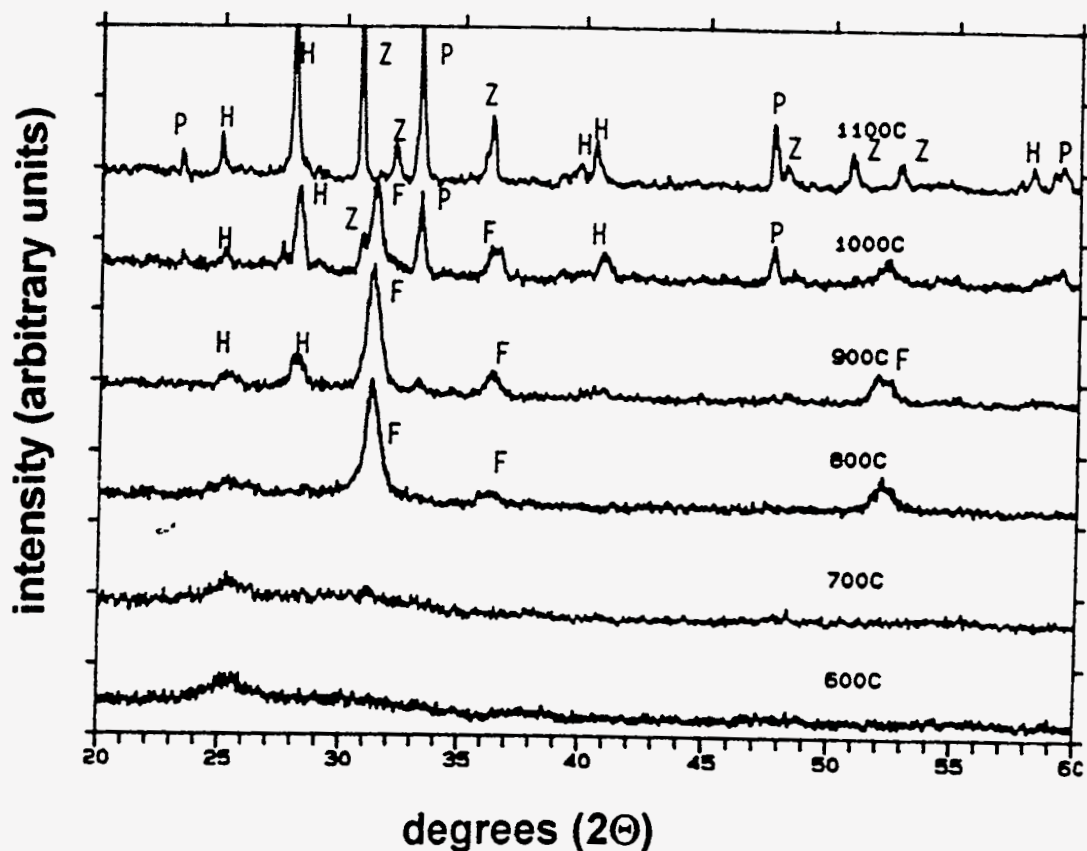


Figure 6.5. Evolution of the SYNROC-B phases, perovskite, hollandite and zirconolite, from the amorphous mixture of nitrates after calcination for 10min at temperatures ranging from 600° C to 1100° C. The material is amorphous to XRD until 800° C, where peaks corresponding to the fluorite-type $\text{CaZrTi}_2\text{O}_7$ (labeled F) appear. Peaks labeled P correspond to perovskite, Z to zirconolite and H to hollandite.

hollandite phase, $\text{BaAl}_2\text{Ti}_5\text{O}_{14}$, appeared, along with very low intensity peaks which corresponded to perovskite, CaTiO_3 . After 10 min at 1000° C, the perovskite and hollandite peaks grew substantially in intensity, and a transformation from fluorite type $\text{CaZrTi}_2\text{O}_7$ to zirconolite type $\text{CaZrTi}_2\text{O}_7$ began. After 10 min at 1100° C all peaks could be indexed to perovskite, hollandite and zirconolite.

Since product formation at 1100° C was too rapid to follow using XRD, the phase development was studied more closely by lowering the calcination temperature to 1000° C

and varying the duration that the samples were in the hot zone of the furnace from 10 min to 20h (see Figure 6.6). At 1000° C, the most intense zirconolite-type peak ($\sim 30.8^\circ 2\Theta$) was more intense than the most intense fluorite-type peak ($\sim 31.4^\circ 2\Theta$). This ratio of zirconolite-type to fluorite-type peak intensity continued to increase as the samples were heated for 1h and 2h. After 15h at 1000° C, this transformation was essentially complete, yielding the full SYNROC-B phase assemblage.

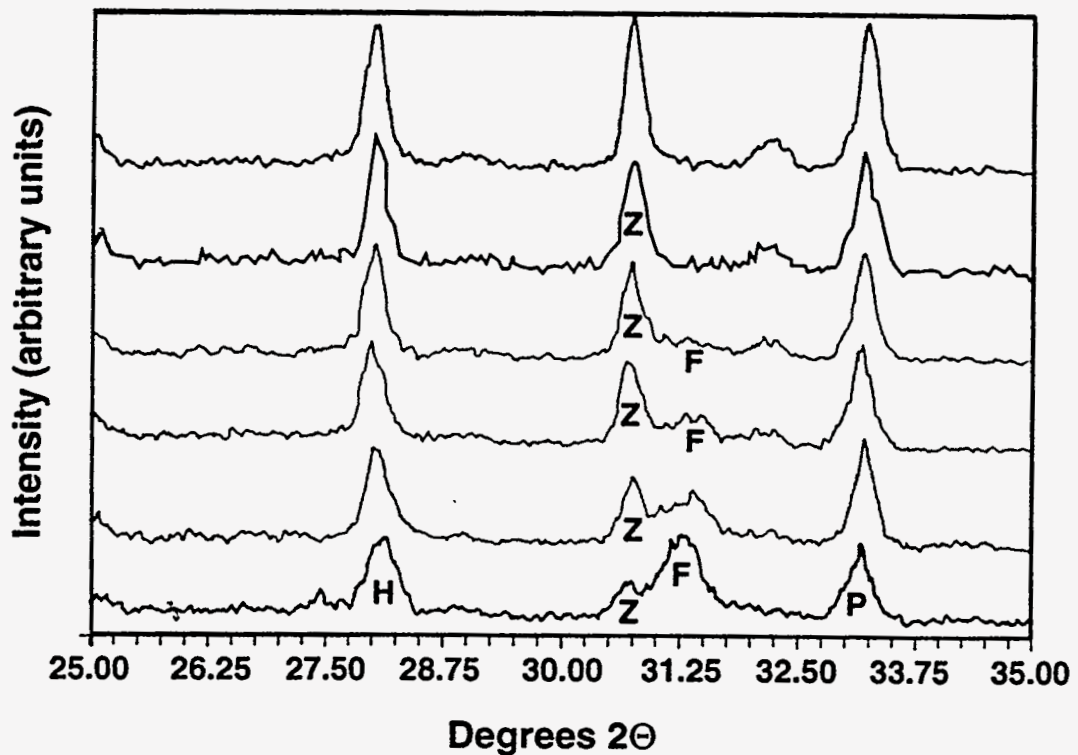


Figure 6.6. X-ray diffraction patterns for SYNROC-B samples heated at 1000° C for (from bottom) 10 min, 30 min, 1h, 2h, and 15h. Peaks labeled P correspond to perovskite, Z correspond to zirconolite, F correspond to fluorite type $\text{CaZrTi}_2\text{O}_7$, and H correspond to hollandite peaks.

The effectiveness of the atomic level mixing achieved through the freeze drying procedure was evident upon comparison of the XRD patterns of the freeze dried precursor and the mechanical mixture (conventional preparation) subjected to similar thermal treatments. Whereas the complete SYNROC-B phase assemblage was formed after only 10 min at 1100° C, a mechanical mixture calcined for >20 h at 1100° C still contained large quantities of the starting materials (binary oxides).

6.2 Preparation of SYNROC-B Constituent Phases

6.2.1 Experimental Procedure

Three separate metal nitrate solutions with stoichiometric elemental ratios of 1.00Ca:1.00Zr:2.00Ti, 1.00Ba:2.00Al:6.00Ti, and 1.00Ca:1.00Ti were prepared for the individual syntheses of zirconolite, hollandite and perovskite, respectively. The freeze drying procedure was identical to that followed in the preparation of SYNROC-B, but different primary drying temperatures were used in accordance with the observed melting points of the solutions. The hollandite precursor and the perovskite precursor were dried at -30° C. The zirconolite precursor was dried at -40° C.

Thermal processing of the precursors was performed using the same furnace as the SYNROC samples. The hollandite samples were calcined in an atmosphere of 6%H₂ in Ar. The perovskite and zirconolite precursors were calcined in pure O₂. Samples were plunged into a preheated furnace at temperatures ranging from 400° C to 1100° C for time periods ranging from 10 min to 15h. Samples of each phase were also prepared by conventional ceramic processing (grind and calcine) of the necessary metal oxides or carbonates. These

mechanically mixed samples were subjected to the same calcination conditions (or longer time periods) as the freeze dried precursors. Characterization of the precursors and products was performed following the identical procedures used for the SYNROC-B samples.

6.2.2 Results and Discussion

6.2.2.1 Hollandite

The XRD pattern for the $\text{BaAl}_2(\text{TiO})_6(\text{NO}_3)_x$ precursor was indistinguishable from that of blank Kapton tape. This is, again, evidence for a lack of long range order in the freeze dried precursors. Calcination of this precursor at 1100°C for 10 min yields a single phase XRD pattern (see Figure 6.7). There exists some confusion in the literature as to whether the empirical formula for the hollandite phase of SYNROC-B is $\text{BaAl}_2\text{Ti}_5\text{O}_{14}$ or $\text{BaAl}_2\text{Ti}_6\text{O}_{16}$. In the early publications of A.E. Ringwood^{1,2}, the phase was referred to as $\text{BaAl}_2\text{Ti}_6\text{O}_{16}$, probably due to analogy with the natural mineral hollandite, $\text{BaMn}_8\text{O}_{16}$. Others have determined that the correct composition is $\text{BaAl}_2\text{Ti}_5\text{O}_{14}$, and attempts at producing a phase of composition $\text{BaAl}_2\text{Ti}_6\text{O}_{16}$ results in the formation of $\text{BaAl}_2\text{Ti}_5\text{O}_{14}$ and "reduced rutile."^{5,6} The most recent determination of the structure of hollandite states that neither of the two compositions exist and the correct representation of the structure is actually $\text{Ba}_{1.14}\text{Al}_{2.29}\text{Ti}_{5.71}\text{O}_{16}$ (which reduces to a 1:2:5, Ba:Al:Ti ratio).⁷ In this work, all compositions given by Ringwood were used. Consequently, the hollandite phase synthesized here contains an excess of titanium. There is no clear evidence, however, for TiO_2 as rutile or anatase, (the most logical impurity resulting from an excess of Ti) in the

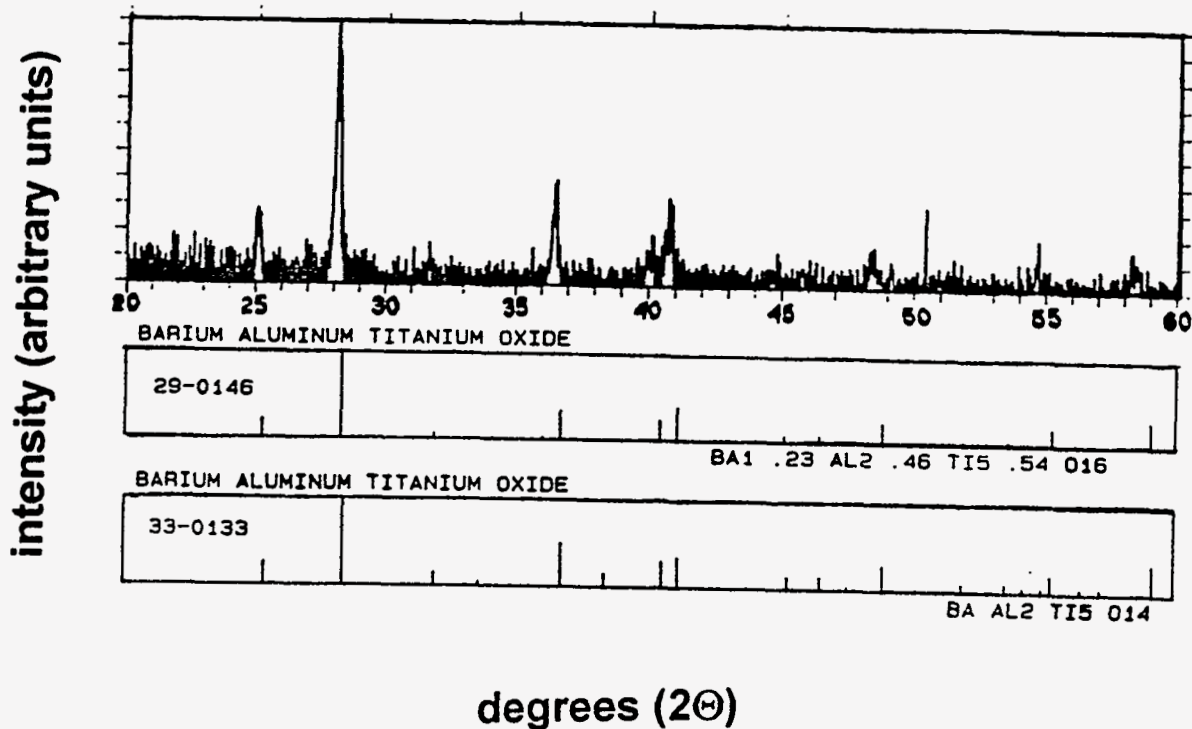


Figure 6.7. The XRD pattern of the hollandite phase obtained from calcination of atomically mixed nitrates for 10min at 1100° C and the JCPDS standard files for the two proposed hollandite phases. The d-spacing data collected in this work are slightly larger than those of both hollandite phases in the JCPDS files.

XRD patterns of the hollandite phases synthesized from freeze dried nitrates. The d-spacings, however, of the material synthesized in this work differed slightly from those reported in the literature for $BaAl_2Ti_5O_{14}$ and $Ba_{1.14}Al_{2.29}Ti_{5.71}O_{16}$. This may have been a result of the extended solid solution formation of which these phases are capable.

The phase development of hollandite was followed using XRD. The hollandite phase began to crystallize from an amorphous mixture of oxides after 10 min at 900° C. Higher temperatures improved the crystallinity of the product. The appearance of

hollandite after 10 min at 900° C in the pure Ba-Al-Ti-O samples corresponded to the temperature where the hollandite-type phase appeared in the SYNROC-B mixture.

The freeze dried precursor has proven to be far more reactive than a mechanical mixture of binary oxides. Whereas complete formation of hollandite occurred after 10 min at 900°C from the freeze dried precursor, no hollandite was evident in the XRD pattern of the mechanically mixed sample even after 40 h at 1100° C. The mechanical mixture reacted to form BaTi₄O₉, BaAl₂O₄, and at least one other unidentified phase. It has been reported elsewhere that a calcination of temperature of 1200° C was also insufficient for the production of the hollandite-type phase from mechanical mixtures of BaO, Al₂O₃, and TiO₂.^{3,8}

6.2.2.2 Zirconolite

All attempts at freeze drying CaZr(TiO)₂(NO₃)_x solutions resulted in partial melting in the freeze dryer, even at a primary drying temperature as low as -40° C (the lowest maintainable sample temperature). Consequently, the resulting precursors suffered phase separation and were not atomically mixed. It appeared that it was the zirconyl nitrate, ZrO(NO₃)₂, that was responsible for the lower melting point of the solution since there was no melting in CaTiO(NO₃)_x solutions of the same ionic concentration at substantially higher temperatures. The mole percentage of Zr in SYNROC-B is minor (~6.8%) compared to that of CaZrTi₂O₇ (25%). The presence of ZrO(NO₃)₂ did not lower the eutectic point of the SYNROC-B nitrate solutions below -40°C, which allowed the preparation of a solid atomic mixture by freeze drying.

6.2.2.3 Perovskite

The XRD pattern of the freeze dried $\text{CaTiO}(\text{NO}_3)_x$ precursor was also indistinguishable from blank Kapton tape. Calcination of this precursor for 10 min at 500°C under 600 torr of pure O_2 resulted in the formation of poorly crystalline (as evidenced by the broadness of the diffraction peaks) CaTiO_3 . However, increasing the calcination temperature resulted in the formation of impurity phases, CaO and TiO_2 (see Figure 6.8). This may have been the result of phase separation due to melting of

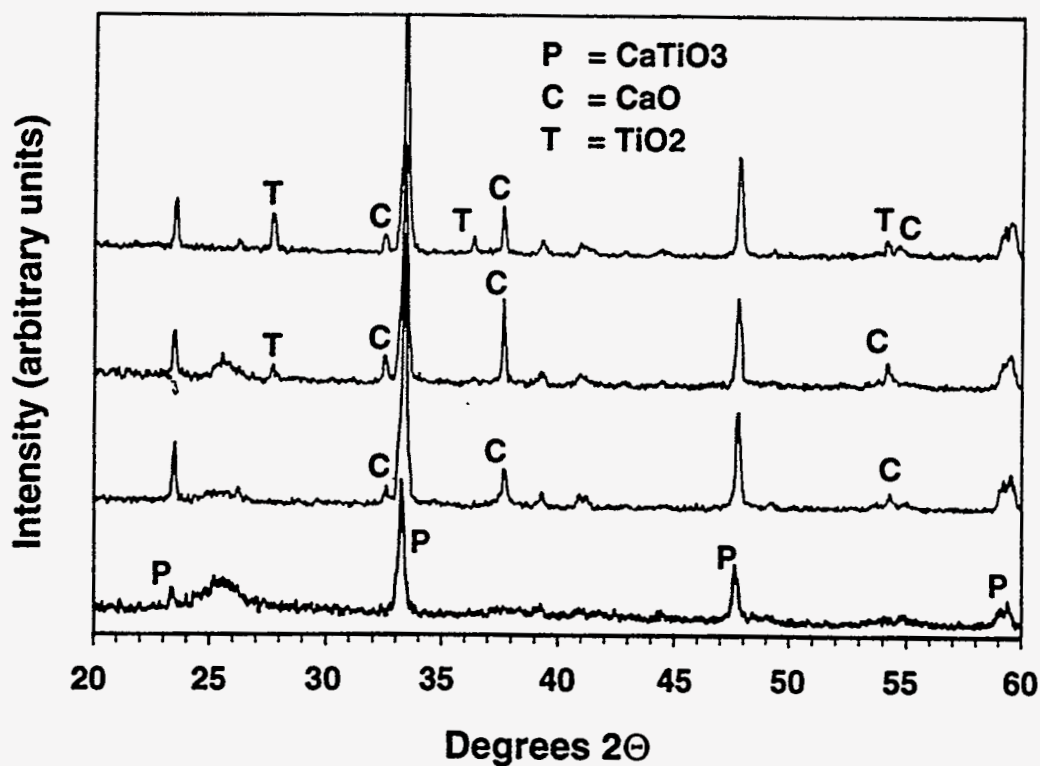


Figure 6.8. X-ray diffraction pattern of the freeze dried, calcium and titanyl nitrate precursor calcined for 10 min at (from bottom) 500°C , 600°C , 800°C , and 1000°C . Peaks labeled P correspond to perovskite, C correspond to CaO (lime), and T correspond to TiO_2 (rutile).

$\text{Ca}(\text{NO}_3)_2$, which is reported to melt at 561°C .⁹ Some powder shrinkage, evidence of melting, was noticed in the perovskite samples. Regardless, the temperature of formation of CaTiO_3 was much lower than it was in the SYNROC-B mixture. In the latter, CaTiO_3 peaks were not apparent until a temperature of 900°C was reached. This significant increase (400°C) in the temperature of appearance of CaTiO_3 may have been due to the presence of excess Zr and Ti resulting in the formation of a fluorite type $\text{Ca}(\text{Zr}_x\text{Ti}_{1-x})\text{Ti}_2\text{O}_7$ solid solution (the fluorite type $\text{CaZrTi}_2\text{O}_7$ with partial Ti^{4+} substitution for Zr^{4+}). This idea is supported by the fact that in the SYNROC mixture, the temperature for phase formation of the zirconolite-type $\text{CaZrTi}_2\text{O}_7$ corresponded to that of CaTiO_3 . It appears that this $\text{Ca}(\text{Zr}_x\text{Ti}_{1-x})\text{Ti}_2\text{O}_7$ solid solution phase separated at higher temperatures to yield the two SYNROC phases, perovskite and zirconolite. When no zirconium was present in the atomic mixture, the perovskite phase formed at much lower temperatures.

6.3 Conclusion

It has been demonstrated that the complete SYNROC-B phase assemblage can be synthesized at ambient pressure (600 torr) through the calcination of atomic mixtures of nitrate salts prepared by freeze drying. Thermal processing of the freeze dried precursor for 10 min at 1100°C or 15h at 1000°C (in a 5% H_2 /Ar atmosphere) yielded the desired product. These regimens are a significant improvement over the conventional preparation proposed by Ringwood,² and the procedure is compatible with the radiological glovebox environment within which HLNW is generally handled. An additional problem which needs to be addressed in the future is sintering. Although the correct phases are present

for immobilization of HLNW as solid solution, the material will need to be sintered into compacts before burial in deep geological formations. Sintering is necessary to reduce the surface area. Leaching rates of HLNW upon exposure to H₂O are dependent upon the surface area. Although the phases have been synthesized in short annealing times at relatively low temperatures (1000° to 1100° C), it may be necessary to use higher temperatures, longer annealing times or higher pressures to fully sinter the materials. These freeze dried powders, due to their uniform, small particle sizes, should sinter at lower temperatures than the large and nonuniform particles resulting from calcination of a mechanical mixture. These issues, however, were not addressed here, and are left for future work.

6.4 Notes and References

- ¹ A. E. Ringwood, *Safe Disposal of High Level Nuclear Reactor Wastes: A New Strategy*, Australian National University Press (Norwalk, Connecticut, 1978).
- ² A. E. Ringwood, S. E. Kesson, N. G. Ware, W. Hibberson, and A. Major, *Nature* **278**, 219 (1979).
- ³ W. J. Buykx, D. J. Cassidy, C. E. Webb, and J. L. Woolfrey, *Am. Ceram. Soc. Bull.* **60**, 1284 (1981).
- ⁴ E. R. Vance, C. J. Ball, M. G. Blackford, D. J. Cassidy, and K. L. Smith, *J. Nuclear Mater.* **175**, 58 (1990).
- ⁵ R. W. Cheary, J. V. Hunt, and P. Calaizis, *J. Aust. Ceram. Soc.* **17**, 11 (1981).
- ⁶ A. G. Solomah, T. M. Hare, and H. Palamour III, *Trans. Am. Nucl. Soc.* **34**, 197 (1980).
- ⁷ S. E. Kesson and T. J. White, *Proc. R. Soc. Lond. A* **405**, 73 (1986).
- ⁸ A. Pring, D. A. Jefferson, and J. M. Thomas, *J. Solid State Chem.* **55**, 125-132.
- ⁹ R. C. Weast, Editor, *CRC Handbook of Physics and Chemistry, 56th Edition*, CRC Press Inc., (Cleveland, 1975).

CHAPTER 7

**PREPARATION OF OXIDE FILMS FROM COMBUSTION OF
NON-AQUEOUS SOLUTIONS**

The preparation of multi-cation oxide films is an important area of synthetic solid state chemistry. Thin films of high temperature superconductors are of particular interest due to the high critical current densities these materials have displayed ($>5 \times 10^6 \text{ A/cm}^2$).¹ These high critical current densities are possible due to the phenomenon of epitaxy (one crystalline phase growing on a crystal face of another phase).² Epitaxy allows for a nearly perfect, single crystal like sheet of superconducting material to be prepared. Since the supercurrents in the high temperature superconducting cuprates are confined to the a-c plane, a film with the b-axis oriented perpendicular to the substrate allows for alignment of the a-c plane, and uninterrupted flow of the supercurrents. Consequently, many of the potential applications of high temperature superconductivity (discussed in section 2.4) require the materials to be in the form of thin films.

As discussed in section 3.2, many of the techniques used for the preparation of thin films of high temperature superconductors require high vacuum conditions. In this work, an open air, atmospheric pressure, deposition method was developed and utilized for the production of thick films of $\text{Ba}_2\text{YCu}_3\text{O}_{7-x}$ and $(\text{Bi,Pb})_2\text{Sr}_2\text{Ca}_2\text{Cu}_3\text{O}_{10}$, and thin films of $\text{Ba}_2\text{YCu}_3\text{O}_{7-x}$. This method is referred to as the flaming solvent spray (FSS) method.³ As with the other synthetic methods discussed in this work, the method introduced in this

chapter takes advantage of the intimate mixing of reactants which can be obtained from a solution. The method consisted of dissolving the necessary metal salts in a flammable solvent, atomizing the solution with an oxidizing gas, igniting the aerosol and allowing the resulting flame to coat a substrate. The flame served to rapidly evaporate/decompose the solvent, trapping the perfect homogeneity of the solution and transferring this homogeneity into the solid state. The flame also provided heat to the substrate, necessary to facilitate diffusion and reaction in the solid state. In the preparation of bulk materials, these two factors (atomic level mixing of reactants and sufficiently high temperatures) led to rapid product formation. In the case of the FSS method, they allowed the product, $\text{Ba}_2\text{YCu}_3\text{O}_{7-x}$, to be obtained in-situ.

When used for the preparation of thick films, the total metal ion concentration of the solution was about 0.06M. This concentration allows rather large particles to impinge upon the substrate. In this case, the method is very much like a normal spray pyrolysis method, with the distinct advantage of supplying its own heat to the substrate. For the production of thin films, the total metal ion concentration of the solution was reduced to $< 0.001\text{M}$. The solute particles resulting from combustion of such a solution are much smaller than those of a more concentrated solution, and approach the limit of a gas phase deposition. With decreasing solution concentration, the method becomes less like a spray pyrolysis method, and more like a chemical vapor deposition.

Three, non-aqueous solvents were used in the method. Preliminary studies, in which most of the mechanical details of the method were developed, were performed with two organic solvents, ethanol and ethylene glycol. The thoroughly studied solvent system

was liquid ammonia. Liquid ammonia was the solvent of choice due to its non-carbonaceous nature. When metal nitrates were dissolved in liquid ammonia (along with appropriate choice of carrier gas and pilot flame), the entire FSS system was free of carbon. Carbon deposits have been found to build up at grain boundaries of high temperature superconducting cuprates and have detrimental effects on material properties.⁴ In addition, the presence of carbon allows the formation of BaCO_3 , which is a relatively stable phase and requires high reaction temperatures for complete decomposition. It can be argued that the advantages of a carbon free system are lost if the deposition takes place in air (a source of CO_2). It was the hope of the author that the high flow rate of the spray and flame would serve to blanket the substrate with a carbon free region. Enclosing the entire system in a nitrogen, argon, or oxygen atmosphere would have been possible. However, the advantages of the method over the current technology (i.e. no need for a vacuum chamber or controlled atmosphere, open air deposition) would become less clear.

Silver was added to some of the samples in an attempt to improve the superconducting properties of the films. The addition of silver to bulk samples of $\text{Ba}_2\text{YCu}_3\text{O}_{7-x}$ has been shown to improve the critical current density,⁵ environmental stability,⁶ contact at interfacial grain boundaries,⁷ and the magnetic properties and Meissner effect (levitation above and suspension below a permanent magnet).⁸ The silver is believed to fill the intergranular spaces in the samples without substituting for copper in the $\text{Ba}_2\text{YCu}_3\text{O}_{7-x}$ lattice.⁵

In the following section, the general considerations which went into the choice of solvent, reagents, carrier gas, pilot flame, and substrate will be reviewed. This will be followed by an overview and some results of the preliminary studies with the organic

solvents. Finally, the experimental procedure and results of the liquid ammonia FSS method for the production of thick and thin films of $\text{Ba}_2\text{YCu}_3\text{O}_{7-x}$ will be discussed.

7.1 General Considerations

7.1.1 Solvent

Three solvents, ethanol, ethylene glycol, and liquid ammonia, were used. The factors that went into the choice for a solvent were; (1) flammability, (2) ability to form stable solutions of yttrium, barium and copper (or Bi, Sr, Ca, Pb, Ag), (3) reasonably low viscosity (to allow good atomization), (4) non-toxicity (e.g., methanol was avoided), and (5) absence of halides (which tend to be volatile and would result in a loss of stoichiometry), sulfur, or phosphorous (which would result in sulfates and phosphates instead of oxides). Liquid ammonia was chosen due to the advantage of being free of carbon in addition to meeting all of the above criteria.

7.1.2 Reagents

The reagents used were $\text{Y}(\text{NO}_3)_3 \cdot 5\text{H}_2\text{O}$, $\text{Ba}(\text{NO}_3)_2$, $\text{Cu}(\text{NO}_3)_2 \cdot 5\text{H}_2\text{O}$ and $\text{Ag}(\text{NO}_3)$, or $\text{Y}(\text{O}_2\text{CCH}_3)_3 \cdot 4\text{H}_2\text{O}$, $\text{Ba}(\text{O}_2\text{CCH}_3)_2$, $\text{Cu}(\text{O}_2\text{CCH}_3)_2 \cdot \text{H}_2\text{O}$ and $\text{Ag}(\text{NO}_3)$. When preparing bismuth based superconductors the reagents used were $\text{Bi}(\text{NO}_3)_3 \cdot 5\text{H}_2\text{O}$, $\text{Sr}(\text{NO}_3)_2$, $\text{Ca}(\text{NO}_3)_2 \cdot 4\text{H}_2\text{O}$, $\text{Pb}(\text{NO}_3)_2$ and $\text{Cu}(\text{NO}_3)_2 \cdot 5\text{H}_2\text{O}$. All were certified 99.9% pure or better by the supplier, Johnson Matthey. Reagents that had waters of hydration were analyzed gravimetrically, as discussed in section 4.1.2, to determine their exact metal contents. These reagents were chosen due to their availability, stability and relatively low cost compared to metal alkoxides

(alternative salts to use in alcohol solutions). These salts also decompose to their oxides without any foreign elemental impurities. Copper(II)tetraamine nitrate, $\text{Cu}(\text{NH}_3)_4(\text{NO}_3)_2$, was used in the liquid ammonia variation due to its environmental stability (with respect to weight gains due to atmospheric moisture) relative to hydrated copper nitrate. This compound was prepared by adding ammonium hydroxide to a concentrated solution of $\text{Cu}(\text{NO}_3)_2 \cdot x\text{H}_2\text{O}$. After the initial precipitation of $\text{Cu}(\text{OH})_2$, further addition of ammonium hydroxide caused dissolution and the appearance of a deep purple color, due to the presence of the $\text{Cu}(\text{NH}_3)_4^{2+}$ ion. $\text{Cu}(\text{NH}_3)_4(\text{NO}_3)_2$ was then be crystallized from this solution by removal (by evaporation) of sufficient water or cooling the solution to 0°C . The exact Cu content of this compound was determined electrogravimetrically, as described elsewhere.⁹ Ammonium nitrate, NH_4NO_3 (reagent grade, Fisher Scientific), which aided in combustion by acting as an internal source of oxygen, was also added to some dilute solutions

For the preparation of thin films, very dilute ($\sim 0.0003 \text{ M}$ in Y) liquid ammonia solutions were used. Obtaining an accurate stoichiometric ratio in weighing such minute quantities was difficult. To circumvent this problem, a stoichiometric, aqueous stock solution of $\text{Y}(\text{NO}_3)_3$, $\text{Ba}(\text{NO}_3)_2$ and $\text{Cu}(\text{NO}_3)_2$ was prepared. Yttrium oxide, Y_2O_3 (99.99%, Johnson Matthey), and copper oxide, CuO (99.999%, Johnson Matthey), were dissolved in aqueous nitric acid in a 1.000 mol Y to 3.000 mol Cu ratio. Barium nitrate, $\text{Ba}(\text{NO}_3)_2$ (99.999%, Johnson Matthey), was then added to this solution to give a 1.000Y:2.000Ba:3.000Cu ratio. The mass of the entire solution was then measured and a mass% of reagents in the solution was calculated. This solution was then stored in a Teflon bottle until needed. For the preparation of thin films, this solution was added dropwise to a flask until a mass corresponding to the desired

amount of metal nitrates was achieved. The flask was then placed in an oven at 90° C until the water and excess HNO₃ evaporated, leaving behind a stoichiometric mixture of yttrium, barium and copper nitrates.

7.1.3 Pilot Flame and Propellant Gas

The choice of pilot flame depended upon many of the same factors that went into the choice of solvent. Natural gas (CH₄) was used as the flame in the ethanol and ethylene glycol variations. This choice was made due to the ease of access to natural gas. The carbonaceous residue from natural gas was considered insignificant when compared to that of the combustion of the organic solvents (or organic acid salts dissolved in the solvent). With the liquid ammonia variation, every effort was made to remove carbon from the system. For this reason, the natural gas burner was replaced with a hydrogen/ oxygen torch.

The choice of propellant gas for the spray was governed, through trial and error, by the gas that best served to sustain a uniform combustion of the solvent. Compressed air proved to be sufficient for the ethanol variation but pure oxygen was needed in the ethylene glycol method. In the liquid ammonia variation, nitrous oxide served to oxidize the ammonia more readily than pure oxygen. The choice of nitrous oxide was consistent with the desire to have the liquid ammonia variation be a carbon free system. The elements of the three solvent systems are given in Table 7.1.

Table 7.1 Anion of reagents, pilot flame, and carrier gas used for the three solvent systems.

	Ethanol	Ethylene Glycol	Liquid Ammonia
Anion	acetates	nitrates	nitrates
Flame	CH ₄ , air	CH ₄ , air	H ₂ , O ₂
Carrier gas	air	O ₂	N ₂ O

7.1.4 Substrate

The substrates employed for thick film production by the FSS process were polycrystalline samples of Al₂O₃, SrTiO₃, YSZ, Si, MgO and stainless steel. The best results for thick films were obtained on MgO (obtained from Transtech Inc.). MgO has been proven to be extremely inert to reaction with the Ba-Y-Cu-O system at temperatures below 1000° C.¹⁰ Single crystal (100 orientation) lanthanum aluminate, LaAlO₃, was used in attempts to produce thin, epitaxial films. LaAlO₃ is also relatively inert with respect to the Ba-Y-Cu-O system.

7.1.5 Substrate Preparation

The preparation of the substrate before deposition is an important aspect. The substrates must be extremely clean for a uniform film to be produced. To assure cleanliness of the substrate, all LaAlO₃ or MgO substrates were soaked in aqua regia (about 3 parts concentrated HCl to 1 part concentrated HNO₃ by volume) for 15 min. Longer soaking times (up to 24 h) caused dissolution of the MgO but had no visible effect on the LaAlO₃. This procedure served both to clean and etch the surface of the substrates prior to deposition. The substrates were then thoroughly washed with distilled and deionized (d.d.) H₂O. The final step

of the cleaning process was soaking the substrates in an ultrasonic bath of isopropanol. This served to degrease the substrates and also remove any loose particles from the surface. After the cleaning procedure, the substrates were left in the isopropanol and handled only with clean stainless steel or Teflon tweezers.

7.2 Preliminary Studies With Organic Solvents

Ethanol and ethylene glycol were the first solvents used in the FSS process for the preparation of thick films. The work done with the organic solvents was mainly preliminary, as liquid ammonia was found to be preferential before the organic solvent systems were thoroughly studied. The work with the ethanol variation, however, served to develop many of the mechanical and technical aspects of the method.

7.2.1 Experimental Procedure

When ethanol was used as the solvent, 0.0200 mol barium acetate, 0.0100 mol yttrium acetate, and 0.0300 mol copper acetate was dissolved in ~1L of an approximately 80% ethanol/ d.d. water mixture (by volume). Approximately 25mL of glacial acetic acid was added to the solution to prevent precipitation of hydroxides and ethoxides. Nitrates could not be used in ethanol solutions due to the low solubility of barium nitrate. When ethylene glycol was used as the solvent, the nitrates of barium, yttrium and copper were dissolved in pure ethylene glycol in the same concentration and stoichiometry. In attempts to improve grain contact and lower the room temperature resistivity of the films, silver (1.5 to 7.5 wt%) was added to some of the solutions as silver nitrate. The ethanol and ethylene glycol solutions were heated, with magnetic

stirring, to about 70° C (boiling point =78.5° C) and 100° C (boiling point=198° C), respectively. They were then sprayed through an atomizing nozzle which consisted of a thin (0.5 mm inner diameter) inner tube through which the solution was fed, surrounded by an outer tube (5 mm inner diameter). The aerosol was created by sending a stream of the oxidizing gas (compressed air for ethanol solutions and pure O₂ for ethylene glycol solutions) through the outer tube of the spray nozzle. The solution was brought from the reservoir to the nozzle by the low pressure created by the Venturi effect. The solution flow rate was controlled at 15mL/min by adjusting the pressure of the carrier gas and maintaining the fluid level of the reservoir at a constant height by use of a manual jack. The flame was ignited by the positioning of a natural gas burner under the spray nozzle, which served as a pilot flame. The spray nozzle and the natural gas burner were motor driven at a rate of 7 r.p.m. with a traverse of 10 cm to assure even coating of two 2.54 cm x 2.54 cm substrates (see Figure 7.1). The substrates were held in place on a stainless steel plate fitted with an insertion heater. They were initially heated to 300° C before the spray was started to prevent thermal shock and cracking of the MgO. Once the flaming spray began the insertion heater was turned off as there was no need for additional heating. The surface temperature of the substrate during deposition was measured at over 800° C for both solvents, by positioning of a chromel-alumel thermocouple in a MgO tube below the substrates.

After deposition, the substrates were taken from the steel plate with stainless steel tweezers and placed in a box furnace (Lindberg, model # 51848) preheated to 550° C. The furnace temperature was increased at 5° C/min to 940° C, where the films were soaked for 2 h. They were allowed to cool to room temperature at 5° C/min and then heated in the same

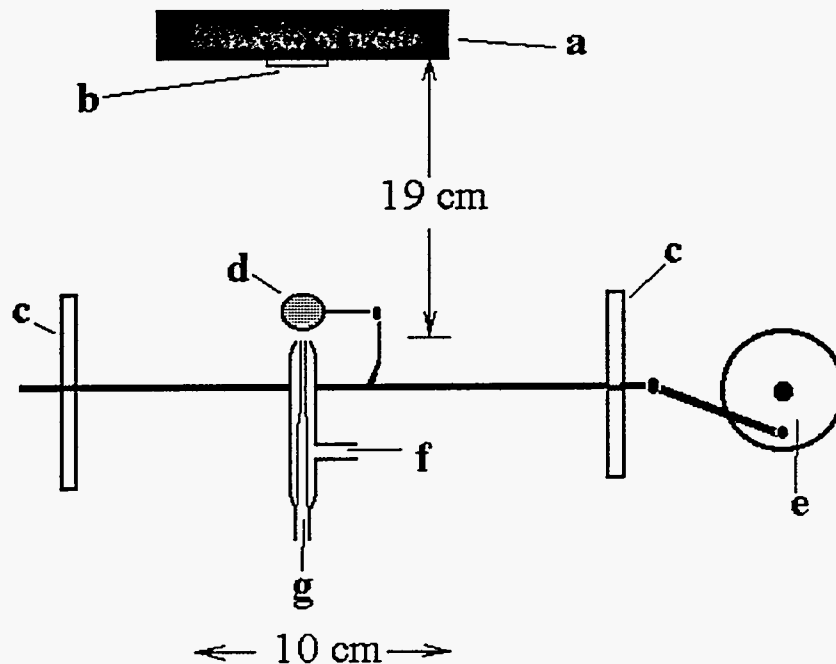


Figure 7.1 A schematic top view of the FSS experimental setup. The tip of the spray gun was fixed at 19 cm from the steel plate. The spray nozzle was motor driven across a region 10 cm in length. The labeled parts correspond a) steel plate, b) substrate, c) Teflon guides, d) natural gas burner (or H_2/O_2 torch), e) 7 or 1 r.p.m. motor, f) carrier gas inlet, and g) solution inlet.

furnace for an additional 24 h at 940°C to allow sintering and reduce the number of weak links between grains. When the films contained silver, the annealing temperature was lowered to 915°C . Metallic silver was suspected of promoting the formation of BaY_2CuO_5 at higher temperatures.¹¹ In order to obtain a low value of x in the formula $\text{Ba}_2\text{YCu}_3\text{O}_{7-x}$ (and the maximum T_c), the final step in the preparation was a 5 h soak at 550°C under oxygen (in a Lindberg horizontal tube furnace fitted with a quartz tube, model #55332) followed by a slow cooling ($1^\circ\text{C}/\text{min}$) to room temperature.

The ethanol process was also employed to prepare thick films in the Bi-Pb-Sr-Ca-Cu-O system. The necessary nitrates were dissolved in the ratio 1.7Bi:0.3Pb:2.0Sr:2.0Ca:3.0Cu in an approximately 80% ethanol/H₂O mixture (by volume). Lactic acid (2-hydroxypropanoic acid) was added to stabilize the bismuth in solution. The remainder of the procedure is identical to the Ba₂YCu₃O_{7-x} process except for the heat treatment. The Bi_{1.7}Pb_{0.3}Sr₂Ca₂Cu₃O₁₀ films were heated to 800° C at a rate of 5° C per minute and soaked at 800° for 10 h. They were then heated at 1° C per minute to 850°, soaked for 10 h and allowed to cool to room temperature at a rate of 5° C per minute.

7.2.2 Results and Discussion

The flaming spray of ethanol and ethylene glycol solutions burned with a green flame due to atomic emission from barium during the production of Ba₂YCu₃O_{7-x} films. When Bi₂Sr₂Ca₂Cu₃O₁₀ films were produced, the flame had a red glow due to atomic emission from strontium. This was strong evidence that some of the reactants had entered the gas phase. There was no visual evidence of liquid material hitting the substrate at a distance of 19 cm.

Although the temperature of deposition (>800° C) was high enough to form the Ba₂YCu₃O_{7-x} phase, the x-ray diffraction (XRD) pattern of "as-sprayed" films displayed peaks corresponding to BaCO₃, with the copper and yttrium presumably present as amorphous phases. The as-sprayed films were dark brown in color, which suggested the presence of metallic copper. After a post anneal at 940° C for 2 h, the Ba₂YCu₃O_{7-x} phase was obtained. A second heat treatment (up to 24 hours) at 940° C resulted in a lower room temperature resistance, presumably due to improved the grain contact in the films. The X-ray

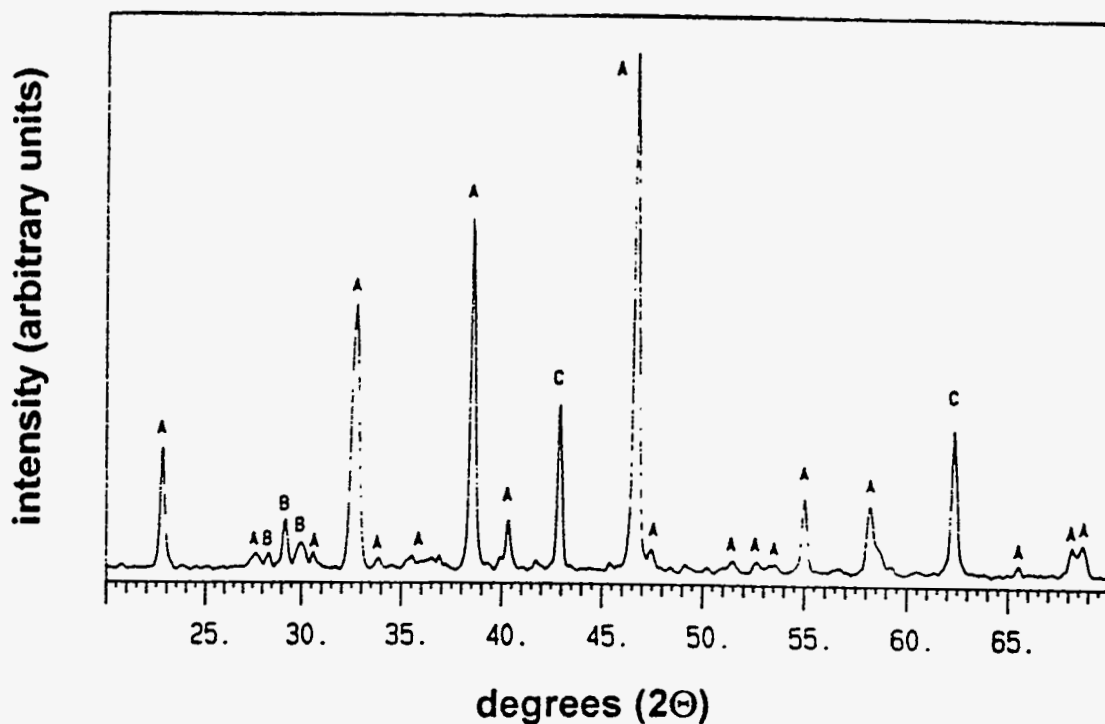


Figure 7.2. An XRD pattern for an ethanol FSS film after thermal processing at 940° C for 24h. The pattern reveals some alignment of the b-axis of $\text{Ba}_2\text{YCu}_3\text{O}_7$ perpendicular to the MgO substrate. Peaks labeled A correspond to $\text{Ba}_2\text{YCu}_3\text{O}_{7-x}$, B to BaY_2CuO_5 , and C to substrate (MgO) peaks.

diffraction data showed $\text{Ba}_2\text{YCu}_3\text{O}_{7-x}$ as the major phase with BaY_2CuO_5 as a minor phase (see Figure 7.2). In addition, MgO peaks from the substrate were observed. The diffraction pattern displayed an increase in the relative intensities of the $0k0$ type peaks due to preferred orientation of the b-axis of $\text{Ba}_2\text{YCu}_3\text{O}_{7-x}$ crystallites perpendicular to the substrate. The extent of the preferred orientation was apparently dependent on the thickness of the film, since it was not noticed in films which showed no substrate peaks. Resistance versus temperature measurements showed a T_c onset at 90 K and a T_{c0} (loss of all resistance) at 60 K

(see Figure 7.3). The addition of 10 mol% silver ($\text{Ag}_{0.1}\text{Ba}_2\text{YCu}_3\text{O}_{7-x}$) raised the T_{c0} to 64 K and improved the pre-transition metallic behavior. The silver was not detected by XRD.

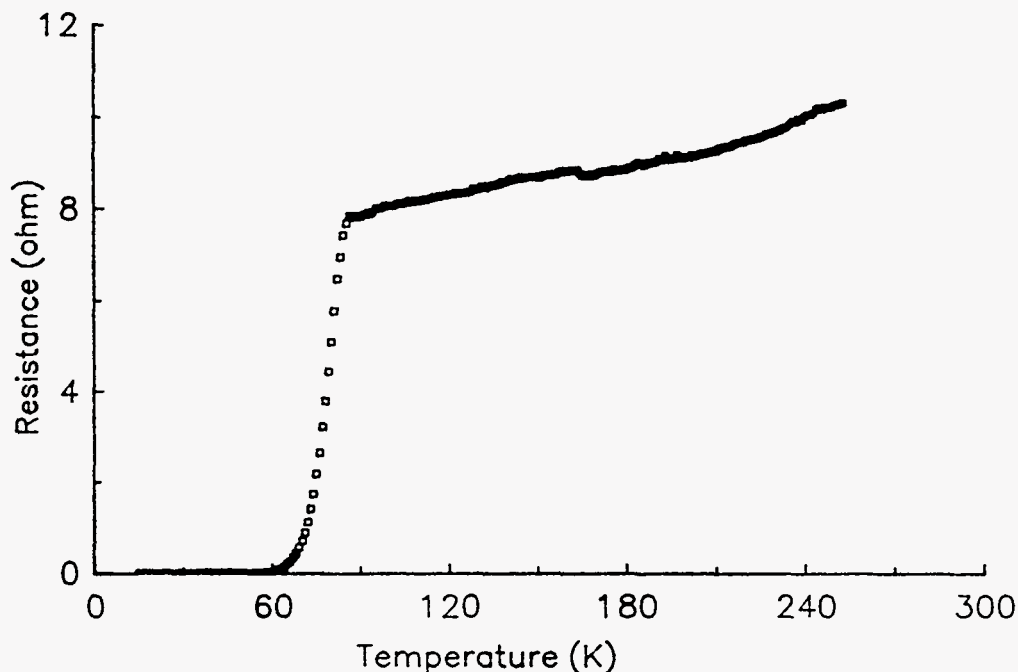


Figure 7.3. The resistivity versus temperature plot for a $\text{Ba}_2\text{YCu}_3\text{O}_{7-x}$ film prepared via ethanol FSS.

The as-sprayed films prepared from ethylene glycol solutions were nearly identical in composition to the ethanol solution films, in that they were brown and the XRD contained only BaCO_3 peaks. After post annealing, XRD patterns indicated that the films contained $\text{Ba}_2\text{YCu}_3\text{O}_{7-x}$ as the major phase. Resistance versus temperature data showed a T_c onset at 85 K and a T_{c0} at 71 K. With silver doped ethylene glycol FSS films of composition $\text{Ag}_{0.5}\text{Ba}_2\text{YCu}_3\text{O}_{7-x}$, XRD revealed that $\text{Ba}_2\text{YCu}_3\text{O}_{7-x}$ was the major phase (see Figure 7.4). Small amounts of BaY_2CuO_5 and metallic silver were also detected by

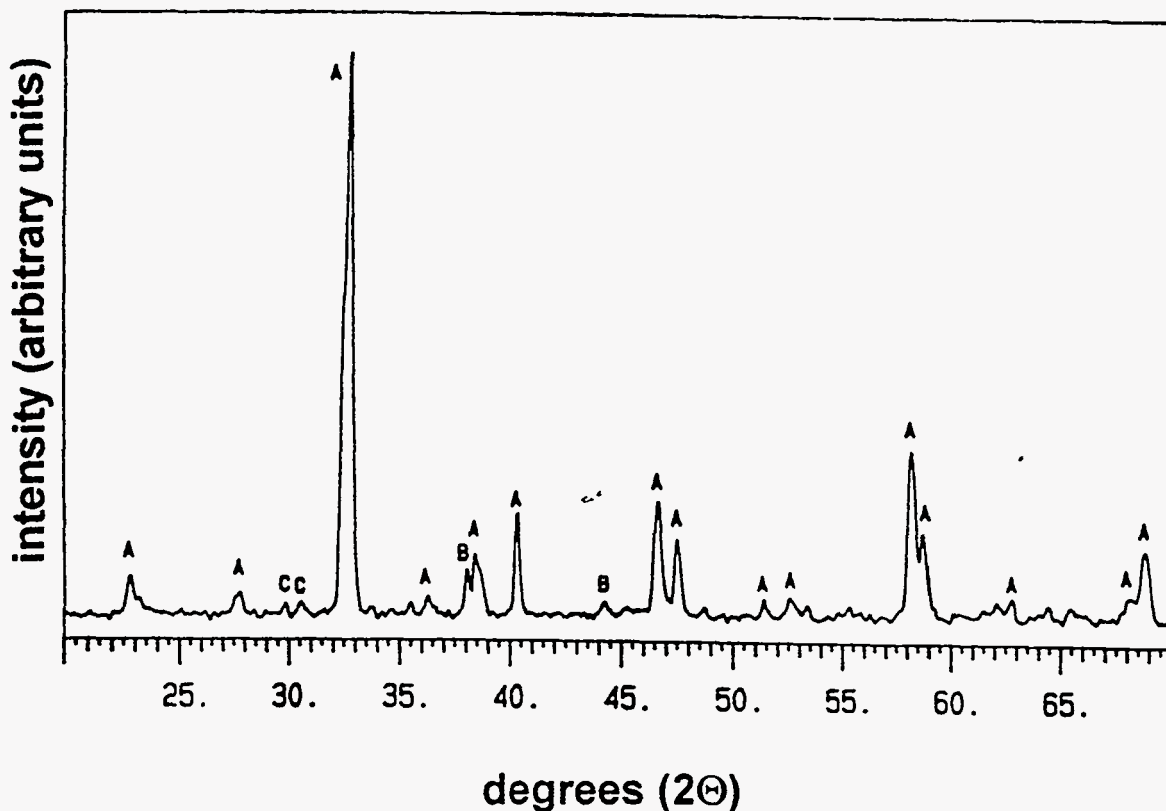


Figure 7.4. An XRD pattern of a film with nominal composition, $\text{Ag}_{0.5}\text{Ba}_2\text{YCu}_3\text{O}_{7-x}$, prepared via ethylene glycol FSS. The peaks labeled A correspond to $\text{Ba}_2\text{YCu}_3\text{O}_{7-x}$, B to metallic silver, and C to BaY_2CuO_5 .

XRD. The amount of BaY_2CuO_5 detected was found to be dependent upon the post annealing temperature. Exceeding 915°C promoted decomposition of $\text{Ba}_2\text{YCu}_3\text{O}_{7-x}$ to BaY_2CuO_5 .¹¹ No increase in the relative intensities of the 0k0 type peaks was evident in the XRD pattern of this ethylene glycol sprayed film, which indicates that the sample had a random orientation. This may have been due to the thickness of the sample (which was thick enough to exclude substrate peaks) or to the lower temperatures used in the thermal processing (915°C as opposed to 940°C). Resistivity measurements on the Ag doped, ethylene glycol FSS films showed a T_c onset at 90K and a T_{c0} at 76 K (Figure 7.5).

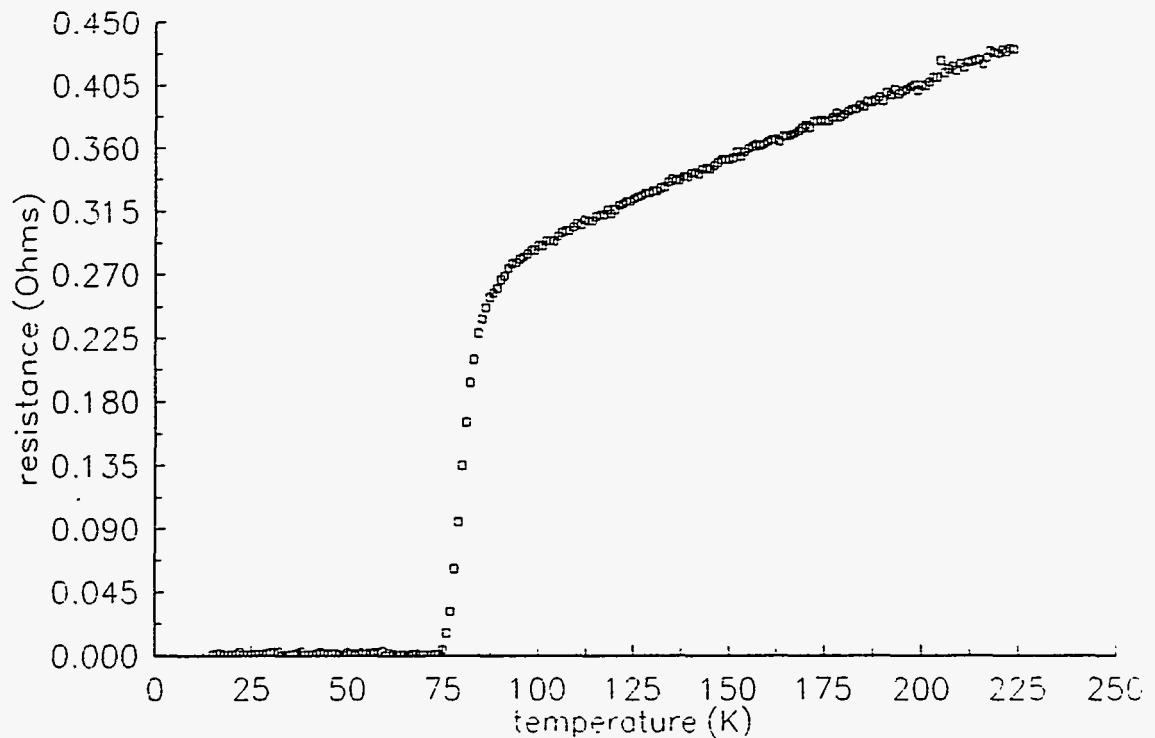


Figure 7.5. The resistance versus temperature plot for a film of nominal composition $\text{Ag}_{0.5}\text{Ba}_2\text{YCu}_3\text{O}_{7-x}$, prepared via ethylene glycol FSS.

The pre-transition resistance was substantially lowered by the addition of silver. The observed increase in T_c with addition of metallic silver to the films is evidence for a large number of weak links in the material. Further evidence for poor grain contact was obtained from scanning electron micrographs of ethylene glycol FSS films. The material was largely deposited in a series of islands, instead of a continuous sheet.

Thick films in the Bi-Pb-Sr-Ca-Cu-O system with nominal composition $\text{Bi}_{1.7}\text{Pb}_{0.3}\text{Sr}_2\text{Ca}_2\text{Cu}_3\text{O}_{10}$ were prepared via ethanol FSS. However, both XRD and resistivity measurements indicated that $\text{Bi}_2\text{Sr}_2\text{CaCu}_2\text{O}_8$ was the major phase and $\text{Bi}_{1.7}\text{Pb}_{0.3}\text{Sr}_2\text{Ca}_2\text{Cu}_3\text{O}_{10}$

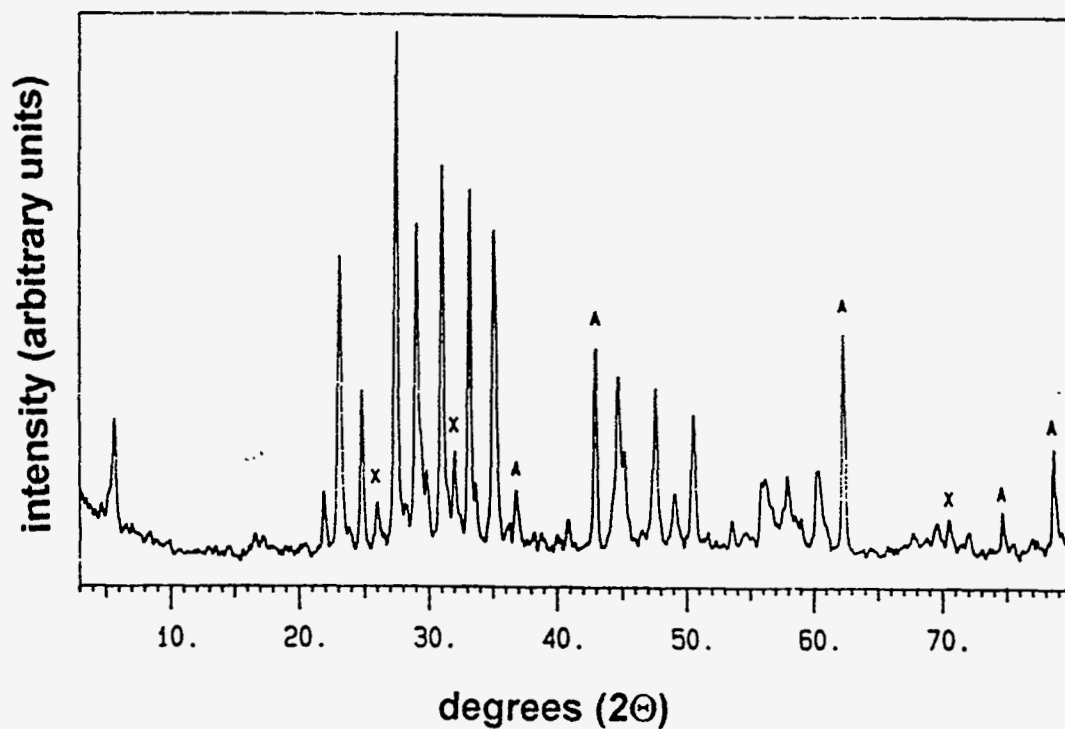


Figure 7.6. The XRD pattern for a film of nominal composition $\text{Bi}_{1.7}\text{Pb}_{0.3}\text{Sr}_2\text{Ca}_2\text{Cu}_3\text{O}_{10}$, prepared via ethanol FSS. Peaks labeled A correspond to MgO (substrate). Peaks labeled X correspond to an unidentified phase

was a minor phase. Substrate (MgO) peaks were also seen in the XRD pattern (see Figure 7.6).

The resistance versus temperature plot for the film (Figure 7.7) showed a small drop in resistance at about 105 K, resulting from the presence of some $\text{Bi}_{1.7}\text{Pb}_{0.3}\text{Sr}_2\text{Ca}_2\text{Cu}_3\text{O}_{10}$.

A sharper drop in resistance occurred at 75 K, due to the large volume fraction of $\text{Bi}_2\text{Sr}_2\text{CaCu}_2\text{O}_8$. Loss of all resistance (T_{c0}) occurred at about 65 K.

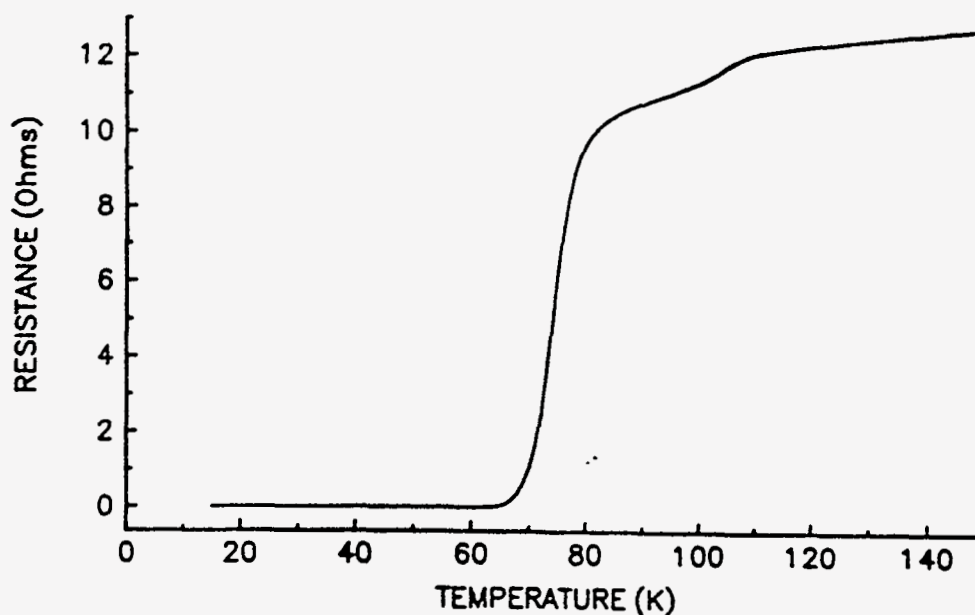


Figure 7.7. The resistivity versus temperature plot for a film of nominal composition $\text{Bi}_{1.7}\text{Pb}_{0.3}\text{Sr}_2\text{Ca}_2\text{Cu}_3\text{O}_{10}$, prepared via ethanol FSS.

7.3 Preparation of Thick Films of $\text{Ba}_2\text{YCu}_3\text{O}_{7-x}$ From Combustion of Liquid

Ammonia Solutions

The liquid ammonia FSS process was the most thoroughly studied system due to the unique factor that the solution, reagents, pilot flame, and carrier gas were all noncarbonaceous. For this system, flow rates of all constituent gases (H_2 , O_2 , N_2O , and N_2) were monitored in attempts to obtain the optimum deposition parameters. The solution concentration was also varied to obtain a maximum superconducting transition temperature, without sacrificing the mechanical integrity of the films (adhesion to the substrate, relatively smooth surface etc.,).

7.3.1 Experimental Procedure

The experimental apparatus was similar to that of the preliminary studies (see Figure 7.1 and Figure 7.8). The same steel plate was used to hold and initially heat the substrates. The flaming spray was motor driven at 7 r.p.m. over a traverse of 10 cm. The liquid ammonia solutions were prepared as follows. The necessary reagents, $Y(NO_3)_3 \cdot xH_2O$, $Ba(NO_3)_2$, and $Cu(NH_3)_4(NO_3)_2$ were placed in a 1000 mL round bottom flask in which a side arm (5 mm inner diameter) was fitted as a gas outlet. The actual amount of reagents added was varied in attempt to obtain optimal superconducting properties. After observing that dilute solutions did not burn as efficiently as more concentrated (0.01M in Y) solutions, it was concluded that the nitrate ion was acting as an internal source of oxygen and aiding in the combustion of the ammonia. When solutions which had concentrations below 0.01 M were used (which corresponds to 0.13 mol of nitrate ion per liter for $Ba_2YCu_3O_{7-x}$), ammonium nitrate was added to the reagents to keep the concentration of nitrate ions constant at ~ 0.13 M. The flask was flushed with dry nitrogen for 15 min to remove H_2O and CO_2 . When the flask was sufficiently flushed, 900 mL of liquid ammonia was condensed from the gas by the use of a cold finger containing a dry ice/acetone slurry. The flask was positioned in an insulated bath of dry ice/acetone on a hot plate equipped with magnetic stirring. The solution was stirred with a Teflon coated magnetic stirring bar to aid in the dissolution of the reagents. Stirring of the solution also served to speed up the condensation of the ammonia by providing better heat transfer between the dry ice and the surface of ammonia. When 900 mL had been collected, the ammonia inlet was replaced with a nitrogen purge to protect the solution from carbon contamination from the atmosphere. Carbon dioxide and ammonia react to form ammonium

carbonate and ammonium carbamate which would serve as potential sources of carbon for barium carbonate formation on the substrate. In order to eliminate all carbon from the system, the natural gas burner used in the preliminary studies with organic solvents was replaced by a hydrogen-oxygen torch. Nitrous oxide (N_2O) was used as the carrier gas to aid in the combustion of the ammonia. A sufficient flame could not be sustained without the use of N_2O .

Four solution concentrations were studied for the ammonia FSS process. These concentrations were stoichiometric quantities of yttrium, barium, and copper nitrates, based on an yttrium nitrate mass of 1.000 g, 2.000 g, 3.000 g, and 4.000 g. These correspond to total metal concentrations (for $Ba_2YCu_3O_{7-x}$ stoichiometry) of 0.016 M, 0.032M, 0.048M and 0.064M, respectively. In some of the 0.016M and 0.032M solutions, silver nitrate was added (to a nominal composition of $Ag_{0.5}Ba_2YCu_3O_{7-x}$) to improve the room temperature resistivity of the films. No silver nitrate was added to the two higher concentrations since the resulting films were thicker, and sufficiently conductive at room temperature.

There were four compressed gases needed in the ammonia FSS process, the flow rates of which were measured with rotameters (see Figure 7.8). The flow rates of hydrogen and oxygen (which served as the source of the pilot flame) were measured with an Omega rotameter (model # N034-39G) capable of reading flow rates between 350 and 9230 mL/min. The N_2 purge served to protect the liquid ammonia solution from atmospheric contamination and also provided additional pressure to raise the solution through the supply tube to the spray nozzle. This flow rate was measured with an Omega rotameter (model #N092-04ST) capable of reading flow rates between 350 and 4750 mL/min. The flow rate of the solution atomizing gas, N_2O , was measured with an Omega rotameter capable of measuring flow rates between

28.3 and 566.8 L/min. The actual flow rate of the solution was determined by recording the amount of time needed to spray a known volume of solution.

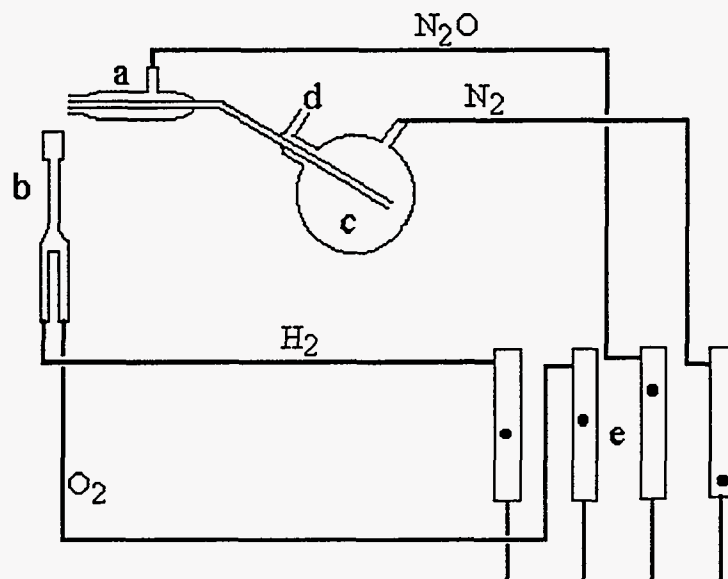


Figure 7.8. A schematic of the experimental setup for ammonia solution FSS. The labeled parts correspond to (a) spray nozzle, (b) hydrogen oxygen torch (pilot flame), (c) liquid ammonia solution reservoir, (d) $N_{2(g)}$ and $NH_{3(g)}$ outlet to oil bubbler, and (e) rotameters. The distance from the spray nozzle to the substrate (not pictured) was constant throughout the experiments at 19 cm..

After deposition, the substrates were removed from the steel plate with stainless steel tweezers and placed in a box furnace (Lindberg, model # 51848) preheated to $550^\circ C$. The furnace temperature was raised at $5^\circ C/min$ to $940^\circ C$, where the films were soaked for 24 h. When the films contained silver, the maximum temperature was lowered from $940^\circ C$ to $915^\circ C$. The final step in the preparation was a 5 h anneal at $550^\circ C$ under oxygen (in a

Lindberg horizontal tube furnace fitted with a quartz tube, model #55332) followed by a slow cooling (1° C/min) to room temperature. The films were stored in a desiccator which was backfilled with dry O₂ to protect them from reaction with water and CO₂.

The thickness of the thick films was measured with digital calipers with a 0.01mm sensitivity. Alternatively, an estimate of the maximum film thickness, T , for films prepared via the FSS method was obtained from the formula;

$$T = \frac{V C F}{A \rho} \quad \text{eq. 7.1}$$

where V is the volume of solution sprayed, C is the concentration of the solution, F is the formula weight of the material sprayed (666.2g/mol for Ba₂YCu₃O₇), A is the approximate area covered evenly by the spray, and ρ is the density of the material deposited. In order for this estimate to be a realistic maximum value, the density was taken to be only 75% of the theoretical density for the given material. For example, the density used in calculation of the thickness of films of Ba₂YCu₃O₇ was 4.78g/cm³, 75% of the theoretical density, 6.38g/cm³. The spray nozzles used in this work, at a distance of 19 cm from nozzle tip to substrate, coated a circular area, 6 cm in diameter. This value, combined with the traverse of 10cm over which the nozzle was motor driven, gave a total area, A , of 88.3cm². Inserting these values, along with a volume of 1L and a concentration of 0.01M, into equation 7.1 gives a maximum film thickness of 158μm. In most depositions, however, only ~500 mL of the solution was sprayed for each substrate. Using this volume in equation 7.1 results in a maximum thickness of 79μm,

which agrees very well with the thickness measurements of $\text{Ba}_2\text{YCu}_3\text{O}_{7-x}$ films using digital calipers.¹²

7.3.2 Results and Discussion

The surface temperature of the substrates during deposition was measured at $>800^\circ\text{C}$. Experiments with powder preparation show that this temperature is high enough to form the $\text{Ba}_2\text{YCu}_3\text{O}_{7-x}$ phase. However no $\text{Ba}_2\text{YCu}_3\text{O}_{7-x}$ was detected by XRD in the films prepared from organic solvents. It was concluded that $\text{Ba}_2\text{YCu}_3\text{O}_{7-x}$ was not forming due to the large amounts of CO_2 produced during combustion of the organic solvents used in the preliminary studies. The presence of CO_2 allowed the formation of barium carbonate, which is very stable and hinders the formation of $\text{Ba}_2\text{YCu}_3\text{O}_{7-x}$.¹³ The presence of BaCO_3 has been shown to necessitate longer reaction times in powder preparation of $\text{Ba}_2\text{YCu}_3\text{O}_{7-x}$.¹⁴ The use of liquid ammonia as the solvent in the FSS method eliminated all carbon from the solution and flame, in an attempt to prevent the formation of barium carbonate on the substrate, and possibly enable the preparation of $\text{Ba}_2\text{YCu}_3\text{O}_{7-x}$ in-situ.

The XRD patterns of thick films prepared by liquid ammonia FSS did show significant amounts of $\text{Ba}_2\text{YCu}_3\text{O}_{7-x}$ before annealing (see Figure 7.9). However barium carbonate was also a major phase. The origin of the carbon is most likely due to contamination from carbon dioxide in the atmosphere. The boiling point of liquid ammonia is -33.4°C . The ammonia is kept cold by the use of a dry ice/ acetone bath. The subliming dry ice leads to relatively high levels of carbon dioxide around the spray. Another possible explanation is that sub-micron BaO crystallites were formed on the substrate which reacted very rapidly with atmospheric

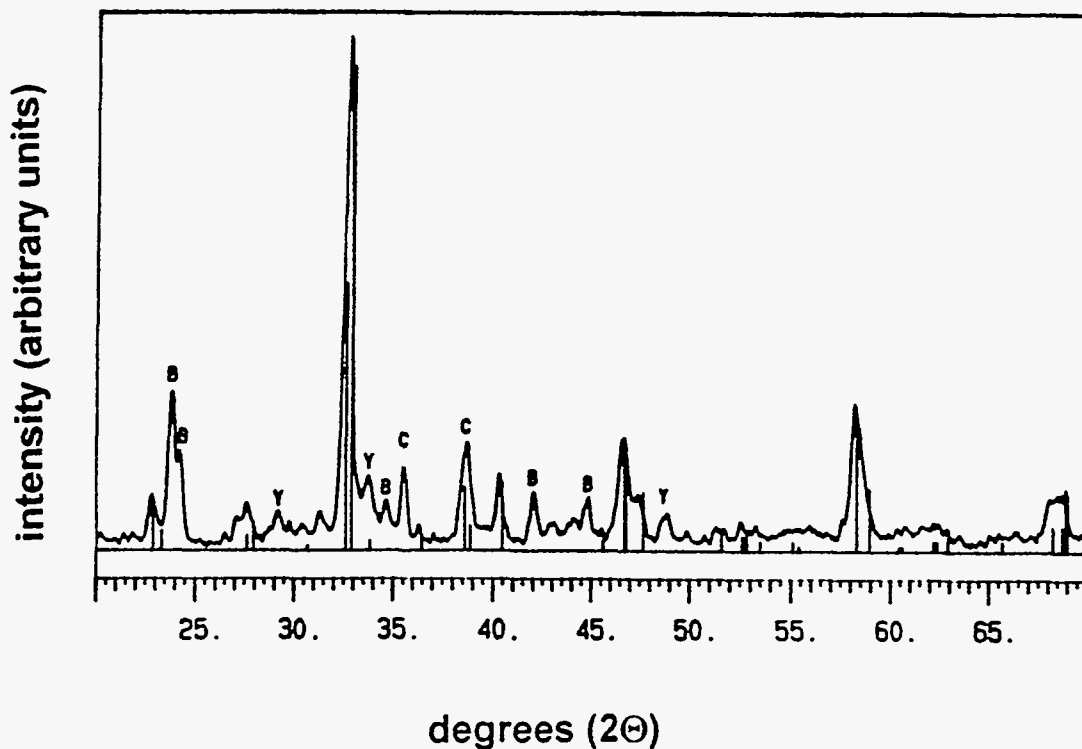


Figure 7.9. An XRD pattern of an ammonia FSS, $\text{Ba}_2\text{YCu}_3\text{O}_{7-x}$ thick film before thermal processing. Significant amounts of $\text{Ba}_2\text{YCu}_3\text{O}_{7-x}$ are present in the pre-annealed sample. The stick pattern of $\text{Ba}_2\text{YCu}_3\text{O}_{7-x}$ is superimposed on the pattern (JCPDS 38-1433). Peaks labeled Y correspond to Y_2O_3 , C to CuO , and B to BaCO_3 .

CO_2 to form BaCO_3 . This reaction may have been completed before the films were analyzed by XRD (which was often less than 15 minutes after preparation).

The XRD patterns obtained for the thermally processed ammonia FSS films revealed $\text{Ba}_2\text{YCu}_3\text{O}_{7-x}$ as the major phase (see Figure 7.10). The diffraction patterns were similar for all solution concentrations studied. However, the highest superconducting transition temperatures were obtained from 0.064M solutions. A distance from spray nozzle to substrate of 19 cm, a

solution flow rate of 12 mL/min, and particular combination of flow rates (which appear in Table 7.2), were found to produce thick films with a transition temperature above 75 K, with a fair reproducibility. The resistivity versus temperature plots for four films deposited under the conditions appearing in table 7.2 are displayed in Figure 7.11. The T_{c0} for the four films ranges from 75 to 88 K.

Table 7.2. Flow rates used in the preparation of thick films of $Ba_2YCu_3O_{7-x}$ via ammonia FSS.

gas	flow rate (L/min)
H ₂	8.62
O ₂	4.83
N ₂	3.50
N ₂ O	93.5

The chemical equation for the complete combustion of the hydrogen and the ammonia in the FSS flame is;



The flow rates above correspond to (assuming ideal gas behavior) 0.38 mol H₂/min, 0.22 mol O₂/min, and 4.18 mol N₂O/min. A solution flow rate of 12 mL/min corresponds to a rate of

9.24g NH₃/min, or 0.54 mol NH₃/min. For complete combustion of the H₂, only 0.19 mol of O₂ is needed, meaning that there is 0.03 mol excess O₂. For combustion of 0.54 mol NH₃, 0.81 mol of N₂O is needed, and over five times this amount is supplied. These calculations show that the environment of the flaming solvent spray is highly oxidizing, and should promote formation of the Ba₂YCu₃O_{7-x} phase.

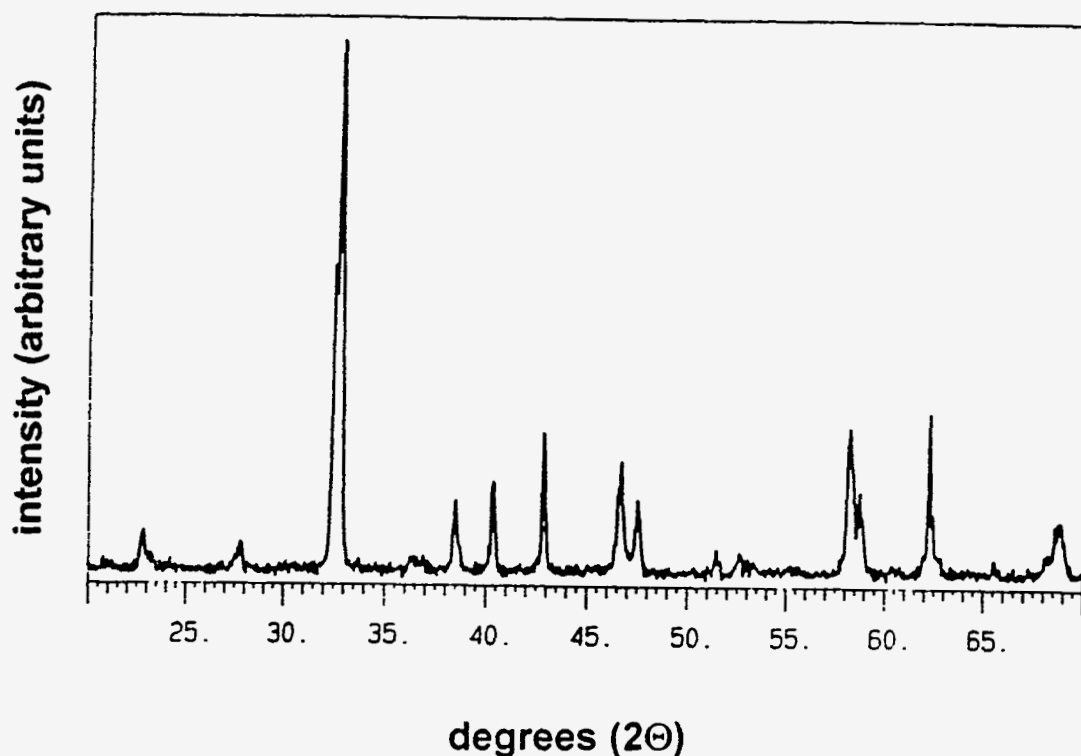


Figure 7.10. An XRD pattern for a thermally processed ammonia FSS Ba₂YCu₃O_{7-x} film deposited from a 0.048M solution. The pattern is typical of the ammonia FSS films. All major peaks can be indexed to Ba₂YCu₃O_{7-x}, except the peaks at ~43°2θ and ~62.5°2θ, which are due to the substrate, MgO.

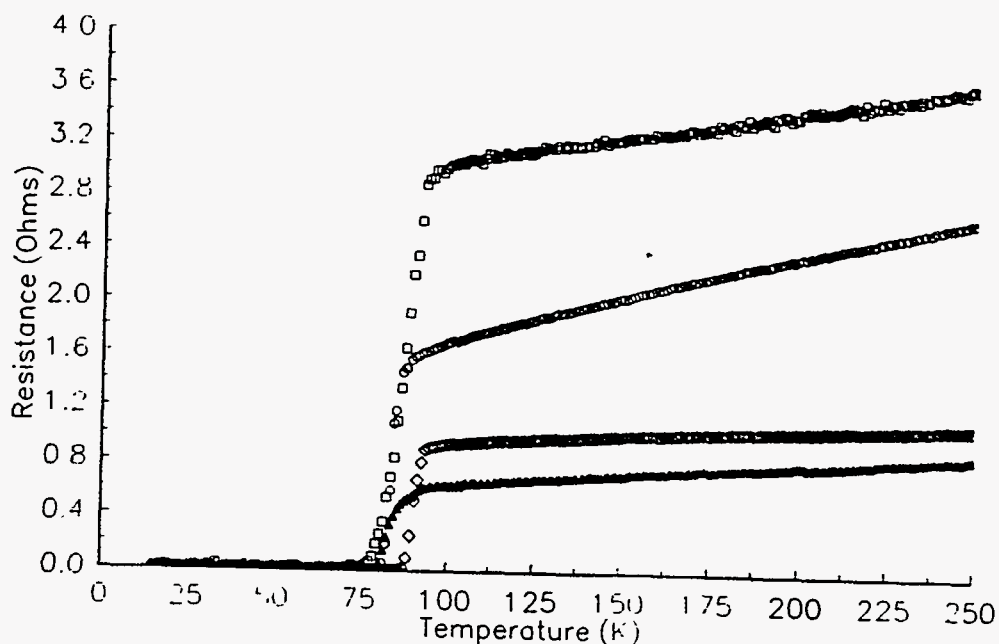


Figure 7.11. Resistance versus temperature plots for four thermally processed films prepared via ammonia FSS.

Although the method could reproducibly synthesize thick films with transition temperatures around the boiling point of liquid nitrogen, there were two serious problems with the films which would have prevented possible applications. (1) The films prepared from solutions with total metal ion concentrations $>0.03M$, although displaying high transition temperatures, had poor adhesion to the substrate. This was evident upon performing a “tape test”. In a tape test, a piece of scotch tape is applied to the surface of film. Poor adhesion to the substrate would become evident if any material is attached to the tape when it is removed from the film. All of the films produced from solutions with total metal ion concentrations $>0.03M$ failed this tape test, even after extended sintering times (24h) at high temperatures ($940^{\circ}C$).

The material removed was very powdery, indicative of a high degree of porosity in the films. In fact, attempts at etching patterns in the films via photolithography (for bolometric response tests) were unsuccessful due to dispersion of the etching agent through the porous film.¹⁵

(2) The transport critical current density of the films was extremely low. Typical values at 20 K were on the order of 200 A/cm². This was also evidence for poor grain contact and porosity in the films. A sample with poor grain contact may display a high transition temperature under low current conditions due to "threads" or pathways of loosely connected superconducting material. When the current is increased, the entire supercurrent must still pass through this same pathway to avoid the normal state. The critical current density in such pathways can be exceeded with very small total currents.

The poor grain contact in the thick films prepared via ammonia FSS was also evident in scanning electron micrographs of the materials. Figure 7.12 shows a scanning electron micrograph of a Ba₂YCu₃O_{7-x} FSS film from a 0.05 M (total metal ion concentration) ammonia before thermal processing. Instead of a continuous sheet of superconducting material, the grains were randomly oriented, much as they are in bulk samples of Ba₂YCu₃O_{7-x}.

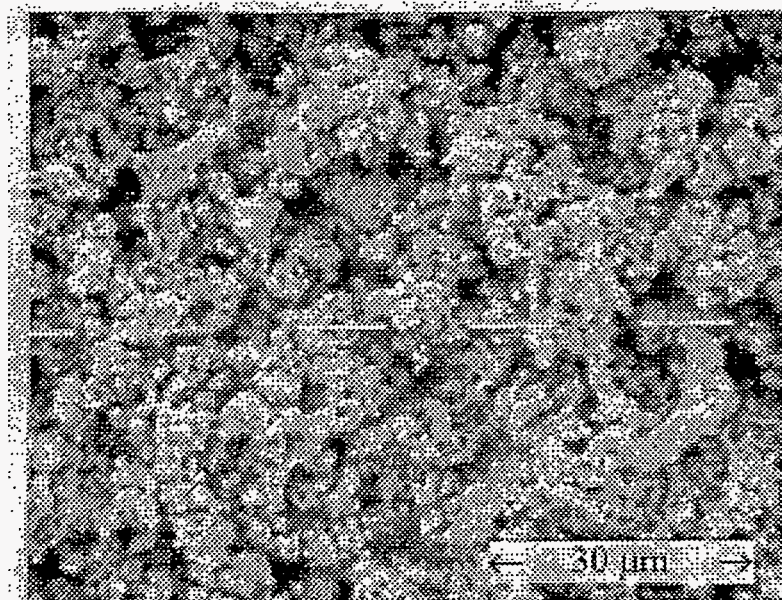


Figure 7.12. A scanning electron micrograph of a Ba₂YCu₃O_{7-x} film prepared via FSS of a 0.05 M ammonia solution. The random orientation of grains and poor grain contact, indicative of a spray deposition, is evident. Each bar=10μm.

A possible factor which could result in the poor grain contact of the FSS films was the particle size of the deposited material. As with bulk powders, the sintering characteristics of the coating on the substrate would have been highly dependent upon the particle size and uniformity. The larger particles produced from the more concentrated solutions may not sinter as easily as the smaller particles deposited from less concentrated solutions. A series of films (Figure 7.13) was prepared by ammonia FSS from different solution concentrations and examined by SEM to probe the particle size and morphology of the deposited material. Figure 7.13A shows a micrograph of an ammonia FSS film sprayed from a solution with a total metal ion concentration of 0.016M. The material resembled a bulk powder with particle sizes of 1 to 3μm, agglomerated into larger particles on the order of 5 to 10 μm. In Figure 7.13B, this same film is shown after thermal processing (in air) for 1h at 940° C. The weak link, porous structure

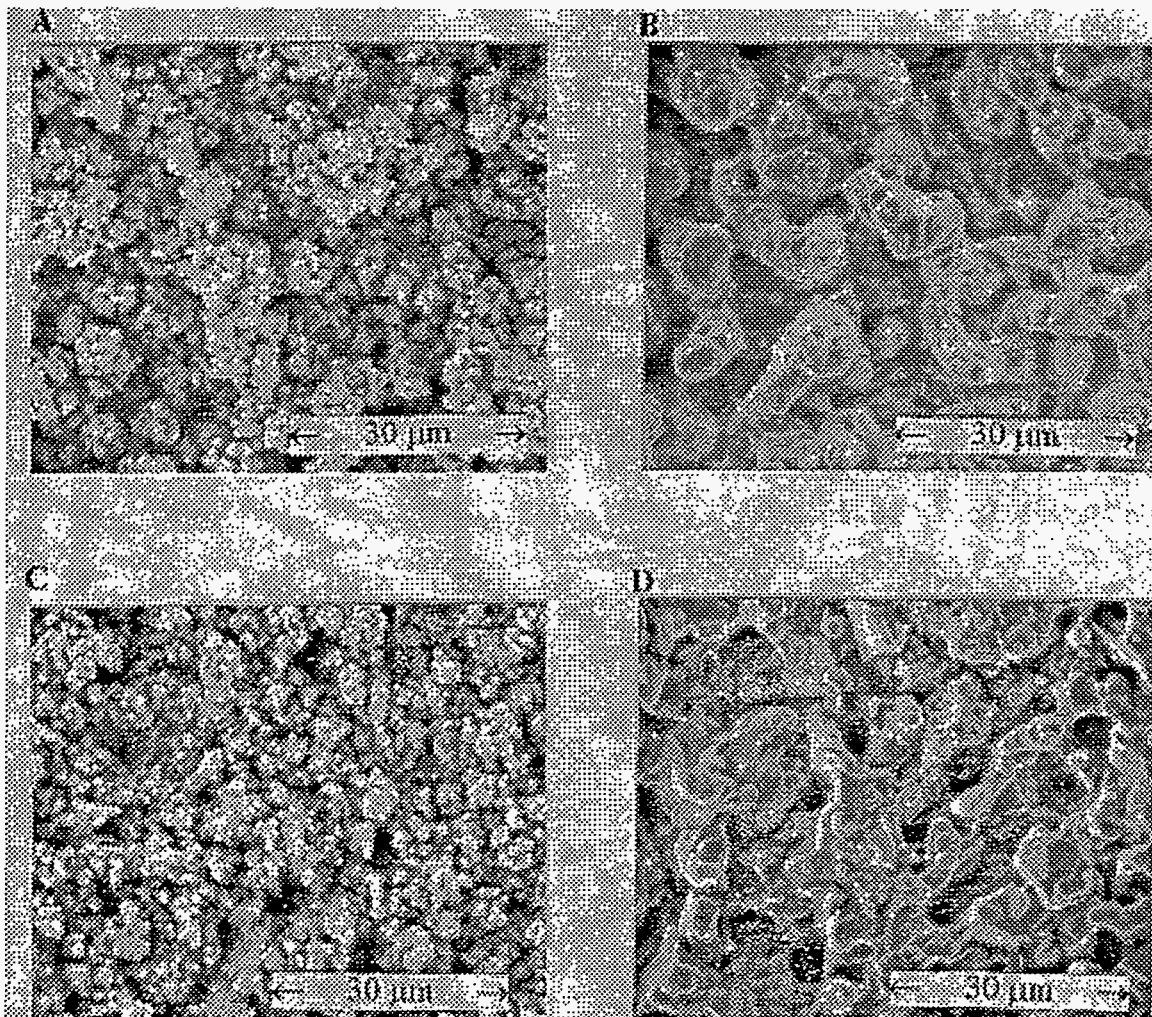
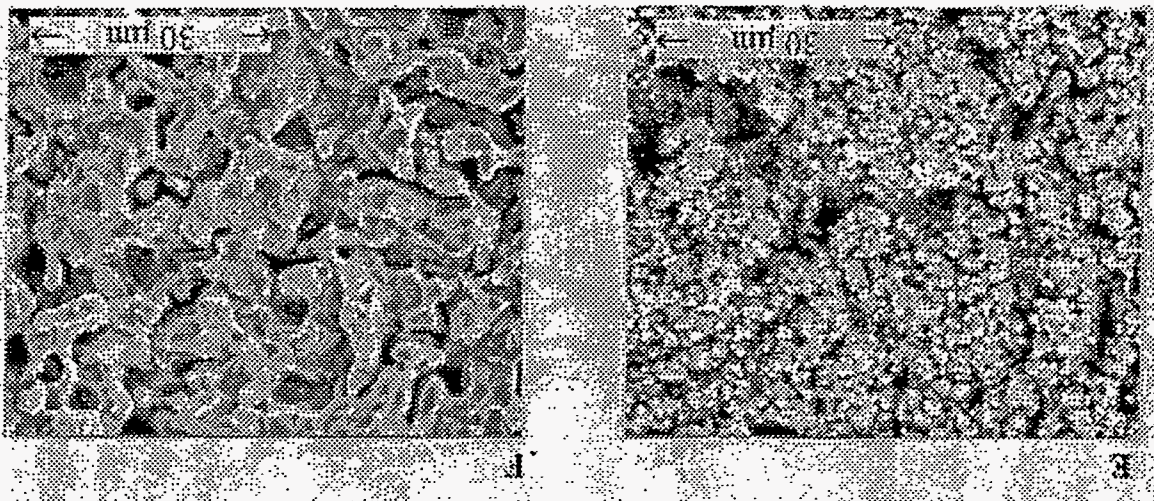


Figure 7.13. Scanning electron micrographs of ammonia FSS films from varying solution concentration. (A) 0.016M as-sprayed film, (B) 0.016M film heated 1h at 940° C, (C) 0.008M as-sprayed film, and (D) 0.008M film heated 1h at 940° C.

of the FSS films was highly evident in this micrograph. The powder sintered into a network of loosely connected circular platelets with a random orientation (XRD of this sample showed no increase in the relative intensities of 0k0 type peaks). The largest crystallites in the micrograph appeared to be about 12 μm in length. Figure 7.13C shows a micrograph of an ammonia FSS film from a 0.008M solution. The material was made up of smaller particles (as expected for a

less concentrated solution) with linear dimensions of $\sim 1\mu\text{m}$. The particles were not as highly agglomerated as the previous sample. The largest agglomerates appeared to be $< 5\mu\text{m}$ in length. Figure 7.13D is the same film subjected to a 1h heat treatment at 940°C . The material had the same, circular plate-like structure but the crystallites appeared to be slightly more defined. The platelets were randomly orientated but there was less of an open network structure and the density of platelets appeared to be higher than that of the previous sample. A scanning electron micrograph, of an ammonia FSS film from a 0.0033M solution can be seen in Figure 7.13E. The particles in this film were submicrometer in diameter, and were agglomerated into larger particles of $\sim 1\mu\text{m}$. The pits, evident as dark spots on the micrograph, were due to the surface roughness of the polycrystalline MgO substrate. Clearly, these rough polycrystalline substrates were not suitable for the production of thin films. Some of the smallest deposited particles $> 50\text{nm}$ evident in the micrograph were observed in these pits (lower right hand corner of Figure 13E). The pits may have provided partial shelter from the flaming spray and prevented

Figure 7.13 (cont.) Scanning electron micrographs of (E) 0.0033M as-sprayed film, and (F) 0.0033M film heated 1h at 940°C .



agglomeration of the particles which were deposited in them. A micrograph of this film, annealed for 1h at 940° C is given in Figure 7.13F. Again, the randomly oriented platelet structure was apparent. The size of the platelets was comparable to those of the 0.008M sample. This may have been the result of more rapid sintering of the smaller particles deposited from the 0.0033M solution. The material had fewer openings and appeared to be a more dense film.

7.4 Preparation of Thin Films From Combustion of Liquid Ammonia Solutions

In attempts to eliminate the poor grain contact and consequent low critical current density of the ammonia FSS films, a variation of the method, utilizing very dilute solutions was developed. If one considers the situation occurring during the FSS process, there are several assumptions that can be reasonably made. During the combustion of an aerosol, it is not the liquid droplets, but gaseous material evaporating from the droplets, that is oxidized.¹⁶ As the solvent evaporates (probably a rapid process considering the high temperatures involved), the concentration of the solute will increase and eventually exceed the solubility level, and result in crystallization. If the deposition takes place before the solvent has completely evaporated, the FSS method is simply a self supporting spray pyrolysis technique. If deposition occurs after nearly all of the solvent has entered the gas phase, the deposition can be thought of as two different processes (see Figure 7.14). In the first situation, particles, which result from the high temperature decomposition of the dissolved salts, impinge upon the substrate. The size of these particles will be dependent upon the initial concentration of the solution. Concentrated solutions will result in partial crystallization before the droplets have completely evaporated and

may result in particles on the order of micrometers. Dilute solutions will result in much smaller particles, possibly approaching the limits of a gas phase deposition. The green color emitted by the FSS flame is evidence for some gas phase emission from barium. It was the hope of the author that decreasing the solution concentration would eliminate the possibility of large particle deposition, and result in a complete, gas phase, or chemical vapor deposition (CVD). A gas phase deposition will allow for more dense films of $\text{Ba}_2\text{YCu}_3\text{O}_{7-x}$ to be produced. Single crystal, 100 oriented LaAlO_3 substrates were used in attempts to produce oriented thin films with high critical current densities.

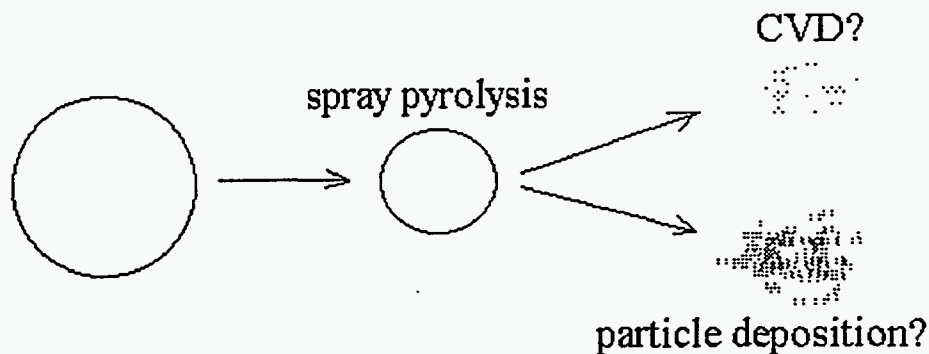


Figure 7.14. A schematic of a single droplet of a liquid ammonia solution during the FSS process. If deposition occurs when some of the ammonia is still in the liquid phase, the method is spray pyrolysis. If deposition occurs when the ammonia has essentially all evaporated, then the concentration of the solution will determine the size of the particles deposited. The optimal situation for the production of a thin epitaxial film is deposition of extremely small particles, approaching a gas phase deposition.

7.4.1 Experimental Procedure

Due to the low masses of reagents used in the preparation of liquid ammonia solutions for FSS, obtaining an accurate stoichiometry by weighing separate reagents would have been difficult. For this reason, an aqueous stock solution of yttrium barium and copper nitrates (the preparation of this stock solution is discussed in section 7.1.2) was used as the source of metal ions. This solution was added to a 1000 mL round bottom flask until an amount corresponding to a total metal ion concentration in the final solution of $\sim 0.0008\text{M}$ was achieved. The flask was then placed in an oven at 90°C until the water and excess HNO_3 evaporated, leaving behind a stoichiometric mixture of yttrium, barium and copper nitrates. When the excess water had evaporated, 15.0 grams of NH_4NO_3 was added and the flask and reagents were flushed with dry nitrogen for 15 min. Liquid ammonia was then condensed into the flask until a volume of 900 mL was collected. The deposition procedure was similar to that of the thick film process and all of the compressed gas flow rates were monitored. However, in the thin film FSS process, the steel plate which had held the substrates in the thick film FSS process was removed and the substrate was held in a steel alligator clip. In addition, the spray nozzle was not motor driven in the thin film FSS process. The flame was allowed to continually coat the substrate. These changes were made for three reasons. (1) It was believed that the steel plate was acting as a heat sink, continually cooling the substrates during deposition. A higher substrate temperature could be reached if the steel plate was removed. (2) Not moving the spray nozzle allowed for a more uniform substrate temperature to be maintained. And (3), the low concentration of metal ions in the solution would result in an extremely thin coating if the spray had been

allowed to coat an area as large as that in the thick film FSS process. The temperature of deposition was monitored by placing the bead of a chromel-alumel thermocouple in contact with the back of substrate (away from the flame), close to the alligator clip. This temperature was not the true deposition temperature. It was monitored only to provide a minimum deposition temperature, that could be used as a parameter to be duplicated when attempting to reproduce a particular experiment. Placing the thermocouple on the deposition side of the substrate would have caused nonuniformities in the coating. The distance from spray nozzle to substrate was 19 cm throughout the experiments. The entire volume of solution was sprayed onto one LaAlO_3 substrate in each experiment. The flow rates used in thin film depositions are listed in Table 7.3.

Table 7.3. Flow rates used in the preparation of thin films of $\text{Ba}_2\text{YCu}_3\text{O}_{7-x}$ via ammonia FSS.

gas	flow rate (L/min)
H_2	8.62
O_2	60.5
N_2	3.50
N_2O	84.9

The thin films were thermally processed under an atmosphere of flowing Ar (1L/min) in the tube furnace previously described, for time periods ranging from 10 min to 2 h at temperatures ranging from 800° C to 920° C. A reduced O_2 partial pressure has been shown to lower the necessary sintering temperature for thin films and bulk samples of

$\text{Ba}_2\text{YCu}_3\text{O}_{7-x}$.^{17,18} The thin films were oxygenated at 450° C for time periods ranging from 2 min to 2 h and furnace cooled under flowing oxygen (1L/min).

7.4.2 Results and Discussion

The thin films produced via the FSS process had the appearance of smoked glass before thermal processing. However, these as-deposited films passed the tape test previously described, indicating a good adhesion between the film and substrate. The temperature of deposition, measured with the thermocouple in contact with the back of the substrate, remained relatively constant throughout the deposition process at ~725° C. The actual deposition temperature was probably higher since the thermocouple was not directly in the ammonia flame.

Figure 7.15 shows the XRD pattern of an ammonia FSS film of $\text{Ba}_2\text{YCu}_3\text{O}_{7-x}$ before annealing (lower pattern) and after a 30 min anneal at 900° C under flowing Ar, followed by furnace cooling to 300° C under flowing O_2 (upper pattern). In the as-deposited film, the majority of peaks in the pattern were attributed to $\text{Ba}_2\text{YCu}_3\text{O}_{7-x}$ or the substrate LaAlO_3 , however, there was an unidentified impurity. Identification of this impurity was complicated due to the high degree of preferred orientation in the sample. The material was nearly completely oriented with the b-axis perpendicular to the substrate, as was evidenced by the increase in relative intensity of the 0k0 type peaks. The ratio of relative intensity of the 050 peak of $\text{Ba}_2\text{YCu}_3\text{O}_{7-x}$ to the 031 peak was 2.92, whereas this ratio has a value of 0.13 in a randomly oriented sample. After the post anneal, this ratio approached infinity, as the 031 peak was extinguished by nearly complete orientation of the $\text{Ba}_2\text{YCu}_3\text{O}_{7-x}$ crystallites with the b-axis

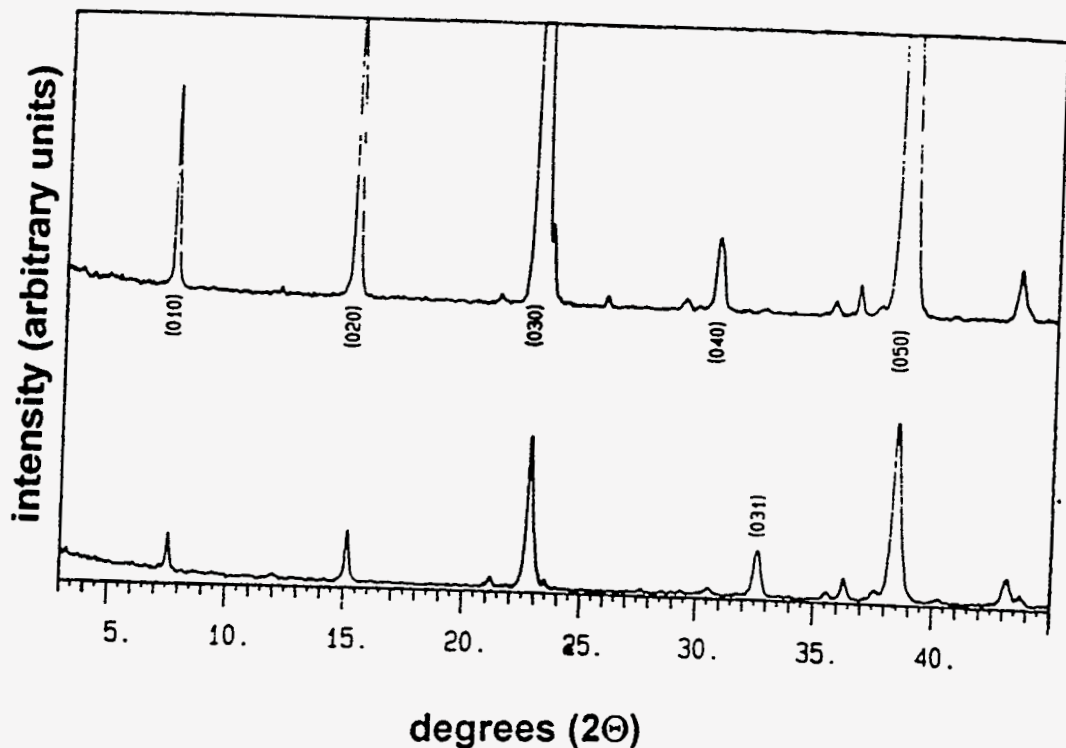


Figure 7.15 The XRD patterns of a thin film of $\text{Ba}_2\text{YCu}_3\text{O}_{7-x}$ as-prepared via ammonia FSS (lower pattern) and the same film, annealed for 30 min under flowing Ar at 900° C (upper pattern). The 031 peak of $\text{Ba}_2\text{YCu}_3\text{O}_{7-x}$, which has the highest relative intensity in randomly oriented samples of $\text{Ba}_2\text{YCu}_3\text{O}_{7-x}$ can be seen in the lower pattern at $\sim 32.8^\circ 2\theta$. The (hkl) values of the intense reflections in the upper pattern are given.

perpendicular to the substrate. It is worth noting at this time that samples prepared by ammonia FSS from concentrated solutions on single crystal LaAlO_3 substrates did not display this level of orientation, even after extended annealing times ($>24\text{h}$) at higher temperatures (940° C).

An estimate of the maximum thickness of this film, obtained from equation 7.1, was $6\mu\text{m}$. However, it is likely that this is a high estimate, since the density of the material deposited

from the dilute solutions was probably much closer to the theoretical density (a value of 75% of theoretical density was used). The resistivity versus temperature plot for this film can be seen in Figure 7.16. The film had a high room temperature resistivity (>500 Ohm/cm), which was indicative of poor grain contact. Thin films of $\text{Ba}_2\text{YCu}_3\text{O}_{7-x}$ prepared by laser ablation¹⁹ typically have a room temperature resistivity of <1 Ohm/cm. The resistivity of the material dropped at ~70K, but did not reach zero above 15K (lowest temperature of data collection).

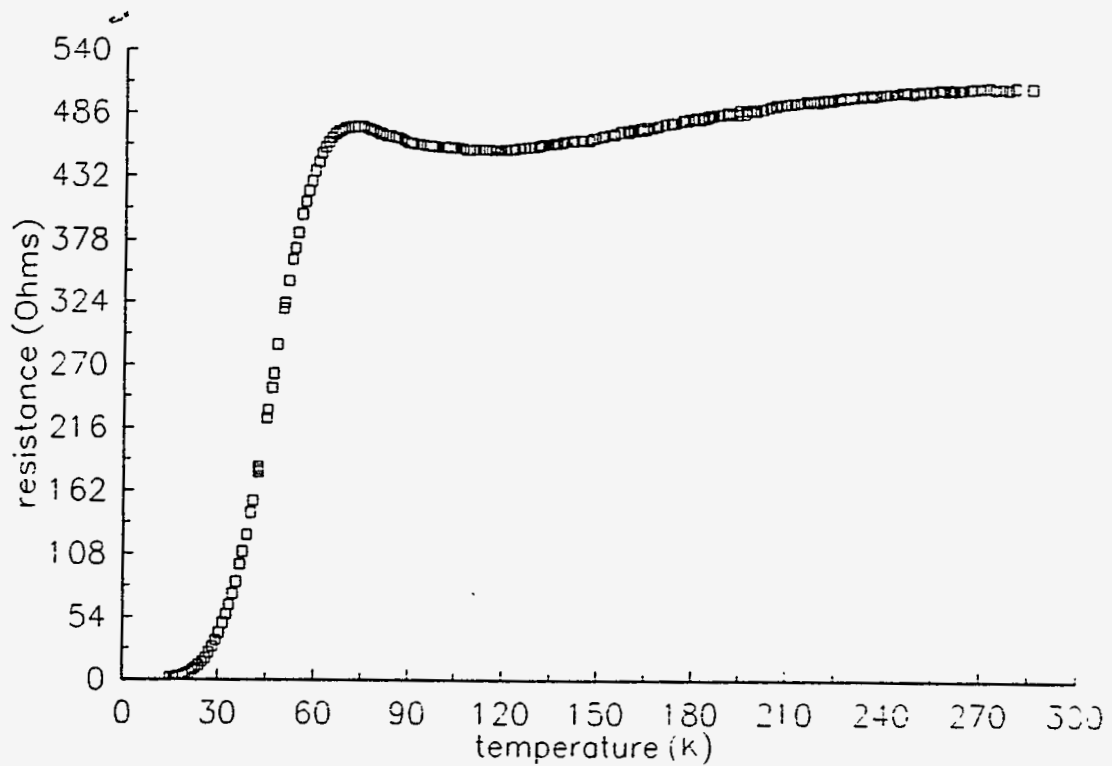


Figure 7.16. The resistance versus temperature plot for an ammonia FSS thin film. The sample does not reach zero resistance above 15K.

Scanning electron micrographs of the as-deposited film (Figure 7.17) revealed that the deposited particles were uniform and less than 500nm in diameter. They appeared to evenly coat the substrate but formed a rough surface at high (2500x) magnification. There appeared to

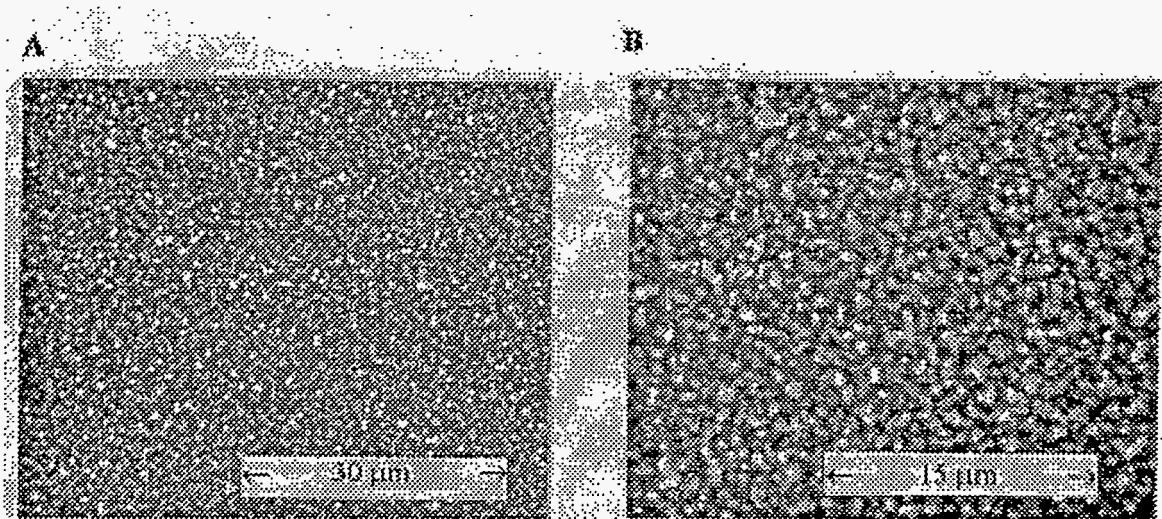


Figure 7.17. Scanning electron micrographs of (A) an as-prepared ammonia FSS thin film, and (B) the same film at higher magnification.

be a fair amount of sintering in the grains closer to the substrate. This may have been due to the fact that these grains were deposited earlier than the grains above and have had time at high temperatures (during subsequent bombardment with the flaming spray) for grain growth and sintering to occur. The coating was more dense than those deposited from the more concentrated solutions. The material, however, was not a single crystalline sheet, and consequently, had a large number of weakly linked grain boundaries (as evidenced by the high room temperature resistivity).

7.5 Conclusions

Chemical vapor deposition has been defined as a process in which “a solid material is deposited from gaseous precursors onto a substrate,” wherein “the deposited phase is produced in-situ via chemical reactions.”²⁰ It has been demonstrated that $\text{Ba}_2\text{YCu}_3\text{O}_{7-x}$ films can be synthesized in-situ by allowing the flame resulting from combustion of liquid ammonia

solutions of metal nitrates to coat a substrate. The maximum temperature obtainable in an ammonia flame is $>3000^{\circ}\text{C}$.¹⁶ These temperatures are sufficient for vaporization of all reactants in the Ba-Y-Cu-O system, and gas phase atomic emission from barium (or strontium) has been observed during the FSS process. Considering these two points (in situ growth and gas phase reactants) it can be concluded that the FSS process is truly a chemical vapor deposition process. However, the properties of the films observed via electrical transport measurements and scanning electron microscopy indicate that not all of the material is deposited from the gas phase and some particle deposition is occurring. The size of these particles is dependent upon the total metal ion concentration of the solution. Although no in-situ deposition of $\text{Ba}_2\text{YCu}_3\text{O}_{7-x}$ from the combustion of organic solvents was observed in this work, others have since reported this observation.²¹

Thick films have been produced which have superconducting transition temperatures above the boiling point of liquid nitrogen. These films, however, had poor adhesion to the substrate and low critical current densities due to a high degree of porosity. Thin films have been produced which have displayed good adhesion to the substrate and epitaxial growth, but as of the time of this writing, have poor superconducting properties. Further optimization of the deposition parameters may improve these properties.

The in-situ growth of $\text{Ba}_2\text{YCu}_3\text{O}_{7-x}$ can be attributed to one of two possible scenarios (or the combination of both). In the first scenario, the $\text{Ba}_2\text{YCu}_3\text{O}_{7-x}$ phase is deposited from gas phase reactants, just as it is in the in situ growth of $\text{Ba}_2\text{YCu}_3\text{O}_{7-x}$ films via metalorganic chemical vapor deposition. In the second scenario, very small, atomically mixed particles of Y_2O_3 , CuO and BaO are deposited on the substrate and rapidly react in the solid state at

deposition temperatures to yield $\text{Ba}_2\text{YCu}_3\text{O}_{7-x}$. An entirely gas phase deposition would yield very smooth, nearly single crystalline, sheets of $\text{Ba}_2\text{YCu}_3\text{O}_{7-x}$. Scanning electron micrographs of the films reveal a particulate morphology which supports the latter scenario.

7.6 Notes and References

- ¹ See for example; L. Luo, X. D. Wu, R. C. Dye, R. E. Muenchausen, S. R. Foltyn, Y. Coulter, and C. J. Maggiore, *Appl. Phys. Lett.* **59**, 2043 (1991).
- ² H. G. Schneider and V. Ruth, Editors, *Advances in Epitaxy and Endotaxy*, VEB Deutscher Verlar fur Grundstoffindustrie (Leipzig, 1971).
- ³ J. McHale, R. W. Schaeffer, A. Kebede, J. Macho, and R. E. Salomon, *J. Supercond.* **5**, 511 (1992).
- ⁴ G. Selvaduray and C. Zhang, *J. Mater. Res.* **7**, 283 (1992).
- ⁵ B. Dwir, M. Affronte, and D. Pavuna, *Appl. Phys. Lett.* **55**, 399 (1989).
- ⁶ Chin-An Chang, *Appl. Phys. Lett.* **53**, 1113 (1988).
- ⁷ P. Strobel, C. Paulsen, and J.L. Tholence, *Solid State Commun.* **68**, 535 (1988)
- ⁸ P. N. Peters, R. C. Sisk, and E. W. Urban, *Appl. Phys. Lett.* **52**, 2066 (1988).
- ⁹ R. W. Schaeffer, Doctoral Dissertation, Temple University, Philadelphia, PA 19122 (1992).
- ¹⁰ C. T. Cheung and E. Ruckenstein, *J. Mater. Res.* **4**, 1 (1989).
- ¹¹ Timothy L. Ward, Toivo T. Kodas, and Altaf H. Carim, *J. Mater Res.* **7**, 827 (1992)
- ¹² The digital calipers were tared to the thickness of a blank substrate and then used to measure the coated substrates. The reliability of thickness measurements of the films was dependant upon the consistency in thickness of the blank substrates.
- ¹³ T. M. Shaw, D. Dinosn P. E. Batson, A. G. Schrott, D. R. Clarke, P. R. Duncombe, *J. Mater. Res.* **5**, 1176 (1990).

- ¹⁴ E. Ruckenstein, S. Narain, and N. L. Wu, *J. Mater. Res.* **4**, 267 (1989).
- ¹⁵ M. Fardmanesh, Personal Communication (Philadelphia, PA, 1993).
- ¹⁶ J. A. Barnard and J. N. Bradley, *Flame and Combustion*, Chapman and Hall Ltd. (New York, 1985).
- ¹⁷ W. H. Poisl and A. C. D. Chaklader, *J. Am. Ceram. Soc.* **76**, 1177 (1993).
- ¹⁸ R. Feenstra, T. B. Lindemer, J. D. Budai, and M. D. Galloway, *J. Appl. Phys.* **69**, 6569 (1991).
- ¹⁹ D. Dijkamp, T. Venkatesan, X. D. Wu, S. A. Shaheen, N. Jisrawi, Y. H. Min-Lee, W. L. McLean, and M. Croft, *Appl. Phys. Lett.* **51**, 619 (1987).
- ²⁰ M. Leskela, H. Molsa, and L. Niinisto, *Supercond. Sci. Technol.* **6**, 627 (1993).
- ²¹ A. T. Hunt, W. B. Carter, and J. K. Cochran Jr, *Appl. Phys. Lett.* **63**, 266 (1993).

CHAPTER 8
SYNTHESIS OF BULK HIGH T_c SUPERCONDUCTORS
FROM ACETATE GLASS PRECURSORS

The solution methods previously discussed were very effective in achieving atomic level mixing and produce extremely high quality materials. It can be argued, however, that they require specialized equipment and have somewhat complicated procedures. In attempts to eliminate these drawbacks, a procedure was developed which has, in practice, the simplicity of conventional ceramic processing, along with the benefits of the solution techniques.¹

As discussed in section 3.1.2, solution methods attempt to maintain, while undergoing a transformation to the solid state, the intimate mixing of ions inherent in a solution. In this work, this mixing was transferred into the solid state by rapid freezing of a solution followed by sublimation (freeze drying), and rapid solvent removal by combustion of a solution aerosol (FSS). Another way to trap the randomness of the solution state would be to use materials that, rather than crystallizing, formed a glass when the solvent was removed. It has been shown that some two and three component systems of metal acetates form glasses when quenched from a melt.^{2,3} Aqueous solutions of metal acetates with various organic additives (ethylene glycol, ethanolamine, citric acid) have been used for the preparation of thick films of Ba₂YCu₃O_{7-x} by a "spin on" method⁴ and a sol gel/spray pyrolysis method.⁵ A solution method utilizing an acetic acid/ethanol mixture

has been used for the preparation of $\text{Bi}_2\text{Sr}_2\text{Ca}_2\text{Cu}_3\text{O}_{10}$.⁶ Presented here is a simple synthesis of $\text{Ba}_2\text{RECu}_3\text{O}_{7-x}$ (RE= Y, Eu, Gd, Nd, La), and $(\text{Bi, Pb})_2\text{Sr}_2\text{Ca}_2\text{Cu}_3\text{O}_{10}$, referred to as the *acetate method*, that requires only a high density alumina (or suitable non-reactive) crucible, a furnace, the necessary reagents, and a standard laboratory hot plate. Samples prepared via the acetate method have been characterized by thermogravimetric analysis, x-ray diffraction (XRD), scanning electron microscopy (SEM), diamagnetic response measurements (using the balance described in section 4.3.2) and four probe dc-resistivity measurements. Substitution studies were also performed in attempts to determine the mechanism of product formation and explain the marked differences in rate of product formation between the acetate method and conventional ceramic processing.

8.1 Experimental Procedure

8.1.1 Reagents

The reagents used for the preparation of $\text{Ba}_2\text{RECu}_3\text{O}_{7-x}$ were $\text{Ba}(\text{O}_2\text{CCH}_3)_2$, $\text{Cu}(\text{O}_2\text{CCH}_3)_2 \cdot \text{H}_2\text{O}$, $\text{Y}(\text{O}_2\text{CCH}_3)_3 \cdot 4\text{H}_2\text{O}$, Eu_2O_3 , $\text{Nd}(\text{NO}_3)_3 \cdot 6\text{H}_2\text{O}$, Gd_2O_3 , and $\text{La}(\text{NO}_3)_3 \cdot 6\text{H}_2\text{O}$. All were 99.9% pure or better (as stated by the supplier Johnson Matthey). Europium nitrate and gadolinium nitrate solutions were prepared from their oxides via dissolution in aqueous nitric acid. The acetates of europium, gadolinium, lanthanum, and neodymium were synthesized in our laboratory from aqueous solutions of their respective nitrates by precipitation of the rare earth carbonate upon addition of ammonium carbonate. The rare earth carbonates were filtered, washed, and dissolved in

acetates were crystallized from this solution after evaporation of sufficient water. The reagents used for the preparation of $(\text{Bi, Pb})_2\text{Sr}_2\text{Ca}_2\text{Cu}_3\text{O}_{10}$ were $\text{Bi}(\text{NO}_3)_3 \cdot 5\text{H}_2\text{O}$, $\text{Sr}(\text{O}_2\text{CH}_3)_2$, $\text{Ca}(\text{O}_2\text{CH}_3)_2$, $\text{Cu}(\text{O}_2\text{CCH}_3)_2 \cdot \text{H}_2\text{O}$, $\text{Pb}(\text{O}_2\text{CCH}_3)_2$, and $\text{NH}_4(\text{O}_2\text{CCH}_3)$. The acetates of yttrium, copper, europium, lanthanum, neodymium, and gadolinium, and bismuth nitrate were analyzed thermogravimetrically, as described in section 4.1.2, to determine their exact water and metal content.

8.1.2 Sample Preparation

$\text{Ba}_2\text{YCu}_3\text{O}_{7-x}$ was prepared by combining 0.0100 mol yttrium acetate, 0.0200 mol barium acetate, 0.0300 mol copper acetate, and 50 mL of glacial acetic acid (Fisher Scientific, minimum purity 99.7%) in 100 mL high density alumina crucible (Coors). This mixture was heated on a hot plate (Corning, model # PC320) and stirred with a Pyrex stirring rod. When a temperature of 118°C was reached the mixture boiled rapidly. The boiling was continued until the volume of the solution decreased to about half of the initial value. At this time a noticeable change in viscosity occurred, marked by a temperature increase to 130°C, leaving behind a viscous, dark blue liquid (which solidified to a dark blue glass if allowed to cool to room temperature). This mixture, now called the precursor, was taken directly from the hot plate and placed in a box furnace (Lindberg, model #51848). The time required to prepare the precursor was less than 15 min. The heat treatment of the precursor consisted of a 5°C/min increase to a soak at 900°C for 2 h in air. The cooling to room temperature was also carried out at 5°C/min. The black product obtained was then heated in a tube furnace (Lindberg, model #55332) under 1 atm of

flowing oxygen at 550°C for 5 h followed by slow cooling to room temperature (1°C/min) to achieve the orthorhombic, fully oxygenated, $\text{Ba}_2\text{YCu}_3\text{O}_7$ phase. The procedure for preparing other $\text{Ba}_2\text{RECu}_3\text{O}_{7-x}$ phases was identical to the $\text{Ba}_2\text{YCu}_3\text{O}_{7-x}$ procedure with 0.010 mol of lanthanum acetate, neodymium acetate, europium acetate, or gadolinium acetate substituted for the 0.010 mol of yttrium acetate.

$(\text{Bi,Pb})_2\text{Sr}_2\text{Ca}_2\text{Cu}_3\text{O}_{10}$ was prepared by combining 0.018 mol $\text{Bi}(\text{NO}_3)_3 \cdot x\text{H}_2\text{O}$, 0.004 mol $\text{Pb}(\text{O}_2\text{CCH}_3)_2$, 0.020 mol $\text{Sr}(\text{O}_2\text{CCH}_3)_2$, 0.020 mol $\text{Ca}(\text{O}_2\text{CCH}_3)_2$, 0.030 mol $\text{Cu}(\text{O}_2\text{CCH}_3)_2 \cdot \text{H}_2\text{O}$, 0.130 mol $\text{NH}_4(\text{O}_2\text{CCH}_3)$, and 200 mL glacial acetic acid in a 400 mL Pyrex beaker. The excess lead acetate was added to account for anticipated losses through sublimation. The mixture was then heated to a boil as in the $\text{Ba}_2\text{YCu}_3\text{O}_{7-x}$ preparation. As the acid boiled away the solution became very viscous and eventually results in a clear blue-violet, highly viscous solution. The glassy state was short lived, as further heating of the mixture resulted in a nearly spontaneous decomposition. The resulting highly agglomerated, dark brown powder was then lightly ground with a mortar and pestle, placed in an alumina crucible and plunged into a furnace pre-set to 800° C. The material was soaked at 800° C, in air, for 20 h, followed by a 1°C /min increase in temperature to a 70 h soak at 850° C. After this time the sample was taken from the furnace and quenched to room temperature.

8.1.3 Mechanistic Studies

Several experiments were performed in attempts to explain the rapid product formation observed in the Ba-Y-Cu-O acetate system. As a comparison, and in order to

evaluate the effectiveness of the method, a solid state mixture of the acetates was prepared. Stoichiometric amounts of yttrium acetate, barium acetate and copper acetate were finely mixed and ground together with an agate mortar and pestle until no inhomogeneities could be seen. This powder was then subjected to the same thermal treatment as the acetate glass precursor. To elucidate the mechanism of product formation, Ba-Y-Cu-O precursor samples (prepared by the acetate method) were heated at 5°C/min to 300°, 400°, 500°, 600°, 700°, and 800°C, and quickly quenched to room temperature. To study the formation of the glassy precursor in the acetate method, several experiments were performed in which the initial composition of the precursor was varied. The acetates were boiled in acetic acid with varying levels of the three reagents. In addition, three samples containing only two of the reagents were boiled in acetic acid (e.g., $\text{Y}(\text{O}_2\text{CCH}_3)_3 \cdot 4\text{H}_2\text{O}$ and $\text{Ba}(\text{O}_2\text{CCH}_3)_2$, $\text{Cu}(\text{O}_2\text{CCH}_3)_2 \cdot \text{H}_2\text{O}$ and $\text{Ba}(\text{O}_2\text{CCH}_3)_2$, etc.), and each acetate was boiled individually. To evaluate the role of copper acetate in the method, copper acetate was completely replaced with zinc acetate, $\text{Zn}(\text{O}_2\text{CCH}_3)_2 \cdot 2\text{H}_2\text{O}$. The acetic acid was also substituted with water in several experiments. After the usual boiling procedure, these mixtures were dried at room temperature in a desiccator containing calcium sulfate (Drierite) and sodium hydroxide (NaOH being added to neutralize the acetic acid vapor) and studied by XRD and SEM to determine the extent of crystallinity.

To evaluate the effectiveness of the acetate method in the synthesis of bismuth based cuprates, a solid state preparation of $(\text{Bi,Pb})_2\text{Sr}_2\text{Ca}_2\text{Cu}_3\text{O}_{10}$ was attempted. The procedure consisted of mixing by grinding with an agate mortar and pestle, until no

inhomogenities were visually apparent, 0.009 mol Bi_2O_3 , 0.004 mol PbO , 0.020 mol SrCO_3 , 0.020 mol CaCO_3 , and 0.030 mol CuO . This powder was then pressed (1kbar) into 0.75 in diameter pellets and subjected to the same thermal treatment as the acetate method samples.

8.2 Characterization of Final Products

8.2.1 $\text{Ba}_2(\text{RE})\text{Cu}_3\text{O}_{7-x}$

The XRD of the final product, prepared via the acetate method, showed single phase (>99%) $\text{Ba}_2\text{YCu}_3\text{O}_{7-x}$. The method also proved to be extremely reproducible as several samples of equal quality (as evaluated by XRD and R vs. T) were prepared in a short time span. The acetate method was also used in the preparation of $\text{Ba}_2\text{EuCu}_3\text{O}_{7-x}$, $\text{Ba}_2\text{GdCu}_3\text{O}_{7-x}$, $\text{Ba}_2\text{NdCu}_3\text{O}_{7-x}$, and $\text{Ba}_2\text{LaCu}_3\text{O}_{7-x}$. The XRD pattern of these final products can be seen in Figure 8.1. The diffraction patterns for $\text{Ba}_2\text{EuCu}_3\text{O}_{7-x}$, $\text{Ba}_2\text{GdCu}_3\text{O}_{7-x}$, and $\text{Ba}_2\text{NdCu}_3\text{O}_{7-x}$ show phase pure material. The $\text{Ba}_2\text{LaCu}_3\text{O}_{7-x}$ pattern had low intensity peaks which were indexed to La_2O_3 . The pattern, however, did not display impurity peaks resulting from barium (e.g., BaCO_3 , $\text{Ba}_2\text{Cu}_3\text{O}_5$) or copper (CuO , $\text{Ba}_2\text{Cu}_3\text{O}_5$) containing phases, suggesting that the La_2O_3 was present due to an error in stoichiometry.

Resistivity measurements, performed on $\text{Ba}_2\text{YCu}_3\text{O}_{7-x}$ samples, showed a T_c onset at 93 K with loss of all resistance at 91 K (Figure 8.2). Extrapolation of the pre-transition line gives an x-axis intercept of ~60 K. Bulk superconductivity in $\text{Ba}_2\text{NdCu}_3\text{O}_{7-x}$, $\text{Ba}_2\text{GdCu}_3\text{O}_{7-x}$ and $\text{Ba}_2\text{EuCu}_3\text{O}_{7-x}$ was confirmed at 77 K using the Meissner balance

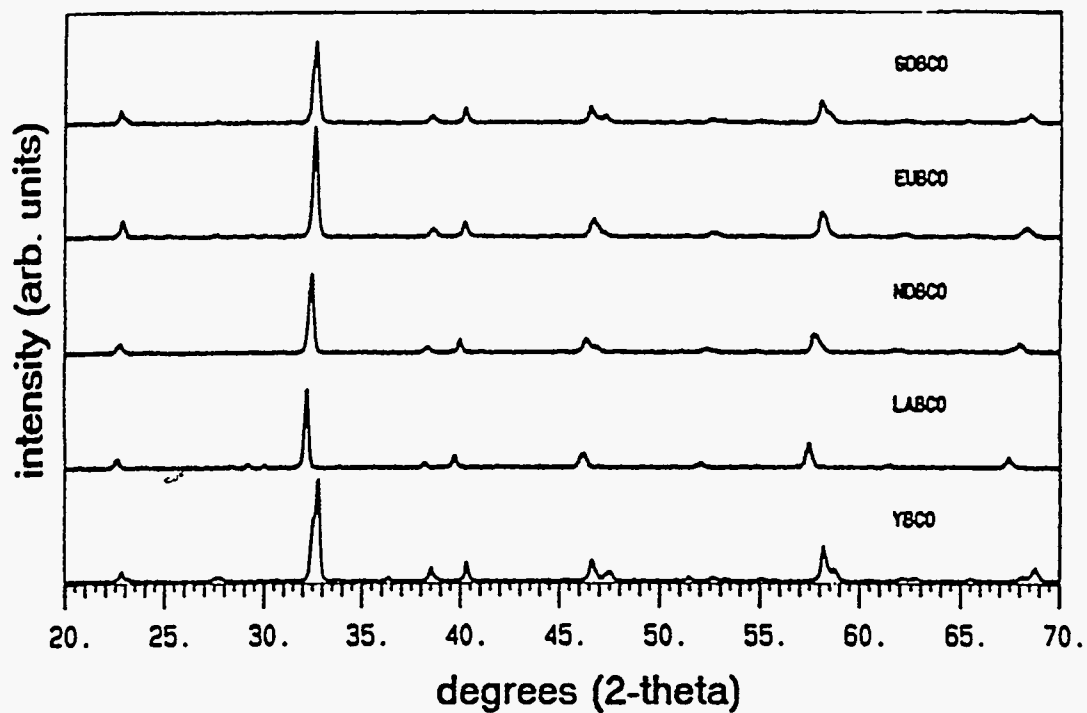


Figure 8.1 The XRD patterns for (from bottom) $\text{Ba}_2\text{YCu}_3\text{O}_{7-x}$, $\text{Ba}_2\text{LaCu}_3\text{O}_{7-x}$, $\text{Ba}_2\text{NdCu}_3\text{O}_{7-x}$, $\text{Ba}_2\text{GdCu}_3\text{O}_{7-x}$, and $\text{Ba}_2\text{EuCu}_3\text{O}_{7-x}$.

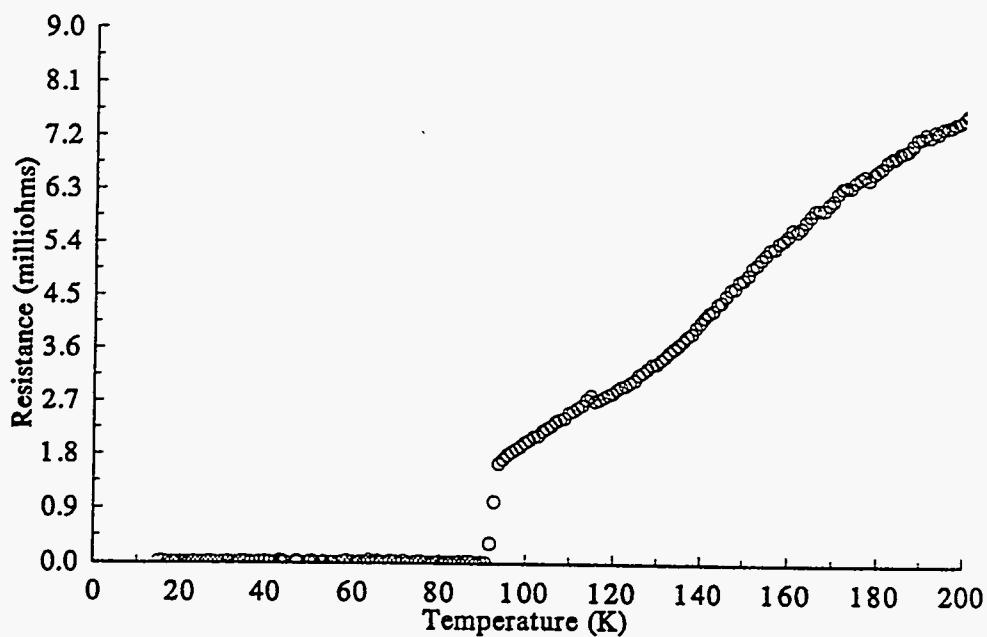


Figure 8.2. The resistance vs. temperature plot for a $\text{Ba}_2\text{YCu}_3\text{O}_{7-x}$ sample, prepared via the acetate method.

described in section 4.3.2 and elsewhere.⁷ The T_c of $Ba_2LaCu_3O_{7-x}$ is too low to observe a Meissner effect at 77 K.

Scanning electron micrographs (Figure 8.3) of $Ba_2YCu_3O_{7-x}$ final products revealed that the material consisted of crystallites on the order of one to two micrometers that were agglomerated into larger particles on the order of ten to twenty micrometers.

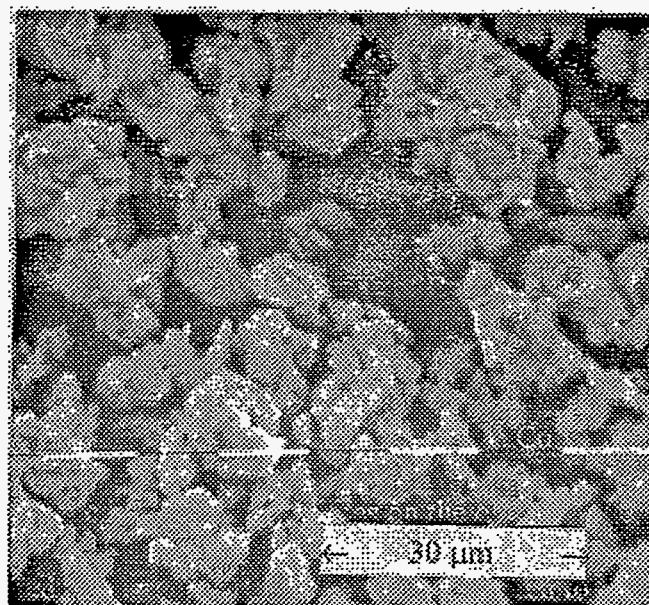


Figure 8.3. A scanning electron micrograph of an $Ba_2YCu_3O_{7-x}$ sample prepared via the acetate method.

8.2.2. $(Bi,Pb)_2Sr_2Ca_2Cu_3O_{10}$

Figure 8.4 shows an XRD pattern of a Bi-Pb-Sr-Ca-Cu-O final product. The patterns revealed that $(Bi,Pb)_2Sr_2Ca_2Cu_3O_{10}$ was the major phase. Although the samples were contaminated with some $Bi_2Sr_2CaCu_2O_8$. A magnetic determination of the T_c was made using the modified Meissner balance described in section 4.3.2. The resulting plot of balance response versus sample temperature can be seen in Figure 8.4. The magnetic

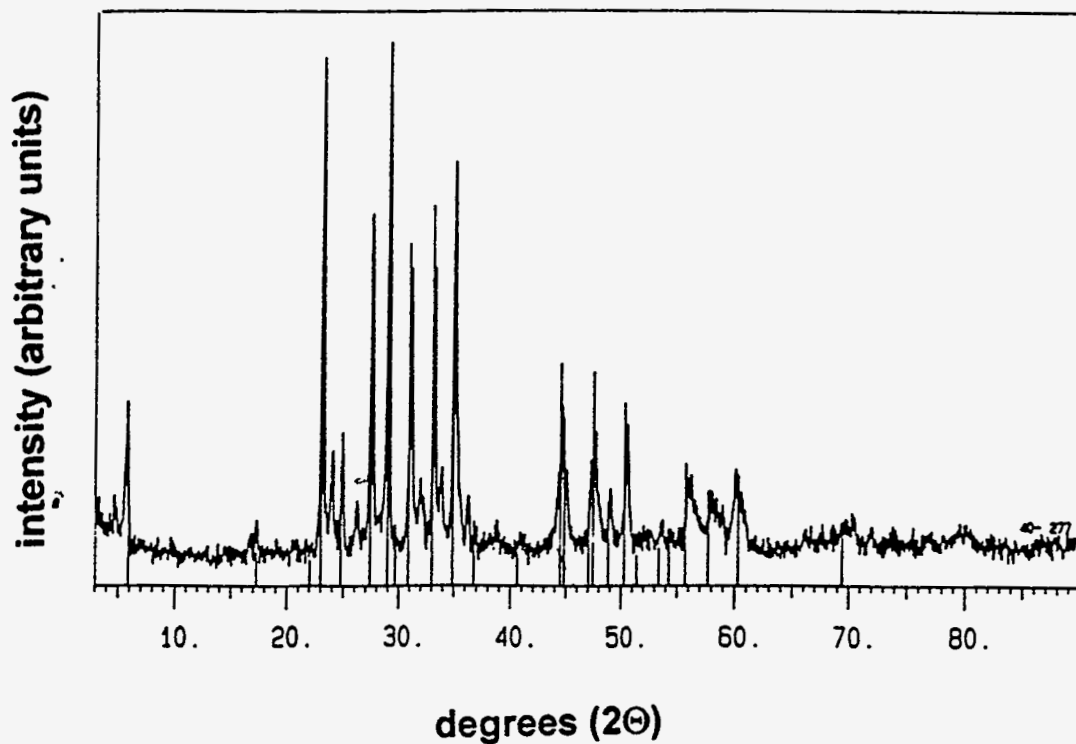


Figure 8.4. The XRD pattern of a $(\text{Bi,Pb})_2\text{Sr}_2\text{Ca}_2\text{Cu}_3\text{O}_{10}$ sample prepared via the acetate method. The JCPDS standard file for $\text{Bi}_2\text{Sr}_2\text{Ca}_2\text{Cu}_3\text{O}_{10}$ is superimposed.

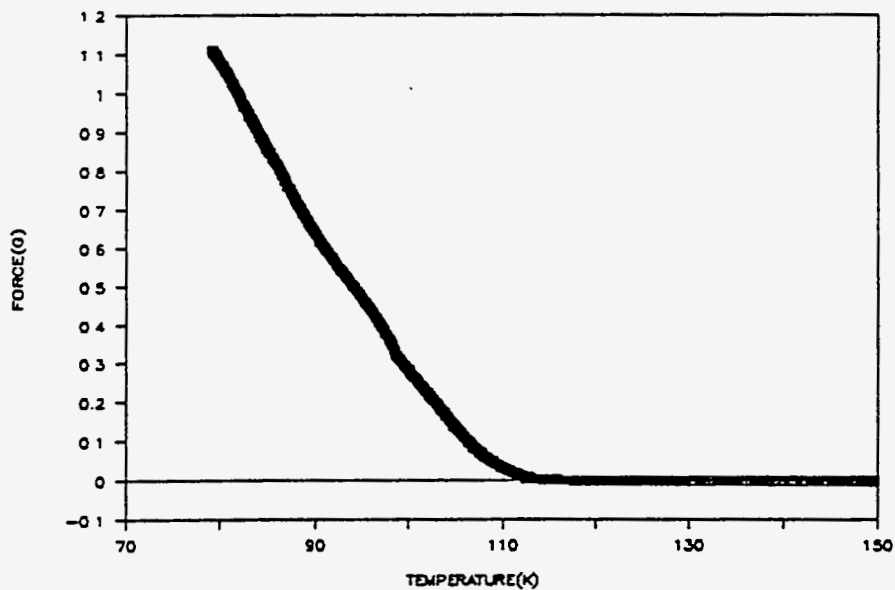


Figure 8.5. A plot of Meissner force versus temperature for a $(\text{Bi,Pb})_2\text{Sr}_2\text{Ca}_2\text{Cu}_3\text{O}_{10}$ sample prepared via the acetate method.

determination for the onset of superconductivity was 111 K (the expected value for $(\text{Bi,Pb})_2\text{Sr}_2\text{Ca}_2\text{Cu}_3\text{O}_{10}$). The conventional preparation of $(\text{Bi,Pb})_2\text{Sr}_2\text{Ca}_2\text{Cu}_3\text{O}_{10}$ from metal oxides and carbonates, subjected to the same thermal treatment, showed no superconductivity (no diamagnetic response) at 77 K.

8.3 Results of Mechanistic Studies

It is clear from the above results that the relatively simple procedure of the acetate method enhanced the product formation of $(\text{Bi,Pb})_2\text{Sr}_2\text{Ca}_2\text{Cu}_3\text{O}_{10}$ over that of the solid state reaction of oxides and carbonates and resulted in high quality, phase pure $\text{Ba}_2\text{RECu}_3\text{O}_{7-x}$. The more interesting questions lie in the mechanism of product formation and origin of the amorphous precursor. The x-ray diffraction pattern of mechanically mixed acetates was compared to the precursor mixed with boiling acetic acid. The diffraction pattern obtained for the mechanically mixed acetates of the Ba-Y-Cu-O system clearly showed the expected peaks of yttrium acetate, barium acetate and copper acetate, whereas the precursor mixed in acetic acid did not display any peaks above the amorphous scattering (see Figure 8.6). As with the freeze dried nitrate precursors, an amorphous XRD pattern was evidence for a lack of long range order in the precursor, a phenomenon consistent with an atomic level mixing of reactants. A difference in the degree of mixing of the two samples was also evident in the final products obtained after heat treatment. When subjected to the same thermal processing, the mechanically mixed acetates produced a mixture of phases; mainly barium carbonate, copper oxide, Y_2BaCuO_5 , and $\text{Ba}_2\text{YCu}_3\text{O}_{7-x}$ (see Figure 8.7).

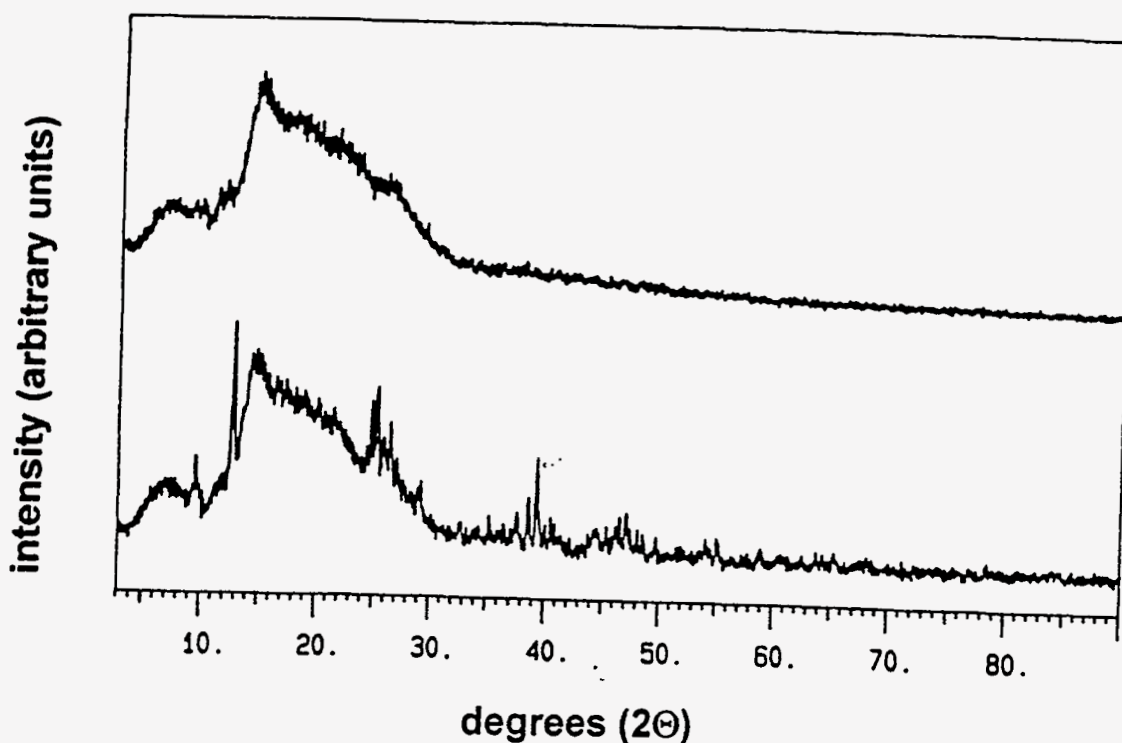


Figure 8.6. The x-ray diffraction pattern of the acetic acid mixed precursor (upper pattern) and mechanically mixed acetates (lower pattern). The large broad diffraction from 3° to 30°2θ is due to the Kapton tape in which the samples were enclosed.

Figure 8.8 shows the x-ray diffraction patterns of Ba-Y-Cu acetate glass samples heated at 5° C/min to varying temperatures and quenched to room temperature. The XRD pattern of the $Ba_2YCu_3O_{7-x}$ precursor sample that was heated to 300°C at 5°C/min primarily consisted of amorphous scattering, with the only identifiable peaks belonging to metallic copper. Metallic copper resulted from the decomposition of copper acetate and the reduction of Cu(II) to Cu(0) by carbon and carbon monoxide produced through the decomposition of the acetate anion and residual acetic acid. At 400°C, the Cu(0) began to

began to oxidize and the main phases present were metallic copper and copper(I) oxide (Cu_2O). In addition, two broad, low angle, unidentified peaks (~ 21.5 and $\sim 27.0^\circ 2\Theta$) were observed at 400°C . At 500°C , 600°C , and 700°C the main phases present were copper(II) oxide (CuO) and barium carbonate. The gradual appearance of barium carbonate peaks (first seen at 500°C) coincided with the diminishing of the intensity of the unknown peaks, suggesting that this unknown phase contained barium. At 600°C , a broad peak was observed, which was centered at $\sim 29.0^\circ 2\Theta$ and steadily narrowed in width and

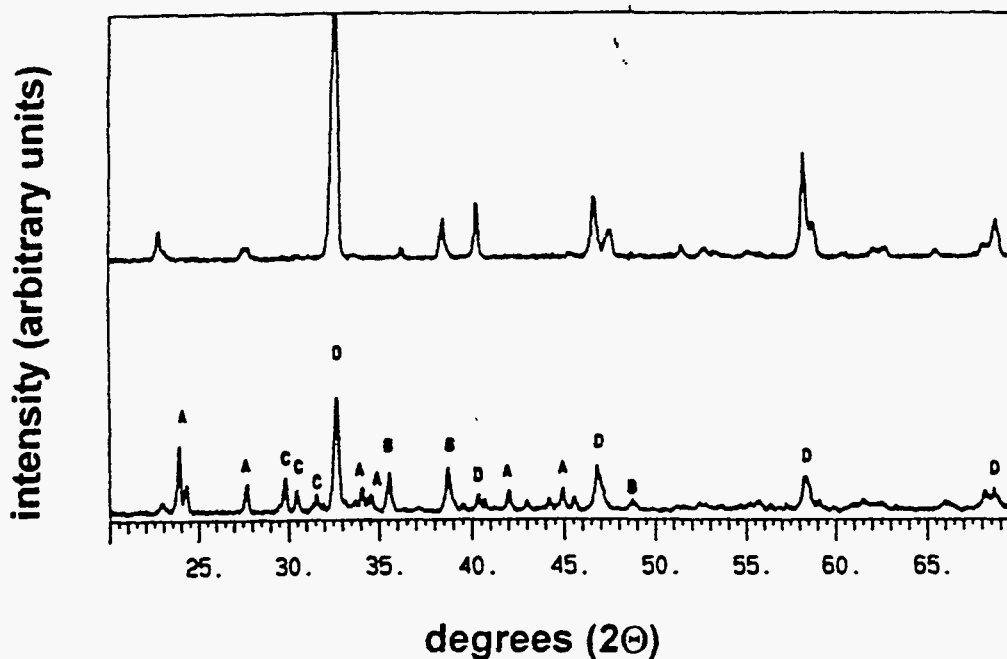


Figure 8.7. The x-ray diffraction patterns of an acetic acid mixed sample (upper pattern) and a mechanical mixture of the acetates, subjected to the same thermal treatment (2h at 900°C). Peaks labeled A correspond to BaCO_3 , B correspond to CuO , C correspond to BaY_2CuO_5 , and D correspond to $\text{Ba}_2\text{YCu}_3\text{O}_{7-x}$

Table 8.1 Nominal composition of metal acetates and solvent in several precursors and the resulting x-ray diffraction.

Y	Ba	Cu	Zn	solvent	diffraction result
1	2	3	0	acet. ac.	amorphous
1	2	0	3	acet. ac.	amorphous
2	0	2	0	acet. ac.	crystalline
0	2	3	0	acet. ac.	crystalline
2	1	1	0	acet. ac.	amorphous
1	1	0	0	acet. ac.	amorphous
1	2	3	0	water	crystalline
1	1	0	0	water	crystalline

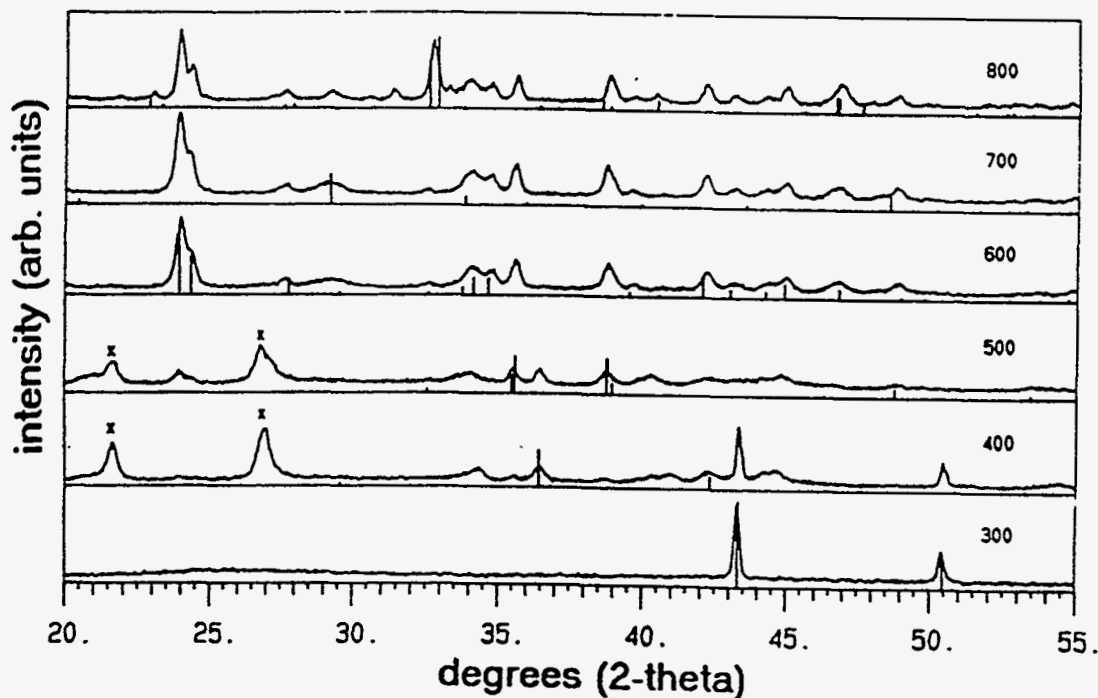


Figure 8.8. The XRD patterns of $\text{Ba}_2\text{YCu}_3\text{O}_{7-x}$ acetate method samples heated from 300° to 800° C. The precursor is completely amorphous except for metallic copper at 300° C. Peaks marked X correspond to an unidentified phase. The stick patterns superimposed are; 300° Cu (metal), 400° Cu_2O , 500° CuO , 600° BaCO_3 , 700° Y_2O_3 , and 800° $\text{Ba}_2\text{YCu}_3\text{O}_7$.

grew in intensity in the 700° and 800°C patterns. This peak was indexed to yttrium oxide.

At 800°C, the main phases present were barium carbonate, copper(II) oxide,

$Ba_2YCu_3O_{7-x}$, and $Y_2Cu_2O_5$. After a 2h soak at 900°C the only identifiable phase was

$Ba_2YCu_3O_{7-x}$.

The formation of the precursor was studied by varying the amounts of the three acetates used in the acetate method. These precursors were then dried under the conditions previously stated and studied by XRD (see Table 8.1) and SEM. The

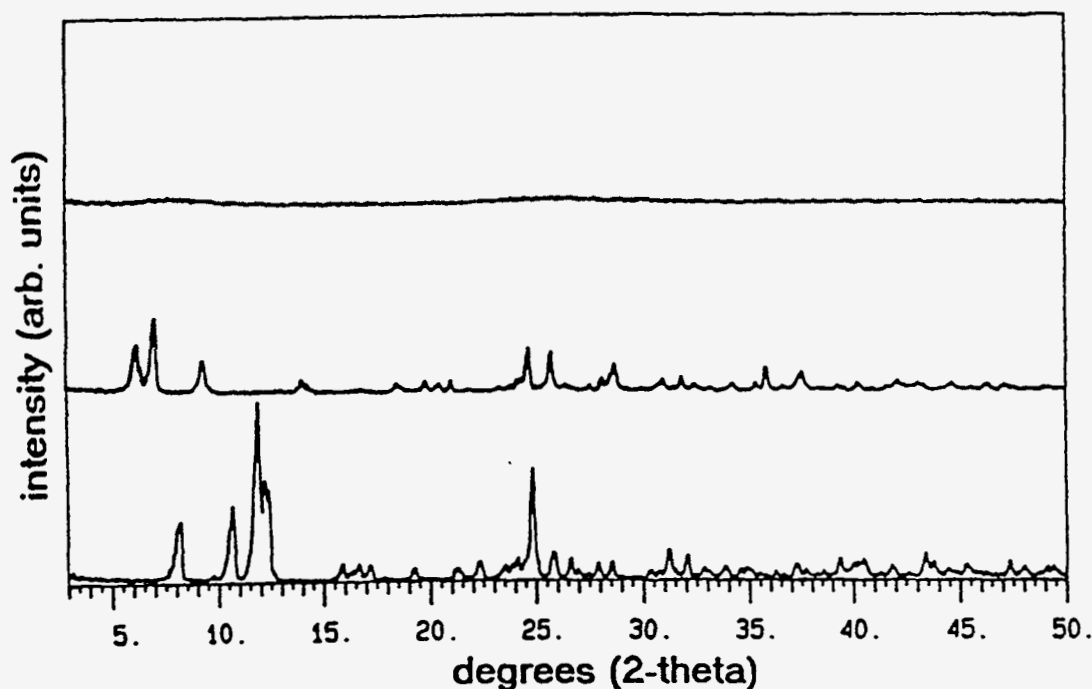


Figure 8.9 X-ray diffraction patterns of (from bottom) the dried precursor of yttrium acetate boiled in acetic acid, barium acetate boiled in acetic acid and a 1:1 mixture (per mole) of yttrium acetate and barium acetate boiled in acetic acid. The two salts are necessary for the amorphous pattern.

micrographs of dried yttrium acetate, barium acetate and acetic acid precursors revealed no crystallinity in the material. In addition, the x-ray diffraction pattern of this precursor consisted of only amorphous scattering (see Figure 8.9), whereas XRD patterns of yttrium acetate boiled individually in acetic acid and barium acetate boiled individually in acetic acid indicated that these materials were highly crystalline.

8.4 Discussion and Conclusions

8.4.1 The Ba-RE-Cu-O Acetate System

The acetate method was a simple, reliable, and time saving method for the production of phase pure, bulk $Ba_2RECu_3O_{7-x}$ superconductors. It was a useful alternative to both the common grind and sinter method and more sophisticated chemical methods. This method should be applicable to the preparation of other rare earth $Ba_2RECu_3O_{7-x}$ superconductors (where RE=Ho, Dy, Sm, Yb, Lu, Er). In addition, the method should allow easy and uniform doping of impurities into high transition temperature superconductors for mechanistic studies.

Although this method produced an amorphous, intimately mixed precursor, and resulted in rapid product formation, the mechanism of mixing was not very clear. Through several experiments, it has been found that the necessary interaction for producing an amorphous precursor occurred through a combination of barium acetate, the rare earth acetate and acetic acid. Table 8.1 shows the result of mixing several varying compositions. The common ingredients for obtaining a glassy, amorphous precursor were barium acetate, a rare earth acetate and acetic acid. Varying the amount of copper (over the

values compiled in Table 8.1), eliminating copper, or substituting it completely with zinc, had no effect on the amorphous structure of the precursor. Eliminating the barium or rare earth acetate, or substituting water for acetic acid resulted in a crystalline precursor.

However, it was not simply one of the two acetates (Y or Ba) that prevented crystallization. When yttrium acetate or barium acetate was boiled separately in acetic acid the result (after drying) was a crystalline material. The two salts were required to achieve the amorphous glass (see Figure 8.10). In fact, 0.010 mol of yttrium acetate would not even completely dissolve in 50 mL of boiling acetic acid. If 0.010 mol (~3.38g) yttrium acetate and 0.010 mol barium acetate were boiled together in 50 mL of acetic acid, the mixture dissolved to yield a clear solution. This effect has been previously observed when $K(O_2CCH_3)$ is added to glacial acetic acid solutions of $Ag(O_2CCH_3)$. The solubility of $Ag(O_2CCH_3)$ increased to over 30 times its initial value upon the addition of $K(O_2CCH_3)$. The authors attributed the increase in solubility to the presence of the acetate anion in solution.⁸ The system of acetates dissolved in acetic acid is analogous to the system of hydroxides dissolved in water.⁹ Only the most electropositive metals (Li, Na, K, Rb, Cs, Ca, Sr, Ba, Ra) form hydroxides that are readily soluble in water.¹⁰ The same is true for acetates in glacial acetic acid (with the exception of $Pb(O_2CCH_3)_2$ and $Cd(O_2CCH_3)_2$ which are both readily soluble in acetic acid).¹¹ When an acetate of a highly electropositive metal dissolves in acetic acid it releases the acetate anion into solution. The acetate anion, being the most basic species possible in the acetic acid solvent system, allows the dissolution of some transition metal acetates just as some transition metal hydroxides (e.g., $Cu(OH)_2$) are soluble in aqueous (basic) sodium hydroxide solutions.¹²

Therefore, barium acetate dissolves in acetic acid and makes "basic" acetic acid which can dissolve transition metal acetates (Y, Cu).

The reason why no crystallization (or very limited crystallization) occurred when the acid was boiled away was less clear. One possibility is that the metal acetates were trapped in a glassy state by an extended network of hydrogen bonds.¹³ The acetate ligand, acetic acid and any residual water, all have hydrogen atoms and oxygen atoms that could participate in hydrogen bonding. However, substituting water for acetic acid, after the boiling and drying, resulted in a crystalline precursor, even though water is very capable of hydrogen bonding. It is possible that the acetic acid removed the waters of hydration from the metal acetates and that these dehydrated acetates were slow to crystallize. The acetic acid may have complexed to the metal acetate or even replaced the waters of hydration in the complex to give an acid-acetate species. The former was indeed the case when barium acetate was boiled in acetic acid. The existence of a barium acetate salt with additional acetic acid ligands, $\text{Ba}(\text{CH}_3\text{CO}_2)_2 \cdot 1.5\text{CH}_3\text{CO}_2\text{H}$, has been reported¹⁴ and was detected in this study by XRD to be the result of boiling acetic acid with barium acetate (see Figure 8.9). The powder x-ray diffraction pattern of yttrium acetate boiled in acetic acid greatly differed from that of yttrium acetate tetrahydrate (as received from Johnson Matthey). Without further investigation, however, the structural change could not be definitely attributed to the additional complexation of yttrium acetate by acetic acid ligands. It is also possible that a double salt was formed which had a high probability of hydrogen bonding to itself, acetic acid, or other acetate ligands. Several double salts of metal acetates, prepared by dissolving the two acetates in glacial acetic acid, have been reported.^{15,16,17}

8.4.2 The (Bi,Pb)-Sr-Ca-Cu-O Acetate System

The procedure for preparation of $(\text{Bi,Pb})_2\text{Sr}_2\text{Ca}_2\text{Cu}_3\text{O}_{10}$ via the acetate method differed slightly from that of the $\text{Ba}_2\text{RECu}_3\text{O}_{7-x}$ preparation due to the differences in solubilities of the $(\text{Bi,Pb})_2\text{Sr}_2\text{Ca}_2\text{Cu}_3\text{O}_{10}$ system acetates. Bismuth acetate proved insoluble in acetic acid. Consequently, bismuth nitrate was used in its place. This resulted in an oxidation-reduction reaction between the oxidizing nitrate anion and the reducing acetate anion upon evaporation of sufficient acetic acid. The result was a near spontaneous decomposition of the acetate glass shortly after its formation. For this reason, the glass formation could be carried out in a Pyrex beaker and the resulting dark brown powder easily transferred to a crucible for the high temperature anneal. Ammonium acetate was added to the $(\text{Bi,Pb})_2\text{Sr}_2\text{Ca}_2\text{Cu}_3\text{O}_{10}$ acetate method preparation to increase the "basic" nature of the acetic acid and thereby increase the solubility of the copper acetate. The acetates of the $(\text{Bi,Pb})_2\text{Sr}_2\text{Ca}_2\text{Cu}_3\text{O}_{10}$ system would not completely dissolve in without the addition of $\text{NH}_4(\text{O}_2\text{CCH}_3)$.

Although not quite as successful with respect to phase purity as in the $\text{Ba}_2\text{YCu}_3\text{O}_{7-x}$ acetate system, the $(\text{Bi,Pb})_2\text{Sr}_2\text{Ca}_2\text{Cu}_3\text{O}_{10}$ acetate system did show marked improvement in the high T_c phase formation over the grind and calcine method. The 110 K T_c phase, $(\text{Bi,Pb})_2\text{Sr}_2\text{Ca}_2\text{Cu}_3\text{O}_{10}$, is extremely difficult to produce with a high degree of phase purity without the use of extremely long firing times (several days). In this study, firing times were limited to 90h. Longer firing times, which would probably have increased the volume fraction of $(\text{Bi,Pb})_2\text{Sr}_2\text{Ca}_2\text{Cu}_3\text{O}_{10}$ present, would have obscured the benefits of the acetate method. Whether or not the acetate method truly achieved atomic

level mixing with the $(\text{Bi,Pb})_2\text{Sr}_2\text{Ca}_2\text{Cu}_3\text{O}_{10}$ system was not clear. Freeze drying (perhaps the most effective means of achieving atomic mixtures) has been used for the preparation of $(\text{Bi,Pb})_2\text{Sr}_2\text{Ca}_2\text{Cu}_3\text{O}_{10}$.¹⁸ Even with the use of freeze dried nitrate precursors, a 37 h anneal at 865°C was needed to reach a maximum volume fraction of $(\text{Bi,Pb})_2\text{Sr}_2\text{Ca}_2\text{Cu}_3\text{O}_{10}$ (although $\text{Bi}_2\text{Sr}_2\text{CaCu}_2\text{O}_8$ formed in minutes). Another study¹⁹ on phase formation in the $(\text{Bi,Pb})_2\text{Sr}_2\text{Ca}_2\text{Cu}_3\text{O}_{10}$ system has shown that $\text{Bi}_2\text{Sr}_2\text{CaCu}_2\text{O}_8$ was still the major phase (with $\text{Bi}_2\text{Sr}_2\text{CuO}_6$, Ca_2PbO_4 and Cu_2O as other impurities) after annealing a mechanical mixture of oxides and carbonates for 100 h at 830°C. Nearly full formation of the $(\text{Bi,Pb})_2\text{Sr}_2\text{Ca}_2\text{Cu}_3\text{O}_{10}$ phase via conventional ceramic preparation has been reported by calcination of the oxides and carbonates at 785° C for 185 h (with three intermittent grindings) followed by sintering of a compact at 850° C for 170 h.²⁰ Considering these studies, as well as the conventional preparations attempted in this work, one can more clearly see the advantages of the acetate method. The shorter firing time achieved through freeze drying may be attributed to the non-carbonaceous nature of the freeze dried nitrate precursor. Calcium carbonate and strontium carbonate formed upon decomposition of the metal acetates are stable phases which require high temperatures for complete decomposition.¹⁰

8.5 Notes and References

- ¹ J. McHale, G. H. Myer and R. E. Salomon, *J. Mater. Res.* **10**, No. 1, (1995).
- ² J. A. Duffy and M. D. Ingram, *J. Am. Ceram. Soc.* **52**, 224 (1969).
- ³ R. F. Bartholomew, and S. S. Lewek, *J. Am. Ceram. Soc.* **53**, 445 (1970).
- ⁴ J. McKittrick and R. Contreras, *Thin Solid Films* **206**, 146 (1991).
- ⁵ M. L. Kullberg, M. T. Lanagan, W. Wu, and R. B. Poeppel, *Supercon. Sci. and Technol.* **4**, 337 (1991).
- ⁶ D. I. dos Santos, U. Balachandran, R. A. Guttschow, and R. B. Poeppel, *J. Non-Cryst. Solids* **121**, 448 (1990).
- ⁷ J. McHale, R. W. Schaeffer, and R. E. Salomon, *J. Chem. Ed.* **69**, 1031 (1992).
- ⁸ S. Peterson and E. K. Dienes, *J. Phys. Chem.* **55**, 1299 (1951).
- ⁹ For a discussion of this topic see chapter 7 of J. Kleinberg, W. J. Argersinger, and E. Griswold, *Inorganic Chemistry*, D.C. Heath and Co. (Boston, Massachusetts, 1960).
- ¹⁰ R. C. Weast (Editor), *CRC Handbook of Physics and Chemistry*, 62nd Edition, CRC Press Inc. (Boca Raton, Florida, 1981).
- ¹¹ For a discussion of the acetic acid solvent system see T. C. Waddington, *Non-Aqueous Solvent Systems*, Academic Press (New York, 1965), or A. K. Holiday and A. G. Massey, *Inorganic Chemistry in Non-Aqueous Solvents*, Pergamon Press (New York, 1965).

- ¹² A. W. Davidson, *J. Am. Chem. Soc.* **50**, 1890 (1928).
- ¹³ D. D. Titus, Personal Communication (Philadelphia, PA, 1993).
- ¹⁴ B. M. Nirsha, A. D. Chubinidze, Y. A. Velikodnyi, B. V. Zhadanov, and V. A. Olikova, *Zh. Obshch. Khim. USSR* **53**, 1631 (1983).
- ¹⁵ A. Davidson and W. McAllister, *J. Am. Chem. Soc.* **52**, 519 (1930).
- ¹⁶ A. W. Davidson and E. Griswold, *J. Am. Chem. Soc.* **57**, 423 (1935).
- ¹⁷ E. Griswold and W. van Horne, *J. Am. Chem. Soc.* **67**, 763 (1945).
- ¹⁸ N. V. Coppa, W. L. Hults, J. L. Smith, and J. Brynestad, *J. Mater. Res.* **9**, 2510 (1994).
- ¹⁹ M. T. Ruiz, G. F. de la Fuente, A. Badia, J. Blasco, M. Castro, A. Sotelo, A. Larrea, F. Lera, C. Rillo, and R. Navarro, *J. Mater. Res.* **8**, 1268 (1993).
- ²⁰ N. Knauf, J. Harwischmacher, R. Müller, R. Borowski, B. Rodeu, and D. Wohlleben, *Physica C* **173**, 414 (1991).

CHAPTER 9

SUMMARY AND CONCLUSIONS

In this dissertation, several solution based methods were utilized for the synthesis of solid state materials. Products were obtained under milder reaction conditions due to a greater degree of reactant mixing. As discussed in Chapter 1, solid state reactions of mechanically mixed reagents are diffusion limited process. Shortening the diffusion paths necessary for complete reaction greatly increases the rate of product formation. This has been experimentally demonstrated in this work using three different means of achieving atomic level mixing, on three different classes of materials.

Freeze drying was used to produce the ternary perovskite-type oxide BaTiO_3 . Conventional preparation of BaTiO_3 from TiO_2 and BaCO_3 requires temperatures in excess of 1000°C for time periods in excess of 24h to achieve phase purity. In this work, freeze dried nitrate precursors yielded phase BaTiO_3 in only 10 min at 600°C . The material produced had a nanocrystalline microstructure which is beneficial for many applications, including the production of thin film capacitors via screen printing. The average particle size of the BaTiO_3 produced from freeze dried nitrate precursors was shown to be highly dependent on the calcination temperature and only slightly dependent on the annealing time. This suggests that BaTiO_3 powders with a desired range of particle sizes could be synthesized through judicious choice of calcination temperature. This

selection of the range of particle size is not possible through conventional ceramic processing and may lead to the application of these freeze dried powders in materials such as nanocrystalline compacts.

In route to the freeze drying preparation of BaTiO_3 , an aqueous procedure was invented¹ for the preparation of solid titanyl nitrate. This material is a stable, water soluble source of titanium and can be used as the starting reagent for a wide range of aqueous titanium chemistry. Prior to the development of this procedure for the preparation of solid titanyl nitrate, aqueous titanium (IV) solutions could only be prepared from TiCl_4 (a volatile, highly moisture sensitive liquid), TiBr_4 , TiF_4 , TiI_4 (volatile moisture sensitive solids), or dissolution of the metal or oxides in hot sulfuric or hydrofluoric acid.² The solid titanyl nitrate has been shown to have a stable formula weight and can be used to prepare accurately stoichiometric solutions.

Titanyl nitrate was also used for the preparation of SYNROC-B from thermal decomposition of freeze dried nitrate precursors. The widespread utilization of SYNROC as a high level nuclear waste immobilization medium is currently hindered by the proposed preparation conditions. These consist of mixing the necessary, binary oxides with ~10wt% high level nuclear waste and hot pressing this mixture at 10×10^7 Pa and 1200°C . Individually, a high pressure or a high temperature is not a problem. But this combination of high pressures and high temperatures introduces a severe safety risk to the environment in which nuclear waste is generally handled. In this work, the complete SYNROC-B phase assemblage, a mixture of CaTiO_3 , $\text{BaAl}_2\text{Ti}_5\text{O}_{14}$, and $\text{CaZrTi}_2\text{O}_7$, was synthesized at 600 torr after only 10 min at 1100°C via thermal decomposition of freeze dried nitrate

precursors. The freeze dried precursor proved amorphous to XRD, a phenomenon consistent with a solid atomic mixture of reactants. This low pressure route to SYNROC synthesis may make the application of the material as an immobilization medium more practical. The solution based aspect of the synthesis is beneficial as well. Currently, high level nuclear waste is evaporated from a solution (many of these solutions are nitrate based) to a "sludge." This sludge would then be mixed with the binary oxides necessary to form SYNROC. Using the freeze drying route, nuclear waste streams could be chemically tailored by addition of the necessary components of SYNROC as water soluble nitrates. The waste solution could then be frozen,³ and after water removal by sublimation, thermally processed to yield SYNROC powders after very short calcination times.⁴

A novel solution based method for the synthesis of thin and thick films of $\text{Ba}_2\text{YCu}_3\text{O}_{7-x}$ was developed. Yttrium, barium and copper nitrates were dissolved in liquid ammonia. This solution was atomized with nitrous oxide and ignited with a hydrogen/oxygen torch. The resulting flame was used to coat a substrate (MgO or LaAlO_3) with superconducting material. The high temperature superconducting cuprate, $\text{Ba}_2\text{YCu}_3\text{O}_{7-x}$, was obtained in-situ through this flaming solvent spray process. The films produced, however, had poor superconducting properties. This was largely the result of poor grain contact in the films. Thin films, deposited from dilute ($<0.0008\text{M}$ total metal ion concentration) solutions grew epitaxially on single crystal LaAlO_3 substrates. Two scenarios were hypothesized to explain the observed in-situ preparation. In the first scenario, gaseous precursors produced in the flame reacted on or near the substrate and

nucleated from the gas phase to form $\text{Ba}_2\text{YCu}_3\text{O}_{7-x}$. This chemical vapor deposition scenario was supported by two pieces of evidence. (1) The maximum temperature of an ammonia/oxygen flame is high enough (3000°C) for volatilization of all reactants to occur. And (2), atomic emission from gaseous barium was observed during deposition. In the second scenario, an atomic level mixture of BaO , CuO and Y_2O_3 particulates are deposited onto the substrate where temperatures are sufficient to facilitate diffusion and reaction in the solid state. This scenario was supported by the observation, from scanning electron micrographs, that the films were rough (at $2500\times$ magnification) and appeared to be comprised of a series of loosely connected grains. The most logical scenario, in the opinion of the author, is that a combination of gas phase growth and particle bombardment was occurring in the flaming solvent spray.

A solution based method for the synthesis of $\text{Ba}_2\text{YCu}_3\text{O}_{7-x}$ and $(\text{Bi,Pb})_2\text{Sr}_2\text{Ca}_2\text{Cu}_3\text{O}_{10}$ was also developed. This method displayed the benefits of a solution method (atomic level mixing of reactants, rapid product formation) but, in practice, had the simplicity of conventional processing. A solution of metal acetates in acetic acid was concentrated (by boiling) until the viscosity of the solution increased and eventually resulted in a glassy state. Thermal processing of this glassy precursor for 2h at 900°C yielded phase pure $\text{Ba}_2\text{YCu}_3\text{O}_{7-x}$, with excellent superconducting characteristics. The precursor proved amorphous to XRD, a phenomenon consistent with a solid atomic mixture of reactants. Substitution studies proved that the interaction necessary for the glass formation is occurring in a combination of yttrium acetate, barium acetate, and acetic acid. The barium acetate is serving to make "basic" acetic acid upon a finite release of the

acetate anion (the most basic species possible in the glacial acetic acid solvent system) into solution. This allowed dissolution of the transition metal acetates, which would dissolve in the concentrations used in the method without the addition of barium acetate.

In summary, the conventional diffusion limited solid state reaction mechanism was circumvented through the use of atomically mixed precursors. The homogeneity inherent in the solution state was trapped, and transferred into the solid state by a number of methods. These solution methods have allowed the synthesis of high quality samples of technologically important materials under comparatively mild reaction conditions.

Notes and References

- ¹ J. M. McHale and N. V. Coppa, Titanate Materials From Freeze Dried Nitrate Solutions, U. S. Patent applied for: DOE application # S-80, 469 (1994).
- ² J. Barksdale, *Titanium, Its Occurrence, Chemistry and Technology, Second Edition*, The Ronald Press Co. (New York, 1966).
- ³ A more efficient means of freezing the solution would be necessary, as millions of gallons of waste need be processed.
- ⁴ N. V. Coppa, Personal Communication (Los Alamos, NM, 1994).

COMPREHENSIVE BIBLIOGRAPHY

- Adachi, S., H. Adachi, K. Stesune, and K. Wasa, *Physica C* **175**, 523 (1991).
- Angus, J. C., and C. C. Hayman, *Science* **241**, 913 (1988).
- Aponte, J. M., and M. Octavio, *J. Appl. Phys.* **66**, 1480 (1990).
- Arya, S. P. S., and H. E. Hintermann, *Thin Solid Films* **193-194**, 841 (1990).
- Awando, M., K. Kani, Y. Takao, and H. Tagaki, *Jpn. J. Appl. Phys.* **30**, L806 (1991).
- Balchev, N., D. Kovacheva, V. Lovchinov, K. Konstantinov, and K. Petrov, *J. Supercon.* **6**, 49 (1993).
- Barboux-Doeuff, S., and C. Sanchez, *Mater. Res. Bull.* **29**, 1 (1994).
- Barksdale, J., *Titanium Its Occurrence, Chemistry, and Technology, Second Edition*, The Ronald Press Co., New York, 1966.
- Barnard, J. A., and J. N. Bradley, *Flame and Combustion*, Chapman and Hall Ltd. (New York, 1985).
- Barth, T., *Norsk. Geol. Tidssk.* **8**, 201 (1925).
- Bartholomew, R. F., and S. S. Lewek, *J. Am. Ceram. Soc.* **53**, 445 (1970).
- Beauger, A., J. C. Multin, and J. C. Neipce, *J. Mater. Sci.* **18**, 3041, (1983).
- Bednorz, J. G., and K. A. Muller, *Z. Phys. B* **64**, 189 (1986).
- Beech, F., S. Miraglia, A. Santoro, and R. S. Roth, *Phys. Rev. B* **35**, 8778 (1987).
- Beretka, J., and T. Brown, *J. Am. Ceram. Soc.* **66**, 383 (1983).
- Bordet, P., C. Chaillout, J. Chevanas, J. L. Hoveau, M. Marezio, J. Karpinski, and E. Kaldis, *Nature* **334**, 596 (1988).

- Briggs, A., B. A. Bellamy, I. E. Denton, and J. M. Perks, *J. Less-Common Metals* **164 & 165**, 559 (1990).
- Brosha, E. L., E. Sanchez, P. K. Davies, N. V. Coppa, A. Thomas, and R. E. Salomon, *Physica C* **184**, 353 (1991).
- Brown, W. E., D. Dollimore, and A. K. Galwey, *Comprehensive Chemical Kinetics, Volume 22, Reactions in the Solid State*, Edited by C. H. Bamford and C. H. F. Tipper, Elsevier Scientific (New York, 1980).
- Buykx, W. J., D. J. Cassidy, C. E. Webb, and J. L. Woolfrey, *Am. Ceram. Soc. Bull.* **60**, 1284 (1981).
- Carreno, T. G., A. Misfud, C. J. Cerna, and J. M. Palacios, *Mater. Chem. Phys.* **27**, 287 (1991).
- Carter, R. E., *J. Chem. Phys.* **34**, 2010 (1961).
- Carter, R. E., *J. Chem. Phys.* **35**, 1137 (1961).
- Cava, R. J., J. J. Krajewski, W. F. Peck Jr., B. Batlogg, L. W. Rupp Jr., R. M. Flemming, W. P. James, and P. Marsh, *Nature* **338**, 328 (1989).
- Cava, R. J., *Scientific American*, August, **42** (1990).
- Chang, C.-A., *Appl. Phys. Lett.* **53**, 1113 (1988).
- Chang, H. J., Y. Doshida, Y. Watanabe, K. Shimizu, Y. Okamoto, R. Akihama, and J. T. Song, *Cryogenics* **32**, 279 (1992).
- Cheary, R. W., J. V. Hunt, and P. Calaizis, *J. Aust. Ceram. Soc.* **17**, 11 (1981).
- Cheung, C. T., and E. Ruckenstein, *J. Mater. Res.* **4**, 1 (1989).

- Clabaugh, W. S., E. M. Swiggard, and R. Gilchrist, *J. Res. Natl. Bur. Stand.* **56**, 289 (1956).
- Coppa, N. V., *Doctoral Dissertation*, Temple University, Philadelphia, PA 19122 (1990).
- Coppa, N. V., G. H. Myer, R. E. Salomon, A. Bura, J. W. O'Reilley, J. E. Crow, and P. K. Davies, *J. Mater. Res.* **7**, 2017 (1992).
- Coppa, N. V., W. L. Hults, J. L. Smith, and J. Brynestad, *J. Mater. Res.* **9**, 2510 (1994).
- Coppa, N. V., A. Bura, J. W. Schwegler, R. E. Salomon, G. H. Myer, and J. E. Crow, *Mat. Res. Soc. Proc. Vol. 180*, 935 (1990).
- Cryot, M., and D. Pavuna, *Introduction to Superconductivity and High Temperature Superconductivity*, World Scientific (Singapore, 1992).
- Cullitty, B. D., *Elements of X-ray Diffraction*, Addison-Wesley Publishing Co (Reading, MA, 1978).
- Das Sharma, A., R. N. Basu, and H. S. Maiti, *J. Mater. Sci.* **11**, 122 (1992).
- Davidson, A. W., and E. Griswold, *J. Am. Chem. Soc.* **57**, 423 (1935).
- Davidson, A. W., and W. McAllister, *J. Am. Chem. Soc.* **52**, 519 (1930).
- Davidson, A. W., *J. Am. Chem. Soc.* **50**, 1890 (1928).
- Dijkamp, D., T. Venkatesan, X. D. Wu, S. A. Shaheen, N. Jisrawi, Y. H. Min-Lee, W. L. McLean, and M. Croft, *Appl. Phys. Lett.* **51**, 619 (1987).
- dos Santos, D. I., U. Balacandran, R. A. Guttschow, and R. B. Poeppel, *J. Non-Cryst. Sol.* **121**, 448 (1990).
- Duckwitz, C. Z., and H. Schamlzried, *Z. Phys. Chem. NF* **76**, 173 (1971).
- Duffy, J. G., and M. D. Ingram, *J. Am. Ceram. Soc.* **52**, 224 (1969).

- Dumas P., and J. A. T. Taylor, *J. Am. Ceram. Soc.* **74**, 2663 (1991).
- Dwir, B., M. Affronte, and D. Pavuna, *Appl. Phys. Lett.* **55**, 399 (1989).
- Feenstra, R., T. B. Lindemer, J. D. Budai, and M. D. Galloway, *J. Appl. Phys.* **69**, 6569 (1991).
- Foltyn, S. R., P. Tiwari, R. C. Dye, M. Q. Le, and X. D. Wu, *Appl. Phys. Lett.* **63**, 1848 (1993).
- Galasso, F. S., *Perovskites and High Tc Superconductors*, Gordon and Breach (New York, 1990).
- Gallagher, P. K., F. Schrey, and F. V. DiMarcello, *J. Am. Ceram. Soc.* **46**, 359 (1963).
- Gao, J., Y. Z. Zhang, B. R. Zhao, P. Out, C. W. Yuan, and L. Li, *Appl. Phys. Lett.* **53**, 2675 (1988).
- Gardner, T. J., and G. L. Messing, *Am. Ceram. Soc. Bull.* **64**, 1498 (1984).
- Golden, S. J., H. Isotalo, M. Lanham, J. Mayer, F. F. Lange, and M. Ruhle, *J. Mater. Res.* **5**, 1605 (1990).
- Goldschmidt, V. M., *Geochemische Verteilungsgesetze der Elemente. VII, VIII*, Skrift. Norske Vidensk Akad. I. Mat. nat. Kl. Oslo, Nos. 2 and 8.
- Grader, G. S., P. K. Gallagher, and D. A. Flemming, *Chem. Mater.* **1**, 665 (1989).
- Graham, H. C., N. M. Tallin, and K. S. Mazdidasni, *J. Am. Ceram. Soc.* **54**, 548 (1971).
- Griswold, E., and W. van Horne, *J. Am. Chem. Soc.* **67**, 763 (1945).
- Gyurov, G., I. Kristova, P. Peshev, and M. V. Abrashev, *Mat. Res. Bull.* **28**, 1067 (1993).
- Hannay, N. B., *Solid State Chemistry*, Prentice-Hall Inc., Englewood Cliffs, NJ, 1967.

- Hatch, L. P., *Am. Sci.* **41**, 410 (1952).
- Hixson, A. W., and W. W. Plechner, *Ind. Eng. Chem.* **25**, 262 (1933).
- Holiday, A. K., and A. G. Massey, *Inorganic Chemistry in Non-Aqueous Solvents*,
Permagon Press (New York, 1965).
- Horowitz, H. S., S. J. McLain, A. W. Sleight, J. D. Druliner, P. L. Gai, M. J. Van
Kavelaar, J. L. Wagner, B. D. Biggs, and S. J. Poon, *Science* **243**, 66 (1989).
- Hulbert, S. F., and J. J. Klawitter, *J. Am. Ceram. Soc.* **50**, 484 (1967).
- Hulbert, S. F., *J. Br. Ceram. Soc.* **6**, 11 (1969).
- Hunt, A. T., W. B. Carter, and J. K. Cochran Jr, *Appl. Phys. Lett.* **63**, 266 (1993).
- Hussain, A. A., and M. Sayer, *J. Supercon.* **4**, 385 (1991).
- Jander, W., *Z. Anorg. Chem.* **163**, 1 (1927).
- Jergel, M., S. Chromik, V. Strbik, V. Smatko, F. Hanic, G. Plesch, S. Buchta, and S.
Valtynova, *Supercond. Sci. Technol.* **5**, 225 (1992).
- Johnson, B. R., K. M. Beauchamp, T. Wang, J. X. Lui, K. A. McGreer, J. C. Wan, M.
Tuominen, Y. J. Zhang, M. L. Mecartney, and A. M. Goldman, *Appl. Phys. Lett.*
56, 1911 (1990).
- Kakihana, M., L. Borjesson, S. Eriksson, and P. Svendlindh, *J. Appl. Phys.* **69**, 867
(1991).
- Karpinski, J., E. Kaldis, E. Jilek, S. Rusiecki, and B. Bucher, *Nature* **338**, 328 (1989).
- Karpinski, J., E. Kaldis, E. Jilek, S. Rusiecki, and B. Bucher, *Nature* **336**, 660 (1988).
- Katayama, S., and M. Sekine, *J. Mater. Res.* **5**, 683 (1990).
- Kesson, S. E., and T. J. White, *Proc. R. Soc. Lond. A* **405**, 73 (1986).

- Kini, A. M., U. Geiser, H-C. I. Kao, K. D. Carlson, H. H. Wang, M. R. Monaghan, J. M. Williams, *Inorg. Chem.* **26**, 1836 (1987).
- Kirchnerova, J., and B. D. Hibbert, *Mat. Res. Bull.* **25**, 585 (1990).
- Kiss, K., J. Madger, M. S. Vukasovich, and R. J. Lockhart, *J. Am. Ceram. Soc.* **49**, 291 (1966).
- Kleinberg, J., W. J. Argersinger, and E. Griswold, *Inorganic Chemistry*, D.C. Heath and Co. (Boston, Massachusetts, 1960).
- Knauf, N., J. Harwischmacher, R. Müller, R. Borowski, B. Rodeu, and D. Wohllebreu, *Physica C* **173**, 414 (1991).
- Kourtakis, K., M. Robbins and P. K. Gallagher, and T. Teifel, *J. Mater. Res.* **4**, 1289 (1989).
- Kourtakis, K., M. Robbins and P. K. Gallagher, *J. Solid St. Chem.* **82**, 290 (1989).
- Kreslin, V. Z., and S. A. Wolf, *Fundamentals of Superconductivity*, Plenum Press (New York, 1989).
- Krishnaraj, P., M. Lelovic, N. G. Eror, and U. Balachandran, *Physica C* **215**, 305 (1993).
- Kubo, T., and K. Shinriki, *J. Chem. Soc. Jpn., Ind. Chem. Sect.* **55**, 49 (1952).
- Kullberg, M. L., M. T. Lanagan, W. Wu, and R. B. Poeppel, *Supercon. Sci. and Technol.* **4**, 337 (1991).
- Kwo, J., *J. Crystal Growth* **111**, 965 (1991).
- Langlet, M., E. Senet, J. L. Deschanvres, G. Delabouglise, F. Weiss, and J. C. Jourbert, *J. Less Comm. Metals* **151**, 399 (1989).

- Lee, H. G., S. D. Park, S. W. Yang, H. S. Shin, and D. Y. Won, *Jpn. J. Appl. Phys.* **31**, L157 (1992).
- Leskela, M., H. Molsa, and L. Niinisto, *Suprecon. Sci. Technol* **6**, 627 (1993).
- Li, Q., O. Meyer, X. X. Xi, J. Geerk, and G. Linker, *Appl. Phys. Lett.* **55**, 1560 (1989).
- Luikov, A. V., *Analytical Heat Diffusion Theory*, Academic Press (1968).
- Luo, L., X. D. Wu, R. C. Dye, R. E. Muenchausen, S. R. Foltyn, Y. Coulter, and C. J. Marriore, *Appl. Phys. Lett.* **59**, 2043 (1991).
- Maeda, H., Y. Tanaka, M. Fukutomi, and T. Asano, *Jpn. J. Appl. Phys.* **27**, L209 (1988).
- Manthiram, A., and J. B. Goodenough, *Nature* **329**, 701 (1987).
- McCarthy, G. J., *Nucl. Technol.* **32**, 92 (1977).
- McGrath, P. J., and R. M. Laine, *J. Am. Ceram. Soc.* **75**, 1223 (1992).
- McHale, J. M., and N. V. Coppa, *Titanate Materials from Freeze Dried Nitrate Solutions*, Patent applied for: DOE Application # S-80, 469 (1994).
- McHale, J. M., P. C. McIntyre, K. E. Sickafus, and N. V. Coppa, To be submitted to the *Journal of Materials Research*, November, 1994.
- McHale, J., G. H. Myer and R. E. Salomon, *J. Mater. Res.* **10**, No.1, (1995).
- McHale, J., R. W. Schaeffer, and R. E. Salomon, *J. Chem. Ed.* **69**, 1031 (1992).
- McHale, J., R. W. Schaeffer, A. Kebede, J. Macho, and R. E. Salomon, *J. Supercond.* **5**, 511 (1992).
- McKittrick, J., and R. Contreras, *Thin Solid Films* **206**, 146 (1991).
- Megaw, H. D., *Proc. Phys. Soc.* **58**, 326 (1946).
- Messing, G. L., S. C. Zhang, and G. V. Jayanthi, *J. Am. Ceram. Soc.* **76**, 2707 (1993).

- Miyatake, T., S. Gotoh, N. Koshizuka, and S. Tanaka, *Nature* **341**, 41 (1989).
- Mogro-Campero, A., L. G. Turner, and E. L. Hall, *J. Appl. Phys.* **65**, 4951 (1989).
- Mogro-Campero, A., L. G. Turner, E. L. Hall, M. F. Garbaskus, and N. Lewis, *Appl. Phys. Lett.* **54**, 2719 (1989).
- Morris, D. E., J. H. Nickel, J. Y. T. Wei, N. G. Asmer, J. S. Scott, U. M. Scheven, C. T. Hultgren, A. G. Markelz, J. E. Post, P. J. Heaney, D. R. Velben, and R. M. Halzen, *Phys. Rev. B* **37**, 9353 (1989).
- Naka, S., F. Nakakita, Y. Suwa, and M. Inagaki, *Bull. Chem. Soc. Jpn.* **47**, 1168 (1974).
- Naray-Szabo, I., *Inorganic Crystal Chemistry*, Akademiai Kiado (Budapest, 1969).
- Negas, T., R. S. Roth, H. S. Parker, and D. Minor, *J. Solid State Chem.* **9**, 297 (1974).
- Nirsha, B. M., A. D. Chubinidze, Y. A. Velikodnyi, B. V. Zhadanov, and V. A. Olikova, *Zh. Obshch. Khim. USSR* **53**, 1631 (1983).
- Nui, C., and C. M. Lieber, *J. Am. Chem. Soc.* **114**, 3570 (1992).
- Onishi, H., H. Harima, Y. Kusakabe, M. Kobayashi, S. Hoshinouchi, and K. Tachibana, *Jpn. J. Appl. Phys.* **29**, L2041(1990).
- Ono, R. H., *MRS Bull.* **8**, 34 (1992).
- Peters, P. N., R. C. Sisk, and E. W. Urban, *Appl. Phys. Lett.* **52**, 2066 (1988).
- Peterson, S., and E. K. Dienes, *J. Phys. Chem.* **55**, 1299 (1951).
- Pfaff, G., *J. Mater. Chem.* **2**, 591 (1992).
- Pfaff, G., *Chem. Mater.* **6**, 58 (1994).
- Phule, P. P., and S. H. Risbud, *J. Mater. Sci.* **25**, 1169 (1990).
- Poisl, W. H., and A. C. D. Chaklader, *J. Am. Ceram. Soc.* **76**, 1177 (1993).

- Pooke, D., R. G. Buckley, M. R. Pressland, and J. L. Tallon, *Phys. Rev. B* **41**, 6616 (1990).
- Poole, C. P., T. Datta, and H. A. Farrah, *Copper Oxide Superconductors*, John Wiley and Sons (New York, 1988).
- Prakash, S., D. M. Umarjee, H. J. Doerr, C. V. Deshpandey, and R. F. Brunshah, *Appl. Phys. Lett.* **55**, 504 (1989).
- Rao, C. N. R., R. Nagarajan, and R. Vijayaraghavan, *Supercond. Sci. Technol.* **6**, 1 (1993).
- Rase, D. E., and R. Roy, *J. Am. Ceram. Soc.* **38**, 102 (1955).
- Raveau, B., C. Michel, M. Hervieu, and D. Groult, *Crystal Chemistry of High Tc-Superconducting Oxides*, Springer-Verlag (New York, 1991).
- Ringwood, A. E., S. E. Kesson, N. G. Ware, W. Hibberson, and A. Major, *Nature* **278**, 219 (1979).
- Ringwood, A. E., *Safe Disposal of High Level Nuclear Reactor Wastes: A New Strategy*, Australian National University Press (Norwalk, CT, 1978).
- Ringwood, T., *Amer. Sci.* **70**, 201 (1982).
- Roth, R. S., *J. Research NBS* **58**, RP 2736 (1957).
- Roy, R., *J. Am. Ceram. Soc.* **60**, 350 (1977).
- Ruckenstein, E., S. Narain, and N. L. Wu, *J. Mater. Res.* **4**, 267 (1989).
- Ruggerio, S. T., and D. A. Rudman, *Superconducting Devices*, Academic Press Inc. (Boston, MA, 1990).

- Ruiz, M. T., G. F. de la Fuente, A. Badia, J. Blasco, M. Castro, A. Sotelo, A. Larrea, F. Lera, C. Rillo, and R. Navarro, *J. Mater. Res.* **8**, 1268 (1993).
- Ruthner, M. J., *Sci. Sintering* **6**, 81 (1974).
- Salama, K., and D. F. Lee, *Supercond. Sci. Technol.* **7**, 177 (1994).
- Sanchez, C., J. Livage, M. Henry, and F. Babonneau, *J. Non-Cryst. Solids* **100**, 65 (1988).
- Schaeffer, R. W., J. Macho, R. E. Salomon, G. H. Myer, J. E. Crow, and P. Wise, *J. Supercon.* **4**, 5 (1991).
- Schaeffer, R. W., Doctoral Dissertation, Temple University, Philadelphia, PA, 1992.
- Scheel, H. J., M. Berkowski, and B. Chabot, *J. Crystal Growth* **115**, 19 (1991).
- Schmalzred, H., *Monographs in Modern Chemistry 12, Solid State Reactions*, Edited By Hans F. Ebel, Verlag Chemie, Deerfield Beach, FL, USA, 1981.
- Schneider, H. G., and V. Ruth, Editors, *Advances in Epitaxy and Endotaxy*, VEB Deutscher Verlag für Grundstoffindustrie (Leipzig, 1971).
- Schnettler, F. J., F. R. Monforte, and W. W. Rhodes, *Sci. Ceram.* **4**, 79 (1968).
- Selinder, T. I., G. Larsson, U. Helmersson, and S. Rudner, *Supercond. Sci. Technol.* **4**, 379 (1991).
- Selvaduray, G., and C. Zhang, *J. Mater. Res.* **7**, 283 (1992).
- Setsune, K., T. Kamada, H. Adachi, and K. Wasa, *J. Appl. Phys.* **65**, 1318 (1988).
- Shaw, T. M., D. Dinos, P. E. Batson, A. G. Schrott, D. R. Clarke, and P. R. Duncombe, *J. Mater. Res.* **5**, 1176 (1990).
- Solomah, A. G., T. M. Hare, and H. Palamour III, *Trans. Am. Nucl. Soc.* **34**, 197 (1980).

- Song, K. H., H. K. Liu, S. X. Dou, and C. Sorrel, *J. Amer. Ceram. Soc.* **73**, 1771 (1990).
- Stastny, P., R. Kuzel, and V. Skacel, *J. Less. Comm. Metals* **164 & 165**, 464 (1989).
- Stockenhuber, M., H. Mayer, and J. A. Lercher, *J. Am. Ceram. Soc.* **76**, 1185 (1993).
- Strobel, P., C. Paulsen, and J.L. Tholence, *Solis State Commun.* **68**, 535 (1988)
- Stroessel, C. H., R. F. Bunshah, S. Prakash, and H. R. Fetterman, *J. Supercon.* **6**, 1 (1993).
- Tabuchi, J., and K. Utsumi, *Appl. Phys. Lett.* **53**, 606 (1989).
- Takemuchi, T., K. Ado, T. Asai, H. Kageyama, Y. Saito, C. Masqueleir, and O. Nakamura, *J. Am. Ceram. Soc.* **77**, 1665 (1994).
- Tejuca, L. G., and J. L. G. Fierro, Editors, *Properties and Applications of Perovskite Type Oxides*, Marcel Dekker Inc. (New York, 1993).
- Templeton, L. K., and J. A. Pask, *J. Am. Ceram. Soc.* **42**, 212 (1959).
- Terashima, T., K. Ijima, K. Yamamoto, Y. Bando, and H. Mazaki, *Jpn. J. Appl. Phys.* **55**, 504 (1989).
- Thampi, K. R., M. Subba Rao, W. Schwartz, M. Gratzel, and J. Kiwi, *J. Chem. Soc. Faraday Trans.* **84**, 1703 (1988).
- Thomas, O., E. Mossang, J. Fick, F. Weiss, R. Madar, J. P. Senateur, S. K. Agarwal, C. Schlenker, M. Ingold, P. Germi, and M. Pernet, *Physica C* **185-189**, 2113 (1991).
- Tsuruoka, T., R. Kawasaki, and H. Abe, *Jpn. J. Appl. Phys.* **28**, L1800 (1989).
- Tunkasiri, T., and G. Rujijanagul, *J. Mater. Sci. Lett.* **13**, 165 (1994).

- Twu, J., and P. K. Gallagher, in *Properties and Applications of Perovskite Type Oxides*, Edited by L. G. Tejuca and J. L. G. Fierro, Marcel Decker Inc. (New York, 1993).
- Vance, E. R., C. J. Ball, M. G. Blackford, D. J. Cassidy, and K. L. Smith, *J. Nuclear Mater.* **175**, 58 (1990).
- Venkatesan, T., E. W. Chase, X. D. Wu, A. Inam, C. C. Cheng, and F. K. Skokoohi, *Appl. Phys. Lett.* **53**, 243 (1988).
- Waddington, T. C., *Non-Aqueous Solvent Systems*, Academic Press (New York, 1965).
- Wagner, C., *Z. Anorg. Allg. Chem.* **236**, 320 (1938).
- Wang, X. Z., M. Henry, J. Livage, and I. Rosenman, *Solid St. Commun.* **64**, 881 (1987).
- Wang, H. S., D. Eissler, W. Dietsche, A. Fischer, and K. Ploog, *J. Crystal Growth* **127**, 655 (1993).
- Ward, T. L., T. T. Kodas, A. H. Carim, D. M. Kroeger, and H. Hsu, *J. Mater. Res.* **7**, 827 (1992).
- Ward, T. L., T. T. Kodas, and A. H. Carim, *J. Mater. Res.* **7**, 827 (1992)
- Weast, R. C., Editor, *CRC Handbook of Physics and Chemistry, 56th Ed.*, CRC Press (Cleveland, Ohio, 1975)
- Weiser, H. B., *Inorganic Colloid Chemistry, Volume II The Hydrous Oxides and Hydroxides*, John Wiley and Sons, Inc. (London, 1935).
- Werme, L., I. K. Bjorner, G. Bart, H. U. Zwicky, B. Grambow, W. Lutze, R. C. Ewing, and C. Magrabi, *J. Mater. Res.* **5**, 1130 (1990).

- West, A. R., *Solid State Chemistry And Its Applications*, John Wiley and Sons
(New York, 1984).
- Xi, X. X., T. Venkatesan, X. D. Wu, A. Inam, C. C. Chang, R. Ramesh, D. M. Hwang,
T. S. Ravi, A. Findikoglu, D. Hemmick, S. Etemad, J. A. Martinez, and B.
Wilkins, *IEEE Trans. Magnet.* **27**, 928 (1991).
- Yamamura, H., A. Watanabe, S. Shirasaki, Y. Moriyoshi, and M. Tanada, *Ceram. Int.* **11**,
17 (1985).
- Zeng, L., Z. Zijiang, L. Zhang, H. Chen, Z. Quain, and D Wu, *Appl. Phys. Lett.* **56**, 1573
(1990).
- Zhang, Z., and C. M. Lieber, *J. Phys. Chem.* **96**, 2030 (1992).